Mouse models to study plasma cells and monoclonal immunoglobulin-related diseases

Maria Victoria Ayala

Ph.D. Thesis

Université de Limoges

University of Limoges

ED 615 - Sciences Biologiques et Santé (SBS)

CNRS UMR7276/ INSERM U1262
CRIBL (Contrôle de la réponse Immune B et Lymphoprolifération)

A thesis submitted to University of Limoges
in partial fulfillment of the requirements of the degree of

Doctor of Philosophy

Immunology, oncology, inflammation and infectiology

Presented and defended by
María Victoria Ayala

On September 11, 2020

Mouse models to study plasma cells and monoclonal immunoglobulin-related diseases

Thesis supervisor: Pr. Christophe Sirac, PhD, University of Limoges

JURY:

President of jury
Pr. Frank Bridoux, MD, PhD, University of Limoges and CHU of Poitiers

Reporters
Pr. Jonathan Wall, PhD, University of Tennessee
Pr. Olivier Decaux, MD, PhD, University of Rennes and CHRU of Rennes

You will succeed if you persevere;
and you will find joy in overcoming obstacles.
Helen Keller

Science never solves a problem without creating ten more.
George Bernard Shawlt

It always seems impossible until it's done.
Nelson Mandela

To my parents,

My sisters,

My friends,

My Poposon,

Advice, like youth, probably just wasted on the young

Mary Schmich, Chicago Tribune – Sunday June 1st 1997- Adapted

Wear sunscreen.

If I could offer you only one tip for the future, sunscreen would be it. The long-term benefits of sunscreen have been proved by scientists, whereas the rest of my advice has no basis more reliable than my own meandering experience. I will dispense this advice now.

Don't worry about the future. Or worry, but know that worrying is as effective as trying to solve an algebra equation by chewing bubble gum. The real troubles in your life are apt to be things that never crossed your worried mind, the kind that blindside you at 4 p.m. on some idle Tuesday.

Do one thing every day that scares you.

Don't be reckless with other people's hearts. Don't put up with people who are reckless with yours.

Don't waste your time on jealousy. Sometimes you're ahead, sometimes you're behind. The race is long and, in the end, it's only with yourself.

Remember compliments you receive. Forget the insults. If you succeed in doing this, tell me how.

Don't feel guilty if you don't know what you want to do with your life. The most interesting people I know didn't know at 22 what they wanted to do with their lives. Some of the most interesting 40-year-olds I know still don't.

Maybe you'll marry, maybe you won't
maybe you'll have children, maybe you won't
maybe you'll divorce at 40, maybe you'll dance the funky chicken on your 75th wedding anniversary...
what ever you do, don't congratulate yourself too much or berate yourself either
your choices are half chance, so are everybody else's

Read the directions, even if you don't follow them.

Get to know your parents. You never know when they'll be gone for good. Be nice to your siblings. They're your best link to your past and the people most likely to stick with you in the future.

Understand that friends come and go, but with a precious few you should hold on. Work hard to bridge the gaps in geography and lifestyle, because the older you get, the more you need the people who knew you when you were young.

Accept certain inalienable truths: Prices will rise. Politicians will philander. You, too, will get old. And when you do, you'll fantasize that when you were young, prices were reasonable, politicians were noble and children respected their elders.

Be careful whose advice you buy, but be patient with those who supply it. Advice is a form of nostalgia. Dispensing it is a way of fishing the past from the disposal, wiping it off, painting over the ugly parts and recycling it for more than it's worth.

But trust me on the sunscreen.

Les conseils, comme la jeunesse, sont probablement gaspillés par les jeunes

Mary Schmich, Chicago Tribune – Dimanche 1er Juin 1997- Adapté

Mettez de la crème solaire.

Si je pouvais vous donner un seul conseil pour l'avenir, ce serait celui-ci: la crème solaire. Les avantages à long terme de la crème solaire ont été démontrés par des scientifiques. A part ça, mon conseil se base sur ma propre expérience un peu décousue, et rien de plus. Voici mon conseil.

N'ayez pas peur de l'avenir. Ou alors: ayez peur, mais sachez que la peur est aussi efficace qu'un chewing gum pour résoudre une équation. Les vrais problèmes dans votre vie sont susceptibles d'être des choses qui ne vous ont jamais traversé l'esprit, du genre qui vous aveugle à 16 heures un mardi inactif.

Chaque jour, faites quelque chose qui vous effraie.

Ne soyez pas imprudent avec le coeur des autres. N'acceptez pas qu'on soit imprudent avec le vôtre.

Ne perdez pas de temps avec la jalousie. Vous êtes parfois en avance, parfois en retard. La course est longue, et à la fin, c'est toujours une course contre soi-même.

Souvenez-vous des compliments et oubliez les insultes. Si vous y parvenez, dites-moi comment vous avez fait.

Ne vous sentez pas coupables si vous ne savez que faire de votre vie. Les gens les plus intéressants sont ceux qui ne savaient pas ce qu'ils allaient faire de leur vie quand ils avaient 22 ans. Les quadragénaires les plus intéressants ne le savent toujours pas.

Vous vous marierez peut-être. Ou peut-être pas.
Vous aurez peut-être des enfants. Ou peut-être pas
Vous divorcerez peut-être à 40 ans, vous danserez peut-être le funky chicken à votre 75e anniversaire.
Quoi qu'il en soit, ne vous félicitez pas trop, et ne vous grondez pas trop. Vous avez une chance sur deux, comme tout le monde.

Lisez les instructions, même si vous ne les suivez pas.

Apprenez à connaître vos parents. On ne sait jamais quand ils partiront pour de bon. Sois gentil avec tes frères et soeurs. Ils sont votre meilleur lien avec votre passé et les personnes les plus susceptibles de rester avec vous à l'avenir.

Sachez que les amis vont et viennent. Mais certains d'entre eux sont précieux, il ne faut pas les perdre. Il faut travailler dur pour vaincre les distances et les différences de mode de vie, parce que plus on vieillit, plus on a besoin de ses amis de jeunesse.

Acceptez certaines vérités: les prix vont augmenter, les politiciens courront après les femmes. Vous aussi, vous vieillirez. Et quand vous serez vieux, vous vous direz que les prix étaient raisonnables, les politiciens étaient nobles, les enfants respectaient leurs parents quand vous étiez jeunes.

Faites attention aux conseils qu'on vous donne, mais soyez patients avec ceux qui vous les donnent. Le conseil est une forme de nostalgie. Donner des conseils, c'est aller repêcher le passé dans le vide-ordures, c'est l'épousseter, repeindre les vilains morceaux et recycler le tout en lui donnant plus de valeur qu'il n'en a.

Mais vous pouvez me faire confiance à propos de la crème solaire.

ACKNOWLEDGEMENTS

I gratefully acknowledge the 4th year funding received from the Fondation ARC

TABLE OF CONTENTS

ACRONYMS AND ABBREVIATIONS

ADCC: ANTIBODY-DEPENDENT CELLULAR CYTOTOXICITY
ADCP: ANTIBODY-DEPENDENT CELLULAR PHAGOCYTOSIS
AG: ANTIGEN
AID: ACTIVATION-INDUCED CYTIDINE DEAMINASE
AL AMYLOIDOSIS: LIGHT CHAIN AMYLOIDOSIS
APC: ANTIGEN-PRESENTING CELLS
APOE: APOLIPOPROTEIN E
APRIL: A PROLIFERATING-INDUCING LIGAND
ASC: ANTIBODY-SECRETING CELL
ATF6: ACTIVATING TRANSCRIPTION FACTOR 6
BCR: B CELL RECEPTOR
BER: BASE EXCISION REPAIR
BIP: IMMUNOGLOBULIN BINDING PROTEIN
BLIMP1: LYMPHOCYTE-INDUCE MATURATION PROTEIN-1
BM: BONE MARROW
B-MEF2: MYOCYTE ENHANCER FACTOR 2
CDR: COMPLEMENTARITY DETERMINING REGION
CH: CONSTANT DOMAINS
CHOP: C/EBP HOMOLOGOUS PROTEIN
CR: CONGO RED
CRAB SYMPTOMS: HYPERCALCEMIA, RENAL IMPAIRMENT, ANEMIA, BONE DISEASE.
CREERT2 RECOMBINASE: TAMOXIFEN-DEPENDENT CRE RECOMBINASE
CSR: CLASS SWITCH RECOMBINATION
CXCR: CHEMOKINE C-X-C MOTIF RECEPTOR
D: DIVERSITY
DC: DENDRITIC CELL
DZ: DARK ZONE
EDEM1: ENHANCING α MANNOSIDASE-LIKE PROTEIN 1
EGFP: ENHANCED GREEN FLUORESCENT PROTEIN
ER: ENDOPLASMIC RETICULUM
ERAD: ER-ASSOCIATED DEGRADATION
FC: FRAGMENT CRYSTALLIZABLE REGION
FDC: FOLLICULAR DENDRITIC CELLS
FISH: FLUORESCENT IN SITU HYBRIDIZATION
FLC: FREE LIGHT CHAINS
FO: FOLLICULAR
FS: FANCONI SYNDROME
GC: GERMINAL CENTER
HC: HEAVY CHAINS
HCDD: HEAVY CHAIN DEPOSITION DISEASE
IF: IMMUNOFLUORESCENCE
IFN-γ: INTERFERON GAMMA
IG: IMMUNOGLOBULIN
IL: INTERLEUKIN
IMID: IMMUNOMODULATOR
IMWG: INTERNATIONAL MYELOMA WORKING GROUP
IRE1α: INOSITOL-REQUIRING ENZYME 1α
IRF4: INTERFERON REGULATORY FACTOR 4
IRF8: INTERFERON REGULATORY FACTOR 8
J: JOINING
LC: LIGHT CHAINS
LCDD: LIGHT CHAIN DEPOSITION DISEASE
LFA-1: LYMPHOCYTE FUNCTION-ASSOCIATED ANTIGEN 1
LZ: LIGHT ZONE
MAB: MONOCLONAL ANTIBODY
MALT: MUCOSE-ASSOCIATED LYMPHOID TISSUE
MDE: MYELOMA-DEFINING EVENT
MGCS: MONOCLONAL GAMMOPATHY OF CLINICAL SIGNIFICANCE
MGRS: MONOCLONAL GAMMOPATHY OF RENAL SIGNIFICANCE
MGUS: GAMMOPATHY OF UNDERTERMINED SIGNIFICANCE
MHC: MAJOR HISTOCOMPATIBILITY COMPLEX
MM: MULTIPLE MYELOMA
MMR: MISMATCH REPAIR
MZ: MARGINAL ZONE
NHEJ: NON-HOMOLOGOUS END JOINING
NK: NATURAL KILLER CELLS
PAX5: PAIRED BOX 5
PC: PLASMA CELLS
PCD: PLASMA CELL DYSCRASIAS
PCL: PLASMA CELL LEUKEMIA
PERK: RNA-DEPENDANT PROTEIN KINASE
PI: PROTEASOME INHIBITOR
PIGR: POLY-IG RECEPTOR
RAG: RECOMBINAISON ACTIVATING GENE
RSS: RECOMBINATION SIGNAL SEQUENCES
SAP: SERUM AMYLOID P COMPONENT
SCT: STEM CELL TRANSPLANTATION
SHM: SOMATIC HYPERMUTATION
SMM: SMOLDERING MULTIPLE MYELOMA (SMM)
TCR: T CELL RECEPTOR
TLR: TOLL-LIKE RECEPTOR
TREG: REGULATORY T CELL
UPR: UNFOLDED PROTEIN RESPONSE
V: VARIABLE
V-CAM1: VASCULAR CELL ADHESION PROTEIN 1
VLA-4: VERY LATE ANTIGEN-4
WM: WALDENSTROM MACROGLOBULINEMIA
XBP1: X-BOX BINDING PROTEIN 1
EBF: EARLY-B-CELL FACTOR
SCF: STEM CELL FACTOR
FTL-3L: FMS-LIKE TYROSINE KINASE 3 LIGAND

INTRODUCTION

Every living creature lives in a threatening world due to daily contact with pathogens, toxic or allergenic substances. Some of them have evolved to have a complex protective system, that we call the immune system. It is a network of cells and molecules capable of distinguishing foreign substances and destroying them. As any dynamic system, its success relies on achieving a perfect balance: getting rid of pathological, toxic, or allergenic agents while avoiding an excessive response that could damage self-tissues.

The immune system can be divided into two types of responses: the innate response and the adaptive response (**Figure 1**). The innate immune response functions as the first line of defense and it includes soluble factors (complement proteins, cytokines, etc.) and different cells such as macrophages, dendritic cells, natural killer cells, etc. It is dependent on the recognition of conserved patterns found in many pathogens and it reacts within hours after encountering the foreign substance. Its main drawback is that it does not generate long-term protective immunological memory. In contrast, the adaptive immune response takes longer to develop but it is more specific to pathogens, has immunological memory, and is highly adaptable. It is composed mainly of antibodies, B cells, and T cells. Furthermore, the adaptive response can be subdivided into a cell-mediated immune response (carried out by T cells), and a humoral immune response (implying B cells and antibodies).

Throughout this manuscript, we will focus on the latter with research mainly centered on the last stage of B cell development, the plasma cell. As we will see later on, their dysfunction or abnormal proliferation can end in the aberrant production of antibodies. Different diseases can arise from the aggregation or deposition of the monoclonal immunoglobulin and they will be further discussed in the following pages.

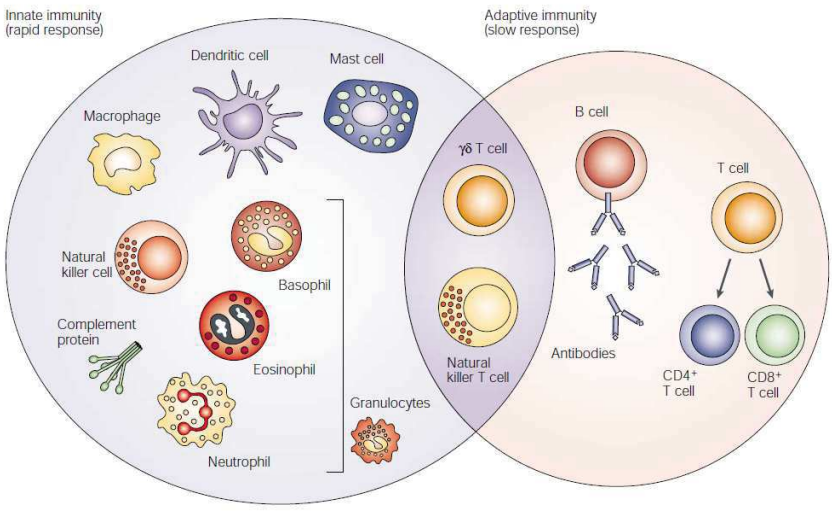

Figure 1- The immune system. The innate responses use phagocytic cells, cells that release inflammatory mediators as well as natural killer cells. The adaptive response involves the proliferation of antigen-specific B and T cells. This occurs when surface receptors bind to a specific antigen.(Dranoff, 2004)

Chapter I. B cell and antibodies

I.1. **The Immunoglobulin**

In 1890, Emil Behring and Shibasaburo Kitasato published a diphtheria antitoxin serum. They explained that infected animals could be cured and healthy animals protected from the infection using serum obtained from immunized rabbits. Mice injected with this serum were immune against tetanus bacilli or tetanus toxin and they called the neutralizing substance "antitoxin" (Kaufmann, 2017). A year after, Paul Ehrlich postulated that immune cells receptors, that he called "side-chains", could recognize a toxin and brake off to circulate through the body (**Figure 2**). He later used the term *Antibody* for these side-chains and the substance they recognized *Antigens* (Bordon, 2016).

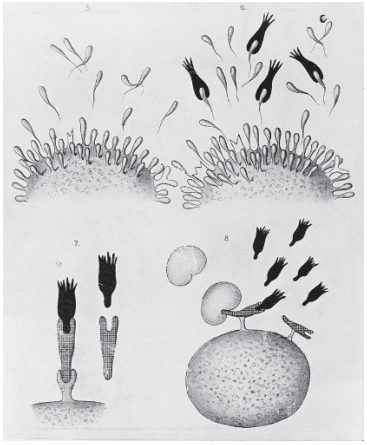

Figure 2- Ehrlich's side-chain theory. Immune cells carry different receptors for a particular substance. When a toxin binds to a receptor, the cell would react by producing more of them to be released into the bloodstream thus neutralizing the toxin. From the Royal Society of London, 66, 424–448 (1900).

It is not almost forty years later that Tiselius and Kabat separated by electrophoresis immunized serum into albumin, alpha-goblulin, beta-globulin, and gamma-globulin fractions (Tiselius and Kabat, 1939) (**Figure 3**). Absorption of the serum against the antigen (Ag) depleted the gamma-globulin fraction, yielding the terms of *Gamma-globulin* and *Immunoglobulin*.

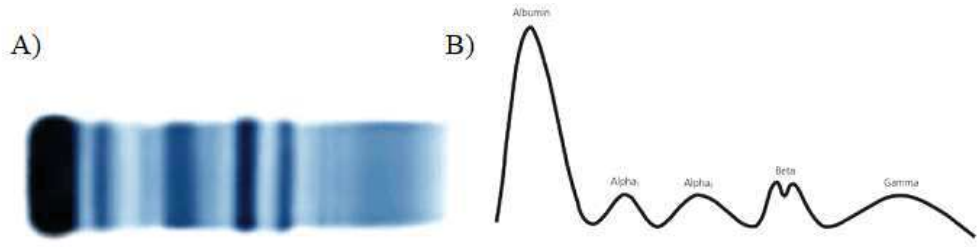

Figure 3- Serum Electrophoresis. A) Normal serum electrophoresis. B) Densitometry tracing of electrophoresis showing the five zones of the high-resolution agarose electrophoresis.

I.1.1. Immunoglobulin structure

The immunoglobulin (Ig) is a glycoprotein composed of two identical light chains (LC), that can be either kappa or lambda, and two identical heavy chains (HC) linked together by disulfide bonds. The HCs determine the Ig class and they can be mu, delta, epsilon, alpha, or gamma (Schroeder and Cavacini, 2010).

Both variable domains (VH and VL) constitute the variable region (Fv) responsible for recognizing and binding to the antigen. They are part of the Fab region of the Ig composed of the V regions, together with the constant region of the LC (CL) and the first constant domain of the HC (CH1) linked by a disulfide bond. The rest of the immunoglobulin is composed of the other HC constant domains (CH2, CH3, and, for IgE and IgM, CH4), also known as the fragment crystallizable region (Fc region) and varies between the different Ig classes. Finally, disulfide bonds in the hinge region of the HC (located in between the CH1 and CH2), stick the HC-LC heterodimers together (**Figure 4**).

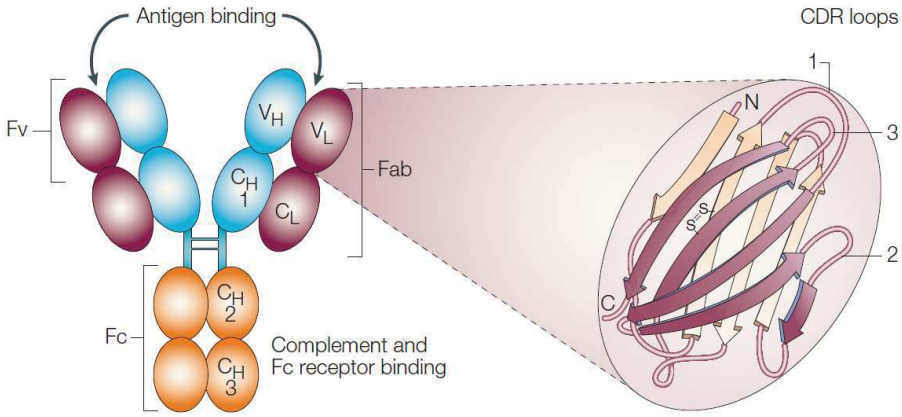

Figure 4- Immunoglobulin structure. Example of an IgG immunoglobulin structure. The HC are covalently linked in the hinge region and the LC are also covalently linked to the HC. The variable domain of both HC and LC compose the antigen-binding region. Within it we can find three loops designated complementarity determining regions (CDRs 1, 2 and 3) which confer the diversity and specificity. The Fc region can interact with effector molecules and Fc receptors. (Brekke and Sandlie, 2003)

I.1.2. Classes of Immunoglobulins

The five primary classes of immunoglobulins are IgG (gamma), IgM (mu), IgA (alpha), IgD (delta), and IgE (epsilon) (**Figure 5**). Differences in the heavy chain allow these immunoglobulins to function in different types and times of the immune response thanks to the Fc region binding to various effector molecules.

IgM is the first circulating immunoglobulin produced following immunization and is involved in the first burst of protective Ig especially through neutralization and complement recruitment. However, its concentration in blood declines rapidly. IgM monomers are arranged in a pentagonal structure thanks to the J chain, which will be described in detail later on. IgD is

mostly found on the surface of B cells serving as antigen-receptor and its role is still poorly understood in B cell development and differentiation into plasma cells and memory B cells.

Other isotypes appear later after immunization and bear affinity maturated V domains with high specificity for the Ag. IgG is the most abundant of the circulating Igs and it can cross blood vessels walls and enter tissue fluids protecting from bacteria, viruses and toxins in the blood and lymph. IgG Fc can recruit complement and bind to Fc receptors expressed by different immune cells like neutrophils, Natural Killer cells (NK) or macrophages to induce antibody-dependent cellular cytotoxicity (ADCC) or antibody-dependent cellular phagocytosis (ADCP) (Bruhns and Jönsson, 2015). IgE Fc attaches to mast cells and basophils and when encountering the antigen, histamine is released. While its main function is to protect against parasites, it is often related to allergic reactions such as atopic dermatitis and asthma. Finally, IgA presents as a dimer, also thanks to the J chain, and is produced mainly in mucous membranes. Polymeric IgA can cross the epithelial cells thanks to their binding to the poly-Ig receptor (pIgR). Cleavage of the pIgR releases IgA in the apical side of the epithelium leading to protective immunity in mucosae. Its presence in the first milk helps protect newborns from gastrointestinal infections (Schroeder and Cavacini, 2010).

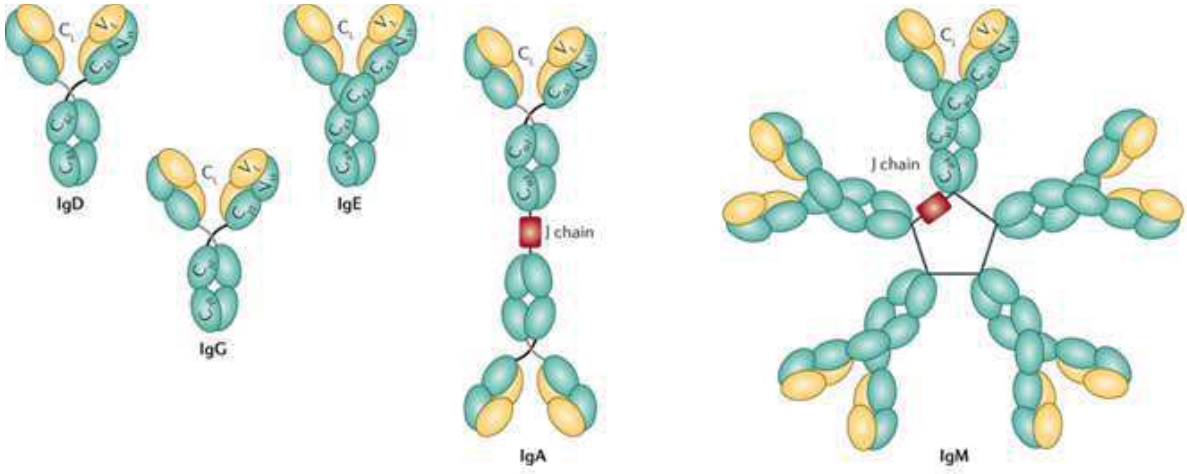

Figure 5- Immunoglobulin classes. Shown here are monomeric IgD, IgE and IgG, along with the dimeric and pentameric forms of IgA and IgM formed thanks to the J chain, schematized in red. Nature Publishing Group. Milestones

I.1.3. Immunoglobulins loci, their rearrangements and modifications

The immunoglobulins loci organization is quite similar between mice and humans (**Figure 6**) although they are found in different chromosomes (Lefranc et al., 2009).

Three distinct types of gene segments, called variable (V), diversity (D), and joining (J), are present in the heavy chain locus in multiple copies. As it will be detailed later on, during B cell

development in the bone marrow (BM), one of each will be selected and recombined to form the variable domain of the heavy chain (Arnaout et al., 2011). The same happens for the light chain that will select one V and J of at least one of the light chains loci (kappa or lambda). However, there is no D segment in these loci (Collins and Watson, 2018). This random pairing of HC and LC, each one with a different combinational rearrangement of those segments, will result in a vast diversity of immunoglobulins capable of recognizing millions of antigens.

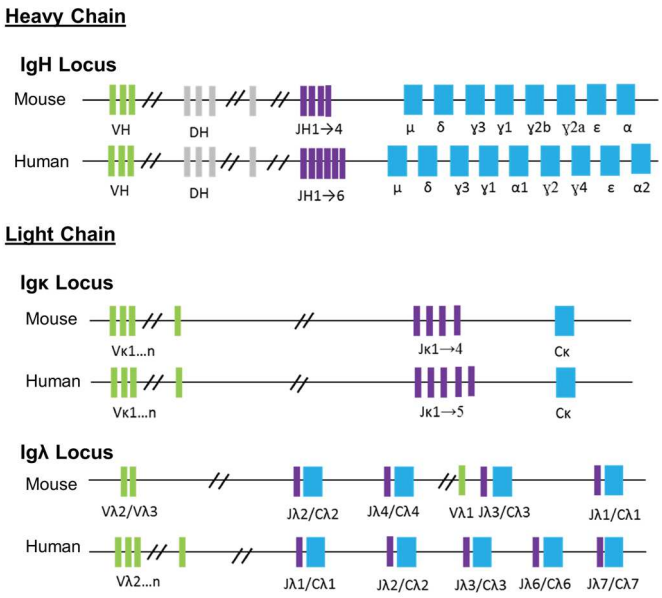

Figure 6- Schematic representation of human and mouse immunoglobulin loci. Variable (V) segments are represented in green, Diversity (D) segments in grey, Junction (J) in violet and the Constant (C) segments in blue. The heavy chain locus (IgH locus) in found in chromosome 14 in humans and 12 in mice. For the light chains, the kappa locus (Igκ locus) is found in chromosome 6 in mice and 2 in humans and lambda (Igλ locus) is in chromosome 16 and 22, respectively.

V(D)J recombination starts with the recognition of conserved recombination signal sequences (RSS), flanking the V, D and J segments, by lymphocyte-specific Recombinaison Activating Gene 1 and 2 (RAG1 and RAG2) endonucleases (Chi et al., 2020; Kim et al., 2015; Schatz and Swanson, 2011). RAG cleavages will be repaired by Non-Homologous End Joining (NHEJ) and these DNA ends can be further diversified before joining by *de novo* insertion of P (palindromic) and nontemplated (N) nucleotides. This imprecise recombination process is useful to increase variable domains diversity but generates 2/3 of nonproductive or out-of-frame transcripts at each recombination that are taken in charge by several mechanisms of RNA surveillance (Chemin et al., 2010; Lambert et al., 2019).

Additionally, another event will seek to increase the affinity for the antigen: Somatic Hypermutation (SHM), also called affinity maturation (Chi et al., 2020; Hwang* et al., 2015; Kinoshita and Honjo, 2001). During this process, point mutations will accumulate in V-regions of the HC and LC during B cell differentiation in germinal centers of secondary lymphoid organs. These mutations are induced by the enzyme Activation-Induced Cytidine Deaminase

(AID) whose expression is restricted to germinal center B cells and results in replacement mutations of cytosine → uracil, a process known as deamination. SHM mutations are mainly concentrated in the complementarity determining regions (CDRs), consisting of the parts of the V domains directly in contact with the antigen (**Figure 4**). This is both due to the selection process for the Ag and the enrichment in AID hotspots in this region (Bak et al., 2014).

Then the damaged DNA will be repaired by Base Excision Repair (BER) or Mismatch Repair (MMR) leading to random mutation rates reaching up to 30 mutations per 1000 base pairs (Bak et al., 2014). SHM can lead to nonfunctional antibodies (misfolded or with premature stop codons due to unfavorable mutations) (Lambert et al., 2019; Stewart et al., 2018) therefore a highly controlled selection process is needed to produce high-affinity antibodies and will be described later on.

As mentioned before, the first Ig produced will be IgM but thanks to another mechanism, called Class Switch Recombination (CSR), the other Igs class can be produced. CSR occurs between switch regions upstream of each Ig CH, comprising tandem repeats of short G-rich sequences that are also mutated by AID but result in double-strand breaks repaired by NHEJ process. The repair of two simultaneous double-strand breaks in distant switch regions can lead to the removal of the intervening sequence and the production of a new HC isotype bearing the same Ag specificity as it carries the same V domain (Xu et al., 2012).

These two mechanisms, SHM and CSR, represented in **Figure 7,** and are tightly controlled by IgH super-enhancers (Eμ and 3'RR) that allow the transcription and accessibility to V domains and switch regions (Kinoshita and Honjo, 2001; Pinaud et al., 2011).

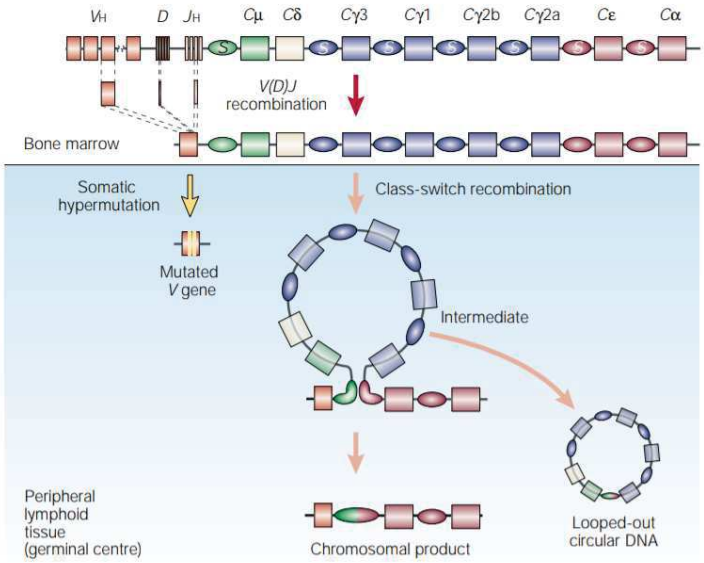

Figure 7- SHM and CSR for further Ig diversity. Schematic representation of mouse IgH locus. With rectangles and ovals representing exons and switch (S) regions, respectively. SHM introduces frequent mutations in the rearranged V exon and CSR brings the downstream constant (C) region exon close to the V exon by deleting between Sμ and another S region upstream of the target C region. Both SHM and CSR occur in the peripheral lymphoid tissues. (Kinoshita and Honjo, 2001)

I.1.4. Immunoglobulin assembly and further modification

While V(D)J recombination, SHM, and CSR play key roles in generating Igs diversity and allow the affinity maturation, they also increase the likelihood of generating a protein incapable of proper folding and assembly. Therefore, B cells rely on the Endoplasmic Reticulum (ER) quality control to eliminate those Igs that cannot be well assembled.

As indicated before, an Ig is a heterodimer of two HCs and two LCs linked by disulfide bonds. Two aminoacids are essential for this: the proline, that will stabilize the domains between them (Steward et al., 2002) and the cysteine, where the bonds inside and between the different domains will occur (Bergman and Kuehl, 1979). Different disulfide bond patterns are present in the Ig subclasses. For example, in the case of the IgG subclasses (IgG1, IgG2, IgG3 and IgG4) we distinguish a total of 12 intra-chain disulfide bonds that follow different patterns, each one associated with an IgG domain (Liu and May, 2012). For instance, the connection in the hinge region of the two HC is achieved by two disulfide bonds for IgG1, while for IgG3 11 bonds are needed. The HC of the IgG1 is linked to the LC by a disulfide bond between its fifth cysteine and the last cysteine of the LC but for IgG3 the third cysteine of the HC and the last cysteine of the LC are involved.

The HC and LC are co-translationally translocated into the ER and the chaperone Immunoglobulin Binding Protein (BiP) will associate with nascent HCs (**Figure 8**) while other proteins, such as ERdj3 and ERdj4, help regulate the process. The interaction between the different Ig domains and BiP is transient for most of them. The exception is the CH1 domain, which will remain associated with BiP until a LC will take over. Therefore, a complete HC without a LC cannot be secreted as it is retained in the ER by BiP. On the contrary, LCs can them be freely secreted (Feige et al., 2010).

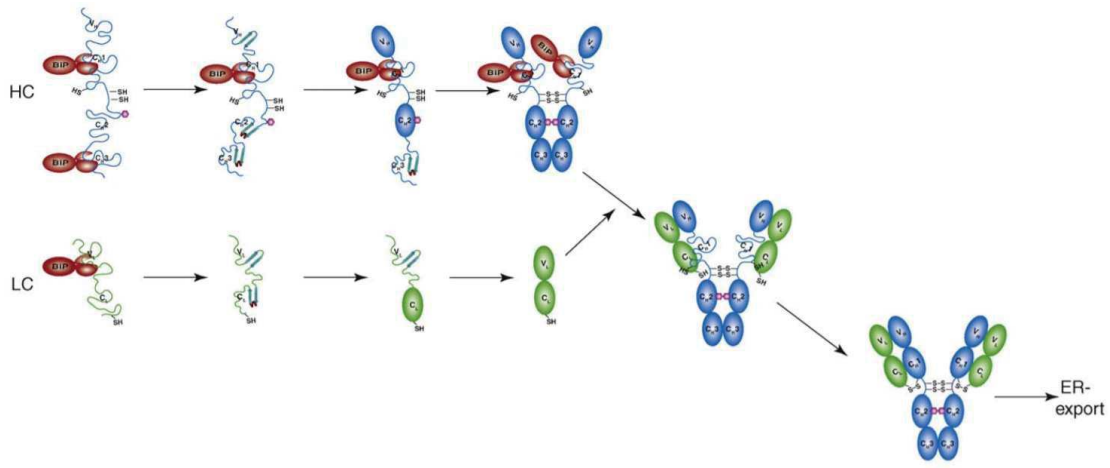

Figure 8- IgG assembly scheme. The folding, glyscosylation and disulfide bonds formation begins cotranslationally in the ER for both the HC (in blue) and the LC (in green). BiP chaperon (in red) interacts with almost every domain transiently before the comple folding of the chain. Once the CH3 domain is folded, HC dimerization is induced and its union stabilized by disulfide bridges in the hinge region. On the contrary, the CH1 domain remains unfolded and stably bound to Bip until it is displaced by a LC. Later the disulfide bridge between the LC and the HC is formed thus generating an IgG that is ready for secretion.(Feige et al., 2010)

The Igs that fail to mature correctly are retrotranslocated to the cytosol where they are degraded by the 26S proteasome in a process known as ER-Associated Degradation (ERAD) (Vembar and Brodsky, 2008). This ER quality control is particularly on high demand in plasma cells (PC), the final differentiation step of B cells, that can produce up to 10000 Igs/sec (Eyer et al., 2017a). The specific mechanisms held by these cells to support such Ig production shall be described in more detail in the following pages.

Finally, immunoglobulin glycosylation affects the assembly, the stability in sera and plays a role in the effector properties of the antibody (**Figure 9**). There are two types of them present in the Igs: the N-glycosylations and the O-glycosylations. The first one appears on asparagine residues within the motif Asn-X-Ser or Thr (Asn: asparagine, Ser: serine and Thr: threonine). Only one N-glycosylation site can be found in the CH2 domain of IgGs but other isotypes can bear up to five N-glycosylations in their CH domains. The presence and the composition of these glycosylations affect the interaction with Fc receptors with consequences on function and stability (Kiyoshi et al., 2017). If germline sequences of V domains are naturally devoid N-glycosylation sites, SHM can randomly create such consensus motifs with potential roles in several diseases including follicular lymphomas (Amin et al., 2015) and AL amyloidosis (Kumar et al., 2019). The latter disease will be one of the focus of study of the present manuscript.

The O-glycosylations are more random and they can occur on Ser or Thr residues (Hayes et al., 2014; Kiyoshi et al., 2017). They are particularly frequent in the hinge regions of IgA and IgG3.

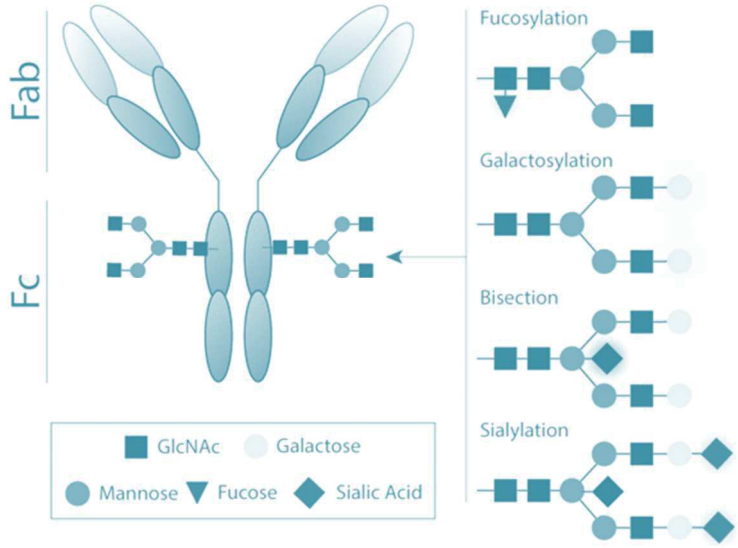

Figure 9- IgG glycosylation. The IgG immunoglobulin has a glycosylation site for a variety of glycans. They result of the combination of mannose, fucose, galactose, sialic acid, etc.(van Erp et al., 2019)

I.2. **B cell development**

To be efficient and capable of recognizing millions of different pathogens while devoid of self-reactivity, the adaptive humoral response requires the production of highly specific antibodies against foreign Ag. To do so, B cells must first produce clonally diverse receptors recognizing all existing Ag and then be activated by their cognate Ag to differentiate into antibody-secreting cells (ASC) or plasma cells. This paradigm of adaptive immunity has been modeled by Sir Macfarlane Burnet as the clonal selection theory (Burnet, 1957) and is possible thanks to the expression of a membrane form of the immunoglobulin, called B cell receptor (BCR) (Cambier et al., 2007; LeBien and Tedder, 2008).

The first phase in B cell development occurs in the BM, where B cells will go through different stages to acquire functional non-autoreactive BCRs (antigen-independent phase). Then, the B cell can exit the BM to reach secondary lymphoid organs where the encounter with their cognate Ag will complete its differentiation in memory B cells and plasma cells (antigen-dependent phase) (**Figure 10**).

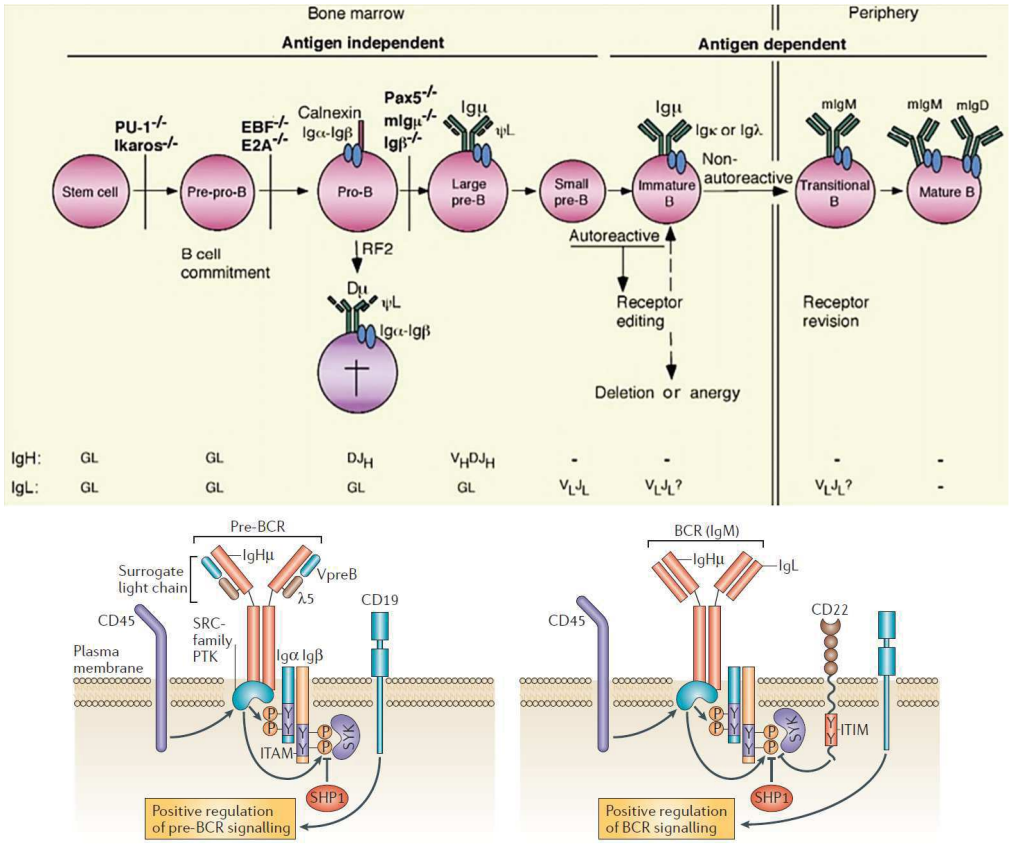

Figure 10- B cell development. Representation of the different phases of B cell development. In the bone marrow we find the antigen-independent phase and in the periphery the phase antigen-dependent. During the different stages of differentiation, the Ig locus is rearranged to express at the surface a pre-B-cell receptor (pre-BCR, represented at the bottom left) comprised of a mu HC and surrogate LC before expressing a mature BCR (represented at the bottom right), formed of rearranged H and L chains. This BCR is capable of binding antigen. Then, B cells undergo a selection process to eliminate self-reactive cells. Cells successfully completing this checkpoint leave the bone marrow to further mature in the periphery. (Meffre et al., 2000; Monroe, 2006)

I.2.1. B cell commitment

B cell lineage commitment depends on a network of transcription factors expressed by hematopoietic progenitors (such as E2A proteins, early-B-cell factor (EBF), Paired Box 5 (PAX-5)) together with external signals brought by BM stromal cells (including IL-7, FMS-like tyrosine kinase 3 ligand (FTL-3L) and stem cell factor (SCF)). They all work together to regulate B cell engagement, allow BCR rearrangements and survival/proliferation of early precursor B cells (pro-B cells) (LeBien and Tedder, 2008; Nutt et al., 2015). Nevertheless, PAX5 appears as the critical transcription factor that irreversibly engages lymphoid progenitors into the B cell fate by repressing linage-inappropriate genes and simultaneously activating B lineage-specific genes, including, *mb-1* and *B29* (coding for Igα and Igβ signaling proteins) and other co-receptors of the BCR (such as CD19) (Cobaleda et al., 2007a).

I.2.2. Antigen-independent phase

Once the cell is engaged into the B cell lineage, it will start by producing its BCR. During the pro-B stage, the rearrangement of the HC genes will begin thanks to the expression of RAG1/2 enzymes and the accessibility of the HC locus. First, the D-J_H rearrangement will take place simultaneously on both alleles. The V-DJ_H rearrangement, on the other hand, is carried out in a sequential way, in a process called allelic exclusion where only one allele is modified, and solely if it is non-productive the second one will be rearranged at its turn (Jung et al., 2006) (**Figure 11**). This sequential rearrangement allows the cell to express a unique HC thus ensuring the mono-specificity of one B cell clone.

The expression of the HC mu leads to the next step in the development as pre-B cells. Without a LC, the surface expression of the HC is possible thanks to a surrogate LC. This chain is formed of two non-covalently associated polypeptides known as VpreB and Lambda 5. In association with the signaling proteins Igα and Igβ, conforms the pre-B cell receptor (Pre-BCR) (Burrows et al., 2002). The signal induced by this pre-BCR allows the survival and the clonal expansion of these cells (large pre-B cells), the arrest of RAG endonucleases expression (thus stopping rearrangements at the HC locus), as well as the generation of a negative retro-control of its own expression by inhibiting the transcription of the genes coding for the surrogate chain. Consequently, following a rapid clonal proliferation, the pre-BCR is no longer expressed in small pre-B cells and the expression of RAG1/2 endonucleases can start again to rearrange LC genes. This begins on one kappa locus first with the goal of generating a functional VJ rearrangement. At the end of this stage, the B cell expresses a complete and functional BCR thus becoming an immature B cell.

The last checkpoint of this phase in B cell development consists in verifying the signal induced by this BCR. Those cells that provoke an intense activation will not leave the BM, as

it is an indication of auto-reactivity, as well as those who induce no signal at all. These cells will go under a re-editing of their BCR by secondary rearrangements of the same kappa allele to produce a new functional BCR. If this is not achieved, the second kappa allele will be rearranged followed by the lambda loci, always assuring the allelic exclusion (Mostoslavsky et al., 2004; Vettermann and Schlissel, 2010). In the end, B cells that succeed at this checkpoint can egress from the BM, enter the blood stream and move to secondary lymphoid organs where the antigen-dependent phase takes place.

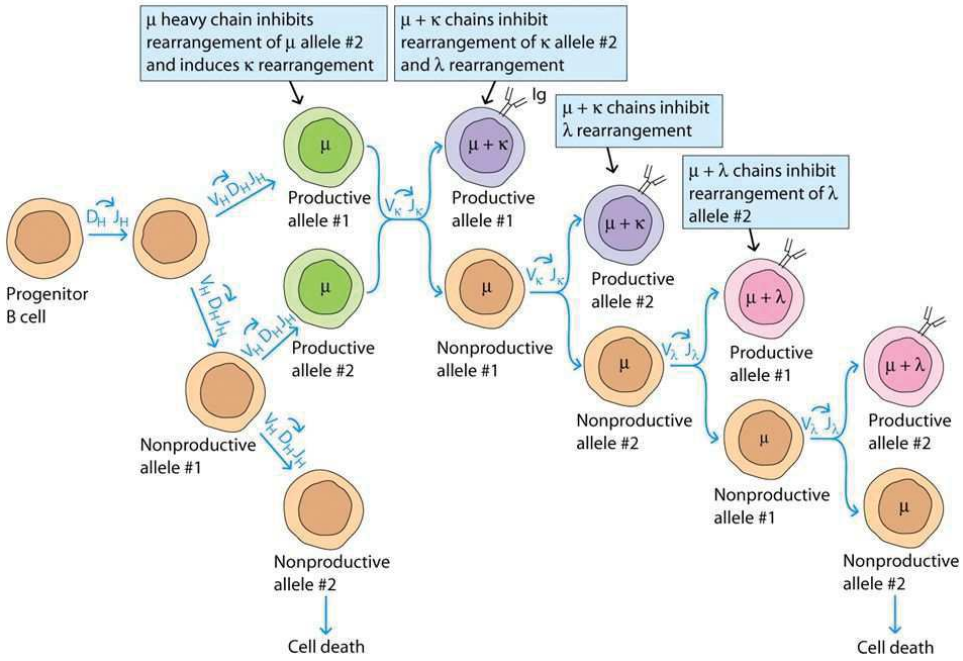

Figure 11- Allelic exclusion. Representation of productive and non-productive V(D)J rearrangements during B cell development. First, after the rearrangement of D_H-J_H, the VH-DJ_H takes place in only one allele. If this rearrangement is non-productive, the second allele will be rearranged. In the case that both allele are non-productive, the apoptosis of this B cell will be induced. On the contrary, with a productive rearrangement of the HC, the V_L-J_L rearrangement takes place first on one kappa allele. Once again, if it is non-productive the other kappa allele will be rearranged before moving to the lambda allele, also in a sequential pattern. B cells that generate non-productive rearrangements will die as they do not express a surface Ig. Partially adapted from Yancopoulos and Alt, 1986 (Yancopoulos and Alt, 1986)

I.2.3. Antigen-dependent phase

The spleen, the tonsils, the lymph nodes and Mucosae-Associated Lymphoid tissue (MALT) are considered secondary lymphoid organs. In those organs, immature naïve B cells will go through transitional stages T1 and T2 before becoming mature B cells (**Figure 12**).

Similar to what happens to immature B cells in the BM, T1 B cells are sensitive to apoptosis or will enter into an anergic state in response to BCR engagement. This happens since some cells that are auto-reactive are able to escape previous controls. T2 B cells, in response to an antigen, can survive, proliferate and become marginal zone (MZ) or follicular (FO) B cells, the latter being involved in the germinal center reaction that will be described later on.

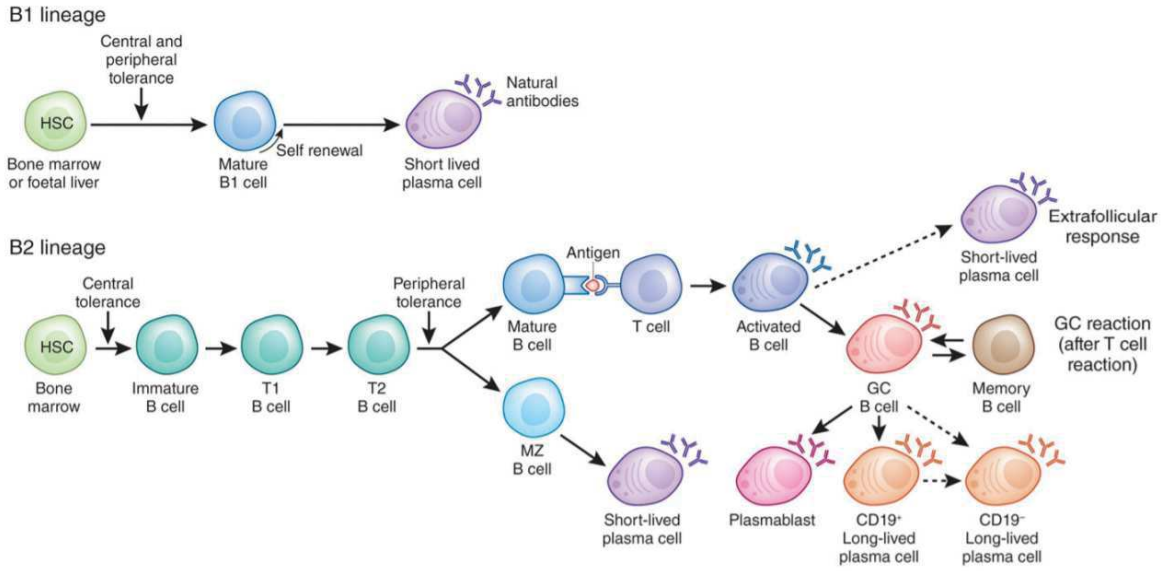

Figure 12 –Peripheral B subsets. The first group of B cells, B1 cells, develop from hematopoietic stem cells (HSC) in the bone marrow or foetal liver. They are self-renewing and are capable of producing natural antibodies implied in self-defence. B2 cells develop in the bone marrow from HSC. After elimination of autoreactive cells, transitional T1 and T2 cells relocate in the spleen. Those immature B2 cells that escape the peripheral tolerance process become Marginal Zone (MZ) B cells or mature follicular (FO) B2 cells. Upon T cell-dependent activation, they will become long-lived plasma cells or memory B cells. MZ cells and B1 cells generate short-live plasma cells. (Schrezenmeier et al., 2018)

I.2.4. B cells sub-populations

I.2.4.1. B1 cells

B1 cells are a small subset of B cells with distinct origins, phenotypes and functions (Shapiro-Shelef and Calame, 2005). Their peculiarity is the production of “natural IgM” antibodies, which are protective against microbial pathogens. Additionally, they are both able of presenting antigen and stimulating T cells while being capable of immunosuppression, due to the production of IL-10 (Petro et al., 2002).

Natural IgM fulfills different distinct functions in host defense and tissue homeostasis but they are multi-specific with low affinity for shared epitopes of different microorganisms. This allows a first line of defense before the development of specific antibodies.

I.2.4.2. B2 cells

I.2.4.2.1. Marginal Zone B cells

A minor population of B2 cells are those from the marginal zone of the spleen (Cerutti et al., 2013; Martin and Kearney, 2002). This organ plays a central role in host defense against blood-borne pathogens thanks to an elevated blood perfusion (**Figure 13**).

Several MZ B cells express poly-reactive BCRs that recognize similar patterns as Toll-like Receptors (TLRs) present in dendritic cells (DCs), macrophages and granulocytes. Therefore,

MZ B cells start a low-affinity antibody response before the production of high-affinity antibodies by Follicular B cells. Additionally, they present a lower threshold for activation, proliferation and differentiation into antibody-secreting cells, known as short-lived plasma cells.

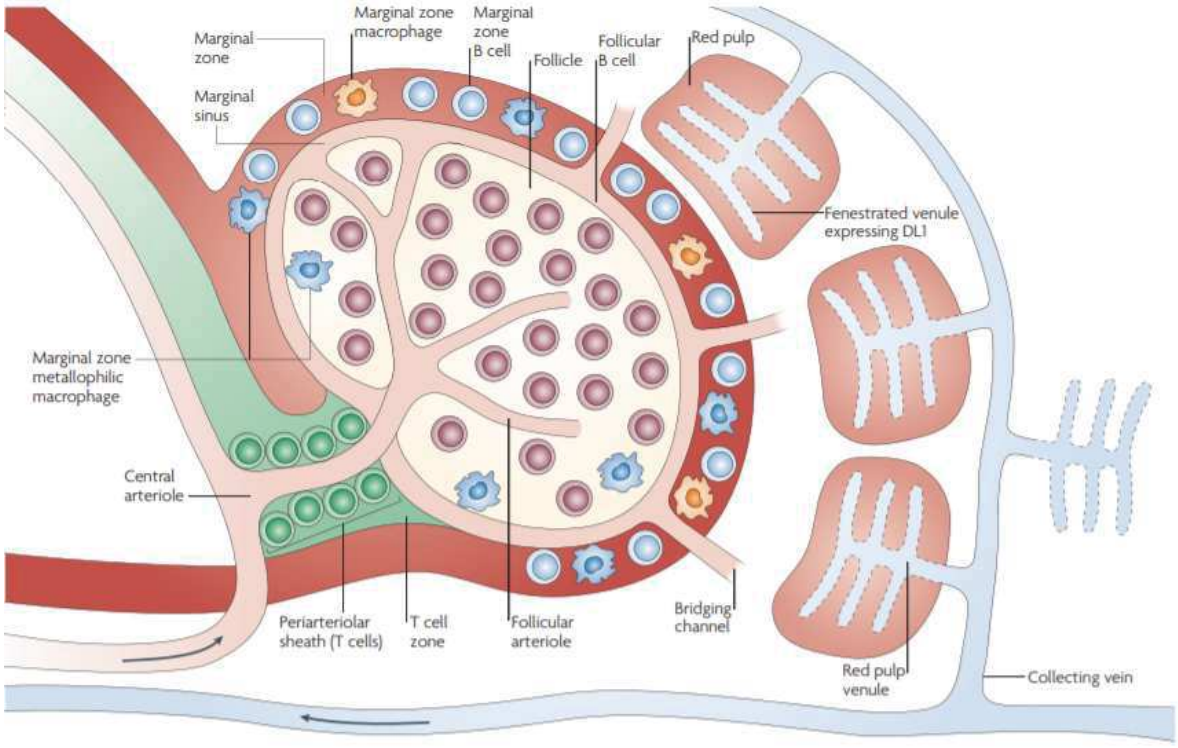

Figure 13 – Schema of spleen anatomy. The spleen is organized into several white pulp areas and a red pulp region. In the white pulp region, we can find specific zones: the marginal zone (with different cell types such as MZ B cells and MZ macrophages), the B cell zone and finally the T cell zone. (Pillai and Cariappa, 2009)

I.2.4.2.2. Follicular Zone B cells

Naïve FO B cells, the major B cell population, can encounter the antigen in secondary lymphoid organs (Pillai and Cariappa, 2009). If they simultaneously receive help from Ag-specific T cells, they can form germinal centers to improve the affinity of their BCR for the Ag, proliferate and differentiate into plasmablasts, plasma cells, or memory B cells.

I.2.5. Germinal Centers

To increase the efficiency and specificity of the antibody against a given Ag, the B cell will go through SHM and CSR as described above. These two events take place in the Germinal Center (GC) of secondary lymphoid organs.

The GC has a structure that can be divided into two zones (**Figure 14**). The first one is the Dark Zone (DZ) characterized by the intense proliferation of B cells that undergo SHM, and the other zone is the Light Zone (LZ) where the selection by the antigen takes place. In the LZ, B cells are found together with Follicular Dendritic Cells (FDC) and follicular helper T cells (Tfh)

(Basso and Dalla-Favera, 2015). This organization is possible thanks to the expression of different receptors on B cells, the Chemokine C-X-C motif receptor 4 (CXCR4) particularly in the DZ and Chemokine C-X-C motif receptor 5 (CXCR5) in the LZ. The FDC plays a central role in the formation of GC as it secretes the ligand for CXCR5. The transit from one zone to the other and the post-GC differentiation of B cells are controlled not only by a cellular network but also of soluble signals (De Silva and Klein, 2015). These signals affect the GC B cells responses through the activation/repression of specific transcriptional programs (**Figure 15**).

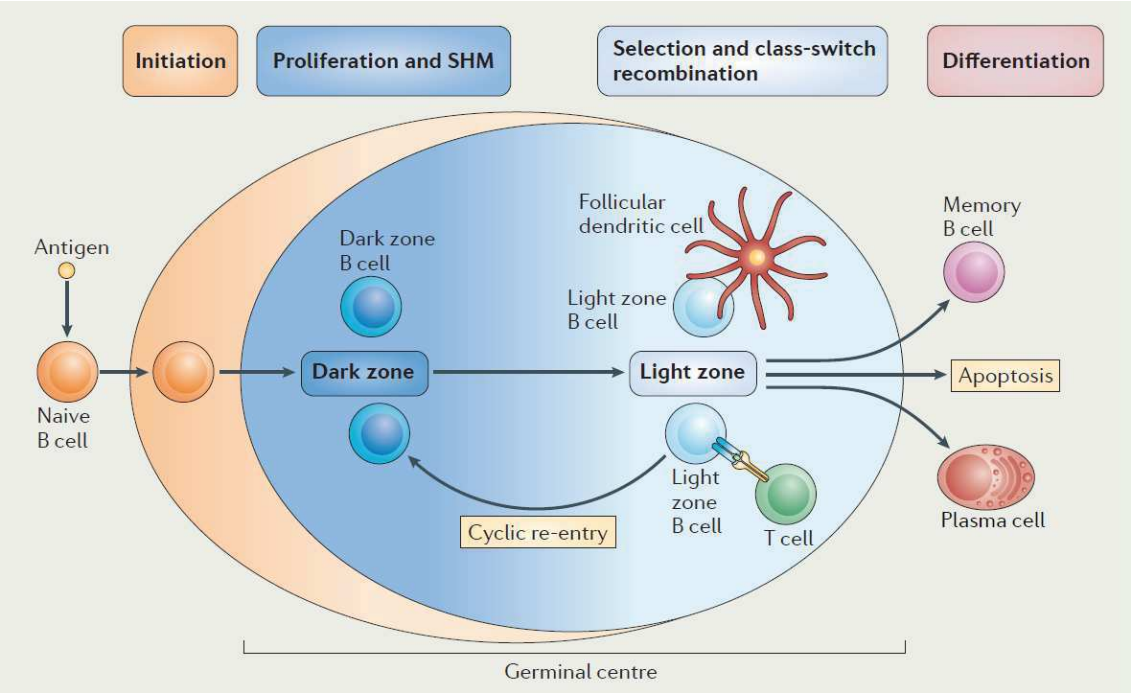

Figure 14 – Germinal Centers. Those B cells with successful V(D)J recombination and functional BCR migrate as naive B cells from the BM to the secondary lymphoid organs. When they encounter the antigen they will be activated by interacting with CD4+ T cells and will get organized into primary follicles to form germinal centres. Here, B cells will go through SHM and CSR in order to generate high-affinity antibodies. The GC structure is comprised of a dark zone, containing highly proliferating B cells, and a light zone containing B cells mixed with follicular dendritic cells, T cells and macrophages. The maturation of B cells involves cyclic re-entries into the different zones of the GC: B cells selected in the LZ return to the DK for further SHM and cell division. At the end, memory B cells and plasma cells will be generated.(Basso and Dalla-Favera, 2015)

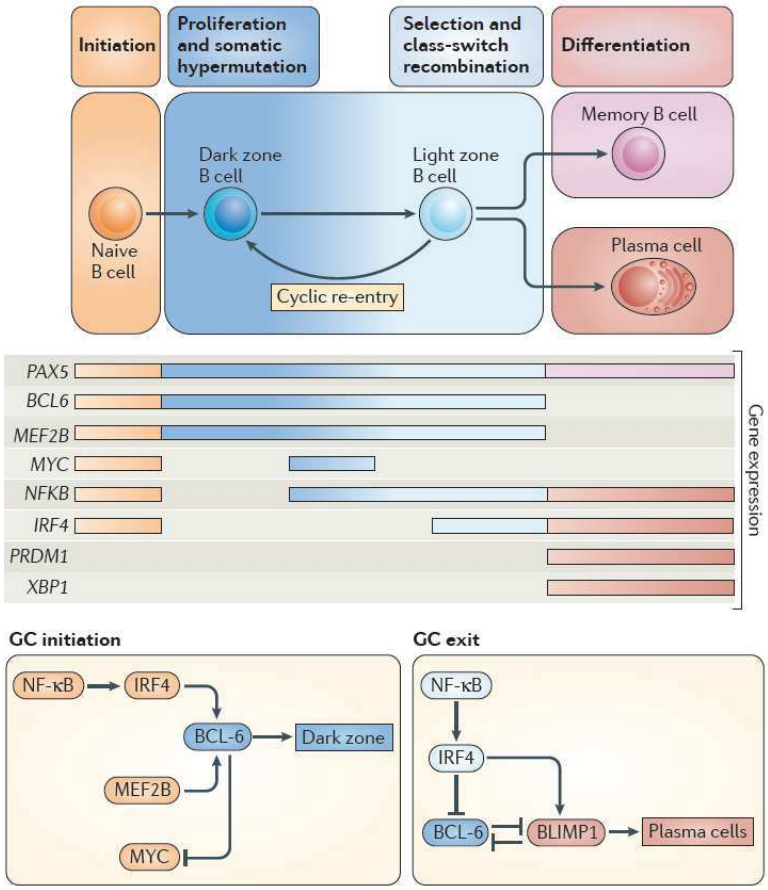

Figure 15 –Transcriptional factors driving the GC reaction. Several transcription factors and modulators are involved in GC regulation. Paired box 5 (PAX5) is expressed throughout the life of mature B cells, except for those are committed to plasma cell differentiation, whereas the expression of B cell lymphoma 6 (BCL-6) and myocyte-specific enhancer factor 2B (MEF2B) is only restricted to the GC stage. For the initiation of the CG, MYC is required as well as for re-entry into the DZ from the LZ. Nuclear factor-κB (NF-κB) and interferon-regulatory factor 4 (IRF4) are expressed during GC initiation, are absent in DZ B cells and then reappear in LZ B cells. PRDM1 (encoding for B lymphocyte-induced maturation protein 1 (BLIMP1)) and XBP1 (which encodes X-box-binding protein 1) is induced in cells that are committed to plasma cell differentiation. All these transcription factors modulate the transcription of each other.(Basso and Dalla-Favera, 2015)

Within the GC, B cells undergo a positive selection based on the capacity of their BCR to interact effectively with the FDCs that present the Ag on their surface as immune complexes (Ac-Ag) fixed on the Complement Receptor 1 (CR1). They will then receive B-cell activating factor (BAFF)-mediated survival signals. The internalization of the Ag allows the B cells to behave as antigen-presenting cells (APCs) and interact with CD4+ follicular helper-like T cells expressing a T cell Receptor (TCR) specific to the Ag-peptide / major histocompatibility complex (MHC) II complex. In turn, they provide B cells survival, proliferation and differentiation signals (Fazilleau et al., 2009b; Ma et al., 2012) (**Figure 16**).

In contrast, those B cells that express a BCR with low affinity will not receive enough survival signals and will undergo apoptosis (Victora and Nussenzweig, 2012). Indeed, the B cells of the GC express the pro-apoptotic receptor Fas (CD95), and the transcription factor B cell Lymphoma-6 (Bcl-6) capable of inhibiting the expression of the anti-apoptotic factor Bcl-2

(Klein et al., 2006; Klein and Dalla-Favera, 2008). Consequently, GC B cells are rapidly engaged in apoptosis in the absence of survival signals (Krammer, 2000; Naito et al., 2007; Wajant, 2002).

Finally, several studies have revealed the dynamic structure of GC with inter-zone migrations allowing several cycles of SHM in order to select B clones expressing very high-affinity BCRs (De Silva and Klein, 2015; Ise and Kurosaki, 2019). In the end, two lines of B cells will emerge from it: the memory B cells and the plasma cells.

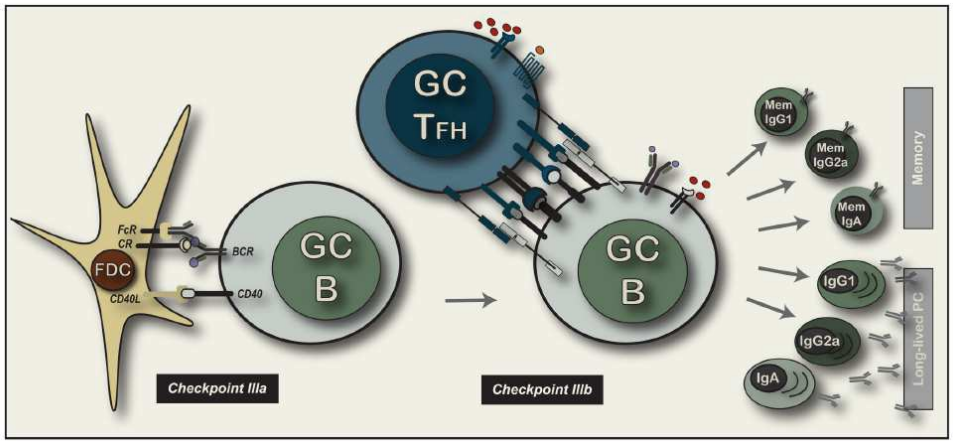

Figure 16 – Schematic representation of the interaction of GC B cells with FDC and Tfh cells. In addition to the signal received through the BCR, FDC provide B cells with cofactors. B cells will process and present the antigen through the MHC-II to T cells that will recognize it through the TCR, completed with CD4. Other interactions, such as CD40 and CD40L, will induce multiple secondary signals (Fazilleau et al., 2009a).

I.2.6. Terminal B cell differentiation: Memory B cells and Plasma cells

Memory B cells arise from the GC by yet incompletely understood mechanisms (Laidlaw et al., 2020; Shinnakasu et al., 2016) and participate in the memory of the immune response. They present their BCR on surface with mostly switched isotypes and high affinity for a given antigen, remaining in the body for several years. In case of reinfection by the same antigen, they can be rapidly activated to induce a quick immune response (Schrezenmeier et al., 2018) (**Figure 17**).

Plasma Cells are the last stage of B cell development and are the actors of humoral immunity as they secrete large quantities of antibodies. They also arise mainly from the GCs even if some short-lived PC can be generated directly from MZ and B-1 B cells (T-independent response). Even though they derived from B cells, PCs are characterized by a complete transcriptional and cellular reprogramming leading to the loss of all B-cell specific markers, such as B220, CD19 and Igα/β, and the gain of others like CD138 in mice and CD38 as well in humans.

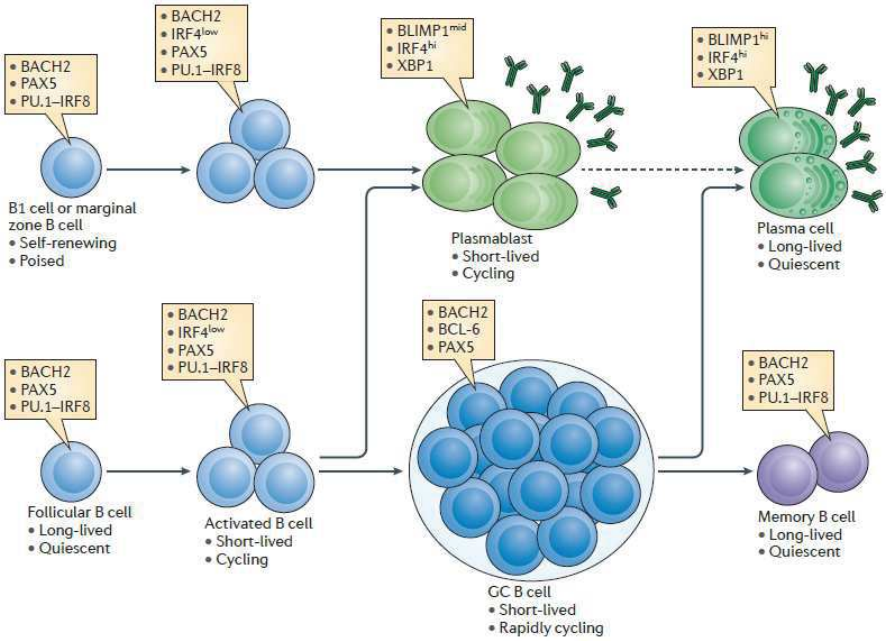

Figure 17 –Summary of the different stages in B cell differentiation. B cells subpopulations found during their development ending into plasma cell differentiation or memory B cells. (Nutt et al., 2015)

I.3. **Plasma cell differentiation**

A small group of B cells will differentiate into PC, going through an intermediate state known as plasmablasts (**Figure 18**). The differentiation is modulated by several cytokines, such as IL-10 and IL-2, and the BCR signal, regarding its intensity and duration (Lechouane et al., 2013; Shapiro-Shelef and Calame, 2005).

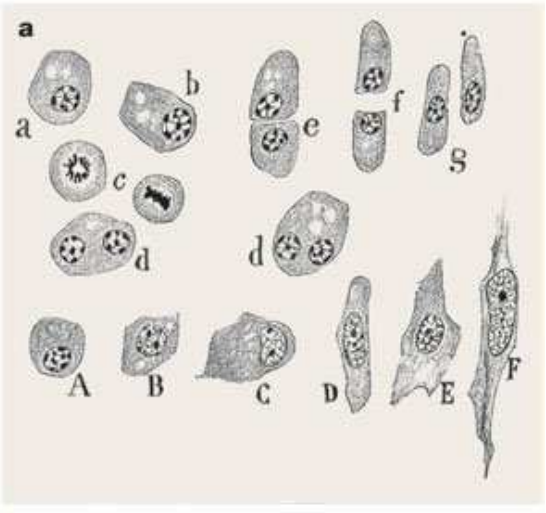

Figure 18 – Plasma cells. Original drawing by Ramón y Cajal describing for the first time, the morphology and development of PCs. (Martínez et al., 2005)

Several other modifications appear at the molecular level: the main B cell factor, Pax5, will be decreased to allow the expression of the transcription and differentiation factor X-Box Binding Protein 1 (Xbp1), the J chain and Lymphocyte-induce Maturation Protein-1 (Blimp1) (**Figure 19)** (Cobaleda et al., 2007b; Roth et al., 2014)**.** The loss of Pax5 is also accompanied

by a decrease in Bcl-6 (Crotty et al., 2010; De Silva and Klein, 2015), BTB Domain and CNC homolog 2 (Bach2) and Interferon Regulatory Factor 8 (IRF8) (Nutt et al., 2015).

PC differentiation is inhibited in GC by Bcl-6 and Bach-2 since they suppress the expression of Blimp1 (Shaffer et al., 2002). The expression of Blimp1, the main transcription factor of PC, is facilitated by several cytokines (such as IL-2, IL-6 and IL-21) and the transcription factor IRF4. This last transcription factor acts in a dose-dependent manner: at low concentrations it promotes GC formation and functions while at higher ones it triggers PC differenciation (Klein et al., 2006; Sciammas et al., 2006).

Thanks to the rise in Blimp1, the expression of the loci IgH and IgL will be increased, and the transcription of Xbp-1 will be stimulated to enable the activation of the PC differentiation program (Reimold et al., 2001). PCs are capable of secreting large quantities of Igs via the Unfolded Protein Response, which will be detailed later on, and it is possible thanks to Xbp-1 expression that induces changes in the ER.

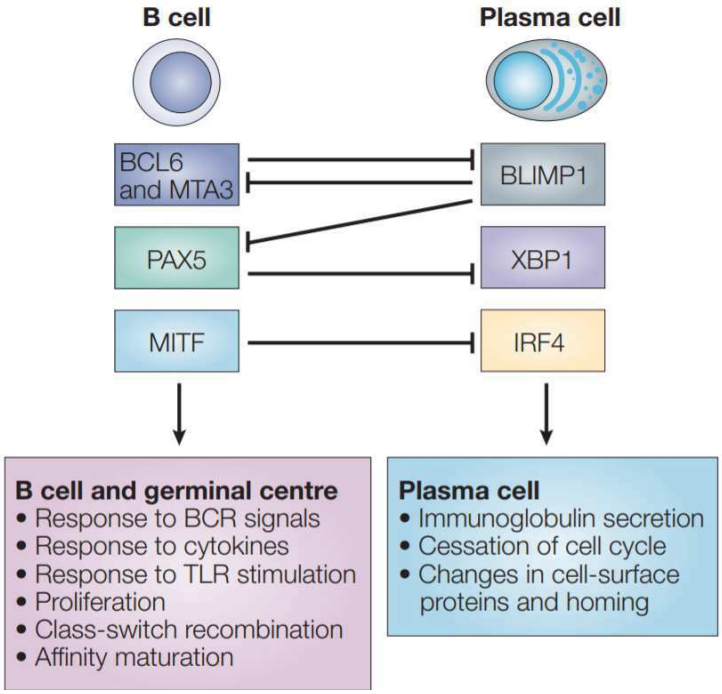

Figure 19- B cells vs. Plasma cells. Different transcription factors will inforce exclusive gene expression programmes in B cells and PC. B-cell lymphoma 6 (BCL6), metastasis-associated 1 family member 3 (MTA3), microphthalmia-associated transcription factor (MITF) and PAX will repress PC development by repressing BLIMP1, XBP1 and interferon-regulatory factor 4 (IRF4). In PCs, BLIMP1 represses B cell gene-expression programmes. This mutual repression prevents PC from appearing unelicited in the GC and the reversion of PCs to B cell stages.(Shapiro-Shelef and Calame, 2005)

I.3.1. Plasma cells subpopulations, survival and localization

Among the different kinds of PC, we can distinguish those with a short life, called short-lived PCs, that arise from a T-independent response and that will produce low affinity antibodies. B cells that are activated by an innate Pattern Recognition Receptor (PRR) (Suresh and Mosser,

2013) recognizing conserved motifs of different pathogens can trigger a rapid response, proliferation and differentiation into these kind of PCs. In the first days of an immune response, short-lived PCs can also be generated from a T-dependent response to fill in the gap before the establishment of PCs secreting high-affinity antibodies.

Another population of PCs are those called long-lived PCs (Lightman et al., 2019) that arise mainly from GC-B cells with a high-affinity Ig and can survive several years in the BM. These PCs can be implied in the production of pathogenic Igs, inducing different diseases that are discussed in the following chapter.

Most ASCs in the secondary lymphoid organs are found in the lymph node medullary cords and in extrafollicular loci of the red pulp of the spleen. Before the PC stage, we can distinguish the plasmablasts, which are migratory ASC that are still dividing. A fraction of the generated plasmablasts will migrate to the BM presumably entering via sinusoidal veins, and the efficient homing depends on CXCR4, receptor for a chemokine (CXCL12) produced in high quantities by stromal cells present in the BM (Roth et al., 2014).

The BM is believed to sustain PC survival by microanatomical niches and it has been shown that their survival depends of different extrinsic factors and the proximity to other cells that secrete them, such as stromal cells. Only those maintained thanks to the microenvironment producing IL-6 or A Proliferating-Inducing Ligand (APRIL), key factor for PC survival (Belnoue et al., 2008), will become Long-lived PCs. PCs adhere to the niche by Very Late antigen-4 (VLA-4) and Lymphocyte function-associated antigen 1 (LFA-1) which have the capacity to interact with other components of the BM such as Vascular cell adhesion protein 1 (V-CAM1), Fibronectin, etc. These long-lived PC cells will be at the origin of most of the PC neoplasms, described in the following Chapter II, explaining their localization and their dependence to the BM microenvironment.

I.3.2. The Unfolded Protein Response

To achieve the massive production of Igs (Corti and Lanzavecchia, 2014; Eyer et al., 2017b; Helmreich et al., 1961; Lanzavecchia, 2018), PCs need to expand their ER to increase the folding and secretory capacity to keep cell protein homeostasis. This increment in activity will induce the stress of the ER, mainly due to the accumulation of misfolded proteins, thus inducing the Unfolded Protein Response (UPR) (Zhang and Kaufman, 2008).

As a consequence of its activation, the capacity to fold proteins and degrade those that are misfolded will be further increased accompanied by the expression of chaperon proteins and stimulation of the degradation of aberrant ones by the ERAD pathway. However, UPR can also act to decrease protein synthesis and if the ER stress remains too high, can end in the apoptosis of the cell (Gass et al., 2004; Janssens et al., 2014). Consequently, PCs require a

specific UPR response to favour protein production at the expense of protein synthesis inhibition and apoptosis.

I.3.2.1. The different UPR pathways

Three different pathways can be described in the UPR (**Figure 20**) (Shapiro-Shelef and Calame, 2005; Zhang and Kaufman, 2008). The first one, called the Inositol-Requiring Enzyme 1α (Ire1α) pathway, is activated by the increment in misfolded proteins in the ER. Due to this accumulation, the chaperone protein BiP that blocked the activity of Ire1α, will be dissociated as it is requested to help fold those proteins. Ire1α will then induce the excision of 26 nucleotides from the RNA coding for Xbp1, generating a change in the reading frame. Thanks to this, a more active form of Xbp1, called Xbp1-s, will be synthesized to induce the overexpression of genes implied in the expansion of ER, the production of chaperone proteins and the increase of glycosylation and secretion capacity.

The second pathway, known as PERK for RNA-Dependant Protein Kinase, is associated with a decrease in protein production to overcome the stress. It is usually suppressed in PCs since their role is to produce great quantities of Igs and also as it leads to the activation of the pro-apoptotic pathway C/EBP Homologous Protein (CHOP) (Ma et al., 2010). This pathway is activated in those cells that are unable to overcome protein misfolding.

Finally, yet importantly, the third pathway is associated to the Activating Transcription Factor 6 (ATF6), also implied in the response to the accumulation of misfolded proteins. If there is no stress, ATF6 should be associated with BiP in the ER. When it is dissociated, it will be transferred to the Golgi to be cleaved into two active forms ATF6 α and β. They will then go to the nucleus to active the genes BIP, CHOP and ER degradation Enhancing α Mannosidase-like protein 1 (Edem1).

The ERAD pathway, allows the exit from the ER to the cytoplasm of those proteins that are aggregated or misfolded for its degradation in the proteasome. Due to this, PCs show higher sensitivity to proteasome inhibitors (PI) as blocking it will rapidly induce the abnormal high accumulation of proteins in the ER thus inducing supplementary stress. The second UPR pathway, PERK, will be activated to induce apoptosis in this case (Meister et al., 2007; Zhou et al., 2014).

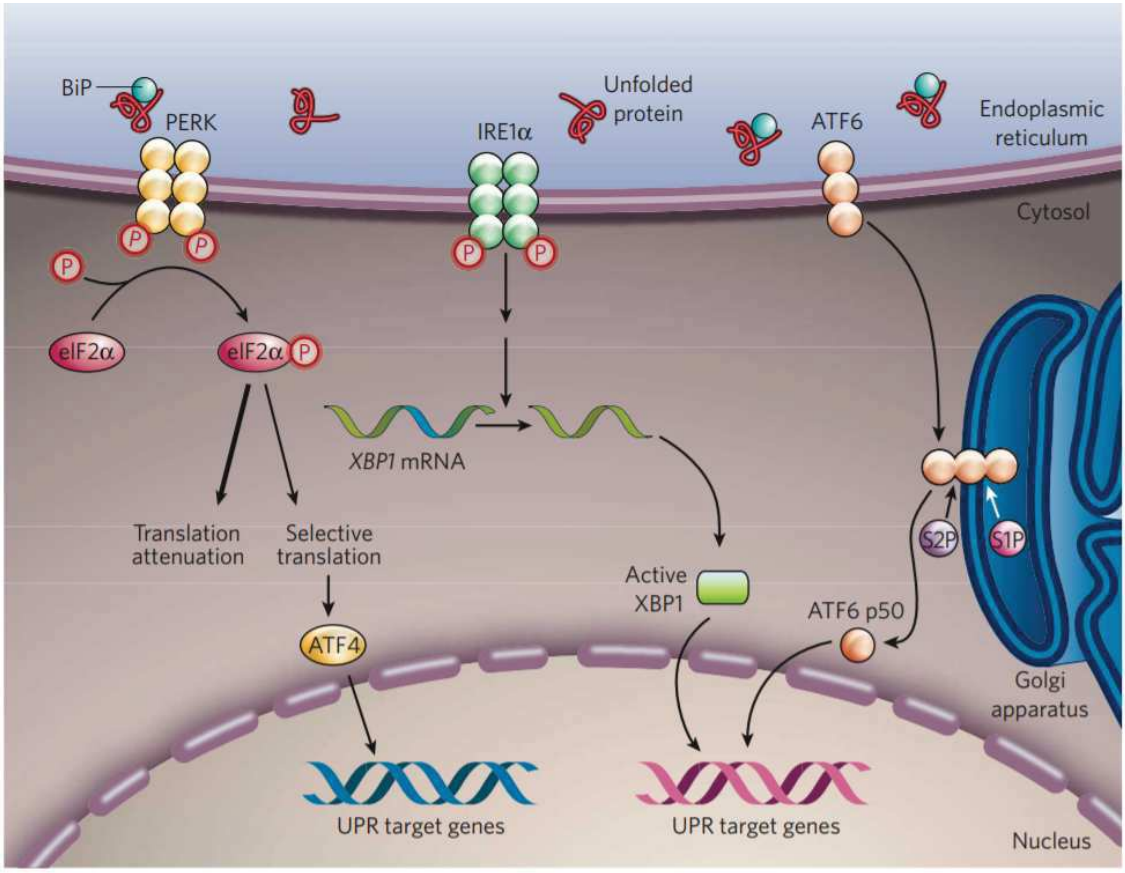

Figure 20- The Unfolded Protein Response. In the absence of stress, the ER chaperone BiP binds to IRE1α, PERK and ATF6, keeping them in an inactive state. During ER stress, BiP preferentially binds to unfolded or misfolded proteins. The release of BiP can result in the activation of one of the three UPR pathways: IRE1α, PERK and ATF6.(Zhang and Kaufman, 2008)

I.3.3. J Chain

The Joining chain or J Chain is a 15kDa protein that can be found covalently associated with dimeric secretory IgA and pentameric IgM. Its exact role in the polymerization of Igs has still not been fully clarified (Castro and Flajnik, 2014).

Although J chain is neither sufficient nor necessary for IgM secretion, it determines the type of IgM polymer produced. Without J chains, hexamers are the main form of IgM secreted and they can bind complement more efficiently than pentamers. Therefore, J chain might regulate the type of humoral response. In the case of IgA, the C-terminal domain of the J chain binds to the pIgR in the basolateral surface of mucosal epithelial cells. This leads to the endocytosis of the complex and its transport by transcytosis to the apical surface of IgA dimers after a proteolytic cleavage that will liberate them.

J chain has been sequenced for human, mouse, cow and rabbit, etc. and identified in several other mammals. The chromosomal location of the J chain gene in mouse is on chromosome 5 whereas in humans is localized on the long arm of chromosome 4 (Knight

and Rhee, 2005). The genomic murine J chain is organized in four exons distributed over 7.3 kb, but unlike Ig genes, they do not undergo rearrangement during B cell differentiation.

Compared with the other Igs, *J chain* gene expression and regulation has not been studied extensively as well as the protein due to its unique structure and biochemical behavior. *J chain* expression is activated by Myocyte Enhancer Factor 2 (B-MEF2) and repressed by Pax5. As seen before, Blimp1 downregulates Pax5, resulting in the expression of genes needed for Ig secretion and the PC phenotype, including J chain (**Figure 21**). Pax5 represses J chain by forming a steric barrier to prevent the binding of positive regulator B-MEF2. Thus, J chain transcript should be expressed when Pax5 is decreased in all PCs, regardless of the isotype expressed.

The exact transcriptional pattern of IgJ in B cell development or other hemapoietic cells is still controversial. Mice expressing a suicide gene (DT-A) under the IgJ promoter were shown to display almost normal humoral response and several studies have observed the expression of IgJ transcripts in pre-B or immature B cell lines. Additionally, its expression in non-IgM/IgA PCs is also controversial (Bjerke and Brandtzaeg, 1990) and it has been suggested that J chain is expressed but quickly degraded in PC with other secreting isotypes, such as IgG, since it will not be associated in multimerization (Mosmann et al., 1978).

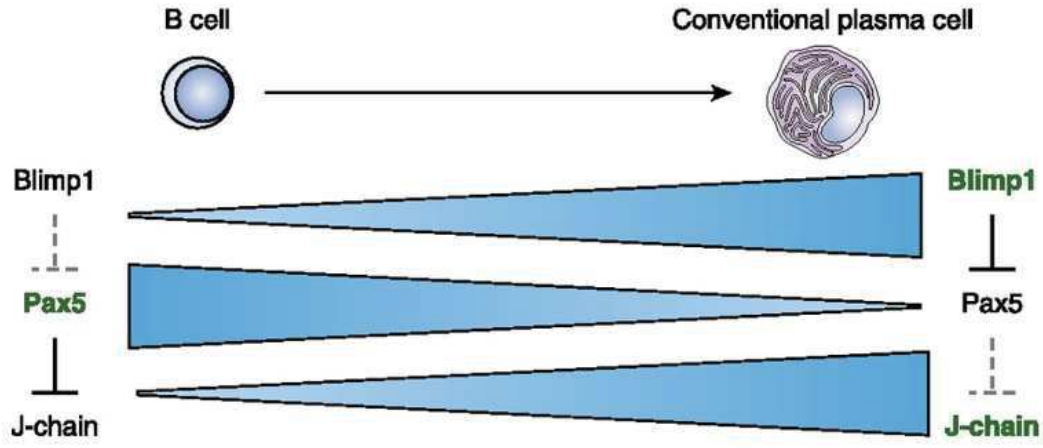

Figure 21- J chain expression. B cells have high levels of Pax5 and it binds to the J chain promoter to prevent expression of J chain. In contrast, Blimp1 is highly expressed in PCs where it represses Pax5 expression and, therefore, indirectly[15] allows for J chain expression.(Castro and Flajnik, 2014)

Chapter II. Plasma Cells Dyscrasias

While all the events leading to the PC differentiation are highly controlled and regulated, some oncogenic events may induce an abnormal proliferation. Plasma cell dyscrasias (PCD) or monoclonal gammopathies are a group of heterogeneous disorders caused by the monoclonal proliferation of these cells mainly in the bone marrow. Due to their function of antibody secretion, these proliferations often come along with the massive production of a monoclonal immunoglobulin. While it is a frequent situation, observed in 3.3% of the population over 50 years (Dispenzieri et al., 2010), in most cases it will remain asymptomatic and revealed only by the monoclonal immunoglobulin peak on a serum or urine electrophoresis. However, the progression of an asymptomatic plasma cell proliferation to an overt multiple myeloma (neoplasm) is about of 1% per year.

II.1. **Monoclonal Gammopathies and Genetic Alterations**

Thanks to the technological advances, such as gene expression profiling, proteomics and fluorescent in situ hybridization (FISH), the genetic characterization of these diseases has greatly improved.

Genetic alterations in monoclonal gammopathies involve, among others, chromosomal gains/deletions and translocations of the Ig loci (Kuehl and Bergsagel, 2012; Paiva et al., 2016). The primary oncogenic events are shared by the different forms of PCD and take place during the events of SHM or CSR in the GC (Bianchi and Munshi, 2015). However, secondary events (translocations, epigenetic modifications, etc.) and the modification of the BM microenvironment will finally lead to the different types of monoclonal gammopathies (van Nieuwenhuijzen et al., 2018).

Primary translocations involving the Ig HC gene 14q32, such as t(11:14) the most common cytogenetic abnormality in AL amyloidosis (Bryce et al., 2009), place the cyclin D1 gene under the control of the hyperactivated superenhancers of the IgH locus (Fiancette et al., 2010; Fonseca et al., 2003). Other translocations are frequent in PC proliferations including t(4:14) (*MMSET/FGFR3* genes translocated to the IgH locus), t(14:16) (*c-Maf*) and t(14:20) (*MAFB*). Most cases of hyperdiploid imply extra copies of the odd-numbered chromosomes such as 3, 5, 7, 9, 11, 15, 19, 21 (Smadja et al., 1998).

For a tumor to develop, multiple hits are usually required, so, for instance, the overexpression of cyclin D1 due to either hyperdiploidy or IgH translocations, is not enough for the disease to progress. Therefore, secondary translocations, oncogenic mutations of NRAS, KRAS, BRAF, copy-number variants, loss of 17p (*TP53*), dysregulation of other factors such as Myc or the NF-κB pathway and/or microenvironmental changes are needed to drive the

clonal evolution (van Nieuwenhuijzen et al., 2018). The most common cancer associated with PCs is multiple myeloma (MM) that evolves from a pre-malignant state, named Monoclonal Gammopathy of Undertermined Significance (MGUS), as it will be detailed next (**Figure 22**).

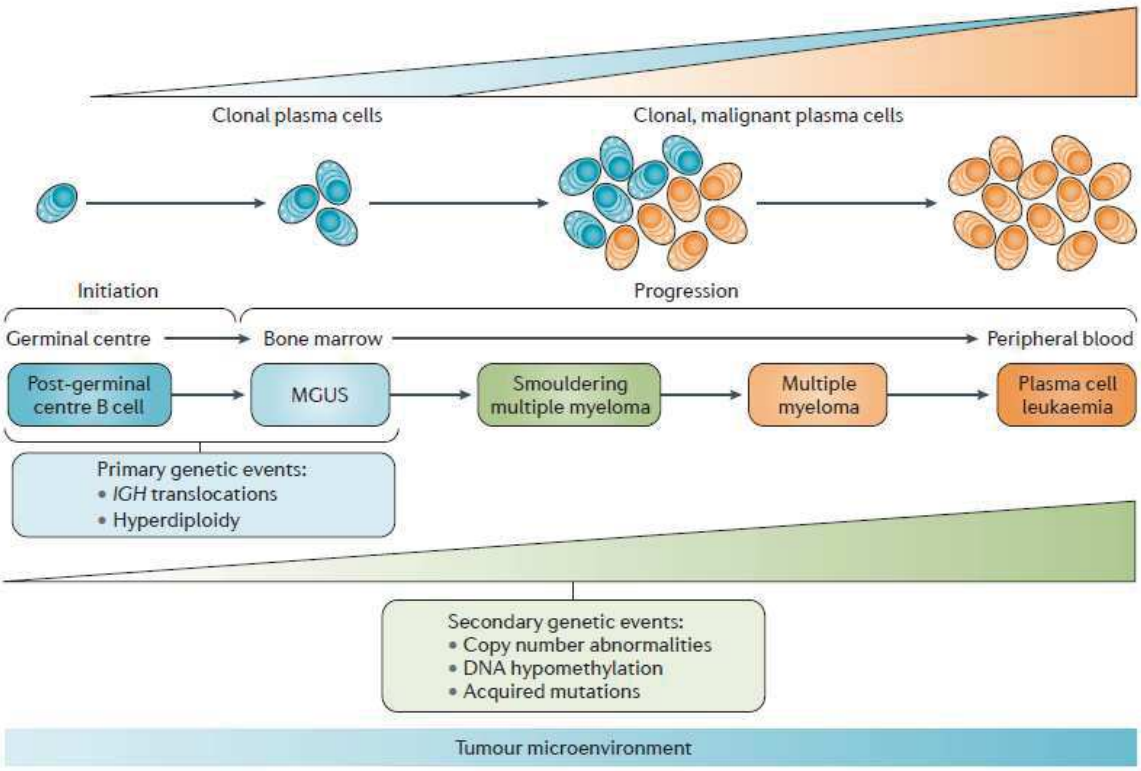

Figure 22- Plasma cell dyscrasias development. Before the appearance of MM, there are precursors disease states each one with different clinical indicators although there are several biological similarities. At first, primary genetic events will take place on the onset of MGUS and include chromosomal translocations or aneuploidy. As the disease evolves from MGUS to SMM, to MM and finally to PCL, the number secondary genetic alterations increases.(Kumar et al., 2017)

II.1.1. Monoclonal Gammopathy of Undertermined Significance

Monoclonal Gammopathy of Undertemined Significance (MGUS) is characterized by the presence of a monoclonal Ig at a concentration of less than 3 g/dL in serum and having less than 10% of monoclonal plasma cells in the BM (**Figure 23**) (International Myeloma Working Group et al., 2010). Despite this, MGUS is considered as a pre-malignant monoclonal proliferation where no damage to organs is observed. It is estimated that around 4% of 50-year old or 7% of people in their 70s have a MGUS (Kyle et al., 2018).

About 80% of MGUS presents with a full monoclonal immunoglobulin in serum mostly IgG (70%), followed by IgM or IgA (15% and 12% respectively) (Dispenzieri et al., 2010; Kyle et al., 2006). In some cases, there can be an imbalance in the stoichiometry of HC/LC ratio, thus LCs can find themselves in a “free” form, called Free Light Chains (FLC). The remaining 20% of MGUS are LC-only MGUS, characterized by an abnormal FLC ratio (kappa to lambda ratio of <0.26 or >1.65) together with the absence of any detectable Ig HC. Translocations involving

the IgH locus (Chr.14) are often found in these LC-only PC proliferations since they frequently switch the HC locus off.

The risk of progression from MGUS to MM or another lymphoproliferative disorder is low, around 1%/ year (Landgren et al., 2009; the International Myeloma Working Group et al., 2010). Since it is not possible to know which patient will progress to a malignant state, these patients should be monitored for potential complications. Several risk factors are used to evaluate it, such as serum FLC ratio and levels of monoclonal Ig (Castillo, 2016). Organ dysfunction, especially kidney and heart, should also be carefully monitor since, as we will discuss later on, some diseases may occur due the nature of the monoclonal Ig component.

Plasma cell disorder	Definition
MGUS	The following three criteria must be met: • Serum monoclonal protein of <3 g/dL • Clonal bone marrow plasma cells of <10% • Absence of end organ damage using the CRAB criteria (hypercalcaemia, renal impairment, anaemia and bone lesions)
SMM	The following two criteria must be met: • Serum monoclonal protein (IgG or IgA) of ⩾3 g/dL, or urinary monoclonal protein of ⩾500 mg/24 h and clonal bone marrow plasma cells of 10–60% • Absence of myeloma-defining events or amyloidosis

MM	The following two criteria must be met:
	• Clonal bone marrow plasma cells of ⩾10% or biopsy-proven bony or extramedullary plasmacytoma
	• Any one or more of the following myeloma-defining events:
	  • Evidence of end organ damage using the CRAB criteria
	  • Hypercalcaemia: serum calcium of >0.25 mmol/L higher than the upper limit of normal or >2.75 mmol/L
	  • Renal insufficiency: creatinine clearance of <40 mL/min or serum creatinine of >177 μmol/L
	  • Anaemia: Hb of >2 g/dL below the lower limit of normal or a Hb value of <10 g/dL
	  • Bone lesions: one or more osteolytic lesions on skeletal XR, CT or PET-CT
	  • **Clonal bone marrow plasma cells of ⩾60%**
	  • **Involved: uninvolved serum free light chain ratio of ⩾100 (involved free light chain level must be ⩾100 mg/L)**
	  • **More than one focal lesion on MRI studies (at least 5 mm in size)**

CT, computed tomography; MGUS, monoclonal gammopathy of unknown significance; MM, multiple myeloma; MRI, magnetic resonance imaging; PET-CT, positron emission tomography/computed tomography; SMM, smouldering multiple myeloma; XR, X-ray.
The new criteria, added in 2014, are indicated in bold.[5]

Figure 23- Diagnostic criteria for PCD. Summary of the different clinical manifestations and criteria use to classify the different PCD according to PC percentage, serum monoclonal Ig and organ damage.(Bird and Boyd, 2019)

II.1.2. Smoldering Multiple Myeloma

Smoldering Multiple Myeloma (SMM) is found between MGUS and active MM. It has been defined by the presence of more than 10% of monoclonal PC in the BM or more than 3 g/dL of a monoclonal Ig without CRAB symptoms (hypercalcemia, renal impairment, anemia, bone disease).

Progression to a malignant state is significantly higher in SMM patients compared to MGUS, ranging from 51% at 5 years to 73% at 15 years (Dispenzieri et al., 2013). Despite this, patients are not treated until progression to MM as they may remain asymtomatic for several years.

II.1.3. Multiple Myeloma

Multiple myeloma is one the most frequent hematological neoplasm, representing 1% of total cancers and about 10% of hematological neoplasm (Rajkumar et al., 2014) characterized by the clonal proliferation of a PC, primarily in the BM. Most people affected with MM are 75 years old and above.

The International Myeloma Working Group (IMWG) criteria for the diagnosis of MM includes the classic CRAB features and what they call three myeloma-defining events (MDEs): 60% or greater clonal PC , a FLC ratio of 100 or greater, provided the absolute level of the involved light chain is at least 100mg/L and more than one focal lesion on MRI that is at least 5mm or greater in size. The presence of at least one of these markers is considered sufficient for a diagnosis of MM.

In terms of the monoclonal Ig found, IgG represents around 50% of cases, followed by IgA and kappa or lambda LC only (20% each). Those with IgD, IgM, biclonal or non-secretory forms are rare, around 1% each (Castillo, 2016).

MM is always preceded by an initial MGUS that then develops into SMM. Rarely, MM can evolve into plasma cell leukemia (PCL), characterized by the circulation of PCs in the peripheral blood (Bird and Boyd, 2019). In recent years, treatments for MM have helped increase the length of survival (Kumar et al., 2017). However, MM remains incurable for the majority of patients as they may become refractory to treatment.

II.1.4. Waldenstrom macroglobulinemia

Waldenstrom macroblobulinemia is a rare type of non-Hodgkin lymphoma, whose diagnosis is carried out by the presence of a monoclonal IgM, the recurrent $MYD88^{L265P}$ somatic mutation (found in more than 90% of patients (Varettoni et al., 2017)) and the clonal proliferation of lymphocytic cells form different stages, from mature B cell to PCs, in BM and other organs (with at least 10% of marrow involvement) (Kapoor et al., 2016). Although WM remains

incurable, with a heterogeneous clinical course, the discovery of genes mutations has improved the understanding of its pathogenesis.

II.2. **Monoclonal gammopathies of clinical significance and Immunoglobulin-induced deposition diseases**

While in most cases the low burden PC clone in PCD may not have a pathological effect *per se*, it can produce a devastating effect by its secreted monoclonal Ig. The monoclonal Ig can be a complete Ig or a fragment of it, such as the LC alone or a truncated HC. These Ig are often unstable and consequently yield a variety of pathologic conditions resulting from their precipitation, aggregation or crystallization in different organs (Bridoux et al., 2015).

In 2012, the term of Monoclonal Gammopathy of Renal Significance (MGRS) has been created to regroup those diseases in which a monoclonal Ig affects the kidney, despite maybe being a MGUS from the hematological point of view (Leung et al., 2012). MGRS is associated with high morbidity due to the renal lesions induced by the monoclonal Ig and a higher mortality. Therefore, while in most cases MGUS patients are not treated, MGRS ones will often be subjected to chemotherapy to suppress the monoclonal Ig-secreting PC. Diagnosis is carried out by evaluation of morphologic alterations (by light microscopy, immunofluorescence (IF) or immunoelectron microscopy), serum and urine protein electrophoresis, immunofixation and serum FLC dosage (Bridoux et al., 2015).

Since other organs can be affected too, such as the heart, skin, periphereal nerves, etc, these Ig-related diseases were further regrouped under the term of Monoclonal Gammopathy of Clinical Significance (MGCS) (Fermand et al., 2018). In most cases, MGCS are due to the direct deposition of monoclonal Ig fragments in organs, leading to their dysfunction. However, the monoclonal Ig can also have indirect effects (such as cytokine release, immune complexes, complement activation, etc.) leading to disease. In **Figure 24**, there is a summary of those MGCS related to the deposition of a monoclonal Ig classified according to the structure of the deposits. Among them, two of the most frequent forms of systemic disease are Light-Chain Amyloidosis (AL Amyloidosis) and Light Chain Deposition Disease (LCDD). As an example, LCDD is found in around 5% of patients with MM, whereas AL Amyloidosis accounts for about 11% (Ronco et al., 2006). Part of my work during this thesis was focused on these two diseases.

	Ultrastructural appearance of deposits	Main characteristics of monoclonal gammopathy	Main organ(s) involved
Organized			
AL amyloidosis	Fibrillar	λ LC (75%), κ LC (25%), IgM <10%	Systemic (heart 80%, kidney 70%)
Type I cryoglobulinemia	Microtubular/crystalline	IgG or IgM	Systemic (skin +++, kidney, peripheral nerve, systemic symptoms [crystal cryoglobulin])
Immunotactoid glomerulopathy/ GOMMID	Microtubular	CLL-like clonal proliferation (50%)	Kidney
Acquired Fanconi syndrome	Crystalline	κ LC (>90%, mostly Vk1)	Kidney (proximal tubulopathy)
Crystal storing histiocytosis	Crystalline	κ LC	Systemic (kidney, cornea, joints, lymphoid tissue)
Crystalline keratopathy	Crystalline	IgG	Cornea
Nonorganized			
MIDD		LCDD: LC only (usually κ LC) (80%, Vk1 and Vk4) HCDD: truncated HC only (mostly γ1 and γ3) LHCDD: LC + truncated HC	Systemic (kidney [~100%, glomerular and tubular basement membrane], liver [30%], heart [30%])
PGNMID		Usually IgG3	Kidney
Macroglobulinosis		IgM	Skin (dermis)

Figure 24- Classification of the main MGCS-related disorders due to the deposition of a monoclonal Ig. We can subdivide the diseases by the form of the deposits, whether they are organized (forming fibrils or crystals) or non-organized.(Fermand et al., 2018)

II.2.1. Non-organized deposits: Light Chain Deposition Disease

Randall-type monoclonal Ig deposition diseases (MIDD) are multi-system Ig-related deposition diseases. LCDD, is the most common form diagnosed (Joly et al., 2019; Ronco et al., 2006; Sayed et al., 2015). Russell E. Randall was the first to describe LCDD back in 1976 (Randall et al., 1976) and is characterized by systemic amorphous deposits composed of monoclonal free light chains. Most cases, up to 80%, involve a Vk1 or Vk4 LC (Denoroy et al., 1994; Fermand et al., 2018) and the hematologic diagnosis is MGRS in about one third of cases, MM accounting for almost all the other cases (Joly et al., 2019). More rare MIDDs involve a CH1-truncated HC (HCDD), sometimes together with a LC (LHCDD) composing the deposits (Bridoux et al., 2017; Joly et al., 2019; Nasr et al., 2012).

In LCDD, amorphous deposits of non-amyloid Ig LC can be found in different organs but kidneys are always involved. When examined ultrastructurally, they do not exhibit a fibrillary structure and are not positive to CR staining (Gokden et al., 2008; Preud'homme et al., 1994). Diagnosis is based on immunohistological analyses of kidney biopsies as MIDDs are characterized by a thickening of tubular and glomerular basement membranes, with linear deposits composed of the monoclonal Ig in IF and sometimes a nodular glomerulosclerosis resembling diabetic nephropathy. EM and Immuno-EM can secure the diagnosis (Bridoux et al., 2015). Patients usually develop chronic glomerular disease due to an abnormal expansion of extracellular matrix components (Collagene IV, Laminine, Fibronectine or Tenasin C)

(Keeling and Herrera, 2005) and mesangial cells, found between the glomerular capillaries (Joly et al., 2019; Ronco et al., 2006).

VLs in this disease have an elevated isoelectric point compared to LC from AL Amyloidosis and this could improve their interaction with the negatively charged proteoglycans found in basal membranes, consequently favouring their deposit (Joly et al., 2019; Kaplan et al., 2007). Moreover, there is a frequent glycosylation of the VL that could increase its tendency to precipitate (Cogné et al., 1991; Decourt et al., 1996; Ronco et al., 2001)

II.2.2. Organized deposits: AL amyloidosis

Amyloidosis refers to a group of rare but serious diseases in which an unfolded protein acquires a β-sheet structure that further leads to its aggregation in an organized way. Up to date there are over 30 amyloid-forming proteins have been described (Eisenberg and Jucker, 2012; Sipe et al., 2016).

First, protobrils are form to finally polymerize into insoluble fibrils that will deposit extracellularly in different tissues and organs. Fibrils are usually formed of about 80% of the causative protein and 20% of other factors, such as Apolipoprotein E (ApoE), Serum Amyloid P component (SAP) or proteoglycans. This other molecules help stabilize the fibrils, promote their formation and prevent their degradation (Pepys, 2006). Since the fibrils deposit in an organized way, when subjected to polarized light after Congo Red (CR) staining, a typical “apple-green” birefringence can be seen (Merlini et al., 2018) (**Figure 25**).

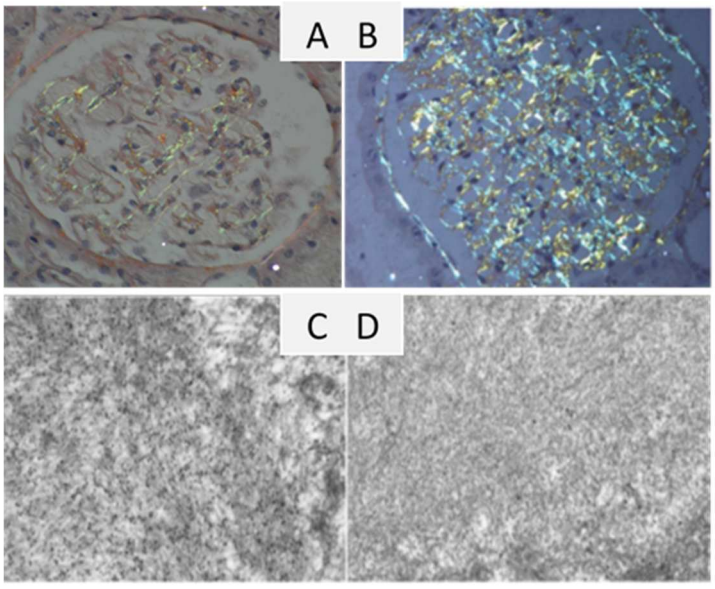

Figure 25- Congo Red staning and Immuno-Electron Microscopy. A-B) Renal AL Amyloidosis confirmed by CR birefrigence and typical gren-yellow dichronisme.under polarized light C) Electron Microscopy of a kidney biospsy and stained with gold-anti-lambda D) same organ but satined with gold- anti-kappa showing no staining thus confirming the type of LC implied. (Desport et al., 2012; Jaccard et al., 2015)

While several proteins can cause amyloidosis, the most common form of systemic amyloidosis is AL Amyloidosis. Here fibrils are formed of a monoclonal free LC and deposits can be found in several organs such as heart, kidney, liver, spleen and the digestive system (Blancas-Mejía and Ramirez-Alvarado, 2013) (**Figure 26**). The gradual accumulation of fibrillar deposits will affect the normal function of the organs and it has also been described that the FLC in excess itself can exert a direct toxicity (Diomede et al., 2014; Jordan et al., 2020; Mishra et al., 2013).

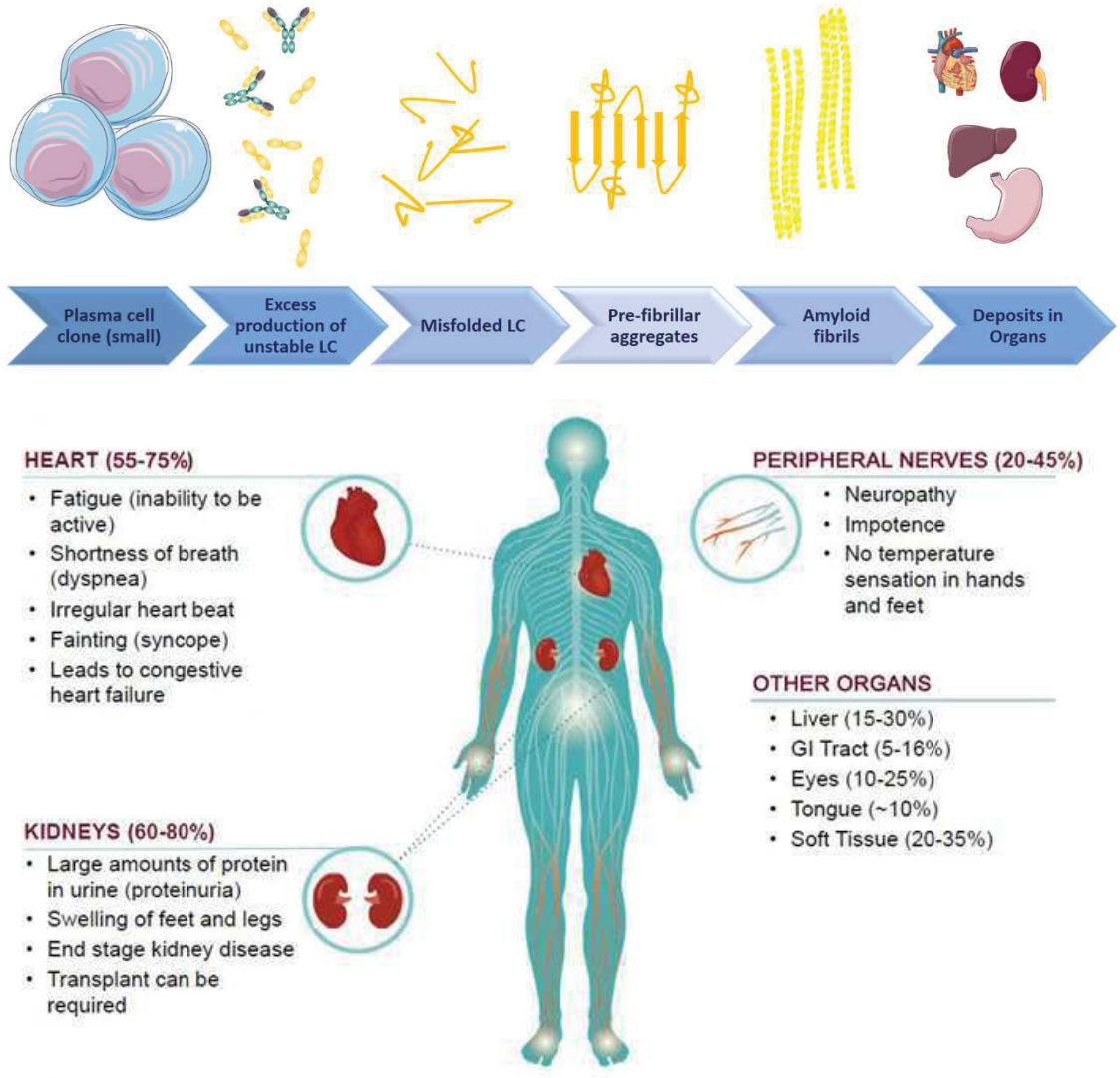

Figure 26 – AL Amyloidosis. Representation of the different steps implied in AL Amyloidosis before the accumulation in the different organs. Most patients have a heart and/or kidney deposits mainly but every organ, except for the central nervous system, can be touched.

Diagnosis is based on the CR birefrengency associated with Ig typing on frozen or pronase-treated paraffin sections (Nasr et al., 2006) while EM and Immuno-EM can help the diagnosis (Bridoux et al., 2015). More recently, mass spectrometry on laser-microdissected amyloid material tends to become a new gold standard for amyloidosis typing (Kourelis et al., 2017).

AL amyloidosis mostly appears associated with MGUS (MGRS) or in association with MM, or WM. The prevalence of the disease rises with age, with a mean age of diagnosis of 65 years, and men and women seem to be affected equally. In France, particularly in the Limousine region, it was shown a yearly incidence of 12.5 per million inhabitants for a period going from 2012 to 2016, which is similar to the Mayo clinic data of the Olmsted County, Minnesota between 1990 and 2015, while in Buenos Aires, Argentina, it was of 6.2 (Aguirre et al., 2016; Duhamel et al., 2017; Kyle et al., 2019).

As it happens in most of the monoclonal Ig-related diseases, each patient has a unique Ig sequence making it more difficult to understand why one Ig will have a tendency to deposit in the form of a fibril, crystal or in a non-organized way. In relation to AL amyloidosis, it has been shown that certain V germline genes can influence the organ tropism (Comenzo et al., 2001; Kourelis et al., 2017; Perfetti et al., 2012) and some mutations may favor fibril formation (Blancas-Mejía et al., 2014). However, up to date, there is no common characteristic described to predict the amyloidogenicity of a FLC.

II.2.2.1. Fibril Formation and structure

Soluble proteins are slowly turned into insoluble amyloid fibrils by a complex process requiring several factors (Merlini and Bellotti, 2003; Ramirez-Alvarado, 2012). Among them, we can find mutations that will change its native conformation thus exposing hydrophobic or protease-sensitive regions, an increase in protein synthesis/accumulation, or an intrinsic propensity to form fibrils (Blancas-Mejía et al., 2014; Wall et al., 1999, 2004).

The formation of a fibrillary nucleus starts with partially folded monomeric proteins and the required concentration needed varies depending on the stability of the LC. Next, after overcoming a lag phase, the fibrillary nuclei are formed and the β-sheet oligomerization takes place, generating the fibrils and its elongation **(Figure 27)**. This last step requires lower concentrations of LC compared to the formation of the first nuclei (Blancas-Mejía et al., 2014; Westermark et al., 2018).

In recent years, thanks to Cryo-Electron Microscopy (Cryo-EM) technique, structural analysis of the different amyloid fibrils have been carried out using patients samples instead of *in vitro* grown fibrils. Swuec *et al.* and Radamaker *et al.* (Radamaker et al., 2019; Swuec et al., 2019) used AL Amyloidosis patients hearts to achieve a high resolution of the *ex vivo* fibrils.

Both studies showed that the fibril density is composed of an asymmetric protofilament formed of 77 to 93 residues exclusively from the VL domain and have the typical 4.9 Å stacking and cross-β architecture. The inner structured core can be divided into two segments and they seem to be spatially contiguous but not directly connected. The individual LC subunits assemble along the fibril elongation axis in parallel β-sheet and each one has nine β- strands. The fibril protein is not glycosylated and the CL domain does not participate to the core fibrils. Consequently, since it is not protected in mature fibrils, it might be completely removed by proteolysis but some short N-terminal CL fragments were shown in the extracts (Swuec et al., 2019).

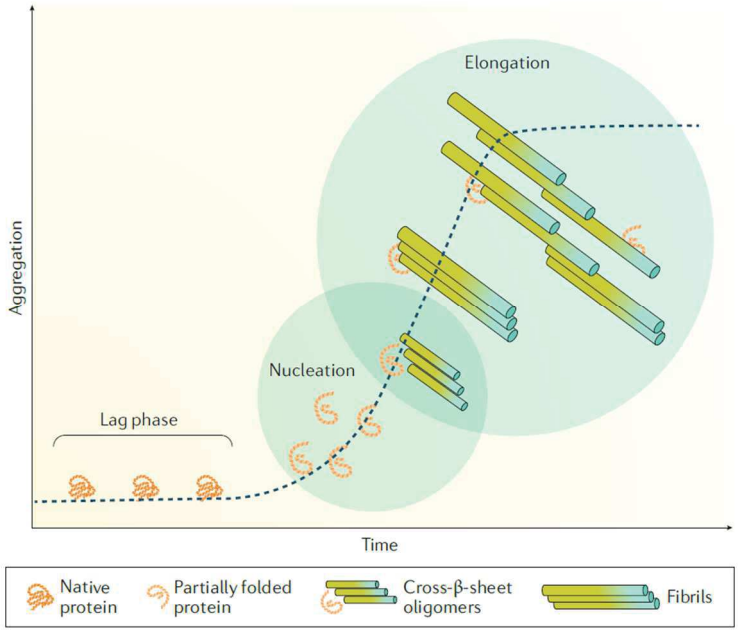

Figure 27- In vitro fibril formation kinetics. The initial Lag phase is overcomed after the formation of fibrillary nuclei. β-sheet oligomers are formed leading to fibril formation and elongation. (Merlini et al., 2018)

II.2.3. Treatments for Ig-induced deposition diseases

Unfortunately, up to date these diseases remain incurable and the choice of treatment is made using a benefit/risk approach while patients clinical history and the organs involved are taken into account (Fermand et al., 2013). The main goal of the currently available treatments is to produce the best hematological response, as the eradication of the PC clone will eliminate the monoclonal Ig implied.

II.2.3.1. Anti-plasma cells therapies

Currently no drug has been specifically approved for AL amyloidosis or LCDD treatment but most treatments regimens are derived from MM. High-dose melphalan has been for several years the first-line treatment for patients that could be eligible for autologous hematopoietic stem cell transplantation (SCT) (Merlini et al., 2018) and Melphalan + Dexamethasone (MDex)

for intermediate and high risk patients (Jaccard et al., 2007). However, after a proven efficacy in MM patients, proteasome inhibitors-containing regimens were gradually imposed and appeared to be specifically efficient in these diseases (Sitia et al., 2007).

As described in the previous chapter, PC are subjected to a higher stress due to the large production of Igs, which induces the UPR response to ease it. The blockage of the proteasome by PI induces the massive accumulation of proteins over the critical threshold and therefore the UPR response balance shifts into the apoptosis pathway. A great advantage of this treatment is that it spares normal hematopoietic cells. Moreover, in the case of AL Amyloidosis, it has been shown that patients PCs are more sensitive to stress. This may be due to the intrinsic characteristics of the pathogenic LC that tends to misfold and aggregate (Oliva et al., 2017). Up to now, bortezomib, carfilzomib and ixazomib have been tested in AL amyloidosis patients (Varga et al., 2019). Weekly subcutaneous treatment of bortezomib, that can be combined with an alkylating agent and dexamethasone, is largely used in the management of these diseases (Fermand et al., 2018).

The immunomodulators drugs (IMiDs) comprise a group of therapeutic compounds analog of thalidomine (glutamic acid derivate). IMiDs can affect the immune system to eliminate the malignant PC, for example by co-stimulating T cells and removing the requirement of a secondary co-stimulation signal from an APCs (Davies et al., 2001). Additionally, they increase the production of IL-2 and interferon-γ (IFN-γ) thus increasing the number of NK cells. These drugs are also capable of inhibiting the cyclin-dependent kinase pathway, downregulating anti-apoptotic proteins and activating FAS-mediated cell death (Jelinek et al., 2016). In this group of drugs we can find lenalidomide and pomalidomide, second generation IMiDs that can be combined with dexamethasone and/or melphalan. However, since PI have proven efficient and that the immunomodulatory agents appeared to be toxic, they have been kept aside and only proposed to patients with refractory disease.

Recently, Venetoclax, a selective oral small-molecule BCL-2 inhibitor has shown value in MM patients, especially those arbouring the t(11:14) translocation, which represents approximatively 60% of AL amyloidosis patients. Some studies reported stunning efficacy in this group of patients (Leung et al., 2018) and a phase-II clinical trial was launched for the treatment of t(11:14)-AL amyloidosis patients (Sidiqi et al., 2020). It is still under debate why t(11:14) translocation involving cyclin D1 is associated with the efficacy af this anti-BLC2 treatment but *Bcl2* expression appears to be often increase in these patients.

Over the years, several monoclonal antibodies (mAbs) targeting PCs have been tested but few were convincing. Daratumumab is the first humanized monoclonal antibody against CD38, a glycoprotein highly expressed on malignant PCs with high efficiency in PC proliferations.

This antibody induces apoptosis by cross-linking as well as antibody-dependent cellular toxicity and complement-dependent cytotoxicity. Two ongoing phase 2 studies have showed, in refractory or relapse patients, a good safety profile and a rapid hematologic response (Kaufman et al., 2017; Roussel et al., 2020). Other biotherapies targeting PCs and currently evaluated for MM, that should also work in MGCS, include anti-SLAM7 antibodies, CD3/BCMA bi-specific antibodies, BCMA-directed antibody drug conjugate and BCMA or CS1 Car-T cells (Parrondo et al., 2020)

II.2.3.2. Anti-amyloid fibrils therapies

Even if PC-targeted therapies have allowed considerable improvement in MGCS management, there is still a need for additional approaches aiming at removing already formed deposits. The main reason is that fibrils, crystals or other aggregates, that are highly resistant to degradation, can remain in organs for several months thus increasing the morbidity and mortality even in patients with good hematological response. In AL amyloidosis, the most severe MGCS, several approaches using mAbs have been developed like the ones directed against the SAP present in the amyloid deposits (Richards et al., 2015) or cryptic epitopes in the fibrils themselves (Edwards et al., 2017; Solomon et al., 2003a).

NEOD001, was a humanized mAb targeting an cryptic epitope on amyloid fibrils and misfolded LCs (Wall et al., 2012). This antibody was supposed to reduce the amyloid burden by neutralizing the amyloidogenic LC and clearing the fibrils through monocyte/macrophage phagocytosis. Unfortunately, the study was discontinued as it was judged unlikely to fit its primary goal of eliminating cardiac deposits. On the same line of treatment, 11-1F4, from the same laboratory and now developed by Caelum Biosciences, is a monoclonal antibody recognizing an epitope on LC amyloid fibrils to induce cell-meditated phagocytosis (Solomon et al., 2003b). It was proven to specifically target organs with amyloidosis on PET/CT imagining of patients (Wall et al., 2010) and several randomized clinical trials are ongoing with encouraging results (Edwards et al., 2017).

Anti-SAP therapy appeared as a promising approach due to its potential to target all kind of amyloidosis. Studies in mice with AA amyloidosis showed tremendous efficiency of the antibody to remove amyloidosis especially through complement dependent cellular phagocytosis (Bodin et al., 2010; Milde et al., 2015). Phase I clinical trials with dezamizumab (a fully humanized monoclonal anti-SAP antibody) demonstrated efficacy in patients (Richards et al., 2015) . However, treatments with anti-SAP require the prior removal of circulating SAP thanks to a small molecule (Miridesap or CPHPC) (Pepys et al., 2002) to avoid therapeutic antibody trapping and formation of immune complexes. Consequently, these treatments required a long period of hospitalization. Despite encouraging results, patient enrollment in

clinical trials were suspended due to an apparent change in the risk-benefit profile of the therapy. Among other compounds, Doxycycline, an antibiotic that was proven to interfere with fibril formation in mice (Ward et al., 2011), tested in combination to bortezomib or standard chemotherapy showed to improve the cardiac outcome and survival of AL amyloidosis patients (Merlini et al., 2011).

Surprisingly as it may seem, green tea has been shown to have anti-amyloidosis characteristics. One of its compounds, Epigallocatechin-3-gallate, already used in ATTR (transthyretin amyloidosis) (Ferreira et al., 2009), could pull the LC to generate a non-toxic aggregate (Hora et al., 2017) and therefore is being tested in patients with cardiac AL-amyloidosis.

Several other therapies are still at preclinical stages. Among them, the team of Jonathan Wall has developed synthetic peptides that specifically bind to all forms of human amyloidosis and were used for amyloid imaging. They now take advantage of these amyloid-reactive peptides to develop therapies. A first approach was to fuse an Ig Fc domain to an amyloid-reactive peptide called p5. While p5 opsonizes amyloid, the Fc domain recruits macrophages for phagocytosis of amyloid fibrils (Foster et al., 2017). Another approach was based on a bifunctional peptide, also called “peptope”, comprising a multiamyloid-reactive peptide fused to a high-affinity peptide epitope recognized by 11-1F4. This pre-targeting approach was found to enhance the reactivity and extend the specifity of 11-1F4 mAb to other amyloidoses in mouse (Wall et al., 2018).

In our laboratory, we have generated a human SAP fusion protein, carrying two Fc domain of a human IgG1 (scFc) (Romeuf and Sirac, 2015). Here, the SAP is used to target and opsonize amyloid deposits. Then the fused Fc domains can recruit phagocytes to eliminate them. In contrast with anti-SAP approach, treatments do not require a prior removal of circulating SAP. This patented fusion protein proved to be efficient into eliminating deposits in a mouse model of AA Amyloidosis.

Part I. Models of Immunoglobulin-induced deposition diseases

Due to the wide spectrum of organs touched and the different Ig involved, understanding each of the Ig-induced deposition diseases is very complex. Despite this, different *in vitro* and *in vivo* models can help untangle the underlying mechanisms and provide new tools to test different therapeutic options for patients.

Putting aside cellular models, that while are very useful to answer basic questions or challenge different hypothesis cannot mimic the global characteristic of these pathologies, the first tests were carried out with huge quantities of the involved Ig. These Ig were obtained from patients' urine, named Bence-Jones proteins, and subsequently injected in mice or rats (Sanders et al., 1987; Solomon et al., 1991). These models showed some of the lesions from the diseases but did not reproduce the pathological course of it in time. However, in the case of AL Amyloidosis, it helped trace the pathway carried out by the Igs in kidneys. First, they are endocytosed by mesangial cells in glomeruli and fibrils are thought to be formed in the lysosomes before being secreted in the extracellular space (Teng et al., 2014).

Tumoral graft models, using transfected Sp2/0 mouse hybridoma cell line with different Igs, were next tested. Mice developed Ig-secreting tumors and could be followed up for several weeks. In the case of a renal disease, called Fanconi Syndrome (FS) in which LC-composed crystals accumulate in renal tubules, this strategy succeeded in reproducing the kidney lesions as well as highlighting the key role of certain amino acids in the CDR1 and CDR3 in the crystallization process. This was done by modifying the Ig sequence thanks to directed mutagenesis (Decourt et al., 1999).

Quickly, the tumoral models were left aside since animal conditions deteriorate in a short lapse and not all diseases could be reproduce with this technique. Therefore, transgenic models become the latest and more efficient strategy to model Ig-induced deposition diseases. One transgenic strategy implied the random insertion of the Ig sequence under a strong promoter that would be express in several tissues. Ward *et al.* (Ward et al., 2011) published an AL Amyloidosis model with circulating FLC below 10µg/ml in which they found few deposits in the stomach. Their model helped to prove that doxycycline could prevent fibril formation but it did not reproduce the systemic involvement of the disease. Other models with a similar approach were published (Nuvolone et al., 2017) or kept unpublished (including ours) because none of them developed overt amyloidosis likely due to the low level of human FLC observed in all these mice.

In 2006, the laboratory published a first model of MGRS (FS) using a knock-in strategy (Sirac, 2006). They inserted the variable domain of a human pathogenic LC gene into its equivalent locus in the mouse, the mouse Ig kappa locus. In the mouse, this human Vκ domain

was spliced to the mouse kappa constant domain (Cκ) producing a chimeric LC. All B and plasma cells were shown to produce the chimeric LC. Similar to what is observed in FS patients, kidney LC deposits and dysfunction were obtained. It was the first direct demonstration that the V domain alone bore the toxicity for organs and that the interruption of LC production reversed the kidney lesions. In this model, total LC was estimated to more than 10mg/ml but mostly associated with the mouse HCs. It was difficult to estimate the level of FLC since there was no available assays for mouse.

Using a similar strategy a model of Heavy Chain Deposition Disease (HCDD), MIDD characterized by the amorphous deposits of truncated HC, was obtained (Bonaud et al., 2015). In these mice, we found several characteristics of the disease but they did not develop a renal insufficiency as patients do.

In both these diseases, we further showed that very low levels of pathogenic Ig (< 20µg/ml) were sufficient to induce organ lesions. However, our first models of transgenic mice with ubiquitous expression of an amyloid LC produced in a similar range (unpublished), were unsuccessful with no amyloidosis development. We hypothesized that it was due to the low level of FLCs since most human LCs associated perfectly well with mouse HCs. In an attempt to increase FLC production, we took advantage of another mouse strain, called DH-LMP2A, which bears an invalidated HC locus but a normal B cell development (Casola et al., 2004) together with an increased PC number (Lechouane et al., 2013), making it the ideal model for high production of free LCs. This strategy has been recently published (Sirac et al., 2018) and will be fully described in the next section.

While mice are the most common animal used in science, around 60%, other animals are also deployed. This is particularly true for AL Amyloidosis, in which a zebrafish transgenic model has been recently developed to study the cardiac AL Amyloidosis (Mishra et al., 2019, 2013) and a *Caenorhabditis elegans* model to study the direct toxicity of amyloidogenic LCs in the heart (Diomede et al., 2014). However, both models remain too far from physiology further illustrating how difficult it is to obtain a reliable model for therapeutic investigation in AL Amyloidosis.

I.1 Glomerulosclerosis and kidney failure in a mouse model of monoclonal immunoglobulin light-chain deposition disease.

As described before, LCDD is a rare disease in which LCs deposit as amorphous aggregates mainly in the kidneys. The accumulation of this LC eventually leads to a renal insufficiency due to a nodular glomerulosclerosis.

We have generated a transgenic mouse model that reproduces the main characteristics of the disease thanks to a well stablished strategy developed in our laboratory. Briefly, the variable domain VJ of the LC of interest is introduced by direct insertion in the kappa locus of the mouse model (Bonaud et al., 2015; Sirac, 2006). By doing this, we were able to obtain high levels of expression of the recombinant LC, with a human V domain and a mouse C domain, by all PCs. Since the pathogenic Ig is the free LC , *i.e.* not associated with a HC, mice were further crossed with DH-LPM2A mice that have the HC locus invalidated while keeping a normal B cell development and more PCs (Casola et al., 2004; Lechouane et al., 2013).

The mouse line obtained, called κF-DH, presents the typical deposits along the tubular and glomerular membranes in the kidney. The accumulation starts at two months and progressively induces a glomerulosclerosis and other lesions along the basal membranes. By the age of 8.5 months, half of them die of renal insufficiency.

The pathogenic LC induces a stress of the ER, as observed in their transcriptome as well as by qPCR of some stress markers. Since a higher ER-stress usually translate into a better response to PI, such as Bortezomib, mice were treated accordingly. As a result, the treated group had an important deposit decrease and regression of renal lesions.

Paper 1- Immunoglobulin light chain toxicity in a mouse model of monoclonal immunoglobulin light-chain deposition disease

S Bender, **MV Ayala**, A Bonaud, VJavaugue, C Carrion, C Oblet, A Rinsant, S Kaaki, Z Oruc, F Boyer, A Paquet, N Pons, B Herve, MO Ashi, A Jaccard, L Delpy, G Touchard, M Cogne, F Bridoux, C Sirac

Blood. 2020 Jun 19:blood.2020005980. doi: 10.1182/blood.2020005980.

Online ahead of print.

PMID: 32559766

American Society of Hematology
2021 L Street NW, Suite 900,
Washington, DC 20036
Phone: 202-776-0544 | Fax 202-776-0545
editorial@hematology.org

Immunoglobulin light chain toxicity in a mouse model of monoclonal immunoglobulin light-chain deposition disease

Tracking no: BLD-2020-005980R1

Sébastien Bender (Centre National de la recherche Scientifique UMR CNRS 7276/INSERM U1262, Université de Limoges, France) Maria Ayala (UMR CNRS7276 INSERM1262, University of Limoges, France) Amélie BONAUD (INSERM U1160, Institut de Recherche Saint-Louis, Saint Louis Hospital, France) Vincent Javaugue (Centre National de l'Amylose AL et Autres Maladies par Dépôt d'Immunoglobulines Monoclonales, Centre Hospitalier Universitaire de Limoges, France) claire carrion (CNRS, France) Christelle Oblet (UMR CNRS 7276 INSERM 1262, France) Alexia Rinsant (University Hospital of Poitiers,) Sihem Kaaki (Service de Pathologie et de Pathologie Ultrastructurale, Centre Hospitalier Universitaire de Poitiers, France) Zeliha ORUC (Centre National de la recherche Scientifique UMR CNRS 7276/INSERM U1262, Université de Limoges, France, France) François BOYER (Centre National de la recherche Scientifique UMR CNRS 7276/INSERM U1262, Université de Limoges, France, France) Agnes Paquet (CNRS, France) Nicolas PONS (Université Côte d'Azur, CNRS, IPMC, Sophia-Antipolis, France) Bastien HERVE (Plateform Biologie Intégrative Santé Chimie Environnement, Université de Limoges 87000 Limoges, France, France) Mohamad Omar ASHI (Centre National de la recherche Scientifique UMR CNRS 7276/INSERM U1262, Université de Limoges, France) Arnaud Jaccard (Centre National de l'Amylose AL et Autres Maladies par Dépôt d'Immunoglobulines Monoclonales, Centre Hospitalier Universitaire de Limoges, France) Laurent Delpy (CNRS, France) Guy Touchard (CHU-University POITIERS France, France) Michel COGNE (Centre National de la recherche Scientifique UMR CNRS 7276/INSERM U1262, Université de Limoges, France) Frank Bridoux (Centre National de l'Amylose AL et Autres Maladies par Dépôt d'Immunoglobulines Monoclonales, Centre Hospitalier Universitaire de Limoges, France) Christophe Sirac (Centre National de l'Amylose AL et Autres Maladies par Dépôt d'Immunoglobulines Monoclonales, Centre Hospitalier Universitaire de Limoges, France)

Abstract:
Light chain deposition disease (LCDD) is a rare disorder characterized by glomerular and peritubular amorphous deposits of a monoclonal immunoglobulin (Ig) light chain (LC), leading to nodular glomerulosclerosis and nephrotic syndrome. We developed a transgenic model using site-directed insertion of the variable domain of a pathogenic human LC gene into the mouse Ig kappa locus, ensuring its production by all plasma cells (PCs). High free LC levels were achieved after backcrossing with mice presenting increased PC differentiation and no Ig heavy chain (HC) production. Our mouse model recapitulates the characteristic features of LCDD, including progressive glomerulosclerosis, nephrotic-range proteinuria and finally, kidney failure. The variable domain of the LC bears alone the structural properties involved in its pathogenicity. RNA sequencing conducted on PCs demonstrated that LCDD LC induces endoplasmic reticulum stress, likely accounting for the high efficiency of proteasome inhibitor-based therapy. Accordingly, reduction of circulating pathogenic LC was efficiently achieved and not only preserved renal function, but partially reversed kidney lesions. Finally, transcriptome analysis of pre-sclerotic glomeruli revealed that proliferation and extracellular matrix remodelling represented the first steps of glomerulosclerosis, paving the way for future therapeutic strategies in LCDD and other kidney diseases featuring diffuse glomerulosclerosis, particularly diabetic nephropathy.

Conflict of interest: No COI declared

COI notes:

Preprint server: Yes; BioRxiv https://doi.org/10.1101/624650

Author contributions and disclosures: SB designed, performed, and analyzed experiments and drafted the manuscript ; MVA performed and analyzed experiments and drafted the manuscript ; AB designed, performed, and analyzed some experiments ; VJ drafted parts of the manuscript and provided general advice ; AR, NQ, SK, CC, CO, ZO and MOA performed and analyzed some experiments ; FB, BH, AP and NP performed the biostatistics and bioinformatics on RNA-seq data ; GT analyzed and provided advices on kidney pathology ; AJ, LD, MC provided general advice and reviewed the manuscript ; FB analyzed data and critically reviewed the manuscript ; CS designed and analyzed experiments, supervised research and wrote the manuscript.

Non-author contributions and disclosures: No;

Agreement to Share Publication-Related Data and Data Sharing Statement: RNAseq datasets are available at GEO under the accession numbers GSE119049 for glomeruli and GSE119048 for PCs. All datasets can be found in the GEO superseries: GSE119050. The token for full access to GEO datasets is: etopeeysfxsflkl.

Clinical trial registration information (if any):

Immunoglobulin light chain toxicity in a mouse model of monoclonal immunoglobulin light-chain deposition disease

(Light chain toxicity in a mouse model of LCDD)

Sébastien Bender[1,2], Maria Victoria Ayala[1]*, Amélie Bonaud[3]*, Vincent Javaugue[1,2,4], Claire Carrion[1], Christelle Oblet[1], Alexia Rinsant[2], Sihem Kaaki[2,5], Zeliha Oruc[1], François Boyer[1], Agnès Paquet[6], Nicolas Pons[6], Bastien Hervé[7], Mohamad Omar Ashi[1], Arnaud Jaccard[1,2,8], Laurent Delpy[1], Guy Touchard[4], Michel Cogné[1,9], Frank Bridoux[1,2,4] and Christophe Sirac[1,2].

*Contributed equally to this work.

[1] Centre National de la recherche Scientifique UMR CNRS 7276/INSERM U1262, Université de Limoges, France.

[2] Centre National de l'Amylose AL et Autres Maladies par Dépôt d'Immunoglobulines Monoclonales, Centre Hospitalier Universitaire de Limoges, France.

[3] INSERM U1160, Institut de Recherche Saint-Louis, Saint Louis Hospital, Paris, France.

[4] Service de Néphrologie et Transplantation, Centre Hospitalier Universitaire de Poitiers, France.

[5] Service de Pathologie et de Pathologie Ultrastructurale, Centre Hospitalier Universitaire de Poitiers, France.

[6] Université Côte d'Azur, CNRS, IPMC, Sophia-Antipolis, France.

[7] Plateform Biologie Intégrative Santé Chimie Environnement, Université de Limoges 87000 Limoges, France

[8] Service d'Hématologie Clinique, Centre Hospitalier Universitaire de Limoges, France.

[9] Institut Universitaire de France

Correspondence: Christophe Sirac, CRIBL laboratory, UMR CNRS 7276 INSERM 1262, CBRS room 110, 2 rue du Dr Marcland, 87000 Limoges, France; e-mail: christophe.sirac@unilim.fr.

Key points

- Human pathogenic Ig light chain fully reproduces LCDD in a transgenic mouse, including glomerulosclerosis and end stage renal failure
- Beside its toxicity for kidney, LCDD light chain induces endoplasmic reticulum stress and sensitizes plasma cells to proteasome inhibitors

Word count:

- Abstract: 198 words
- Main text: 3997 words
- 6 figures
- 8 supplemental figures
- 6 supplemental tables
- 1 supplemental methods
- Number of references: 54

Abstract

Light chain deposition disease (LCDD) is a rare disorder characterized by glomerular and peritubular amorphous deposits of a monoclonal immunoglobulin (Ig) light chain (LC), leading to nodular glomerulosclerosis and nephrotic syndrome. We developed a transgenic model using site-directed insertion of the variable domain of a pathogenic human LC gene into the mouse Ig kappa locus, ensuring its production by all plasma cells (PCs). High free LC levels were achieved after backcrossing with mice presenting increased PC differentiation and no Ig heavy chain (HC) production. Our mouse model recapitulates the characteristic features of LCDD, including progressive glomerulosclerosis, nephrotic-range proteinuria and finally, kidney failure. The variable domain of the LC bears alone the structural properties involved in its pathogenicity. RNA sequencing conducted on PCs demonstrated that LCDD LC induces endoplasmic reticulum stress, likely accounting for the high efficiency of proteasome inhibitor-based therapy. Accordingly, reduction of circulating pathogenic LC was efficiently achieved and not only preserved renal function, but partially reversed kidney lesions. Finally, transcriptome analysis of pre-sclerotic glomeruli revealed that proliferation and extracellular matrix remodelling represented the first steps of glomerulosclerosis, paving the way for future therapeutic strategies in LCDD and other kidney diseases featuring diffuse glomerulosclerosis, particularly diabetic nephropathy.

Introduction

Monoclonal gammopathies of renal significance (MGRS) are characterized by renal lesions due to monoclonal immunoglobulins (Ig) produced by a non-malignant B or PC clone.[1] They comprise tubulopathies caused by LC accumulating in the proximal or distal tubules, or glomerulopathies, most frequently AL amyloidosis and Randall-type monoclonal Ig deposition disease (MIDD).[2] MIDD are characterized by linear amorphous deposits of a monoclonal LC (LCDD) or a truncated HC (HCDD) along the tubular and glomerular basement membranes (BMs), around arteriolar myocytes and in the mesangium, eventually leading to diabetic-like nodular glomerulosclerosis. Clinical manifestations include glomerular proteinuria with progressive kidney failure.[3–5] In LCDD, the most frequent form of MIDD, involved LCs are mostly of the κ isotype, with a striking overrepresentation of the Vκ4 variable (V) domain. Cationic V domains and/or complementarity determining regions (CDR) could account for their propensity to deposit along negatively charged BMs.[6,5,7] However, little is known about the pathogenic mechanisms involved in glomerular damage leading to proteinuria and glomerulosclerosis. Herrera and colleagues showed the acquisition of a myofibroblast phenotype by mesangial cells exposed to purified LCDD LCs.[8–11] Similarly to diabetic nephropathy (DN),[12] these changes came along with the increased production of PDGFβ and TGFβ, resulting in excessive generation of extracellular matrix (ECM) proteins. However, since most of these experiments relied on acute exposure to pathogenic LC, they deserve to be confirmed in a model reproducing the progressive development of glomerular lesions observed in MIDD. We recently developed a transgenic mouse model of MIDD in which the continuous production of a truncated HC from a HCDD patient by PCs led the main pathologic features of HCDD, but neither glomerulosclerosis nor kidney dysfunction was observed.[13] In the present study, we developed a transgenic mouse

model of LCDD, κF-DH, using targeted insertion of a human LC gene into the mouse κ locus, coupled to a deletion of the HC genes, to obtain high levels of circulating pathogenic free LC (FLC)[14]. This strategy proved efficient with the induction of a full-blown LCDD and gave new insights into the pathophysiology of the disease and into the toxicity of monoclonal LCs for PCs.

Methods

Mice

Gene targeting into the murine Igκ locus was performed as previously described.[15] The procedure is detailed in the supplemental Methods and Figure 1A. As described elsewhere[14] and in the supplemental methods, LC transgenic mice (κF) were backcrossed with the DH-LMP2A (DH) strain to produce only free LCs (Figure 1A). LCDD mice, corresponding to the double homozygous DH and κF strain (κF-DH) were analysed throughout this study. Primers used are in Supplemental Table 1. DH-LMP2A mice[16] were kindly provided by S. Casola (IFOM, Milan, Italy). All animals are under a mixed genetic background (BALB/C x 129SV x C57/BL6) and were maintained in pathogen-free conditions and analyzed at 2, 6 and 8 months except when otherwise stated. All experimental procedures have received the approval of our institutional review board for animal experimentation and of the French Ministry of Research (N° 7655-2016112211028184).

In vivo treatment, surgery and biochemical parameters

For long-term treatment, mice were treated with Bz 0,75mg/kg[17,13] (Velcade®, Janssen Cilag) and cyclophosphamide (Endoxan®, Baxter) (2mg/kg) once a week during 2 months. Bz was injected subcutaneously and cyclophosphamide was injected intraperitoneally. To test the sensitivity of PCs to PI, we injected for 2 consecutive days a sub-optimal dose of Bz as

previously described.[13] Biochemical parameters were measured on a Konelab 30 analyser with a creatinine enzymatic test (ThermoFisher Scientific). Urine albumin concentrations were measured using a mouse albumin ELISA kit (Abcam).

Pathologic studies, ELISA and Western Blot analysis

Kidney samples were processed for light microscopic examination, immunofluorescence and electron microscopic studies, as previously described.[13] Some specific techniques and the lesion scores protocol are described in the supplemental methods. Serum were analysed for the presence of κLC by ELISA and western blots as previously described.[15,13] The list of antibodies is in supplemental Table 2.

Glomeruli extraction

Isolation of kidney glomeruli from mice was derived from Takemoto and al.[18] Briefly, mice were perfused in the heart with magnetic 4.5µm diameter Dynabeads. Kidneys were minced, digested by Dnase I (Roche) and collagenase IV (Sigma-Aldrich), filtered, and glomeruli were isolated using a magnetic rack. In our hands, this technique could not be applied to kidneys presenting advanced sclerosis likely due to the lack of access of the beads to the glomerular capillaries.

Flow cytometry and PC enrichment

Intracellular staining was performed using the Intraprep™ kit (Beckman Coulter). Flow cytometry analysis were performed on a BD Pharmingen LSRFortessa® cytometer. Data were analyzed with BD FACSDiva software (BD Biosciences). PC enrichments were performed using the mouse $CD138^+$ PC isolation kit (Miltenyi Biotec).

Transcriptional analysis

Total RNA from purified glomeruli or PCs were obtained using miRNeasy Mini kit (Quiagen) and purity (RIN > 7) was assayed with the Bioanalyzer RNA 6000 Nano (Agilent). 500 ng of RNA was used to generate RNA sequencing libraries. Alternatively, reverse transcription was

performed using high capacity cDNA reverse transcription kit (Applied Biosystems), with random hexamers. Relative quantification was performed with Premix Ex Taq or SYBR Premix Ex Taq (Takara) on cDNA samples (10 ng per reaction). Quantification of the gene of interest was analyzed by ΔCt method with IgJ used as housekeeper gene. Probes are listed in Supplemental Table 1.

RNA sequencing

Libraries were generated from 500 ng of total RNA using Truseq Stranded mRNA kit (Illumina), quantified with Qubit dsDNAHS assay kit (Invitrogen) and pooled. 4nM of this pool were loaded on a Nextseq 500 high output flowcell and sequenced on a NextSeq 500 platform (Illumina) with 2×75bp paired-end chemistry. Bioinformatic pipelines for mapping and filtering and tools for pathways analysis are described in supplemental Methods. Gene Expression Omnibus (GEO) accession numbers for the RNAseq datasets reported in this paper are: GSE119049 for glomeruli and GSE119048 for PCs (GEO superseries: GSE119050).

Statistical analysis

The statistical tests used to evaluate differences between variables were carried out using Prism GraphPad software (GraphPad Software, Inc). Statistical significance were determined using the non-parametric Mann-Whitney test to assess two independent groups and the log-rank (Mantel-Cox) test for survival analyses. p values < 0.05 were considered significant.

Results

An efficient transgenic strategy to produce high amounts of human pathogenic LCs in mouse. LCDD mice, as described in the methods (Figure 1A and B), closely recapitulate the features of monoclonal gammopathy with an elevated number of PCs producing the

human/mouse chimeric monoclonal FLC. Indeed, LCDD mice presented with about 10% of PCs in spleen (as compared to about 1% in WT mice), of which 95% produced the transgenic LC (Figure 1, C and D). Serum FLC levels were similar to those observed in patients with LCDD,[19] progressively increased with age and lasted during the life-span of the animals. Bence-Jones proteinuria was readily detectable in 5 month-old mice (Figure 1E).

Severe kidney failure induces premature death of LCDD mice. κF-DH mice (n=12 in two independent cohorts) were monitored daily from the fifth month for external signs of morbidity (see methods). Median survival was 8.5 months, with the first mouse sacrificed at 6 months and the last one at 14 months (Figure 2A). DH mice (n=10 in two independent cohorts) were used as control (similarly to κF-DH mice, they do not produce complete antibodies). At 14 months, all control mice were healthy (Figure 2A). Increased albuminuria was observed in 8-month-old κF-DH mice (Figure 2B). Mice sacrificed at humane endpoints showed heavy albuminuria, reaching up to 24.80 g/L (mean 8.30 ± 2.63 g/L) (Figure 2B), together with high serum creatinine (135.58 ± 19.23 vs 7,89 ± 0.47 and 9,20 ± 1.33µM/L in 8 month-old wild-type (WT) and DH controls mice, respectively) confirming a severe kidney failure in these mice (Figure 2C). Macroscopic observations revealed pale and atrophic kidneys (Supplemental Figure 1). Altogether, these results confirmed that the short life span of κF-DH mice is due to end-stage renal failure.

Pathogenic human LCs recapitulate renal lesions of LCDD. Pathologic studies were carried out on 2 and 6-month-old κF-DH mice and in mice sacrificed at humane endpoints. As early as 2 months, immunofluorescence analysis revealed linear LC deposits along glomerular (Figure 3A) and medullary tubules BMs (Supplemental Figure 2). At 6 months of age, an intense LC staining was observed along all BMs in the renal medulla and cortex, and into

mesangial space of the glomeruli (Figure 3A and Supplemental Figure 2) but kidneys showed normal tubular and glomerular structures (Figure 3A and Supplemental Figure 2). In contrast, mice sacrificed at humane endpoints displayed an absence of detectable LC reabsorption in proximal tubules, with massive staining of tubular BMs, mesangium and Bowman's capsule, and diffuse nodular appearance of glomerular deposits (Figure 3A and Supplemental Figure 2). Corticomedullary dedifferentiation suggestive of severe renal failure was observed (Supplemental Figure 2). Periodic acid schiff (PAS) staining confirmed thickening of tubular BMs, mesangial extracellular matrix expansion with mesangial cell proliferation and mesangiolysis, nodular glomerulosclerosis with glomeruli enlargement (Figure 3B). Focal areas of interstitial fibrosis with inflammatory infiltrates mainly composed of granulocytes/macrophages ($CD11b^+$) and T cells ($CD3^+$) (Supplemental Figure 3) were observed around sclerotic glomeruli and dilated tubules (Figure 3B). Electron microscopy revealed characteristic linear "powdery punctuate" deposits on the inner aspect of glomerular BMs and the outer aspect of tubular BM, diffuse thickening of tubular and glomerular BMs, and expanded mesangial areas with massive accumulation of electron-dense material (Figure 3C). Finally, immunoelectron microscopy using gold-labelled anti-mouse κLC confirmed the κ composition of the deposits (Figure 3D). Lesions of thrombotic microangiopathy with widening of the subendothelial zone by electron lucent material were seen in some glomeruli from 6 month-old mice and in most glomeruli from mice sacrificed at humane endpoints (Figure 3, C and D). Similarly to the patient from whom the LC gene was extracted,[20] κF-DH mice also yielded LC deposits in other organs including lung, liver and heart (Supplemental Figure 4). Collectively, kidney lesions observed in κF-DH mice fully recapitulate the human pathological features of MIDD and are consistent with premature death due to end-stage kidney failure.

Early induction of cell cycle and ECM remodelling are involved in LC-induced glomerulosclerosis. Having demonstrated that most 6-month-old κF-DH mice presented with early renal lesions of LCDD (Figure 3), we sought to compare their glomeruli transcriptome to that of control mice. RNA-seq performed on purified glomeruli revealed a total of 360 and 475 genes expressed differentially in κF-DH mice compared to WT and DH controls, respectively (abs(log2FC) $\geq$ 0.7, FDR $\leq$ 0.05) (Figure 4A and Supplemental Figure 5A). Among these genes, 192 were deregulated compared to both controls, with 155 upregulated and 37 downregulated genes (Supplemental Figure 5A and B). We performed a C2 canonical pathway analysis from the Molecular Signatures Database (MSignDB v6.2)[21,22] which revealed that the cell cycle (mitotic) was the main modified pathway (Figure 4B and Supplemental Table 3). All deregulated genes involved in the cell cycle were upregulated (Figure 4A, Supplemental Figure 5A and B and Supplemental Table 3). Beside the cell cycle, we found 24 deregulated genes involved in the matrisome pathway (18 upregulated, 6 downregulated), including the previously described upregulation of Tenascin C (Tnc) and CTGF, known to be involved in glomerulosclerosis and interstitial fibrosis (Figure 4, A and B, supplemental Figure 5B and Supplemental Table 3)[12,23,10]. However, we did not find any activation of pathways related to TGFβ despite its established role in glomerulosclerosis. Immunostaining for Ki67 (Figure 4C and D) and Tenascin C (Supplemental Figure 6) in 6-month-old mice confirmed extensive cell cycle and ECM remodelling, respectively, in the glomeruli of κF-DH mice.

LCDD LC induces endoplasmic reticulum (ER) stress and sensitizes PC to proteasome inhibitors (PI). Several studies tend to demonstrate that the production of a pathogenic monoclonal Ig or Ig fragment could influence PC fitness and sensitivity to treatments through a general cellular stress involving ER stress, decreased autophagy and oxidative stress.[13,24] To

determine if such cellular stress occurred in PCs producing LCDD LC, we performed RNA-seq on magnetically sorted spleen PCs (>80%) of κF-DH mice compared to WT mice producing polyclonal complete Igs and to DH mice producing polyclonal FLCs. Our data revealed a total of 1946 and 809 expressed genes deregulated in LCDD LC-producing PCs compared to WT and DH controls, respectively (abs(log2FC) $\geq$ 0.7, FDR $\leq$ 0.05). Among these deregulated genes, 722 and 376 were upregulated and 1224 and 433 were downregulated, respectively (Figure 5A). Only genes similarly deregulated in both comparisons (κF-DH *vs* WT and κF-DH *vs* DH) were considered for further analysis (Supplemental Figure 7A). This restricted the analysis to 180 and 213 genes, respectively upregulated and downregulated in κF-DH *vs* both controls (Supplemental Figure 7A and B). C2 canonical pathway analysis (MSignDB v6.2) found that among upregulated genes, the only significant pathways were related to the unfolded protein response (UPR) (Figure 5B and Supplemental Table 4). Genes of the UPR pathway upregulated in κF-DH PCs *vs* each control (WT and DH) are indicated on the MA-plots (Figure 5A) showing that they were not only upregulated but, as expected, also highly expressed in PCs.[25] Activated pathways in each comparison are depicted in supplemental Figure 7C. GO biological process analysis showed that nine out of the twenty most significant overlaps and the three most significant pathways were related to topologically incorrect proteins and ER stress, further suggesting that the activation of the UPR was likely due to the pathogenic LCDD LC (Figure 5C and Supplemental Table 5). Downregulated genes were associated with ECM modification, hematopoietic lineage and G protein-coupled protein signalling (Supplemental Table 6). We performed real-time PCR on selected genes (Herpud1, Hspa5, Ddit3, Xbp1s) and confirmed a similar tendency for upregulation of genes involved in UPR even if, consistent with RNA-Seq analysis, no increase in Xbp1s was observed (Figure 5D). We next verified if such ER stress could sensitize PCs to PI.[13] We treated mice with suboptimal doses of bortezomib (Bz) for

two consecutive days to evaluate the level of PC depletion. This protocol led to a partial (about 2 fold) reduction of the absolute number of PCs in WT and DH mice (45.16 % and 57.54 % of depletion, respectively) as previously demonstrated.[13] In contrast, PC depletion in κF-DH mice was far more efficient than in control mice with a mean depletion of 84.46 % corresponding to 6.44 fold reduction in absolute PC number (Figure 5E).

Removal of circulating LC leads to a rapid decrease of renal LC deposits and protects mice from kidney failure. The efficient response to PI prompted us to evaluate the effect of LC removal on renal lesions evolution. Weekly injections of Bz plus cyclophosphamide were performed on 6-month-old mice during 2 months and compared to age-matched untreated mice. All mice were subsequently sacrificed at the end of the treatment for histological studies. The treatment led to an almost complete (> 90% of reduction) and sustained depletion of circulating κLC (Figure 6A). Treatment completely protected mice from kidney dysfunction (Figure 6B) and early death (Figure 6C) and treated mice presented significantly less abundant renal LC deposits as compared to non-treated mice (Figure 6D and E). Interestingly, kidney lesions after treatment (at 8 months) were also significantly lower as compared to younger mice at 6 months (Figure 6D and E). PAS staining showed glomeruli of smaller size in treated κF-DH mice as compared to 6-month-old mice and EM analysis revealed less marked glomerulosclerosis and the absence of thrombotic microangiopathy-like lesions, despite persistence of diffuse thickening of glomerular BMs (Figure 6D). While serum creatinine was significantly increased in non-treated mice associated with an increase of serum FLC, it was maintained at normal levels in treated mice (Figure 6A and B), which, compared to control 6-month-old mice, showed slight but non-significant increase in albuminuria (Figure 6F) and no rise of serum FLC (Figure 6A).

Discussion

We herein described the first transgenic mouse model fully reproducing specific renal lesions and kidney dysfunction observed in human LCDD. We previously characterized another model of MIDD using a similar transgenic strategy, *i.e.* targeted insertion of a human truncated γ1 HC obtained from a patient with biopsy-proven HCDD, into the mouse κ locus.[13] In this model, the pathogenic Ig induced kidney lesions closely resembling those observed in human MIDD, except glomerulosclerosis, a hallmark of HCDD,[5] and glomerular dysfunction. We first suspected the role of genetic background (C57/BL6 and 129SV)[26–28] but we could not exclude that the low level of circulating HC (~30-40 µg/ml) precluded pathological progression of the disease. In the present LCDD mouse model, we used a new strategy to obtain high levels of circulating human FLC.[29,14] We inserted the pathogenic V domain of a human LC into the κ locus and crossed the mice with DH-LMP2A mice that display increased PC development in the absence of Ig heavy chains.[16,30,14] Production of a chimeric FLC occurred in virtually all PCs and κLC serum levels reached 1g/l in κF-DH mice, which is similar to that observed in LCDD patients.[19] Similar productions were obtained in other unpublished models of MGRS,[14] making this strategy a powerful tool to study the pathogenicity of monoclonal LCs *in vivo*.

Accordingly, κF-DH mice recapitulate progressive glomerular lesions closely resembling those observed in MIDD patients, with linear monoclonal κLC deposits along glomerular and tubular BMs and in the mesangium, with glomerular enlargement and mesangial hyper cellularity, resulting in albuminuria. The lesions eventually lead to nodular glomerulosclerosis and end-stage kidney failure within the first year. Then we first confirmed that the V domain bears alone the pathogenic properties of LCCD LCs, similarly to what we shown in a model of LC-induced Fanconi syndrome.[15] It does not mean that C domain could not play a positive

or negative role in the deposition process and it would have been interesting to compare with the full length human LC. Unfortunately, our attempts to obtain such a model with insertion of the complete cDNA in the κ locus were unfruitful with very low expression of the transgene (unpublished data). Tumor graft models could be advantageously use to compare full length with chimeric LC or to test V domain mutations that could be involved in the deposition of the LC.[20,31] If the pathological lesions slowly progress during the first months, the occurrence of kidney dysfunction with increased serum creatinine, appears to be more sudden and unpredictable, requiring careful follow-up of mice after the sixth month. All these features make the κF-DH mice an accurate model to study the pathophysiology of MIDD, but also other kidney diseases featuring nodular glomerulosclerosis, particularly DN. Indeed, κF-DH mice recapitulate all the criteria used to validate the glomerular lesions of DN as established by the Diabetic Complications Consortium[32] and could be advantageously used to decipher common pathways involved in mesangial cell proliferation and ECM expansion leading to glomerulosclerosis. Nodular glomerulosclerosis has been widely studied, especially in the context of DN[33,32,34] and LCDD,[35,8,11] highlighting a role for TGFβ signalling and PDGF. However, due to the lack of relevant animal models reproducing the chronic progression of kidney lesions, it is still unclear whether TGFβ and PDGF are early mediators of glomerulosclerosis or if they are involved latter, enhancing and accelerating terminal fibrosis of the glomeruli. When we performed RNA sequencing on glomeruli from 6-month-old LCDD mice which display abundant LC deposits but no glomerulosclerosis, we did not find any activation of the TGFβ or PDGF pathways despite already present ECM deregulation, as indicated by the overexpression of Tenascin C.[12,10,36] Tenascin C is an ubiquitous component of the expanded glomerular ECM in pathologic conditions, including DN.[37] More specifically, it has been characterized as one the main component of abnormal ECM produced by mesangial cells following LCDD LC exposure but not AL LC, likely due

to the concomitant overexpression of matrix metalloproteinases (MMPs) that degrade ECM components in the latter case.[9,10] We observed a slight but significant increase of CTGF, known for its pro-fibrotic properties in damaged tissues including the kidney.[23,38] The most prominent early effect of LC deposition in our model was the induction of proliferation, as observed by RNA-seq and Ki67 staining. This result is consistent with the presence of hypercellularity and enlargement of glomeruli that precede glomerulosclerosis and kidney dysfunction. Similar studies in mice with more advanced disease stages or in treated *vs* non-treated mice, deserve to be carried out to decipher the sequential molecular events leading to glomerulosclerosis, but our results suggest that TGFβ overproduction and its consequences are secondary events following LC-induced proliferation of mesangial cells and production of abnormal ECM. Understanding the pathways linking LC deposition and cellular proliferation should likely give new insights in the pathophysiology of the disease.

Recent studies have highlighted the efficiency of PI-based treatment in patients with MIDD, as already demonstrated in AL-amyloidosis.[39–42,19,5] We confirmed this observation in our mouse model. This regimen led to a rapid hematological response with almost complete and sustained depletion of circulating FLC leading to a significant improvement in kidney lesions. Interestingly, kidney lesions were significantly decreased compared to those observed in animals at age corresponding to the beginning of treatment, highlighting a possible "cleaning" mechanism leading to the elimination of the LC deposits. This improvement in kidney lesions was also characterized by normalization of the glomerular size and the absence of thrombotic microangiopathy-like lesions occasionally observed in six-month-old mice. Although complete recovery was not achieved after 2 months as observed by electron microscopy, the treatment was sufficient to maintain normal serum creatinine levels. This result is in accordance with studies of human diseases, including DN[43,44] which showed that glomerulosclerosis at early stages can be reversed with efficient treatment, although this

process in humans can take several years. In mouse models, however, the reversibility was demonstrated after short term treatment in DN[45,46] or hypertension-related glomerulosclerosis.[47] Accordingly, we demonstrated the almost complete reversibility of kidney lesions in LCDD-induced glomerulosclerosis following LC depletion. Further studies are needed to confirm if long-term LC removal could lead to complete renal recovery, to decipher the involved mechanisms and to test therapeutic strategies that could accelerate this process. In this latter view, it seems that therapy based on mesenchymal stem cells could be a valuable approach, as demonstrated in rodent models of glomerulopathies[48,49] or more recently in *ex vivo* models of monoclonal LC-induced glomerular damages.[50] Our model also enabled us to analyse the intrinsic toxicity of pathogenic monoclonal LC for PCs. Similarly to what was shown in patients with MIDD[51,19,5,7] and in the HCDD model,[13] PCs producing LCDD LC are highly sensitive to PI. We assume that mouse PCs are quite different from dysplasic human PCs, in that genomic alterations other than the sole LC production could explain such sensitivity. However, on the contrary, differences in PI sensitivity in our model uniquely depends on the presence of the human LC since PCs are otherwise strictly identical. We showed that these PCs display a high ER stress and more generally, an overexpression of genes involved in the response to misfolded or unfolded proteins. Similar results have been obtained with PCs forced to express heavy chain only,[52] truncated HC[13] or truncated LC,[53] Collectively, we hypothesize that the high sensitivity to proteasome inhibitors is likely related to the impaired capacity of PCs to cope with the production of an abnormal, aggregation-prone, monoclonal LC, as observed in AL amyloidosis.[24] Using our transgenic strategy, we now have developed several mouse models expressing human LC from other MGRS, including AL amyloidosis and Fanconi syndrome,[14] which will serve to determine if all pathogenic LC are toxic for PCs and to decipher the common pathways leading to ER stress and PI sensitivity.

We describe here the first mouse model fully recapitulating the features of MIDD, including glomeruloslerosis and end stage kidney disease. Compared to other models of chronic kidney diseases, the development of kidney dysfunction relies on the natural causing factor (*i.e.* monoclonal LC) without any chemical or physical induction or genetic mutations artificially triggering the disease.[54] Consequently, such a model will likely be useful to understand the molecular mechanisms leading to glomerulosclerosis in MIDD but also other chronic kidney diseases such as diabetic nephropathy. It also confirms the toxicity of abnormal LC for PCs and will likely serve to design and test new therapeutic strategies for MIDD and other related diseases.

Acknowledgments

The authors thank the staff of the BISCEm technical platforms at the University of Limoges (Animal facility, cell cytometry, microscopy, transgenesis and bioinformatics facilities), the Department of Pathology of Poitiers, L. Magnol and K. Vuillier for access to the Konelab 30 analyser and A. Garot for helpful discussions. This work was supported by grants from Fondation Française pour la Recherche contre le Myélome et les Gammapathies monoclonales, Limousin committees of Ligue nationale contre le cancer, Fondation pour la Recherche Médicale, Agence régionale de la santé and Institut Universitaire de France. S.B. is supported by Centre Hospitalier Universitaire Dupuytren Limoges and Plan National Maladies Rares. M.V.A., A.B. and M.O.A were funded by fellowships from Région Limousin (now Région Nouvelle Aquitaine), French ministry of research and Agence de Valorisation de la recherche de l'université de Limoges. M.V.A is funded by a fellowship from Fondation ARC pour la recherche sur le cancer.

Author contributions

SB designed, performed, and analyzed experiments and drafted the manuscript ; MVA performed and analyzed experiments and drafted the manuscript ; AB designed, performed, and analyzed some experiments ; VJ drafted parts of the manuscript and provided general advice ; AR, NQ, SK, CC, CO, ZO and MOA performed and analyzed some experiments ; FB, BH, AP and NP performed the biostatistics and bioinformatics on RNA-seq data ; GT analyzed and provided advices on kidney pathology ; AJ, LD, MC provided general advice and reviewed the manuscript ; FB analyzed data and critically reviewed the manuscript ; CS designed and analyzed experiments, supervised research and wrote the manuscript.

Conflict-of-interest disclosure

The authors declare no competing financial interests.

References

1. Leung N, Bridoux F, Hutchison CA, et al. Monoclonal gammopathy of renal significance: when MGUS is no longer undetermined or insignificant. *Blood*. 2012;120(22):4292–4295.
2. Bridoux F, Leung N, Hutchison CA, et al. Diagnosis of monoclonal gammopathy of renal significance. *Kidney Int.* 2015;87(4):698–711.
3. Preud'homme JL, Aucouturier P, Touchard G, et al. Monoclonal immunoglobulin deposition disease (Randall type). Relationship with structural abnormalities of immunoglobulin chains. *Kidney Int.* 1994;46(4):965–972.

4. Preud'homme JL, Aucouturier P, Touchard G, et al. Monoclonal immunoglobulin deposition disease: a review of immunoglobulin chain alterations. *Int. J. Immunopharmacol.* 1994;16(5–6):425–431.
5. Bridoux F, Javaugue V, Bender S, et al. Unravelling the immunopathological mechanisms of heavy chain deposition disease with implications for clinical management. *Kidney Int.* 2017;91(2):423–434.
6. Kaplan B, Livneh A, Gallo G. Charge differences between in vivo deposits in immunoglobulin light chain amyloidosis and non-amyloid light chain deposition disease. *Br. J. Haematol.* 2007;136(5):723–728.
7. Joly F, Cohen C, Javaugue V, et al. Randall-type monoclonal immunoglobulin deposition disease: novel insights from a nationwide cohort study. *Blood*. 2019;133(6):576–587.
8. Russell WJ, Cardelli J, Harris E, Baier RJ, Herrera GA. Monoclonal light chain--mesangial cell interactions: early signaling events and subsequent pathologic effects. *Lab. Investig. J. Tech. Methods Pathol.* 2001;81(5):689–703.
9. Keeling J, Herrera GA. Matrix metalloproteinases and mesangial remodeling in light chain–related glomerular damage. *Kidney Int.* 2005;68(4):1590–1603.
10. Keeling J, Herrera GA. An in vitro model of light chain deposition disease. *Kidney Int.* 2008;75(6):634–645.
11. Herrera GA, Turbat-Herrera EA, Teng J. Animal Models of Light Chain Deposition Disease Provide a Better Understanding of Nodular Glomerulosclerosis. *Nephron*. 2016;132(2):119–136.
12. Yang CW, Hattori M, Vlassara H, et al. Overexpression of transforming growth factor-beta 1 mRNA is associated with up-regulation of glomerular tenascin and laminin gene expression in nonobese diabetic mice. *J. Am. Soc. Nephrol. JASN*. 1995;5(8):1610–1617.
13. Bonaud A, Bender S, Touchard G, et al. A mouse model recapitulating human monoclonal heavy chain deposition disease evidences the relevance of proteasome inhibitor therapy. *Blood*. 2015;126(6):757–765.
14. Sirac C, Herrera GA, Sanders PW, et al. Animal models of monoclonal immunoglobulin-related renal diseases. *Nat. Rev. Nephrol.* 2018;14(4):246–264.
15. Sirac C, Bridoux F, Carrion C, et al. Role of the monoclonal kappa chain V domain and reversibility of renal damage in a transgenic model of acquired Fanconi syndrome. *Blood*. 2006;108(2):536–543.
16. Casola S, Otipoby KL, Alimzhanov M, et al. B cell receptor signal strength determines B cell fate. *Nat. Immunol.* 2004;5(3):317–327.
17. Neubert K, Meister S, Moser K, et al. The proteasome inhibitor bortezomib depletes plasma cells and protects mice with lupus-like disease from nephritis. *Nat. Med.* 2008;14(7):748–755.
18. Takemoto M, Asker N, Gerhardt H, et al. A new method for large scale isolation of kidney glomeruli from mice. *Am. J. Pathol.* 2002;161(3):799–805.
19. Cohen C, Royer B, Javaugue V, et al. Bortezomib produces high hematological response rates with prolonged renal survival in monoclonal immunoglobulin deposition disease. *Kidney Int.* 2015;88(5):1135–1143.
20. Khamlichi AA, Rocca A, Touchard G, et al. Role of light chain variable region in myeloma with light chain deposition disease: evidence from an experimental model. *Blood*. 1995;86(10):3655–3659.
21. Subramanian A, Tamayo P, Mootha VK, et al. Gene set enrichment analysis: A knowledge-based approach for interpreting genome-wide expression profiles. *Proc. Natl. Acad. Sci.* 2005;102(43):15545–15550.
22. Liberzon A, Birger C, Thorvaldsdóttir H, et al. The Molecular Signatures Database Hallmark Gene Set Collection. *Cell Syst.* 2015;1(6):417–425.

23. Gupta S, Clarkson MR, Duggan J, Brady HR. Connective tissue growth factor: potential role in glomerulosclerosis and tubulointerstitial fibrosis. *Kidney Int.* 2000;58(4):1389–1399.
24. Oliva L, Orfanelli U, Resnati M, et al. The amyloidogenic light chain is a stressor that sensitizes plasma cells to proteasome inhibitor toxicity. *Blood*. 2017;129(15):2132–2142.
25. Tellier J, Shi W, Minnich M, et al. Blimp-1 controls plasma cell function through the regulation of immunoglobulin secretion and the unfolded protein response. *Nat. Immunol.* 2016;17(3):323–330.
26. Zheng F, Striker GE, Esposito C, Lupia E, Striker LJ. Strain differences rather than hyperglycemia determine the severity of glomerulosclerosis in mice. *Kidney Int.* 1998;54(6):1999–2007.
27. Ma L-J, Fogo AB. Model of robust induction of glomerulosclerosis in mice: importance of genetic background. *Kidney Int.* 2003;64(1):350–355.
28. Qi Z, Fujita H, Jin J, et al. Characterization of susceptibility of inbred mouse strains to diabetic nephropathy. *Diabetes*. 2005;54(9):2628–2637.
29. Sirac C, Bender S, Jaccard A, et al. Strategies to model AL amyloidosis in mice. *Amyloid Int. J. Exp. Clin. Investig. Off. J. Int. Soc. Amyloidosis*. 2011;18 Suppl 1:40–42.
30. Lechouane F, Bonaud A, Delpy L, et al. B-cell receptor signal strength influences terminal differentiation. *Eur. J. Immunol.* 2013;43(3):619–628.
31. Decourt C, Rocca A, Bridoux F, et al. Mutational analysis in murine models for myeloma-associated Fanconi's syndrome or cast myeloma nephropathy. *Blood*. 1999;94(10):3559–3566.
32. Brosius FC, Alpers CE, Bottinger EP, et al. Mouse models of diabetic nephropathy. *J. Am. Soc. Nephrol. JASN*. 2009;20(12):2503–2512.
33. Chen S, Jim B, Ziyadeh FN. Diabetic nephropathy and transforming growth factor-beta: transforming our view of glomerulosclerosis and fibrosis build-up. *Semin. Nephrol.* 2003;23(6):532–543.
34. Hu C, Sun L, Xiao L, et al. Insights into the Mechanisms Involved in the Expression and Regulation of Extracellular Matrix Proteins in Diabetic Nephropathy. *Curr. Med. Chem.* 2015;22(24):2858–2870.
35. Zhu L, Herrera GA, Murphy-Ullrich JE, Huang ZQ, Sanders PW. Pathogenesis of glomerulosclerosis in light chain deposition disease. Role for transforming growth factor-beta. *Am. J. Pathol.* 1995;147(2):375–385.
36. Fu H, Tian Y, Zhou L, et al. Tenascin-C Is a Major Component of the Fibrogenic Niche in Kidney Fibrosis. *J. Am. Soc. Nephrol. JASN*. 2016;
37. Truong LD, Pindur J, Barrios R, et al. Tenascin is an important component of the glomerular extracellular matrix in normal and pathologic conditions. *Kidney Int.* 1994;45(1):201–210.
38. Sonnylal S, Shi-wen X, Leoni P, et al. Selective Expression of Connective Tissue Growth Factor in Fibroblasts In Vivo Promotes Systemic Tissue Fibrosis. *Arthritis Rheum.* 2010;62(5):.
39. Kastritis E, Wechalekar AD, Dimopoulos MA, et al. Bortezomib with or without dexamethasone in primary systemic (light chain) amyloidosis. *J. Clin. Oncol. Off. J. Am. Soc. Clin. Oncol.* 2010;28(6):1031–1037.
40. Jaccard A, Comenzo RL, Hari P, et al. Efficacy of bortezomib, cyclophosphamide and dexamethasone in treatment-naïve patients with high-risk cardiac AL amyloidosis (Mayo Clinic stage III). *Haematologica*. 2014;99(9):1479–1485.
41. Reece DE, Hegenbart U, Sanchorawala V, et al. Long-term follow-up from a phase 1/2 study of single-agent bortezomib in relapsed systemic AL amyloidosis. *Blood*. 2014;124(16):2498–2506.

42. Patel K, Dillon JJ, Leung N, et al. Use of Bortezomib in Heavy-Chain Deposition Disease: A Report of 3 Cases. *Am. J. Kidney Dis. Off. J. Natl. Kidney Found.* 2014;
43. Fioretto P, Steffes MW, Sutherland DE, Goetz FC, Mauer M. Reversal of lesions of diabetic nephropathy after pancreas transplantation. *N. Engl. J. Med.* 1998;339(2):69–75.
44. Yang H-C, Fogo AB. Mechanisms of disease reversal in focal and segmental glomerulosclerosis. *Adv. Chronic Kidney Dis.* 2014;21(5):442–447.
45. Pichaiwong W, Hudkins KL, Wietecha T, et al. Reversibility of structural and functional damage in a model of advanced diabetic nephropathy. *J. Am. Soc. Nephrol. JASN*. 2013;24(7):1088–1102.
46. Conway BR, Betz B, Sheldrake TA, et al. Tight blood glycaemic and blood pressure control in experimental diabetic nephropathy reduces extracellular matrix production without regression of fibrosis. *Nephrol. Carlton Vic*. 2014;19(12):802–813.
47. Aldigier JC, Kanjanbuch T, Ma L-J, Brown NJ, Fogo AB. Regression of Existing Glomerulosclerosis by Inhibition of Aldosterone. *J. Am. Soc. Nephrol.* 2005;16(11):3306–3314.
48. Kunter U, Rong S, Djuric Z, et al. Transplanted mesenchymal stem cells accelerate glomerular healing in experimental glomerulonephritis. *J. Am. Soc. Nephrol. JASN*. 2006;17(8):2202–2212.
49. Lv S, Liu G, Sun A, et al. Mesenchymal stem cells ameliorate diabetic glomerular fibrosis in vivo and in vitro by inhibiting TGF-β signalling via secretion of bone morphogenetic protein 7. *Diab. Vasc. Dis. Res.* 2014;11(4):251–261.
50. Herrera GA, Teng J, Zeng C, et al. Phenotypic plasticity of mesenchymal stem cells is crucial for mesangial repair in a model of immunoglobulin light chain-associated mesangial damage. *Ultrastruct. Pathol.* 2018;42(3):262–288.
51. Kastritis E, Migkou M, Gavriatopoulou M, et al. Treatment of light chain deposition disease with bortezomib and dexamethasone. *Haematologica*. 2009;94(2):300–302.
52. Zhou P, Ma X, Iyer L, Chaulagain C, Comenzo RL. One siRNA pool targeting the λ constant region stops λ light-chain production and causes terminal endoplasmic reticulum stress. *Blood*. 2014;123(22):3440–3451.
53. Srour N, Chemin G, Tinguely A, et al. A plasma cell differentiation quality control ablates B cell clones with biallelic Ig rearrangements and truncated Ig production. *J. Exp. Med.* 2016;213(1):109–122.
54. Betz B, Conway BR. An Update on the Use of Animal Models in Diabetic Nephropathy Research. *Curr. Diab. Rep.* 2016;16(2):18.

Figure legends:

Figure 1: **Strategy to produce high amounts of a human kappa light chain (**κLC) **in mouse.** (A) The strategy consists in replacing the Jκ segments in a wild-type (WT) unrearranged mouse κ locus by a human VJ exon/neomycin cassette. The absence of the Jκ segments in the newly recombined κ locus blocks all possibilities of endogenous rearrangements. A cre-mediated deletion of the neomycin resistance gene leads to the production of a chimeric human VJ/mouse κ constant light chain. (B) Breeding with DH-LMP2A (DH) mice enables the production of only free light chain (FLC) by B and plasma cells (PCs). (C) Flow cytometry analysis of PCs isolated from spleen and stained with an anti-mouse CD138 and an anti-mouse κ antibodies. Note the increase of PCs in DH models compared to WT and that nearly all PCs are κ+/CD138+ in κF-DH mice. (D) Western blot analysis of the produced κLC in sera of κF-DH, DH and WT mouse with an anti-mouse κ antibody (top) and with an anti-human Vκ4 variable domain (bottom). The bands appears at the expected size of 25 kDa and the anti-human Vκ4 antibody reveals only the chimeric κLC of the κF-DH mice. (E) Serum and urine levels (in µg/mL) of κFLC in 2 months and 5 months-old κF-DH mice compared to 5 months-old DH and WT mice. The κFLC levels increase in κF-DH mice with age. Serum results are expressed in log scale, means are ± SEM.

Figure 2: **Survival analysis and kidney function in κF-DH mice.** (A) Kaplan-Meier overall survival analysis of κF-DH mice (n=12) compared to DH-mice (n=10). Note the short 8.5 months median survival for κF-DH mice compared to DH-mice (all alive at 14 months). (B) Urine albumin and (C) serum creatinine levels in 2 to 8-month-old κF-DH, DH and WT mice, and in κF-DH mice at humane endpoint (ɵ). Urine albumin in κF-DH mice started to increase at 8 months while a strong increase of serum creatinine appeared only in unhealthy mice.

Survival data were analyzed using log-rank (Mantel-Cox) test and comparisons between 2 groups were calculated using the non-parametric Mann-Whitney test. Means are ± SEM and only significant *p* values are indicated. *$p < 0.05$; **$p < 0.01$; ***$p < 0.001$; ****$p < 0.0001$.

Figure 3: **Kidney sections analysis of** κF-DH **mice.** (A) Immunofluorescence microscopy on frozen kidney sections of κF-DH mice using an anti-mouse κ antibody at 2 and 6 months and at humane endpoint, compared to DH control mice. κLC deposits in κF-DH are detectable as soon as the age of 2 months and become intense with age along tubular and glomerular basement membrane and in the mesangium. Lesion scores are indicated (see methods). Original magnification x200. (B) Periodic acid Schiff (PAS) staining performed on paraffin embedded kidney sections showing tubular basement membranes thickening and nodular glomerulosclerosis with mesangial expansion of the extracellular matrix and mesangial cell proliferation. Note the massive enlargement of glomeruli in κF-DH mice. Original magnification x200. (C) Electron microscopy analysis showing in the left panel linear electron-dense deposits in the inner aspect of the glomerular basement membrane (arrowhead). Subendothelial space is extremely widened consistent with thrombotic microangiopathy-like lesions (asterisk). Original magnification x8,000. The right panel shows granular electron-dense deposits in the mesangium (arrow-head). Original magnification x10,000. (D) Immunoelectron microscopy (original magnification x40,000). Presence of anti-κ gold-conjugated particles along the inner aspect of glomerular basement membrane (arrow-head). All data are representative of at least 3 kidneys in each group.

Figure 4: **Glomerular transcriptomic analysis of** κF-DH**.** (A) MA plots of normalized transcript values from κF-DH vs WT (left) and κF-DH vs DH (right) glomeruli (n=4 DH and κF-DH mice and n=5 WT mice). Examples of overexpressed genes in the cell cycle (red) and

matrisome (blue) pathways are represented. (B) Top 20 enriched pathways based on the C2 canonical pathways from the Molecular signature database (MSignDB v6.2). All differentially expressed genes in κF-DH compared to both WT and DH glomeruli (see supplemental Figure 5A) are included in the analysis (155 upregulated and 37 downregulated genes). FDR *q*-value of the overlaps are represented on the bar graphs. (C) Intracellular Ki67 staining on frozen kidney sections of κF-DH compared to DH mice, the analysis was performed on 5 months-old mice. Glomeruli are surrounded and positive cells appear in red (arrowhead). (D) Mean of Ki67 positive cells in glomeruli of a complete kidney section of κF-DH compared to DH mice (n=4 of each strain). Note the increase of Ki67 positive cells in κF-DH glomeruli compared to DH mice. Means are ± SEM and comparisons between 2 groups were calculated using the non-parametric Mann-Whitney test. *$p < 0.05$

Figure 5: **Endoplasmic reticulum (ER) stress and sensitivity to proteasome inhibitors (PI) of** κF-DH **PCs.** (A) MA plots of normalized transcript values from κF-DH vs WT (top) and κF-DH vs DH (bottom) PCs (n=3 mice of each strain). Overexpressed genes, common in both comparisons, from the REACTOME UPR pathway are represented. (B) Significantly enriched pathways based on the C2 canonical pathways from the Molecular signature database (MSignDB v6.2). Analysis was done on the 180 up-regulated genes in κF-DH *vs* both controls (WT and DH PCs). FDR *q*-value of the overlaps are represented on the bar graphs. (C) GO biological process enrichment analysis. The enrichment was done on the 180 up-regulated genes in κF-DH *vs* both controls (WT and DH PCs). FDR *q*-value of the overlaps are represented on the bar graphs. (D) Quantitative transcriptional analysis of ER stress markers Herpud1, Hspa5, Ddit3 and Xbp1s in sorted CD138+ PCs of κF-DH, DH and WT mice. The increase of Herpud1, Hspa5, Ddit3 but not Xbp1s in κF-DH transcripts corroborates the transcriptomic analysis (n = 4 mice of each group) (E) Comparison of the

absolute number of splenic CD138+ PCs between proteasome inhibitor treated (T) mice and non-treated (NT) mice. Percentage of depletion for each group is indicated over the bars (N = 5-8 mice of each group in 3 independent experiments). Means are ± SEM and comparisons between 2 groups were calculated using the non-parametric Mann-Whitney test. ns, non-significant; * $p < 0.05$; ** $p < 0.01$

Figure 6: **Effect of bortezomib/cyclophosphamide-based therapy on survival, renal lesions and function of kF-DH mice.** (A) Serum LC levels (µg/mL) and (B) serum creatinine levels in treated (n=6) and non-treated (n=7) κF-DH mice during the 8 weeks of treatment. Note the absence of kidney dysfunction in treated mice. Statistics at d54 compared end of treatment or sacrifice with d0 (C) Kaplan-Meier overall survival analysis of non-treated versus treated kF-DH mice during the 8 weeks of treatment (from the age of 6 to 8 months). Note that none of the treated mice died during the course of the treatment while half of the non-treated control mice died. Results are from 2 independent experiments (D) Lesions analysis on kidney sections by immunofluorescence microscopy (top), light microscopy (middle) and electron microscopy (bottom) between κF-DH mice at the beginning of the treatment and mice treated/non-treated at the end of the treatment. Note that deposits revealed by immunofluorescence in non-treated mice or mice at the beginning of the treatment totally disappeared in treated mice. LCDD suggestive lesions are also absent in treated mice (no glomerulosclerosis or thrombotic microangiopathy-like lesions). Original magnification x200. (E) Comparison of kappa LC deposits in kidney of κF-DH mice at the age of the beginning of the treatment (6-month-old kF-DH, n = 5) and the kidneys of treated and non-treated mice at the end of the treatment. Evaluation of total deposits, glomerular and tubular, were performed with an anti-mouse kappa LC staining by 4 different experimenters in n = 2 blinded experiments. (F) Urine albumin levels in treated (κF-DH T) and non-treated (κF-DH NT)

mice at the end of treatment compared to six-month old mice (κF-DH). Survival data were analyzed using log-rank (Mantel-Cox) test and comparisons between 2 groups were calculated using the non-parametric Mann-Whitney test. Means are ± SEM and only significant *p* values are indicated. *$p < 0.05$; **$p < 0.01$; ***$p < 0.001$; ****$p < 0.0001$. All statistics at 8 months corresponded to end of treatment or sacrifice at humane endpoint. [a] n= 3 mice.

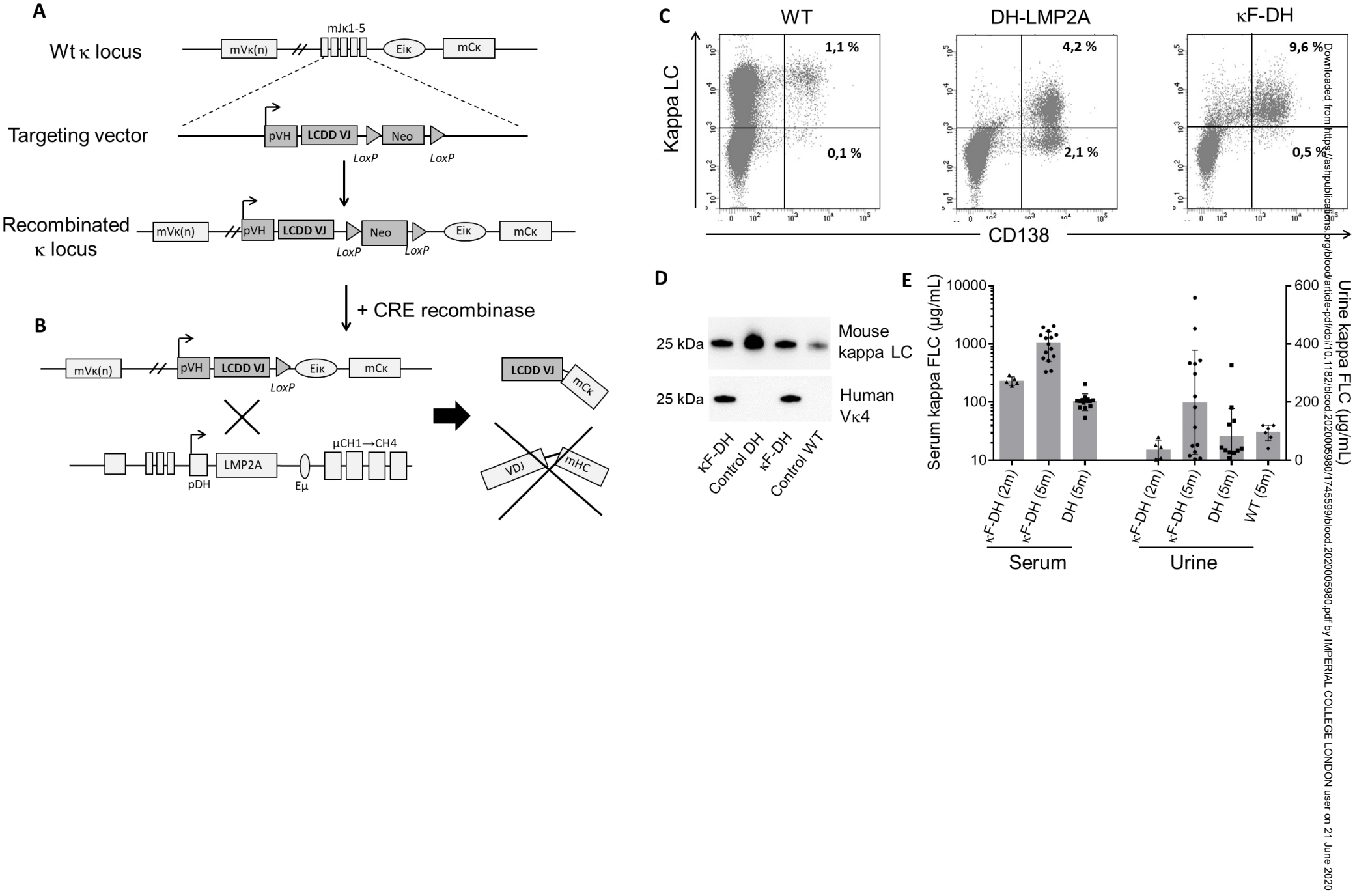

Figure 1

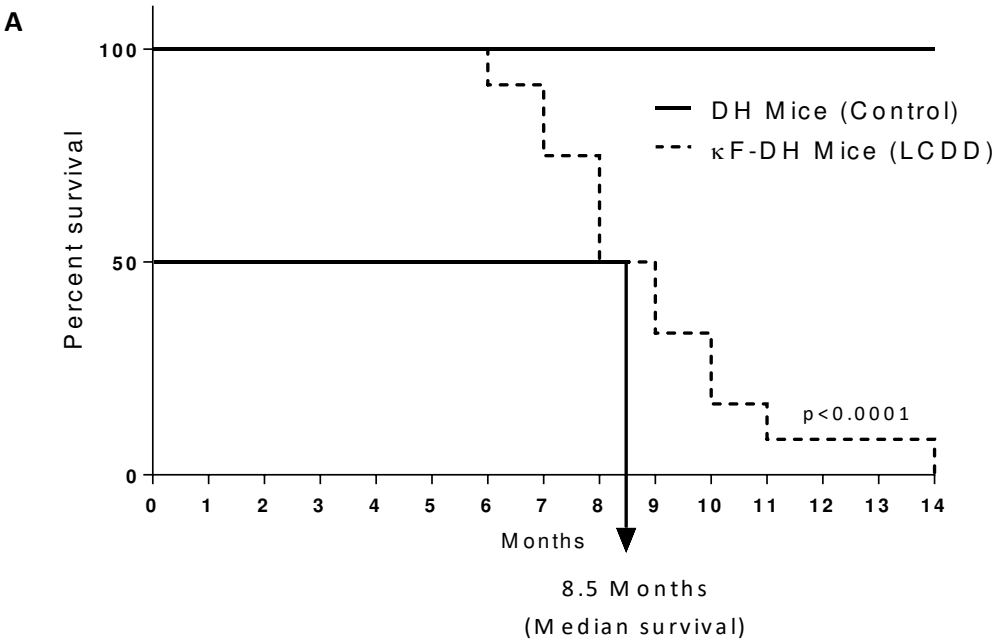

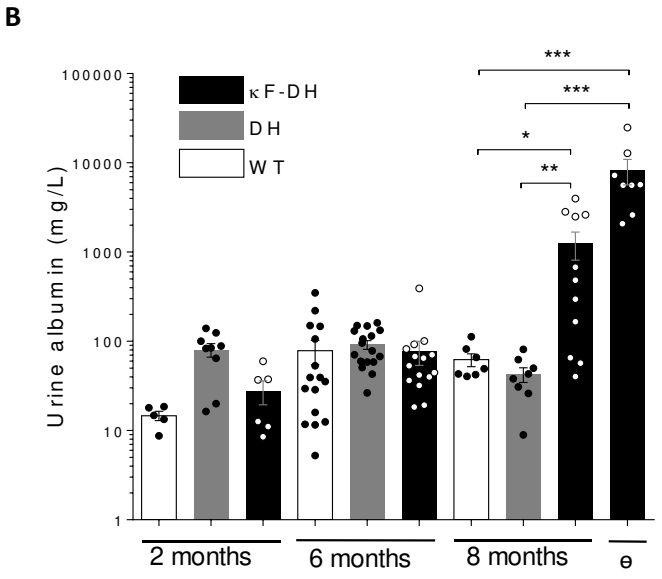

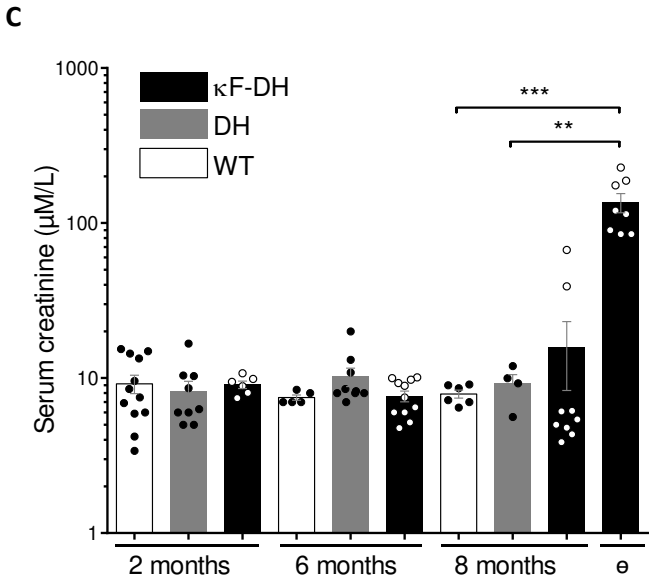

Figure 2

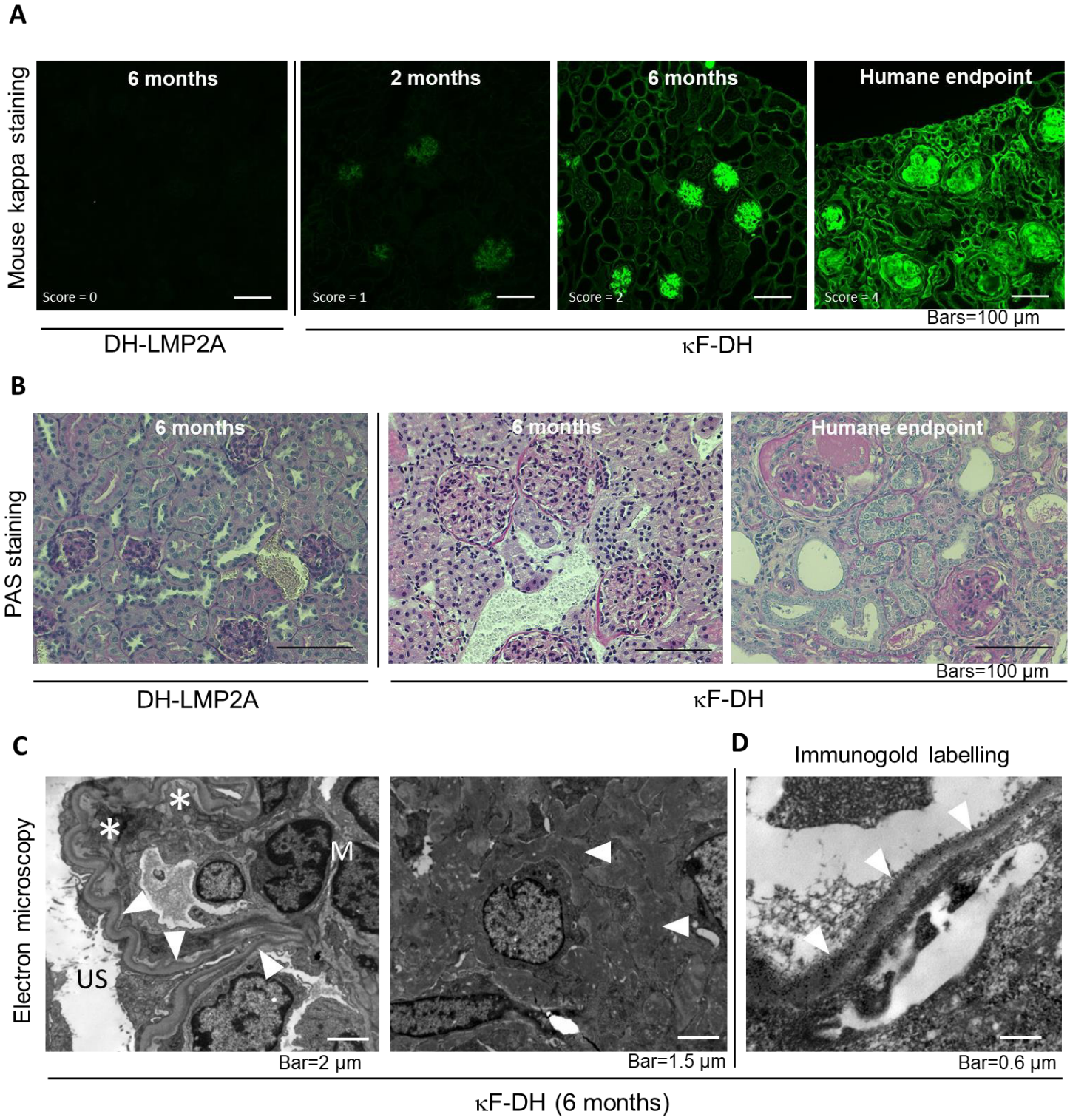

Figure 3

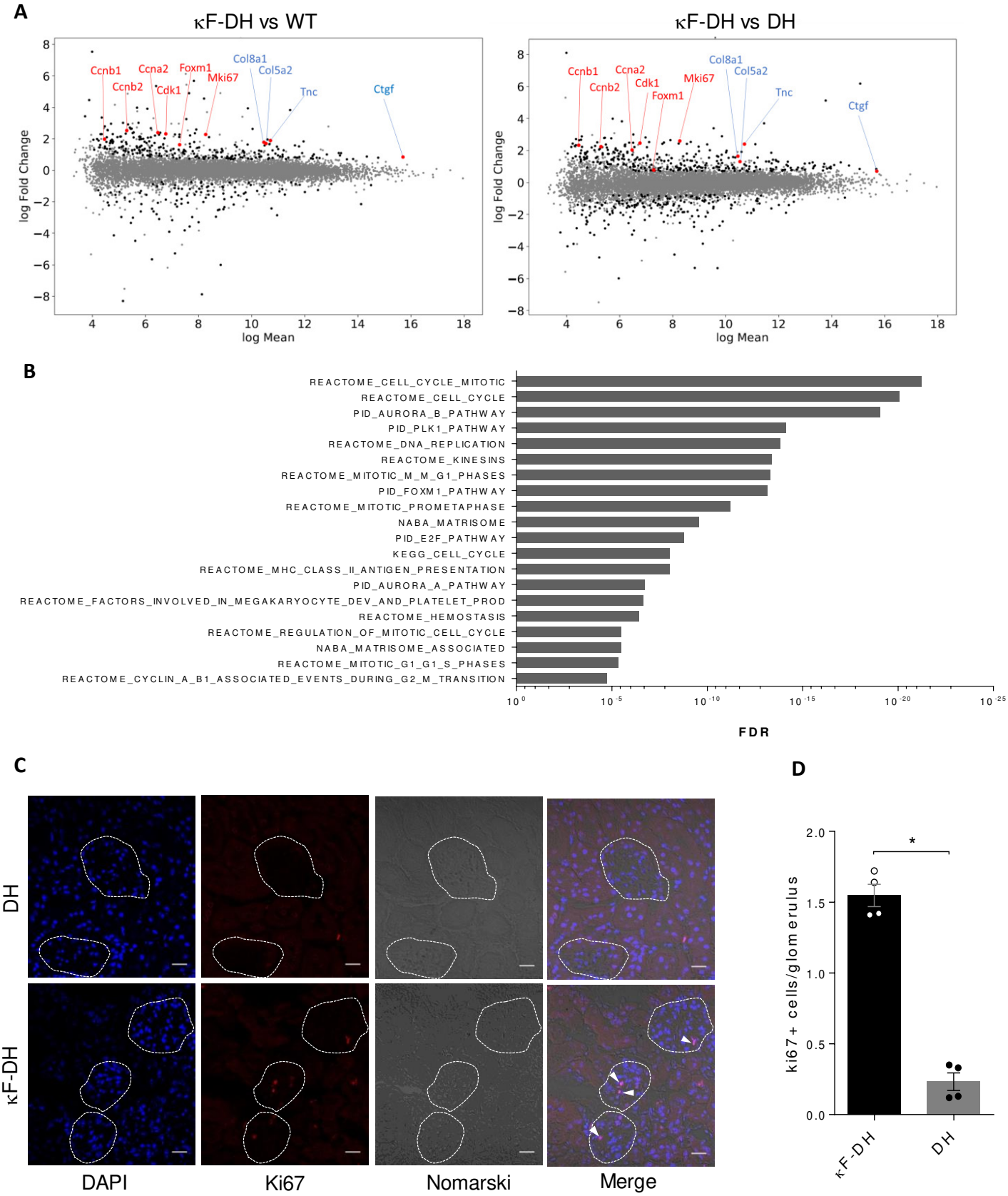

Figure 4

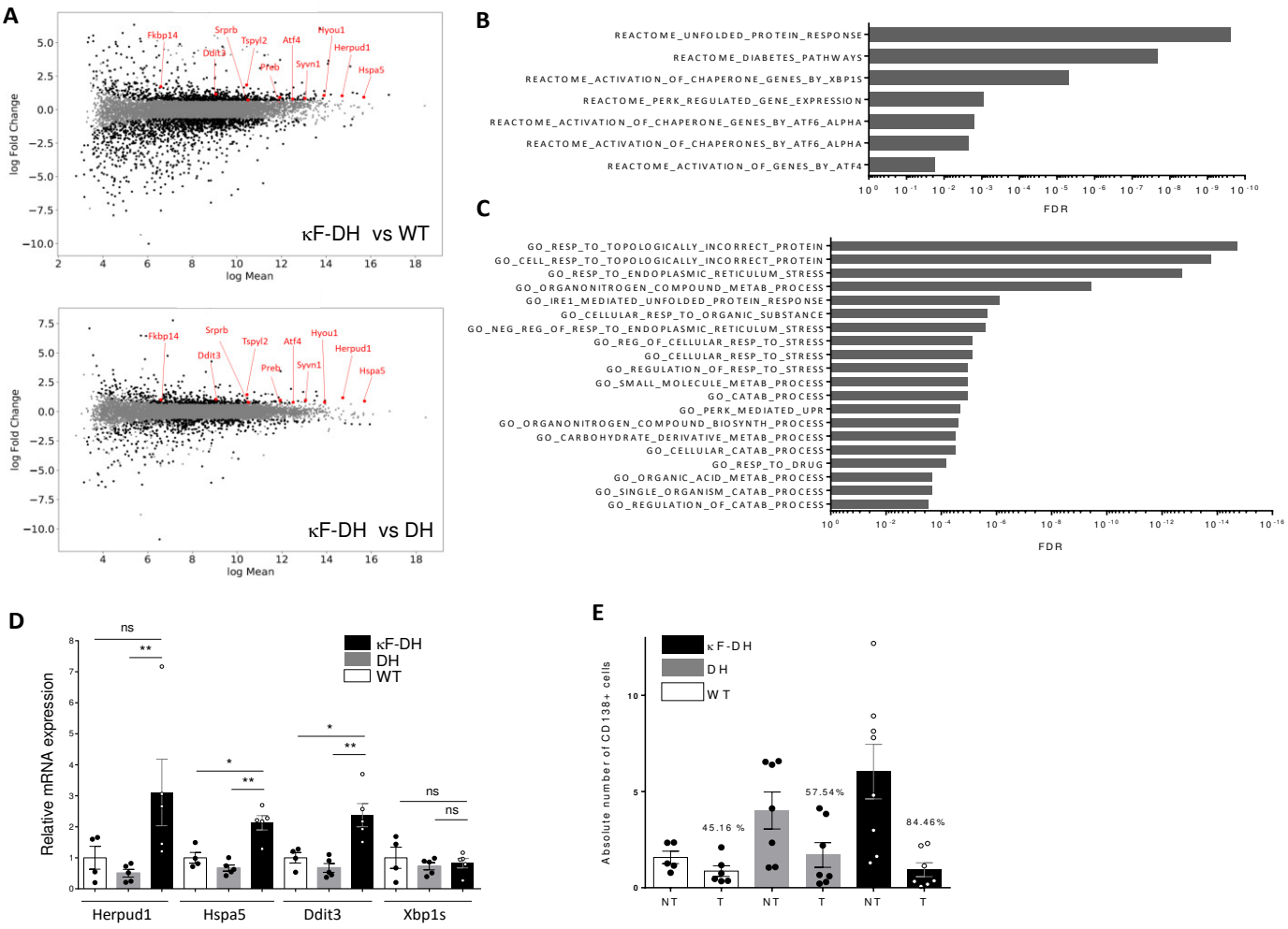

Figure 5

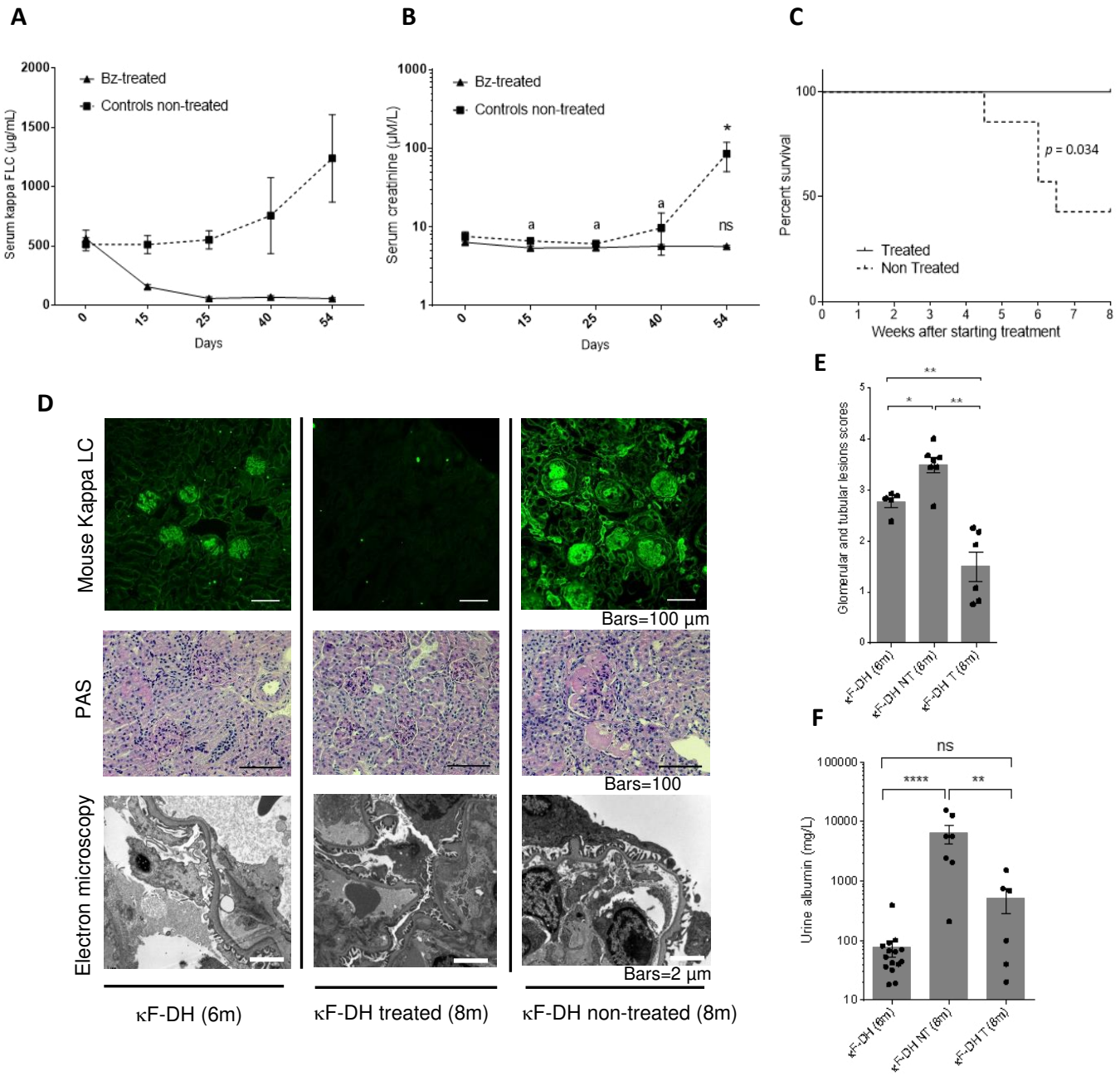

Figure 6

I.2 The challenge in developing an animal model for systemic AL amyloidosis.

While AL Amyloidosis is the most frequent type of systemic amyloidosis, it suffers from the lack of models despite all the efforts worldwide to obtain one. One of the main problems, not only in the research of AL Amyloidosis but in science in general, is that non-productive results or those that do not respond to expectations are put aside, regarded as a failure, or most of the time not shared with the scientific community. This ends up in a waste of precious information and time in the search for better tools for patient management and understanding of the disease.

For almost twenty years now, the laboratory has tried by different strategies to obtain a model for AL Amyloidosis. The first models consisted in the random insertion of an amyloidogenic LC under the control of strong ubiquitous or B cell specific promoters. This always resulted in low levels of circulating LC (below 20µg/ml, which is in the range of FLC in healthy patients) and no amyloid formation. We unquestionably associated the absence of amyloidosis to the low level of free LC in these mice. Consequently, we generated a transgenic mouse line (λS mice) expressing a full-length human lambda LC obtained from a patient with a severe form of AL amyloidosis and additional crossing with DH-LMP2A mice (Casola et al., 2004) resulted in high levels of circulating FLC (λS-DH mice). The development of this model and the encouraging results we recently obtained will be discussed as preliminary results in section I.2.2 of the Results. More recently, we generated a transgenic rat line that is described below.

I.2.1 Rat model expressing a human AL Amyloidosis kappa light chain

Rats present a physiology closely related to humans, as mice do, but they are considered more sensitive to pathogenic lesions and organ failure (Becker and Hewitson, 2013; Iannaccone and Jacob, 2009; Nauta et al., 2000). Since mice were long considered resistant to amyloidosis in general and AL amyloidosis in particular (Buxbaum, 2009), we tried to apply our transgenic strategy to rats.

Thanks to a grant obtained from the French foundation for rare diseases, we generated the first rat model expressing a human AL amyloidosis LC. We used our knock in strategy in the kappa locus using two CRISPRs/Cas9 and a full-length amyloidogenic kappa LC as donor sequence obtained from a patient with severe kidney AL amyloidosis.

Despite the lack of an equivalent DH-LMP2A rat model, we hoped that low levels of pathogenic free LC could be enough to exert a direct toxicity in the organs. Unfortunately, despite a very good expression by most B and plasma cells, we did not detected any deposits or toxicity in this model, likely due, to the good association of human LCs with rat HC, giving rise to only very low levels of free LCs. However, we think that our model could be useful for the amyloid community in search of alternatives to *in vitro* models to test LC toxicity. In the future, with the accelerated creation of new rat models thanks to the CRISPR/Cas9 technology, we also believe that it will be possible to increase the FLC production hoping to obtain amyloid deposits.

Paper 2- Rat model expressing a human AL amyloidosis kappa light chain

MV Ayala, S Bender, I Anegon, S Menoret, F Bridoux, A Jaccard, C Sirac

Submitted to *Amyloid* as a Letter to the editor.

Amyloid

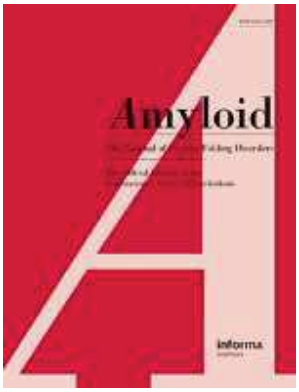

Rat model expressing a human AL Amyloidosis kappa light chain

Journal:	*Amyloid*
Manuscript ID	DAMY-2020-0148
Manuscript Type:	Letter to the Editor
Date Submitted by the Author:	10-Jul-2020
Complete List of Authors:	Ayala, Maria; Limoges University, CRIBL UMR CNRS 7276 INSERM U1262 Bender, Sébastien; Limoges University, CRIBL UMR CNRS 7276 INSERM U1262; University Hospital Centre of Limoges, National referency centre for AL amyloidosis Anegon, Ignacio; University of Nantes, Centre of research in transplantation and immunology, UMR 1064 INSERM Menoret, Séverine ; University of Nantes, Transgenic rats and immunophenomics platform, INSERM 1064 and SFR François Bonamy CNRS UMS3556 Bridoux, Franck; University Hospital Centre Poitiers, Nephrology; University Hospital Centre Poitiers, National Referency centre for AL amyloidosis Jaccard, Arnaud; University Hospital Centre of Limoges, Hematology; University Hospital Centre of Limoges, National referency centre for AL amyloidosis sirac, christophe; Limoges University, CRIBL UMR CNRS 7276 INSERM U1262; University Hospital Centre of Limoges, National referency centre for AL amyloidosis
Keywords:	AL amyloidosis, Transgenic rat, immunoglobulin light chain, rat and mouse model

Rat model expressing a human AL Amyloidosis kappa light chain

Ayala, MV[1]; Bender, S[1]; Anegon, I[2]; Menoret, S[3]; Bridoux, F[1]; Jaccard, A[1];Sirac, C[1]*

[1]*CNRS UMR7276/INSERM U1262, University of Limoges, Limoges, France and French national reference centre for AL amyloidosis and other monoclonal Ig deposition diseases, University hospital of Limoges and Poitiers, France*

[2]*Centre of research in transplantation and immunology, UMR 1064 INSERM, University of Nantes, Nantes France*

[3]*Transgenic rats and immunophenomics platform, INSERM 1064 and SFR François Bonamy CNRS UMS3556, Nantes France.*

*Corresponding author : Christophe SIRAC (UMR CNRS 7276/INSERM U1262, CBRS-Faculté de Médecine, 2 rue du Dr Marcland, 87025 LIMOGES, France)

E-mail: christophe.sirac@unilim.fr

Research on AL amyloidosis suffers from the lack of a reliable animal model that could allow a better understanding of the pathophysiology of the disease and the design of new innovative therapeutic strategies. Even if few mouse models demonstrated the presence of amyloid fibrils, none of them was sufficiently reproducible and physiologically relevant. Other models in non-mammals (worm, zebrafish) were of invaluable interest to decipher several aspects of the disease but remain too far from physiology to consider them enough for therapeutic investigation [1]. Hereby we describe the first transgenic rat expressing an amyloidogenic human immunoglobulin (Ig) light chain (LC).

We have transposed our knock-in strategy used in mice [1] into rats as they could display less resistance to amyloidosis. A patient (ptR) with AL amyloidosis that presented a small excess of VK1-33 kappa free light chain (FLC) (96,5 mg/L FLC at diagnosis) was selected. The patient had some cardiac involvement with NYHA-II and NT-proBNP 194 ng/L but mainly kidney deposits with creatinine and albumin levels at 114 µmol/L and 15,5 g/L, respectively. The rat knock-in model (rR) was generated using CRISPR-Cas9 SgRNA microinjections in zygote, allowing the replacement of Jκ segments in the rat κ locus by the cDNA coding for the complete monoclonal κLC obtained from ptR (Supp. Fig.1A). All experimental procedures have been approved by our institutional review board for animal experimentation and of the French Ministry of Research (APAFIS#16248-2018072412155739). Human Ig κLC is expressed in most B and plasma cells together with rat HC (Supp. Fig.1B). Production of the human LC was evaluated in serum by ELISA for total κLC and Freelite assay (Binding site) for FLC (Figure 1A). The human κLC was readily detected in serum (928.3 µg/ml ± 144.3; mean ± SEM, n=14)

but seemed to be mainly associated with the rat heavy chains (HC) since FLC were not in excess (15.7 µg/ml ± 4.7, n=7). This is further illustrated by the native western blot carried out on serum showing that most κLC is associated with a 150 kDa band corresponding to full length IgG (Figure 1B). Accordingly, urine human κLC was 26.3 µg/ml ± 7.2 (n=15) which is similar to what we found in WT mice [2]. Organs sections from 12 and 24 months old rats showed no evidence of amyloid deposits (n=3 for each age). Immunofluorescence microscopy on frozen kidney, heart, liver and spleen are shown on Figure 1C. Despite abundant LC reabsorption in proximal tubules, kidneys showed normal tubular and glomerular structures with negative Congo Red (CR) under polarizing light with no apparent amyloid deposits (Figure 1C). Since, several studies showed that amyloid LC may exert direct toxicity for organs even in the absence of amyloid fibrils [3,4], we analysed kidney function in 18 month-old rats (n=5). Creatinine levels were 29 µmol/l ± 6.348 which is in a normal range for rats [5]. Moreover, rats seemed to have a normal life span, with no sign of morbidity or deaths in a two-year lapse.

Despite the efficient κLC production by most B and plasma cells, FLC remained low in this model, due to an efficient association of human LCs with rat HCs. This likely account for the absence of amyloid deposits in organs. In mice, we overcame this problem using DH-LMP2A model, which generate B and plasma cells without HCs [1]. Unfortunately, such a model does not exist yet in rats. While our first attempt of modelling AL Amyloidosis in rats does not fulfil its main purpose, *in vivo* production of amyloid LC will be useful to better understand its direct cellular toxicity on mesangial cells or cardiomyocytes. Our study emphasizes the difficulty to develop reliable AL amyloidosis *in vivo* models in rodents and the discrepancies concerning the toxicity of amyloid LC for organs compared to humans, in whom low levels of amyloidogenic LC are enough to exert organ damage. Unraveling these discrepancies could help understand the key factors that could be targeted for novel therapies and further characterizing the disease.

Conflict of Interest

The authors declare that the research was conducted in the absence of any commercial or financial relationships that could be construed as a potential conflict of interest

Funding

This work was supported by grants from Fondation Maladies Rares "Small animal models and rare diseases" program N°20161209. MVA was funded by fellowships from Région Limousin (now Région Nouvelle Aquitaine) and Fondation ARC pour la Recherche sur le Cancer. BS is supported by Centre Hospitalier Universitaire Dupuytren Limoges and Plan National Maladies Rares.

Acknowledgments

The authors thank the staff of the BISCEm technical platforms at the University of Limoges (Animal facility, cell cytometry and microscopy), the Department of Pathology of Poitiers and TACGENE for the CRISPR-Cas9Sg RNA synthesis and selection.

Bibliography

[1] Sirac C, Herrera GA, Sanders PW, Batuman V, Bender S, Ayala MV, et al. Animal models of monoclonal immunoglobulin-related renal diseases. Nat Rev Nephrol 2018;14:246–64. https://doi.org/10.1038/nrneph.2018.8.

[2] Bender S, Ayala MV, Bonaud A, Javaugue V, Carrion C, Oblet C, et al. Immunoglobulin light chain toxicity in a mouse model of monoclonal immunoglobulin light-chain deposition disease. Blood 2020:blood.2020005980. https://doi.org/10.1182/blood.2020005980.

[3] Keeling J, Teng J, Herrera GA. AL-amyloidosis and light-chain deposition disease light chains induce divergent phenotypic transformations of human mesangial cells. Lab Invest 2004;84:1322–38. https://doi.org/10.1038/labinvest.3700161.

[4] Jordan TL, Maar K, Redhage KR, Misra P, Blancas-Mejia LM, Dick CJ, et al. Light chain amyloidosis induced inflammatory changes in cardiomyocytes and adipose-derived mesenchymal stromal cells. Leukemia 2020;34:1383–93. https://doi.org/10.1038/s41375-019-0640-4.

[5] Keppler A, Gretz N, Schmidt R, Kloetzer H-M, Groene H-J, Lelongt B, et al. Plasma creatinine determination in mice and rats: An enzymatic method compares favorably with a high-performance liquid chromatography assay. Kidney Int 2007;71:74–8. https://doi.org/10.1038/sj.ki.5001988.

Legend to figures:

Figure 1. (A) κFLC dosage in patient serum at diagnosis and rR rat serum and total κLC dosage in serum and urine from rR rats. (B) Non-denaturing Western Blot revealed with an anti-human Vκ1 showing the human κLC association in a full-length Ig molecule (150kDa). A slight cross-reactivity with the rat Ig can be observed (CTL= negative control rat). Inset: the 25kDa band corresponding to the human κFLC can be seen only after a longer exposure time. (C) Immunofluorescence microscopy of kidney, heart, spleen and liver sections stained with anti-human κLC-FITC and Congo Red (CR), x200. CR was negative under polarizing light for all sections (not shown). Unmerged images are shown for the kidney only (top panel). Asterisks indicate glomeruli.

Supplemental Figure 1:

Supp. Fig. 1. (A) Transgenic strategy used to generate the knock-in rR rats. The targeting vector containing the amyloidogenic human κLC gene flanked by the 5' and 3' arms of the rat J κ locus was introduced by microinjection in zygote pronucleus together with two cas9/sgRNA ribonucleotides targeting the J κ locus from the rat. Not to scale. (B) Flow cytometry analysis of total spleen cells with anti-rat IgM and anti-human κLC. Percentages for each gate are indicated.

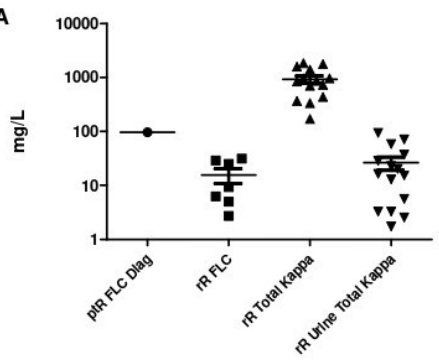
A
10000
1000
100
10
1
mg/L
pIR FLC Diag
rR FLC
rR Total Kappa
rR Urine Total Kappa

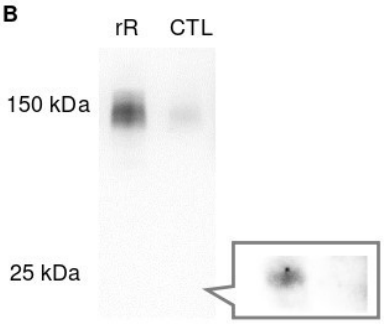
B
rR
CTL
150 kDa
25 kDa

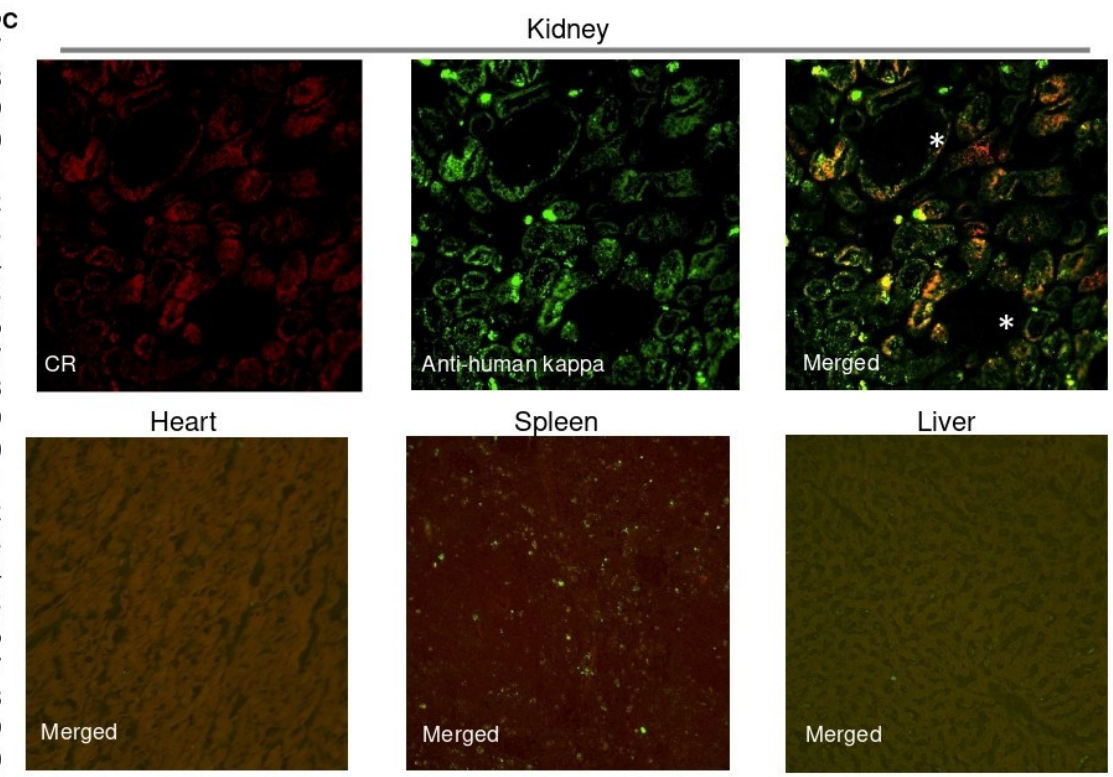
C
Kidney
CR
Anti-human kappa
Merged
Heart
Merged
Spleen
Merged
Liver
Merged

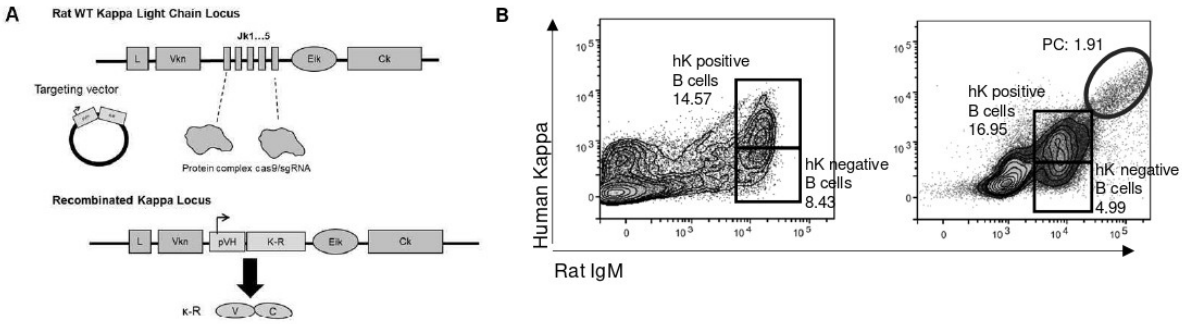
A
Rat WT Kappa Light Chain Locus
JK1...5
L
Vkn
Ek
Ck
Targeting vector
Protein complex cas9/sgRNA
Recombinated Kappa Locus
L
Vkn
pVH
K-R
Ek
Ck
κ-R
V
C
B
Human Kappa
Rat IgM
hK positive
B cells
14.57
hK negative
B cells
8.43
PC: 1.91
hK positive
B cells
16.95
hK negative
B cells
4.99

I.2.2 The pursuit of an animal model for systemic AL amyloidosis

As explained above, a mouse model of AL amyloidosis was created in the laboratory on a similar strategy as the LCDD model (knock-in in the kappa locus and crossing with DH-LMP2A mice). We herein used a full-length human λLC since we were not confident with a chimeric LC composed of a human Vλ domain spliced on a mouse Cκ.

In the next section, presented as preliminary results, we describe this model. We carefully followed up mice at different ages and organs were tested for CR positive staining but unfortunately, no deposits were observed despite levels of free LC exceeding those in the patient.

Therefore, we tried to trigger the amyloid formation by different strategies *in vivo* with no success until we obtained, thanks to a collaboration with Michael Ehrmann's group, fibrils and seeds formed *in vitro* by the VL domain alone. Interestingly, fibrils from the same the full length LC were never obtained, highlighting an inhibitory role of the C domain in amyloidosis formation.

In preliminary results described below, such VL seeds injected in our mouse model gave rise to AL amyloidosis deposits, composed also of the transgenic LC, mostly in heart and spleen. This yearned result opens new lines of investigation to find what protease or process could cause the release of the V domain from the full-length LC, needed for fibril formation, with obvious consequences on therapeutic options. Interestingly, this could also explain why different LC subgroups present specific organ tropisms.

Preliminary results (*ongoing*) - The pursuit of an animal model for systemic AL amyloidosis

MV Ayala, S Bender, L Pedroza, M Merdanovic, V Javauge, A Bonaud, A Rinsant, S Kaaki, C Oblet, C Cogné, M Ehrmann, F Bridoux, A Jaccard, C Sirac

Ayala, MV[1,2]; Bender, S[1,2]; Pedroza, L[3]; Merdanovic, M [3]; Javauge, V[1,2,5]; Bonaud, A[4]; Rinsant, A[5]; Kaaki, S[5]; Oblet C[1]; Cogné, M[1]; Ehrmann, M[3]; Bridoux, F[2,5]; Jaccard, A[1,2,] ; Sirac, C [1,2]

[1]CNRS UMR7276/INSERM U1262, University of Limoges, Limoges, France
[2]French national reference centre for AL amyloidosis and other monoclonal Ig deposition diseases, France
[3]University Duisburg-Essen, Centre for Medical Biotechnology, Essen, Germany
[4]INSERM U1160, Institut of Research Saint Louis, Paris, France.
[5]Department of nephrology, University hospital, Poitiers, France

RESULTS

High levels of production of an amyloidogenic lambda free light chains in mouse is not enough *per s*e to induce AL amyloidosis

For the generation of the transgenic mouse, patient λS-PT was chosen with a Vλ6-57 AL Amyloidosis. This LC gene is well known for being frequently implicated in renal AL amyloidosis. Patient FLC levels at diagnosis were 99.8 mg/L and had 12% of medullar plasma cells (PC) infiltration. The patient presented with cardiac involvement (NYHA-I) as well as kidney deposits (**Figure 1A**) (creatinine: 194 µmol/L and urine albumin 80% with 5.76 g/24 hours proteinuria).

The production of the pathogenic human λS-LC, whose sequence was obtained from the previously mentioned λS-PT patient, was carried out via an adapted method of our Immunoglobulin (Ig) kappa knock-in strategy. Here we introduced the complete human λ-LC sequence in the mouse kappa locus, replacing the Jκ segments, instead of only the human VJ exon sequence spliced on the mouse constant domain, as done for previous models (1). All further kappa rearrangements in homozygous mice are no longer possible and since in mice k/λ ratio expression is of 95:5 (2), this strategy ensures the production by almost all B and PC of the transgenic monoclonal λ- LC.

We have previously noticed that transgenic LCs can associate with the endogenous mouse heavy chains (HC). Therefore, to guarantee the production of unbound free LC, mice were further crossed with DH-LMP2A mice. This mouse line has its HC locus invalidated thanks to the targeted insertion of the Epstein Barr virus protein LMP2A while allowing a normal B cell development and an increased PC numbering (3–5) (**Figure 1B**). Double homozygous λS-DH thus produce only free LC (FLCs) with a high number of PC, mimicking some of the features of monoclonal gammopathies (**Figure 1C**).

As the λS is a fully human LC, FLC serum levels were evaluated by the routine Freelite® assays and showed a median of 387.1 µg/ml ± 68.51 (mean ± SEM, n=14) which is 4 fold more than in the patient λS-PT at diagnostic and similar to the control transgenic mouse line use κR-DH (described in Methods) with a mediam of 359.4 µg/ml ± 68.69 (mean ± SEM, n=5) (**Figure 1D**). We also confirmed the presence of the human Vλ6-LC by Western blot using a mouse anti-Human Vλ6 antibody obtained from Alan Solomon's lab (6) (**Figure 1E**).

In λS-DH mouse line, LCs were highly detectable by immunohisto-fluorescence in tubules of the kidney, corresponding to the reabsorption of the λLC, and in extrafollicular zones of the spleen (PCs). However, there was no overt Congo Red (CR) positive staining colocalized with the LCs by fluorescence and a total absence of apple-green birefringence under polarizing light in any organ, even in old mice (**Figure 2**). Additionally, mice had a normal lifespan compared to control DH-LPM2A mice (*data not shown*) with no signs of morbidity. Creatinine and albumine levels at 8 months old were 4.40 µM/L ± 1.51 (mean ± SEM, n=5), and 43.93 µg/ml ± 9.54 (n=6), respectively, which is comparable to DH-LPM2A mice (3). Altogether, these results showed that the transgenic amyloid LC does not display apparent toxicity despite high levels of circulating FLC.

Unfruitful attempts to trigger fibril formation *in vivo*

While several studies have been carried out *in vitro* for AL amyloidosis, regarding the biochemistry of the amyloidogenic LC or direct organ toxicity (7–9), *in vivo* information of the disease formation remains unclear. In an attempt to trigger fibril formation *in vivo*, we tried several strategies following the logic of the biological knowledge available for amyloid diseases.

Although it has been mainly studied for AA amyloidosis (10) or Aβ and tau proteins (implied in Alzheimer's disease), amyloid cross-seeding can occur when oligomers composed of one misfolded protein induce fibril formation of a different protein (11–14). Since AA amyloidosis (amyloid formed from serum AA protein in a chronic inflammation context) can be easily induced experimentally in mice by different approaches (15–17) we decided to do so in our transgenic mice by injecting amyloid-enhancing factor (AEF) obtained from an AA amyloidosis mouse. While AA Amyloidosis was generated, there was no co-immunostaining of birefringent deposits with the λS-LC (**Figure 3A**). We further used as AEF AL amyloid extracts obtained from the heart of a transplanted patient suffering from a λ-type AL amyloidosis. We hypothesized that such fibrils composed of λ-LC could better work for a cross-seeding in our mouse model. However, its injection in λS-DH mice was unfruitful to induce AL amyloidosis (*images not shown*). Altogether, these results tend to indicate that *in vivo* cross-seeding of AL amyloidosis is not feasible.

Given that, unfortunately, we did not have available tissues from λS-PT, it was not possible to test direct seeding with fibrils from this patient. However, we had serum of λS-PT available from its routine follow-ups. In the hope that the serum would contain the oligomers, or seeds, that could trigger fibrils formation in the transgenic line λS-DH, mice were injected with patient serum containing ~10µg of FLC. Unfortunately, once again, it did not generate amyloid

deposits in the λS-DH mice (**Figure 3B**). We cannot conclude that it was because we did not inject enough FLC or if serum does not contain efficient AEF.

Additionally, focusing on the *in vitro* conditions used to form fibrils, where it has been shown that most of the amyloidogenic LCs aggregate from pH 2.0 to pH4.0 (18), we used an established protocol to create metabolic acidosis in mice (19). At the end of the induced metabolic acidosis, we observed no effect in fibril formation *in vivo,* as there were no CR positive deposits in analysed organs (spleen, kidney) (**Figure 3C**).

Forcing the production of misfolded amyloid LC with proteasome inhibitor treatment

In AL amyloidosis patients, proliferating PCs have accumulated mutations that could decrease their ability to fold the LCs correctly. This could account for the production by these PCs of oligomers or at least some misfolded LCs (20). According to this idea, we thought that maybe healthy PCs from our mouse model only produced a native form of the pathogenic LC and/or degraded faster the misfolded LCs, consequently limiting the appearance of amyloid oligomers. In an attempt to force mouse PCs into accumulating and secreting misfolded LCs, we took advantage of one of the mechanism of action of the widely used proteasome inhibitor Bortezomib (Bz). By blocking the proteasome, Bz induces the accumulation of unfolded proteins in the ER (mostly Ig in PCs), eventually leading to apoptosis through the terminal UPR pathway (21).

λS-DH mice were treated with a sub-optimal dose of Bz, previously shown to induce a slight but significant decrease in PC number (22,3). Strikingly, the levels of LC detected by ELISA 15 days post-treatment were two folds higher than the control (797 µg/ml ± 100.6 vs. 494 µg/ml ± 90, respectively). This increase was not expected but it was suggested that inhibiting intracellular protein degradation in PCs could lead to increased Ig secretion (23) and could be consistent with the secretion of misfolded Ig (20).

Flow cytometry conducted three months after the end of the treatment showed that the PC populations in spleen and bone marrow (**Figure 4A**) were similar to control (**Figure 1B**), indicating a complete recovery from the Bz treatment. When organs were observed by IF and CR staining (**Figure 4B**), all mice were negative for deposits despite the huge reabsorption of λS-LCs in kidney tubules.

***In vitro* fibril formation using the Variable Domain *vs* Full-Length amyloidogenic LC.**

Since no λS LC-composed fibrils were available from the patient, we decided to try to produce such fibrils *in vitro*. This part of the study was conducted in collaboration with Michael Ehmann's group in Germany. We provided them with the purified full-length λS-LC and they produced *in house* the VL domain from the λS-LC as described in the methods. Heparin-induced fibril formation *in vitro* using purified λS-VL was quite easy to obtain and confirmed by Thioflavin T staining (ThT) (**Figure 5A**) and Atomic Force Microscopy (AFM) (**Figure 5B**). Interestingly, attempts to form fibrils with the full- length λS-LC were unsuccessful even for extended times (up to 12 days) (**Figure 5B**). We only detected some amorphous aggregates that stained faintly for ThT (*not shown*). Seeding with short fragments of pre-formed fibrils (hereafter "seeds") induced fibril formation in few hours for λS-VL (**Figure 5A and C**) and its addition slightly improved fibril formation from full-length λS-LC (**Figure 5C**). However, it required several days to obtain only short non-branching fibrils, which sharply contrasted with the few hours needed to form full fibrils with the λS-VL (**Figure 5C**). Higher concentration of full- length λS-LC with seeds λS-VL induced an accumulation as aggregates rather than fibrils and full- length λS-LC alone did not form fibrils either (**Figure 5D**).

To better mimic *in vivo* conditions, we then tried to induce fibrils in the presence of mouse or human sera. Seeds and λS-VL were directly diluted in sera from WT or λS-DH mice and from λS-PT patient, and supplemented with heparin as described in the Methods. Strikingly, none of these conditions gave rise to amyloid fibrils even after 5 days of incubation (**Figure 5E**).

Eureka! Obtaining AL amyloid deposits *in vivo*

Having obtained amyloid fibrils composed by the λS-VL domain, we though to use them as AEF in λS-DH mice. Mice were injected with a mix of λS-VL-seeds / λS-VL-fibrils and their organs analysed at 2 and 4 months. While there were no CR positive deposits in kidney, the spleen and the heart presented with overt amyloid deposits, which were confirmed under polarizing light. CR positive deposits co-localized the anti-human λ-LC staining (**Figure 6A** and **B**). Additionally, deposits in heart and spleen were still detectable 4 months after the injection, highlighting the stability of amyloid deposits (**Figure 7**).

κR-DH mice, expressing a monclonal non-amyloidogenic κ-LC, were used to verify in one hand if the seeds + fibrils injected are sufficient or not to induce amyloidosis, and on the other hand to check if cross-seeding with another monoclonal LC is possible. As seen in **Figure 6**, 2 months after the injection, we did not detect apple-green deposits in heart (**Figure 6A**). Spleen presented with small amorphous aggregates, some of them staining for CR but birefringence is difficult to conclude and we did not observe co-staining with the anti-κLC (**Figure 6B**).

Even if we did not detect amyloidosis in control mice injected with seeds +fibrils mix, we could not definitely exclude that amyloidosis in λS-DH mice was formed only by the injected material rather than elongated by the transgenic λ-LC. However, seeds and fibrils are composed exclusively by the VL domain that should not be recognized by the anti-λ antibody mainly directed against the constant region of the LC. To definitely conclude on the specificity of the antibody used for IF studies, we carried out western blot analysis showing that our anti-λ antibody is specific for the constant part of the human λ-LC and does not recognize the VL seeds (**Figure 8A**). By contrast, an anti-Vλ6 antibody readily detected the seeds together with the transgenic λ-LC (**Figure 8B**). These results endorse the fact that the amyloid deposits are formed, not only by the injected seeds and fibrils, but are elongated with the full-length LC produced by the mouse.

DISCUSSION AND PERSPECTIVES

Thanks to our innovative transgenic approach, we were able to obtain deposition diseases mouse models producing higher levels of FLC than the patients from whom we obtained the LC gene (1). However, in the case of our mouse model of amyloidosis, and contrary to our other mouse models of MGRS (24,3), serum levels do not seem to be the sole factor for amyloid formation in mice, as we did not observe fibril deposits in any organ and at any age.

Our multiple attempts to trigger amyloidosis in our model, including cross-seeding with AL or other amyloid materials, injection of serum from the patient, metabolic acidosis and finally, forcing of misfolded LC production by PCs using bortezomib, were all unsuccessful, emphasizing the resistance of mice to AL amyloidosis.

Since the cross-seeding with fibrils obtained from other patients did not work, as the light chain sequence differs from the one present in our mice, we searched to produce *in vitro* fibrils with the λS-LC. Results from this *in vitro* study first confirmed previous works indicating that VL is more prone to form amyloid fibrils than the full-length LC (9,25–27). In fact, in our hands, the full-length LC was incapable of fibril formation on its own. We also showed that, while λS-VL presented a strikingly high propensity to form amyloid when mixed with VL-seeds, full-length LC poorly formed short and non-branching fibrils in the same conditions.

It is still under debate whether the constant domain of the LC participate or not to amyloid nucleation and/or elongation and if so, what role exactly it plays (28,29,25,27). Mass spectrometry (MS) analysis have shown that AL amyloidosis always contain at least some constant domain fragments (30,31), which in fact is in accordance with routine immunophenotyping mostly using antibodies reacting with CL domains. However, neither the proportion of CL vs VL, nor the sizes of the CL parts in amyloid fibrils are known.

Cryo-Electron Microscopy (EM) studies have recently shed lights on this question, showing that AL fibrils contains mostly VL and that short N-terminal parts of the CL domain can be found in the fibril extracts but do not participate to the fibril core (32,33). Consequently, partial CL fragments could be recognized by antibodies and found in MS studies, without being directly involved in fibril formation. In fact, the total absence of full-length LC in both Cryo-EM studies is consistent with a negative role of the CL domain in AL amyloidosis. In our case, it could also explain the absence of amyloidosis in our mice since only the full-length LC is produced.

Another striking result from our *in vitro* study is the complete inhibition of fibril formation when serum from mice or from λS-PT was added to an otherwise highly amyloidogenic mixture (seeds + λS-VL). If such result could have been expected with serum from WT or λS-DH mice, we were more surprised by the serum from the patient λS that we thought to contain misfolded LCs or oligomers prone to form fibrils. This result highlights the discrepancies between "pure" *in vitro* studies where optimal conditions of buffer, pH and temperature are applied to purified proteins, and *in vivo* conditions, in which the amyloid protein is diluted in saturating non-amyloid serum proteins and imposed pH and buffer.

Despite this disappointing observation, we decided to inject λS-VL fibrils and seeds in λS-DH mice to try to trigger AL amyloidosis. In these preliminary experiments, we decided to inject both since we could not predict if one form is better than the other one. Much to our satisfaction, and in contrast with the *in vitro* data, this yielded amyloid deposits in heart and spleen two months later and remained at least up to 4 months. Since the *in vitro*-produced VL cannot be detected by the antibody use for IF, the positive staining indicated that the seeds or the pre-formed injected fibrils were elongated by full-length LC. Moreover, these deposits seem to be stable, as they were not eliminated 4 months after the injection even if we do not know yet if amyloidosis is increased or not at this time point (not enough mice analysed). We confirmed

that amyloidosis observed in mice is not the sole accumulation of the injected fibrils since no or very few amyloid fibrils were observed when injected in another mouse model producing a monoclonal non-amyloidogenic κ-LC (κR-DH). This experiment also further reaffirmed that cross-seeding is not efficient in AL amyloidosis.

We are now conducting MS and immune-EM studies to confirm the nature of the amyloid deposits. However, our first results are highly encouraging, showing that the injection of seeds+ VL-fibrils, probably combined with the high levels of the same full-length amyloid LC in mice, are efficient to induce AL amyloidosis *in vivo*.

Currently, other cohorts of mice were injected with seeds and VL-fibrils to consolidate our first data and to observe organs at longer time points. Even if deposits in heart were expected since λS patient suffered from cardiac dysfunction, we envisioned kidney lesions, as it was the main organ involved. Consequently, we will carefully follow up kidney (albuminuria, creatinine) and cardiac functions (NT-proBNP) in mice up to 6 months after the injections and at different time points. A confirmation that mice do not develop kidney AL amyloidosis could shed new lights on the discrepancies between human and mouse.

Additionally, we will inject soluble λS-VL, that were recently obtained from a French CRO (Proteogenix, Schiltigheim, France), to verify whether it could bear alone the capacity to prime amyloidosis in mice. Absence of amyloid deposits would mean that amyloidogenic VL fragments are not sufficient to nucleate fibrils and that some other component is missing in mice to recreate the conditions needed for the disease to develop as in humans.

Finally, if we confirm the requirement of VL fragments to induce amyloidosis in mice, as observed *in vitro*, it raises the question of how such fragments are produced in human and why they are not produced in mouse. Morgan et al. suggested that LC dimers from AL amyloidosis patient unfold faster than non amyloidogenic LCs, making them more susceptible to endoproteolysis that could release the amyloidogenic VL domain (26). The hypothesis of partial

endoproteolysis was recently reinforced by the Cryo-EM studies as discussed above (32,33). Searching for proteases implicated in such partial degradation of the LCs could help untangle the pathophysiology of this disease. This could also explain the different organ tropism of amyloid LC subgroups (IGLV6-57 in kidney, IGLV1-44 in heart) (34,35) if a specific protease present in a certain organ is responsible for degrading the circulating monoclonal LC. Degradomes from mouse and human have been recently studied thanks to the availability of their whole genome. Results showed that human degradome is composed of 553 proteases and homologues while the mouse one has at least 628 components (36). A comparative study of these proteases in mouse and human, with functional assays to determine their propensity to degrade CL domains from amyloid LCs, could help finding candidates, immediately becoming key targets in the treatment of AL amyloidosis.

Altogether, these exciting preliminary results obtained after 20 years of trials and errors highlight the difficulty to develop animal models of human diseases. Many experiments are still needed to confirm and to better understand amyloidosis induction in our model. However, to our knowledge, λS-DH mouse model stands as the first *in vivo* model presenting overt AL amyloidosis in organs typically involved in the human disease and consequently, represents a precious tool to evaluate new therapeutics.

MATERIALS AND METHODS

LC gene extraction and sequencing

The human monoclonal LC genes used in the study were obtained from bone marrow (BM) aspirates as previoulsly described (22,3). The AL λLC cDNA was extracted from a patient with biopsy-proven AL amyloidosis (λS-PT). The LC is derived from the Vλ6-57 germline gene (95,53% homologous) rearranged on a Jλ3*02 junction segment (92,11% homologous) and a constant Cλ3 domain. The κLC gene used to generate the κR-DH model was extracted from a patient with multiple myeloma and cast nephropathy (κR-PT), with no amyloidosis in the kidney biopsy and no other clinical argument to suspect amyloidosis.

Transgenic mice models generation

To generate the transgenic mice models (λS-DH and κR-DH) two similar strategies were used as previously described (24,3). For λS-DH, the complete cDNA coding for the selected human monoclonal λLC was introduced in place of the mouse Jκ segments in the κ locus thus generating a fully human LC. For κR-DH, only the cDNA coding for the variable/junction domains (VJ) was introduced, generating in the mouse a chimeric human/mouse LC composed of the human VJ domain and the mouse Cκ domain as previously described (24,3).

Mice were crossed with DH-LMP2A mice, kindly provided by S. Casola (IFOM, Milan, Italy) (5). The transgenic strategy for λS-DH is showed in **Figure 1A** and was previously described (37). The two models produced similar levels of free LC. Mice were maintained in pathogen-free conditions, with food and water *ad libitum*, unless otherwise stated. All experimental procedures have been approved by our institutional review board for animal experimentation and of the French Ministry of Research (APAFIS #7655-2016112211028184).

LC dosing

Serum were analyzed for the presence of FLC using Freelite™ (The Binding Site, Birmingham, UK) assay on BNII nephelometer (Siemens healthcare, Herlangen, Germany) according to according to the manufacturer's instruction. Additionally, total LCs were dosed by ELISA, as previously described (3,22,24) using appropriate antibodies (**Table 1**). Plates were read at 405nm using a Multiskan FC® spectrophotometer (Thermo scientific).

Western Blot

Serum proteins were separated by non-reducing SDS-PAGE (10%) and transferred onto polyvinylidene difluoride membranes (Millipore). Membranes were blocked in 5% milk Trisbuffered saline (TBS), following by incubation with desired antibodies in 3% milk TBS (**Table 1**), washed three times with TBS 0.1 % tween and revealed by chemiluminescence (ECL, Pierce).

Flow cytometry

Intracellular staining was performed using the Intraprep™ kit (Beckman Coulter). Flow cytometry analysis were performed on a BD Pharmingen LSRFortessa® cytometer and data were analyzed with Flowlogic™ Software (Miltenyi Biotec). Corresponding antibodies are listed in the **Table 1**.

Histological studies

Organ samples were processed for immunofluorescence (IF) studies, as previously described (22). In brief, IF was performed on OCT-included organs and snap frozen in isopentane using a Snap Frost 2 (Excilone). Cryosections of 9µm were fixed with cold acetone, blocked with phosphate-buffered saline (PBS) and bovine serum albumin (BSA) 3% and then stained with appropriate antibodies (**Table 1**). For Congo Red (CR) staining, 2.87mM CR alkaline solution

was freshly prepared by adding NaOH 1% following a five-minute staining before washing with PBS. Slides were observed on a NiE microscope (Nikon).

Biochemical parameters determination

Biochemical parameters were measured on overnight urine collection and blood samples were obtained by retro-orbital puncture under anesthesia. Serum concentrations of creatinine were measured on a Konelab 30 analyser with a creatinine enzymatic test (ThermoFisher Scientific). Urine albumin concentrations were measured using an albumin mouse ELISA kit (Abcam), according to the manufacturer's recommendations.

Cell line generation

To express the λ-LC *in vitro*, the corresponding cDNA obtained from the patient was amplified and cloned in a modified pCpGfree plasmid (Invivogen, San Diego, USA) containing the neomycin resistance gene. Series of transfections in the murine hybridoma/myeloma cell line SP2/0 (ATCC® CRL-1581™) were performed using Cell line Nucleofactor kit V (Amaxa/Lonza, Basel, Switzerland) and a Nucleofactor II device (Amaxa/Lonza, Basel, Switzerland). Positive clones were then selected using neomycin (1mg/mL, Fisher Bioreagent, Pittsburg, USA).

Expression and purification of human recombinant λS Full-Length free LC

Full-length free LC secretion in 7-day culture supernatant was quantified as previously described using ELISA. The selected best producing SP2/0-λS clone was cultured in a mini-bioreactor system (CELLine CL 350, Integra Biosciences) and the secreted FLC collected according to manufacturer's instructions. All collected samples were pooled and FLC was purified by Binding Site (Birmingham, UK).

Expression and purification of recombinant human Variable Domain (VL)

Recombinant human λS-VL was periplasmatically expressed in *E.coli* BL21 strain based on the pet12a vector (Novagene). After a cold osmotic shock to release the periplasmatic fraction, the proteins were purified by size exclusion chromatography using Superdex 200 preparation grade columns (GE Healthcare) in 10 mM Hepes, 100 mM NaCL, pH 7.6. Protein concentrations were determined by BCA assay (Thermo Fisher Scientific) and SDS-PAGE.

Heparin induced fibrilization of λS-VL or λS-LC

For aggregation assays, 33 µM of λS-VL was incubated in aggregation buffer (10 mM Hepes, 100 mM NaCl, pH 7.6) at 59°C for 10 min followed by the addition of 5 mM DTT and 0.8 µg/µl Heparin sodium salt and the incubation at 37°C and 300 rpm for two days. Fibrillation was confirmed by Tht fluorescence and Atomic Force Microscopy (AFM). Regarding λS-LC, 6.5 µM or 20 µM were incubated as mentioned before for four days in the case of higher concentration and up to 12 days for the lower one.

***In vitro* seeding assays**

λS-VL seeds were prepared by sonication of λS-VL fibrils 20 seconds at an amplitude of 90% using an Ultrasonic homogenizer (Bandelin). Addition of 1.6 µM seeds to the λS-VL aggregation assay mentioned above yielded fibrils within 30 min of incubation at 27°C, 300 rpm. 1.6 µM λS-VL fibril seeds prepared as mentioned above were incubated with 6.5 µM λS-LC in aggregation buffer for 4 days at 37°C, 300 rpm. 1.6 µM λS-VL fibril seeds prepared as mentioned above were incubated with 20 µM λS-LC in aggregation buffer for 2 days at 37°C, 300 rpm.Fibrillization was confirmed by Tht fluorescence and AFM.

***In vitro* fibril formation assays in serum.**

1,6 µM λS -VL fibril seeds prepared as mentioned above were incubated with 16.5 µM λS-VL in WT mouse, λS-DH or λS-PT serum at 37°C, 300 rpm. Fibril presence was confirmed by AFM.

***In vivo* assays:**

- **Cross seeding + AA induction**

3 months-old mice λS-DH (n=3) were injected intravenously (i.v.) with 100µl (~100µg) of human AL amyloidosis fibrils purified using Pras water extraction method (38). Mice were sacrificed at different times and organs were analyzed by IF and CR staining. AA amyloidosis were induced in 6 months-old mice (n=2) using AEF from AA amyloidosis-induced mice (spleen extracts) and complete freund reagent (Sigma) emulsion (200µl, 50/50 V/V) injected intraperitoneally. Mice were sacrificed 4 weeks later and spleen and kidney were analyzed by congo red staining and immunofluorescence.

- **Patients serum injection**

12- months old λS-DH mice (n=3) were injected i.v. with 100 µl of λS-PT serum containing ~10 µg of free λ LC. Mice were euthanized at different times after the injection (1 month, 2 months and 3 months).

- **Acidosis**

18-months old λS-DH mice (n=3) were put under acidosis with 0.28M NH_4Cl pH 6.88 in their water bottles. Mice were subjected to 14 days of acidosis followed by 14 days of rest with water *ad libitum* and finalized with 14 additional days under acidosis, then sacrificed. Organs samples were frozen for histological studies.

- **Low-dose Bortezomib**

6-month old λS-DH mice (n=3) were regularly injected subcutaneously (sc) ten times with Velcade® (Bortezomib) at a dose of 0.25mg/kg. The dose was chosen taking into account previous experiences (22) not to fully deplete plasma cells. The proper concentration was obtained through dilution in sterile PBS (Eurobio) according to mice weight at start of the experience. All injections were performed under Isoflurane (Arkema) anesthesia. Mice were euthanized at different times (15 days, 2 months and 3 months after last Bz injection). Organs samples were frozen for histological studies.

- **λS-VL fibrils+ seeds *in vivo* injection**

8-months old λS-DH and κR-DH mice (n=4) were injected by i.v. with 200µg of LPS free 1:1 mixture of λS-VL seeds and λS-VL fibrils. A set of 2 mice were euthanized at different times post-injection (2-months and 4-months). Organs samples were frozen for histological studies.

Figure 1.

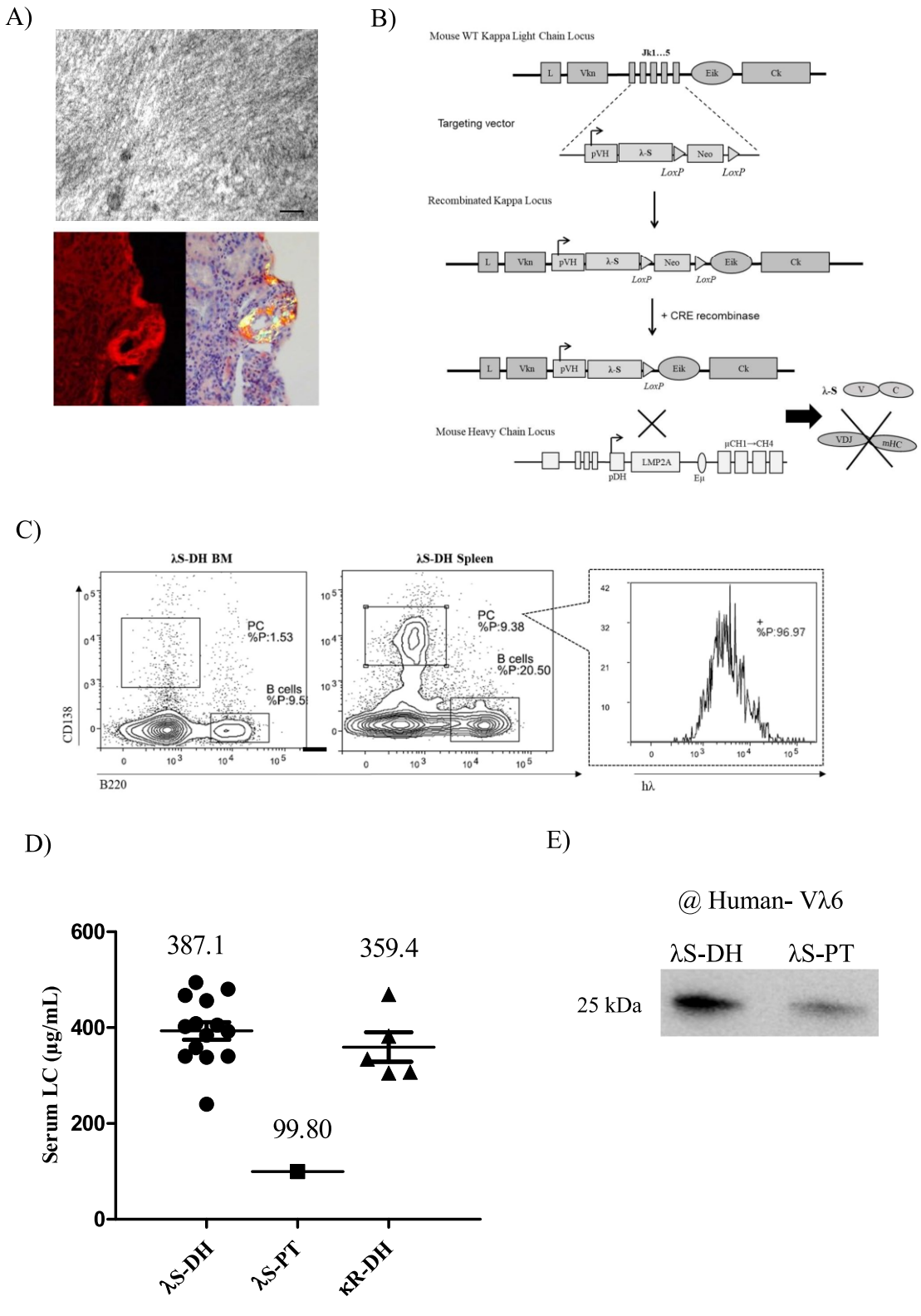
A)
B)
Mouse WT Kappa Light Chain Locus
Jk1…5
L
Vkn
Eik
Ck
Targeting vector
pVH
λ-S
Neo
LoxP
LoxP
Recombinated Kappa Locus
+ CRE recombinase
Mouse Heavy Chain Locus
μCH1→CH4
LMP2A
pDH
Eμ
VDJ
mHC
V
C
C)
λS-DH BM
λS-DH Spleen
PC
%P:1.53
B cells
%P:9.5
PC
%P:9.38
B cells
%P:20.50
+
%P:96.97
CD138
B220
hλ
D)
E)
@ Human- Vλ6
λS-DH
λS-PT
25 kDa
Serum LC (μg/mL)
600
400
200
0
387.1
99.80
359.4
λS-DH
λS-PT
κR-DH

A) Electron microscopy analysis of λS-PT kidney (up) showing the amyloid fibrils. Congo red (CR) staining (bottom left) is positive under immunofluorescence microscopy and confirmed under polarizing light (bottom right).

B) Strategy to produce high amounts of a human lambda light chain (LC) in mouse consisting of replacing the Jk segments in a WT unrearranged kappa locus by a human LC/neomycin cassette. Thanks to the absence of the Jk segments in the newly recombined kappa locus, all endogenous rearrangements are blocked. Later, the neomycin resistance is deleted by a cre-mediated deletion. Further crossing with DH-LMP2A (DH) mice assures the production of only free light chain (FLC) by B and plasma cells (PC).

C) Flow cytometry analysis of spleen and bone marrow cells from λS-DH mice stained with anti-mouse CD138 and B220 antibodies. Intracellular staining with anti-human lambda antibodies shows that almost all PCs are lambda positive.

D) Serum LC levels (in μg/mL) of lambda FLC for λS-DH mice or λS-PT patient and kappa LC for κR-DH control mice. Means for λS-DH and κR-DH are shown while for λS-PT patient represents the dosage at diagnosis.

E) Denaturing western blot analysis of the produced λS-LC in sera of λS-DH compared with λS-PT serum stained with an anti-human Vλ6 antibody. The LC band appears at the expected size (25kDa).

Figure 2.

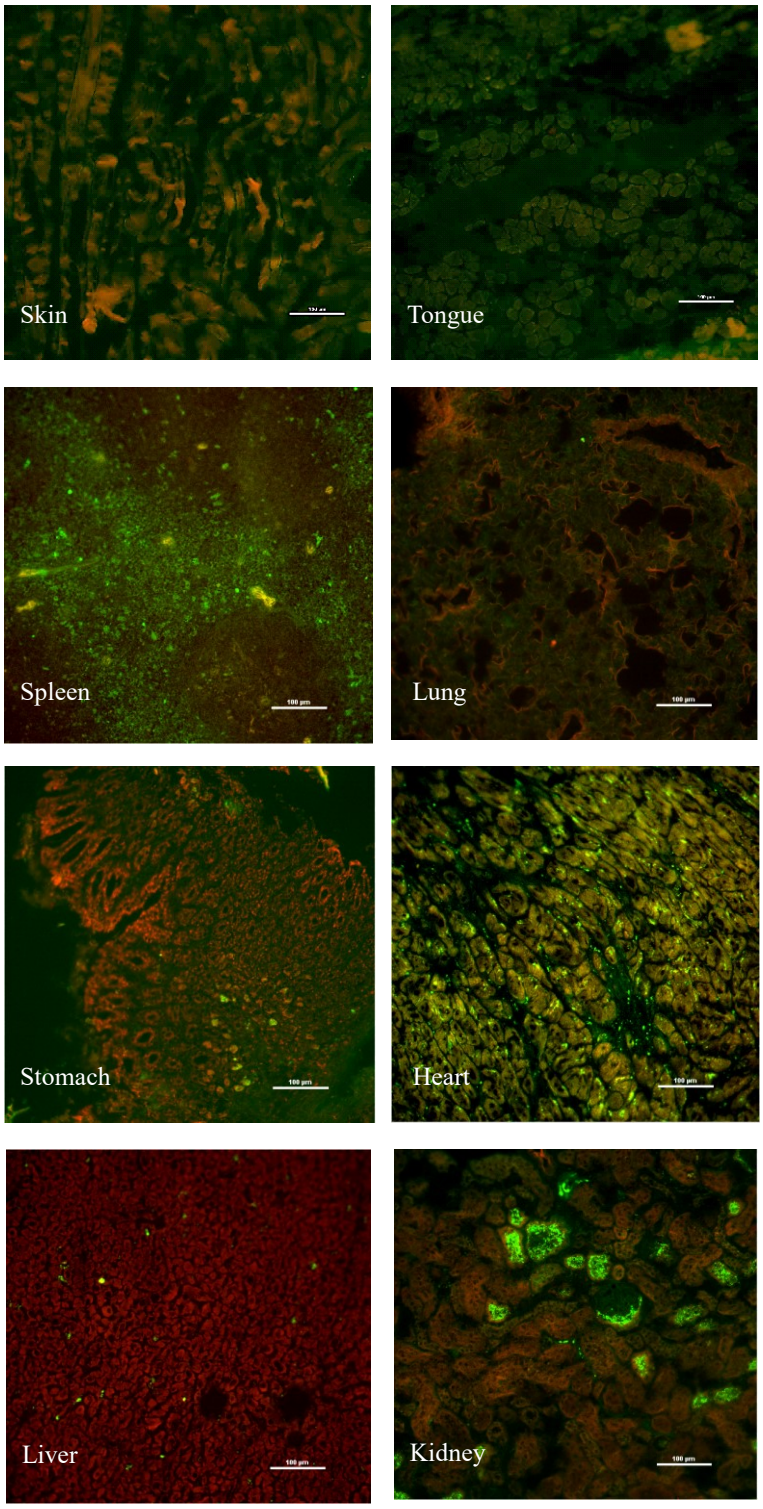

Immunofluorescence microscopy on frozen organ section of λS-DH old mice stained using CR and anti-human lambda antibody. The LC is highly detectable in kidneys and spleen. The heart also shows some positive staining while the liver and stomach denote de presence of few PCs. Original magnification x200. Scale bars: 100μm.

Figure 3.

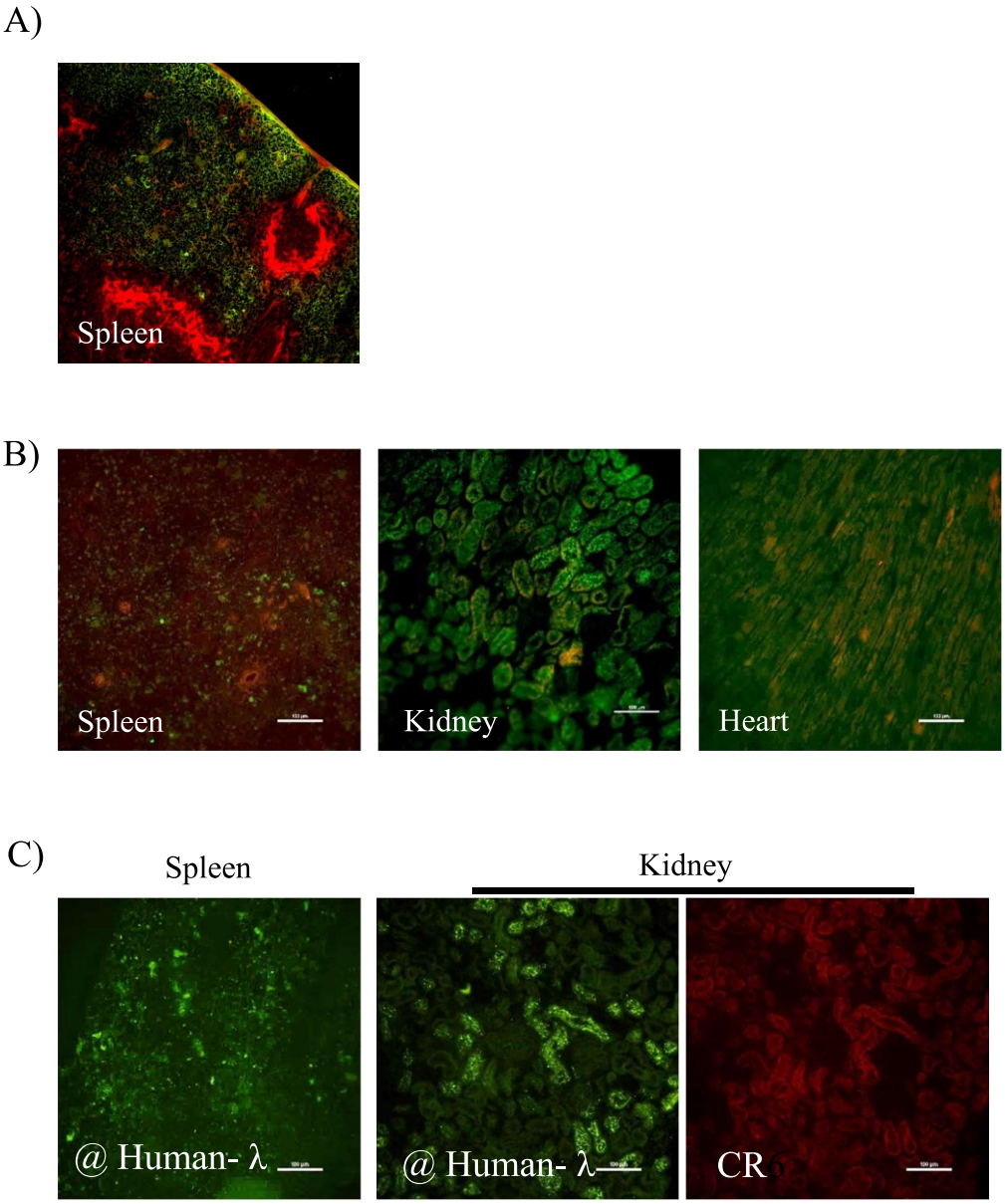

A) Immunofluorescence microscopy on frozen spleen section of AA amyloidosis-induced mouse. While there is positive CR staining, it does not co-localize with the lambda LC (green). Original magnification x40.

B) Immunofluorescence microscopy on frozen organs sections of λS-DH mice injected with patient sera. No CR positive was observed. Original magnification x200. Scale bar: 100µm.

C) Immunofluorescence microscopy on frozen organs sections of λS-DH mice submitted to systemic acidosis. The unmerged images for kidney are shown. Original magnification x200. Scale bar: 100µm.

Figure 4.

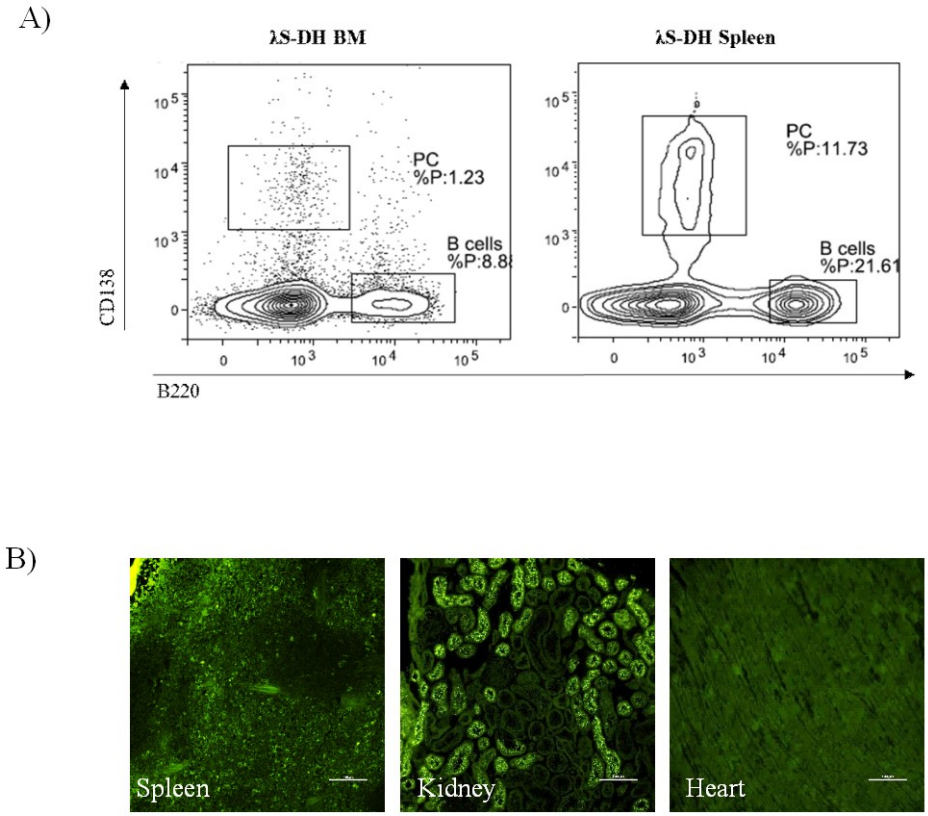

A) Flow cytometry analysis of spleen and bone marrow cells from λS-DH mouse treated with low dose bortezomib (bz) stained with anti-mouse CD138 and B220 antibodies showing a recovery in PC numbering at sacrifice.

B) Immunofluorescence microscopy on frozen organs sections of λS-DH mice treated with low dose bz. Original magnification x200. Scale bar: 100μm.

Figure 5.

A)

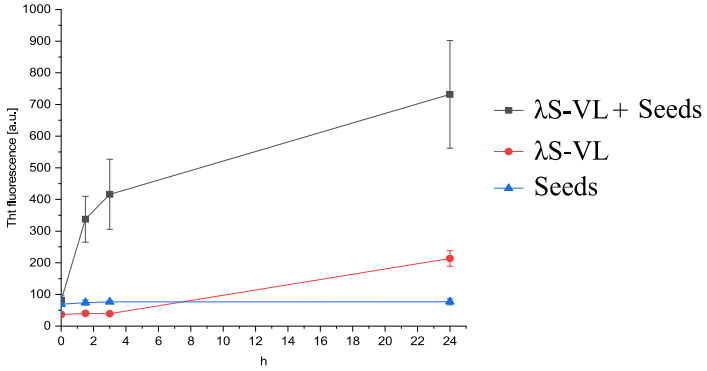

B)

de novo

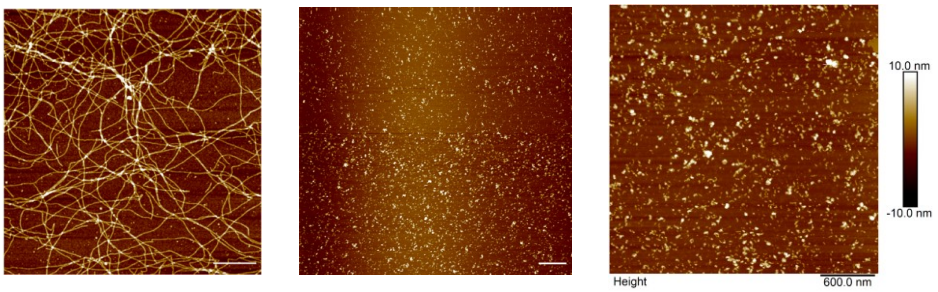

λS-VL (2 days) λS-LC (4 days) λS-LC (12 days)

C)

Seeding

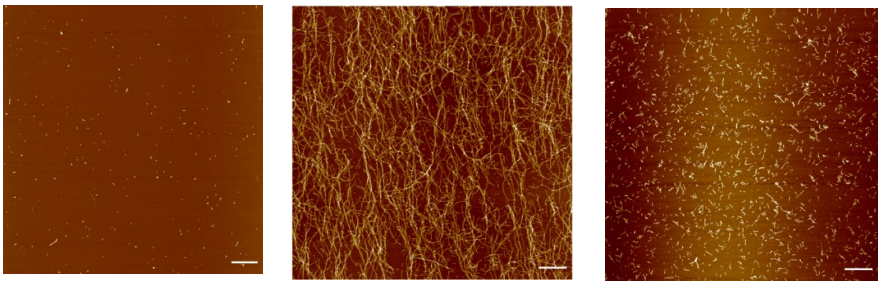

Seeds Seeds + λS-VL (5 hours) Seeds + λS-LC (4 days)

D)

Higher concentration

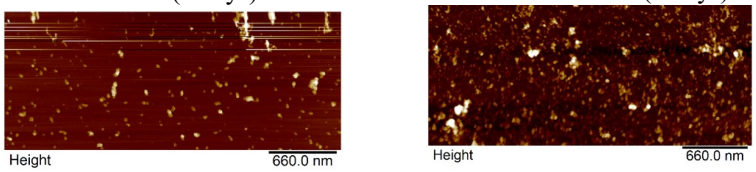

E)

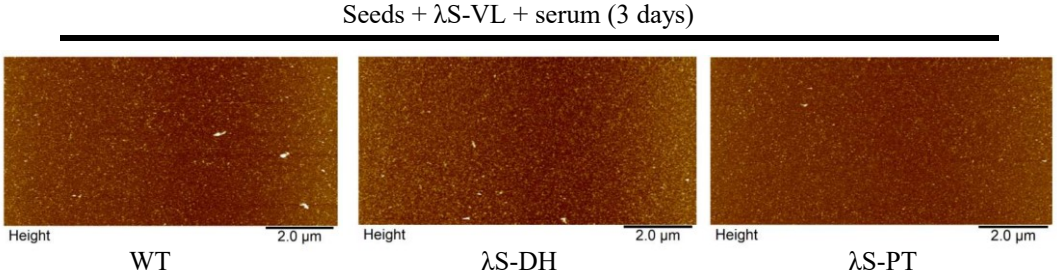

WT λS-DH λS-PT

A) Follow-up of fibril formation by fluorescent signal using thioflavine t (Tht) (exited at 440nm and measured at 480nm). Different aliquots were analyzed at the indicated time points. When seeds are added, λS-VL fibril formation is rapidly induced (2hours) compared to λS-VL alone (2 days). Seeds alone do not form fibrils at any analysed time.

B) *de novo* fibril formation assay using λS-VL or full-lenght λS-LC showing that the λS-LC does not form fibrils, even after 12 days as seen by atomic force microscopy (AFM). Scale bars: 1 μM (White) or 600nm (black) and Height profile -10 to 10 nm.

C) Seeding assays with λS-VL seeds combined with λS-VL or λS-LC. As observed in the AFM images, short fibrils are obtained with using the full-length LC and thanks to the seeds fibril formation process is accelerated. White Scale bars: 1 μM. Height profile -10 to 10 nm.

D) Assays with higher quantities of λS-LC alone or with seeds. Height profile -10 to 10 nm and scale bar of 600nm. No fibril formation is observed by AFM at 4 days for λS-LC) or 2 days for λS-LC+ seeds.

E) Fibril formation assays in sera (wild type mouse (WT), λS-DH mouse or λS-PT patient) combined with seeds and λS-VL. AFM after 3 days shows no fibrils.

Figure 6.

A)

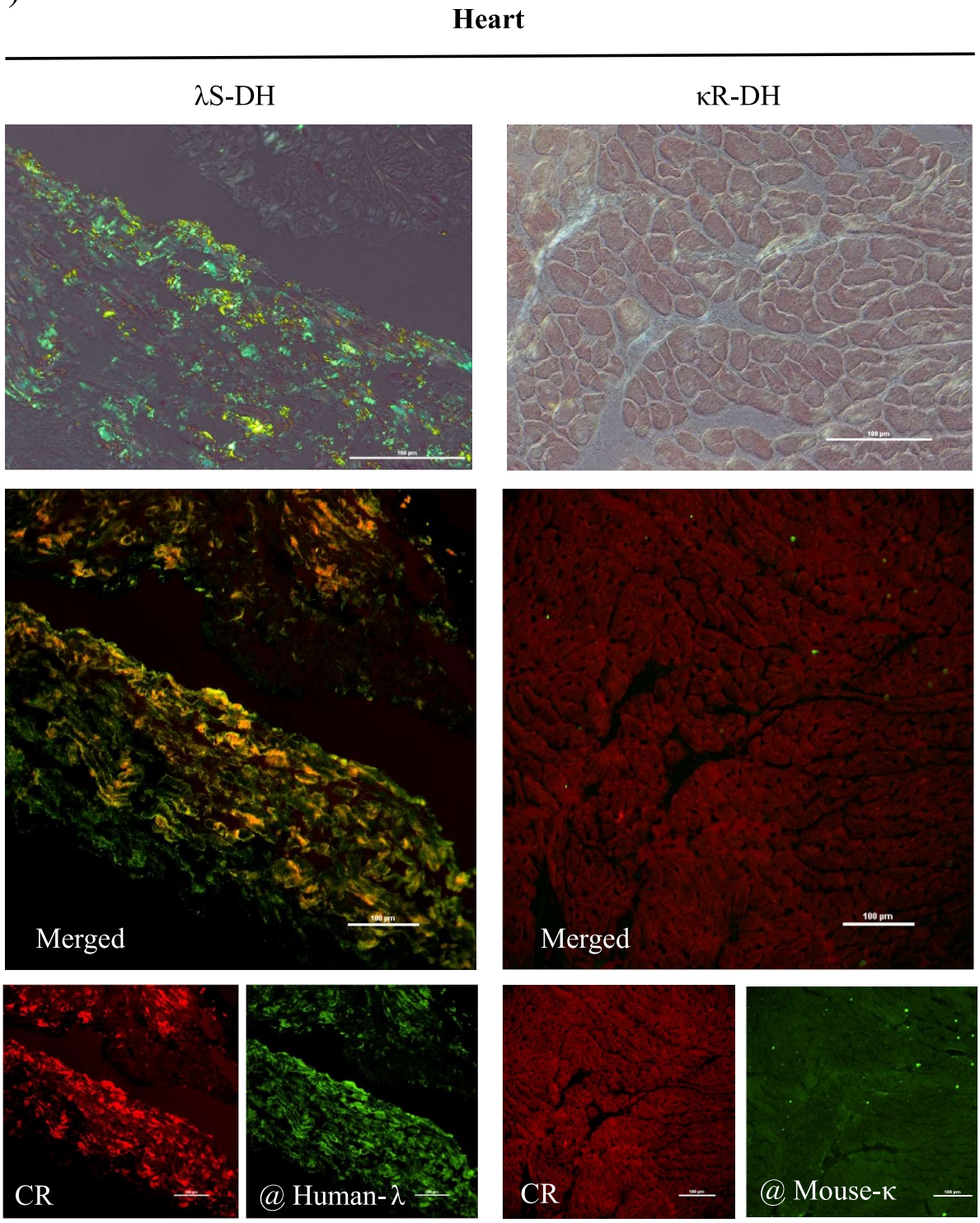

B)

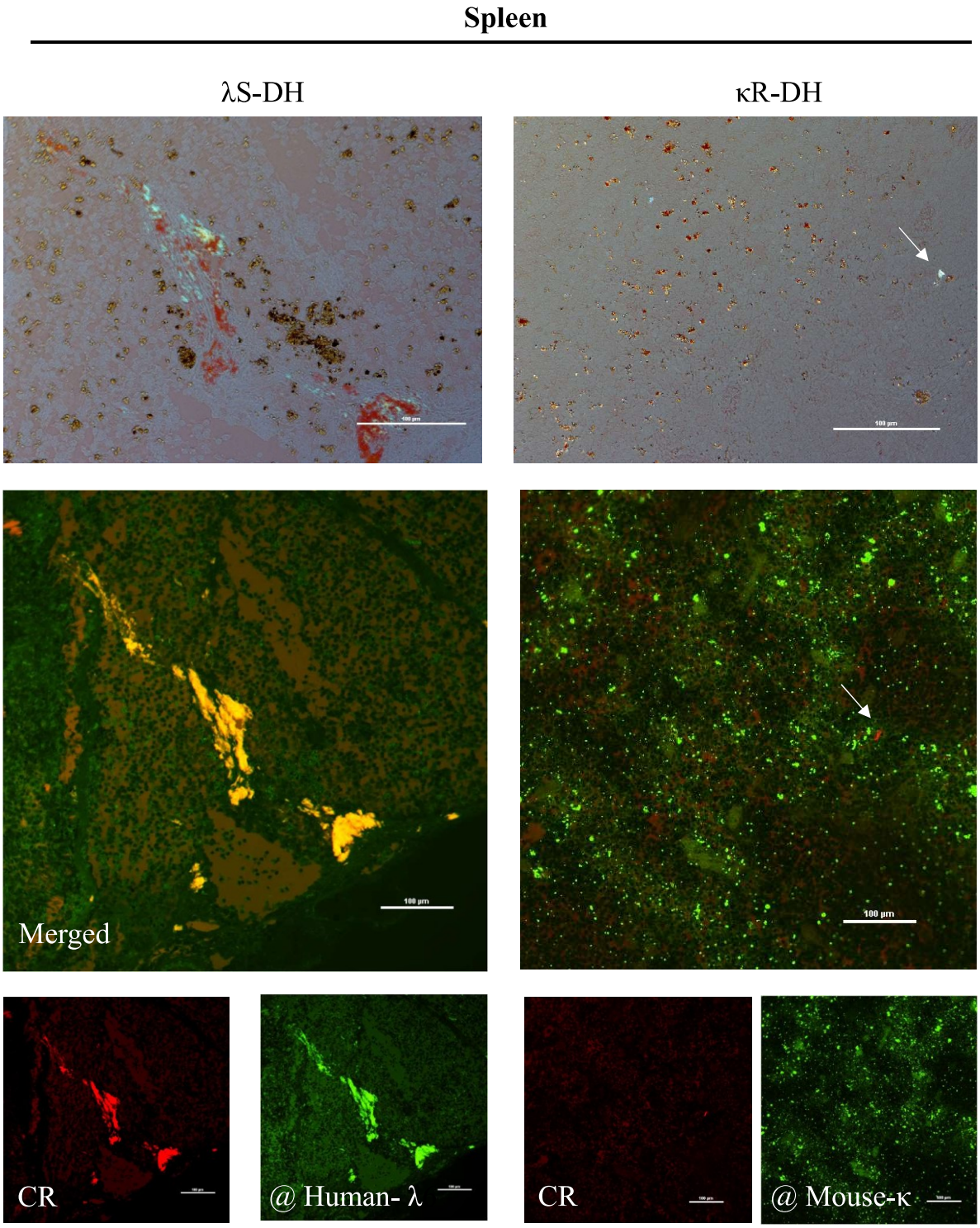

A) Heart sections analysis of λS-DH or control κR-DH mice two months after the injection of a mix of seeds plus λS-VL fibrils. Upper image corresponds to polarizing light. For λS-DH (left) large quantities of apple-green birefringent areas are observed while κR-DH (right) remained negative only showing pale-white areas. By immunofluorescence (middle), the co-localization of CR and lambda LC is confirmed for λS-DH. The unmerged images are shown at the bottom. Original magnification x200. Scale bar: 100μm.

B) Spleen sections analysis of λS-DH or control κR-DH mice two months after the injection of a mix of seeds plus λS-VL fibrils. Upper image corresponds to polarizing light. For λS-DH (left) scattered quantities of apple-green birefringent areas are observed while κR-DH (right) showed red-brown aggregates that were not CR positive (bottom left). By immunofluorescence (middle), the co-localization of CR and lambda LC is confirmed for λS-DH. For κR-DH, one small "fibril" appears (arrow, bottom right CR) but it is not co-stained for κ-LC (bottom, right). The unmerged images are shown at the bottom. Original magnification x200. Scale bar: 100μm.

Figure 7.

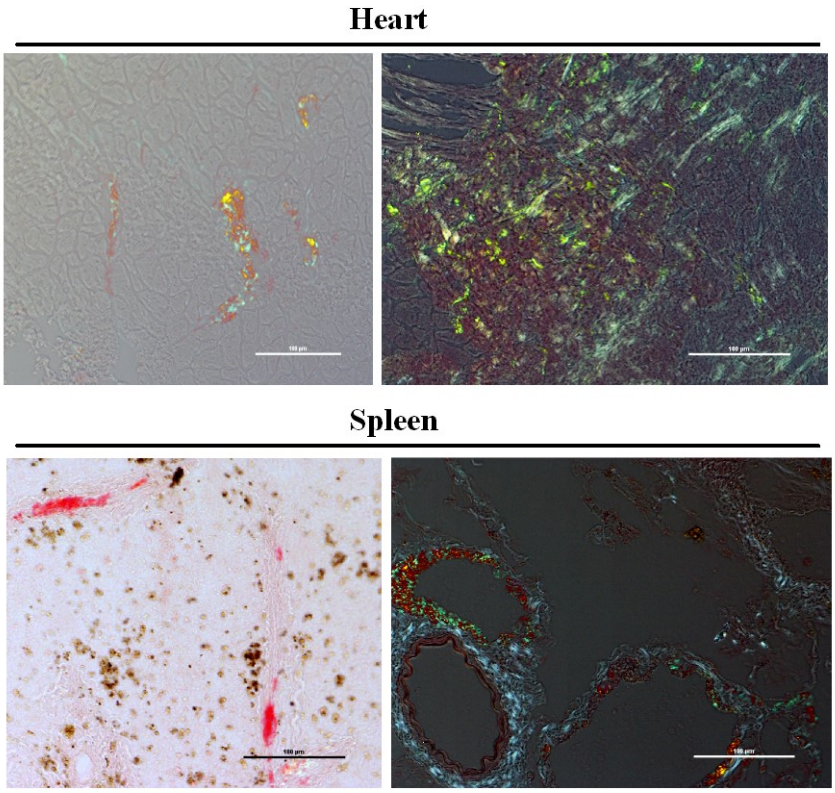

Heart and spleen sections analysis by polarizing light of λS-DH mice four months after the injection of seeds + λS-VL fibrils. Positive apple-green birefringent areas are still observed. Original magnification x200. Scale bar: 100µm.

Figure 8.

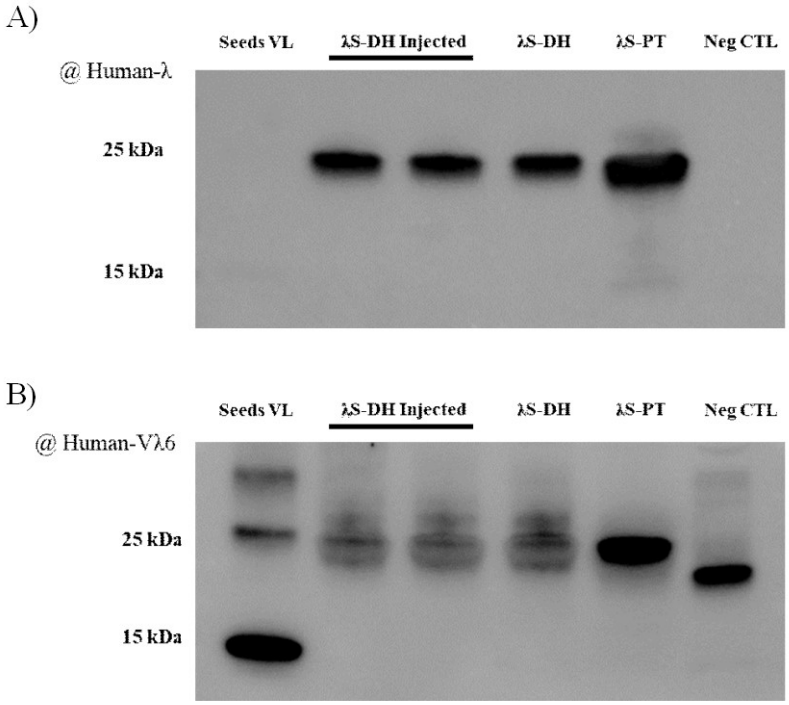

A) Denaturing western blot analysis using the anti-human lambda antibody used for immunofluorescence staining for λS-VL, λS-DH mice (λS-VL+ seed injected and non-injected), λS-PT and negative control (neg CTL = κR-DH). As shown, it recognized only the full-length LC (band at 25kDa) and not the λS-VL.

B) Denaturing western blot analysis using the anti-human VL6 antibody for the same samples. The λS-VL (band at 15kDa mainly) is recognized as well as the full-length LC (band at 25kDa). Since it is a mouse antibody, the negative control (κR-DH serum) reveals positive due to the secondary-HRP anti-mouse antibody used.

Table 1. List of antibodies.

Antibody	Reactivity	Clone	Source	Conjugate	Applications
Anti-B220	Mouse	RA3-6B2 (Becton Dickinson)	Rat	BV421	Flow cytometry
Anti-CD138	Mouse	281-2 (BD Biosciences)	Rat	APC	Flow cytometry
Anti-human VL6	Human	Monoclonal (from A. Solomon's lab)	Mouse	Unconjugated	Western-Blot
Anti-lambda	Human	Polyclonal (southernBiotech)	Goat	Unconjugated or AP	ELISA
Anti-lambda	Human	Polyclonal (Beckman Coulter)	Goat	Unconjugated, AP, HRP	ELISA
Anti-lambda	Human	Polyclonal (Dako)	Rab (Fab'2)	FITC	Flow cytometry+ IF + Western-Blot
Anti-kappa	Mouse	Polyclonal (Southern Biotech)	Goat	Unconjugated or AP	ELISA
Anti-IgG	Rabbit	Polyclonal (Beckman Coulter)	Goat	HRP	Western-Blot
Anti-IgG	Mouse	Polyclonal (Beckman Coulter)	Goat	HRP	Western-Blot

BIBLIOGRAPHY

1. Sirac C, Herrera GA, Sanders PW, Batuman V, Bender S, Ayala MV, et al. Animal models of monoclonal immunoglobulin-related renal diseases. Nat Rev Nephrol. 2018 Feb 19;14(4):246–64.

2. Popov AV, Zou X, Xian J, Nicholson IC, Brüggemann M. A Human Immunoglobulin λ Locus Is Similarly Well Expressed in Mice and Humans. J Exp Med. 1999 May 17;189(10):1611–20.

3. Bender S, Ayala MV, Bonaud A, Javaugue V, Carrion C, Oblet C, et al. Immunoglobulin light chain toxicity in a mouse model of monoclonal immunoglobulin light-chain deposition disease. Blood. 2020 Jun 19;blood.2020005980.

4. Lechouane F, Bonaud A, Delpy L, Casola S, Oruc Z, Chemin G, et al. B-cell receptor signal strength influences terminal differentiation. Eur J Immunol. 2013 Mar;43(3):619–28.

5. Casola S, Otipoby KL, Alimzhanov M, Humme S, Uyttersprot N, Kutok JL, et al. B cell receptor signal strength determines B cell fate. Nat Immunol. 2004 Mar;5(3):317–27.

6. Davern S, Tang LX, Williams TK, Macy SD, Wall JS, Weiss DT, et al. Immunodiagnostic capabilities of anti-free immunoglobulin light chain monoclonal antibodies. Am J Clin Pathol. 2008 Nov;130(5):702–11.

7. McWilliams-Koeppen HP, Foster JS, Hackenbrack N, Ramirez-Alvarado M, Donohoe D, Williams A, et al. Light Chain Amyloid Fibrils Cause Metabolic Dysfunction in Human Cardiomyocytes. Khodarahmi R, editor. PLOS ONE. 2015 Sep 22;10(9):e0137716.

8. Merlini G. AL amyloidosis: from molecular mechanisms to targeted therapies. Hematology. 2017 Dec 8;2017(1):1–12.

9. Blancas-Mejía LM, Ramirez-Alvarado M. Systemic Amyloidoses. Annu Rev Biochem. 2013 Jun 2;82(1):745–74.

10. Johan K, Westermark G, Engström U, Gustavsson A, Hultman P, Westermark P. Acceleration of amyloid protein A amyloidosis by amyloid-like synthetic fibrils. Proc Natl Acad Sci U S A. 1998 Mar 3;95(5):2558–63.

11. Fu X, Korenaga T, Fu L, Xing Y, Guo Z, Matsushita T, et al. Induction of AApoAII amyloidosis by various heterogeneous amyloid fibrils. FEBS Lett. 2004 Apr 9;563(1–3):179–84.

12. Moreno-Gonzalez I, Edwards III G, Salvadores N, Shahnawaz M, Diaz-Espinoza R, Soto C. Molecular interaction between type 2 diabetes and Alzheimer's disease through cross-seeding of protein misfolding. Mol Psychiatry. 2017 Sep;22(9):1327–34.

13. Ren B, Zhang Y, Zhang M, Liu Y, Zhang D, Gong X, et al. Fundamentals of cross-seeding of amyloid proteins: an introduction. J Mater Chem B. 2019;7(46):7267–82.

14. Yan J, Fu X, Ge F, Zhang B, Yao J, Zhang H, et al. Cross-Seeding and Cross-Competition in Mouse Apolipoprotein A-II Amyloid Fibrils and Protein A Amyloid Fibrils. Am J Pathol. 2007 Jul;171(1):172–80.

15. Solomon A, Weiss DT, Schell M, Hrncic R, Murphy CL, Wall J, et al. Transgenic Mouse Model of AA Amyloidosis. Am J Pathol. 1999 Apr;154(4):1267–72.

16. Simons JP, Al-Shawi R, Ellmerich S, Speck I, Aslam S, Hutchinson WL, et al. Pathogenetic mechanisms of amyloid A amyloidosis. Proc Natl Acad Sci. 2013 Oct 1;110(40):16115–20.

17. Watanabe K, Uchida K, Chambers JK, Tei M, Shoji A, Ushio N, et al. Experimental Transmission of AA Amyloidosis by Injecting the AA Amyloid Protein Into Interleukin-1 Receptor Antagonist Knockout (IL-1raKO) Mice. Vet Pathol. 2015 May;52(3):505–12.

18. Blancas-Mejia LM, Misra P, Dick CJ, Marin-Argany M, Redhage KR, Cooper SA, et al. Assays for Light Chain Amyloidosis Formation and Cytotoxicity. In: Gomes CM, editor. Protein Misfolding Diseases [Internet]. New York, NY: Springer New York; 2019 [cited 2020 Aug 2]. p. 123–53. (Methods in Molecular Biology; vol. 1873). Available from: http://link.springer.com/10.1007/978-1-4939-8820-4_8

19. Nowik M, Kampik NB, Mihailova M, Eladari D, Wagner CA. Induction of Metabolic Acidosis with Ammonium Chloride (NH_4Cl) in Mice and Rats – Species Differences and Technical Considerations. Cell Physiol Biochem. 2010;26(6):1059–72.

20. Cooley CB, Ryno LM, Plate L, Morgan GJ, Hulleman JD, Kelly JW, et al. Unfolded protein response activation reduces secretion and extracellular aggregation of amyloidogenic immunoglobulin light chain. Proc Natl Acad Sci U S A. 2014 Sep 9;111(36):13046–51.

21. Zhou P, Ma X, Iyer L, Chaulagain C, Comenzo RL. One siRNA pool targeting the λ constant region stops λ light-chain production and causes terminal endoplasmic reticulum stress. Blood. 2014 May 29;123(22):3440–51.

22. Bonaud A, Bender S, Touchard G, Lacombe C, Srour N, Delpy L, et al. A mouse model recapitulating human monoclonal heavy chain deposition disease evidences the relevance of proteasome inhibitor therapy. Blood. 2015 Aug 6;126(6):757–65.

23. Pengo N, Scolari M, Oliva L, Milan E, Mainoldi F, Raimondi A, et al. Plasma cells require autophagy for sustainable immunoglobulin production. Nat Immunol. 2013 Mar;14(3):298–305.

24. Sirac C, Bridoux F, Carrion C, Devuyst O, Fernandez B, Goujon J-M, et al. Role of the monoclonal kappa chain V domain and reversibility of renal damage in a transgenic model of acquired Fanconi syndrome. Blood. 2006 Jul 15;108(2):536–43.

25. Blancas-Mejía LM, Horn TJ, Marin-Argany M, Auton M, Tischer A, Ramirez-Alvarado M. Thermodynamic and fibril formation studies of full length immunoglobulin light chain AL-09 and its germline protein using scan rate dependent thermal unfolding. Biophys Chem. 2015 Dec 1;207:13–20.

26. Morgan GJ, Kelly JW. The Kinetic Stability of a Full-Length Antibody Light Chain Dimer Determines whether Endoproteolysis Can Release Amyloidogenic Variable Domains. J Mol Biol. 2016 23;428(21):4280–97.

27. Rennella E, Morgan GJ, Kelly JW, Kay LE. Role of domain interactions in the aggregation of full-length immunoglobulin light chains. Proc Natl Acad Sci U S A. 2019 15;116(3):854–63.

28. Klimtchuk ES, Gursky O, Patel RS, Laporte KL, Connors LH, Skinner M, et al. The Critical Role of the Constant Region in Thermal Stability and Aggregation of Amyloidogenic Immunoglobulin Light Chain. Biochemistry. 2010 Nov 16;49(45):9848–57.

29. Blancas-Mejía LM, Misra P, Ramirez-Alvarado M. Differences in Protein Concentration Dependence for Nucleation and Elongation in Light Chain Amyloid Formation. Biochemistry. 2017 Feb 7;56(5):757–66.

30. Lavatelli F, Perlman DH, Spencer B, Prokaeva T, McComb ME, Théberge R, et al. Amyloidogenic and associated proteins in systemic amyloidosis proteome of adipose tissue. Mol Cell Proteomics. 2008;7(8):1570–83.

31. Vrana JA, Gamez JD, Madden BJ, Theis JD, Bergen HR, Dogan A. Classification of amyloidosis by laser microdissection and mass spectrometry–based proteomic analysis in clinical biopsy specimens. Blood. 2009 Dec 3;114(24):4957–9.

32. Radamaker L, Lin Y-H, Annamalai K, Huhn S, Hegenbart U, Schönland SO, et al. Cryo-EM structure of a light chain-derived amyloid fibril from a patient with systemic AL amyloidosis. Nat Commun. 2019 Dec;10(1):1103.

33. Swuec P, Lavatelli F, Tasaki M, Paissoni C, Rognoni P, Maritan M, et al. Cryo-EM structure of cardiac amyloid fibrils from an immunoglobulin light chain AL amyloidosis patient. Nat Commun. 2019 Dec;10(1):1269.

34. Comenzo RL, Zhang Y, Martinez C, Osman K, Herrera GA. The tropism of organ involvement in primary systemic amyloidosis: contributions of Ig V(L) germ line gene use and clonal plasma cell burden. Blood. 2001 Aug 1;98(3):714–20.

35. Merlini G, Dispenzieri A, Sanchorawala V, Schönland SO, Palladini G, Hawkins PN, et al. Systemic immunoglobulin light chain amyloidosis. Nat Rev Dis Primer. 2018 Dec;4(1):38.

36. Puente XS, Sánchez LM, Overall CM, López-Otín C. Human and mouse proteases: a comparative genomic approach. Nat Rev Genet. 2003 Jul;4(7):544–58.

37. Sirac C, Herrera GA, Sanders PW, Batuman V, Bender S, Ayala MV, et al. Animal models of monoclonal immunoglobulin-related renal diseases. Nat Rev Nephrol. 2018 Apr;14(4):246–64.

38. Pras M, Schubert M, Zucker-Franklin D, Rimon A, Franklin EC. The characterization of soluble amyloid prepared in water. J Clin Invest. 1968 Apr;47(4):924–33.

Part II. Inducible mouse model to study plasma cells

The molecular mechanisms leading to the differentiation of B-lymphocytes into PC are now well known, but few studies have been done to understand their fate later on as well as their deregulation in the case of PCD. This is mainly due to the lack of reliable mouse models to specifically study PCs.

Several studies have shown that PC, together with expressing the different monomeric Ig isotypes, express the J chain and that the *IgJ* gene is active at very early steps of PC differentiation (Kang et al., 1998). Consequently, we considered it could be a good exclusive marker of PCs , allowing the follow up of these cells *in vivo*.

To confirm this, we generated a transgenic mouse model expressing the enhanced Green Fluorescent Protein (eGFP) under the *IgJ* gene enhancer/promoter to follow J Chain expression during B cell differentiation. This IgJ^{eGFP} mouse line helped us confirm that IgJ appears as an early marker of terminal differentiation, even before CD138, representing an exquisite tool for *in vivo* PC imaging and follow up.

Based on this first model, via the Phenomin Consortium (laureate project of the PHENOMIN 6th call in 2016), a conditional deletion mouse model in PC using a Tamoxifen-dependent Cre recombinase (Cre^{ERT2} recombinase) under the control of the regulatory elements of *IgJ,* was analyzed. In contrast with existing models, deletion or activation of genes through CRE/Lox recombination would specifically target PCs and would let the evaluation of the impact of genetic modifications in this population.

To characterize the $IgJ^{CreERT2}$ model, we crossed it first to a reporter model (ROSA-lsl-tdTomato) to monitor Cre recombinase activity. With it, we confirmed the efficacy of tamoxifen induction of the Cre^{ERT2} recombinase and its specific activity in PCs, which proved to be the only targeted population. Next, using our previously described HCDD model bearing a floxed CH1 domain-coding exon crossed with $IgJ^{CreERT2}$, this result was confirmed. Additionally, this last model highlighted the toxicity of a truncated HC in preliminary experiments.

Paper 3- New models to study plasma cells in mouse based on the restriction of IgJ expression to antibody secreting cells.

MV Ayala, A Bonaud, S Bender, JM Lambert, F Lechouane, C Carrion, M Cogné, V Pascal, C Sirac.

Submitted to as a pre-print to *bioRxiv (MS ID#: BIORXIV/2020/249441)* before its planned submission to *Frontiers in Immunology* as a Brief Research report.

New models to study plasma cells in mouse based on the restriction of IgJ expression to antibody secreting cells.

Maria Victoria Ayala [1,2], Amélie Bonaud[3], Sébastien Bender [1,2], Jean-Marie Lambert[1], Fabien Lechouane[1], Claire Carrion[1], Michel Cogné[1], Virginie Pascal[1,] and Christophe Sirac[1,2*]

[1]CNRS UMR7276/INSERM U1262, University of Limoges, Limoges, France
[2]French national reference centre for AL amyloidosis and other monoclonal Ig deposition diseases, France
[3]INSERM U1160, Institut of Research Saint Louis, Paris, France.

*Corresponding author : Christophe SIRAC (UMR CNRS 7276/INSERM U1262, CBRS-Faculté de Médecine, 2 rue du Dr Marcland, 87025 LIMOGES, France)

E-mail: christophe.sirac@unilim.fr

Keywords: abnormal plasma cell proliferation, J Chain, inducible mouse model, truncated immunoglobulin

Conflict of Interest: The authors declare that the research was conducted in the absence of any commercial or financial relationships that could be construed as a potential conflict of interest

AUTHOR CONTRIBUTIONS

MVA designed, performed, analyzed experiments and wrote the manuscript; SB, FL and AB performed and analyzed some experiments and drafted parts of the manuscript; JML, CC and VP performed and analyzed some experiments; SC designed and supervised research and wrote the manuscript.

FUNDING

This work was supported by grants from Fondation Française pour la Recherche contre le Myélome et les Gammapathies monoclonales, Limousin committees of Ligue nationale contre le cancer, Agence régionale de la santé and Institut Universitaire de France. MVA was funded by fellowships from Région Limousin (now Région Nouvelle Aquitaine) and Fondation ARC pour la Recherche sur le Cancer. BS is supported by Centre Hospitalier Universitaire Dupuytren Limoges and Plan National Maladies Rares. FL and AB were funded by French government fellowships. JML was funded by French government fellowships and Ligue national contre le cancer.

ACKNOWLEDGMENTS

The authors thank the staff of the BISCEm technical platforms at the University of Limoges.

ABSTRACT

Plasma cells (PC) represent the last stage of B cell development and are mainly characterized by their capacity of secreting large quantities of antibodies. They can be implicated in a broad-spectrum of neoplastic disorders, including Multiple Myeloma, Waldenstrom macroglobulinemia or Monoclonal Gammopathy of Clinical Significance, all characterized by the abnormal proliferation of a PC clone. Up to date, there are only few reporter models to specifically follow PC development, migration and homing in mouse and none allowing the genetic manipulation of these cells. We created a transgenic mouse model in which a green fluorescent protein gene was placed under the control of the well-characterized regulatory elements of the murine immunoglobulin J (IgJ) chain locus. Thanks to this model, we demostrated that IgJ is an early and specific marker of antibody secreting cells (ASCs) and appears before the expression of CD138, making it a good candidate to targeted genetic modifications of plasma cells. Therefore, a conditional deletion model using a Tamoxifen-dependent Cre recombinase inserted into the IgJ locus was characterized. Using a reporter model, we showed that, in contrast with existing models of B cell lineage genetic modification, the activity of the CRE recombinase only affects ASCs after tamoxifen treatment. Additionally, we used this model in a functional *in vitro* assay, to show that Ig modifications directly affect plasma cell survival. These two new mouse models, IgJ^{GFP} and $IgJ^{CreERT2}$ represent exquisite tools to study PCs. In pathology, the $IgJ^{CreERT2}$model opens new frontiers for *in vivo* genetic modifications of PCs to better reflect the pathophysiology of PC-related diseases.

INTRODUCTION

Plasma cells (PC), dedicated to the secretion of large amounts of antigen-specific immunoglobulins, represent the final stage of B cell lineage differentiation. The transcriptional program involved in the transition from B cell to PC has been extensively investigated in the past few years revealing two sets of transcription factors that are mutually opposite: those involved in the B cell identity and maintenance like Pax5, Bcl6 or Bach2 and those that control PC differentiation like Blimp1, Irf4 or Xbp1 [1–9]. However, few studies make it possible to understand the mechanisms involved after the differentiation, leading to migration, death or on the contrary to the exceptionally long survival of these cells, as well as their deregulation in the case of clonal plasma cell proliferations such as Monoclonal Gammopathy of Undertemined Significance (MGUS) or Multiple Myeloma (MM). One reason is the lack of models to specifically follow PCs in mouse and to turn on/off genes specifically in this lineage. The current murine models of inducible gene invalidation in the B cell lineage only allow deletion at relatively early stages of development ($CD19^{Cre}$, $CD21^{Cre}$). For instance, many models of overexpression of oncogenes normally involved in the development of PC proliferation resulted in general B hyperplasia or B cell tumor developments mainly because the oncogene was expressed throughout B cell development rather than restricted in the plasma cell compartment [10–12]. Currently, models with germinal center B cell-specific Cre expression ($AID^{CreERT2}$ or $IgG1^{Cre}$) represent the latest stage of B cell differentiation [13,14]. They can be useful to study the early stages of PC differentiation or transformation but remain useless for fully differentiated PCs. One reason for this lack of PC-specific Cre-deleter model is the difficulty to find a true PC-specific promoter to induce expression of Cre only in PCs. Genes overexpressed in PCs are often expressed earlier during B cell development or in other immune cell lineage (Prdm1, Irf4)[15,16]. Prdm1 promoter-driven reporter genes has been extensively used to decipher PC differentiation and homing[17,18] since Blimp1 is highly expressed in PCs[19]. However, it was shown that GFP is also expressed in other immune cells[20,21] precluding the usage of its promoter for a PC-specific Cre-deleter strain. In the absence of such strain, Tellier *et al*. advantageously used the ubiquitous tamoxifen-inducible Rosa26-

Cre^{ERT2} strain to study the role of Blimp1 and Ifr4 in mature PCs[22]. However, such approach also induced Cre-driven deletion in other cells expressing these genes and cannot be used to delete or activate genes or oncogenes specifically in PCs.

Immunoglobulin Joining (IgJ)-chain is a 15 kDa peptide expressed by antibody secreting cells (ASCs) and required for correct assembly of pentameric IgM and dimeric IgA [23]. Several studies have demonstrated that PCs producing monomeric Ig isotypes also express this peptide but it still remains controversial to what extent [24–26]. The exact stage of production during B cell development and differentiation into PC remains unknown but promoter activity and transcriptional studies have revealed that IgJ is expressed at very early steps of PC differentiation [27], before the requirement for Blimp1 over-expression [28]. Older studies also showed IgJ expression in pre-B and mature B cells[24].

In the present study, we first created a transgenic murine model that expresses the eGFP under the control of the murine IgJ gene enhancer/promoter [27] to follow IgJ expression during *in vivo* and *in vitro* differentiation of B-cells into PC. We show that, in contrast to previous assumptions, almost all ASC express the J-chain, independently of the secreted IgH isotype and its expression is mainly restricted to ASCs with a low expression in GC B cells. In contrast with other PC reporter models based on Prdm1 expression pattern[17,18], no other hematopoietic lineage yielded GFP expression making this model a unique tool to specifically access PCs localization. IgJ appears as an early marker of terminal differentiation before the expression of CD138, making of it an ideal promoter for a conditional deletion model in PCs. Consequently, we characterized a new model in which a tamoxifen-dependent Cre recombinase (Cre^{ERT2} recombinase) was placed under the control of this promoter in a knock-in transgenic mouse model. For the characterization of its targeted activity, mice were further crossed with a reporter mouse line. This model relies on the expression of a fluorescent protein, tdTomato, after elimination of a floxed STOP cassette. Thanks to it, we were able to show that Cre^{ERT2} recombinase activity is strictly restricted to PCs *in vivo* and *in vitro*. Furthermore, we confirmed this specificity in a model of Heavy Chain Deposition Disease (HCDD) [29], yielding a floxed CH1 domain in a transgenic human heavy chain. In preliminary

experiments *in vitro*, we showed that deletion of the CH1 domain had a negative impact on plasmablast differentiation without affecting other stimulated B cells thus confirming the specific toxicity of truncated/abnormal Ig for PCs as already shown with truncated LCs[30]. Overall, the IgJ^{CreERT2} model appears as an exquisite new tool to study PC development, maintenance and deregulation.

METHODS

Generation of transgenic mice.

The IgJ-GFP construct includes the 1.1kb NdeI/NheI genomic fragment harboring IgJ enhancer activity previously described[27] and the 1.4 kb IgJ promoter followed by *EGFP* gene from pMOD-ZGFPsh vector (Cayla Invivogen), all flanked by two insulators from chicken β-globin gene locus [23]. A neomycine resistance cassette follows this construct. CK35 embryonic stem cells were electroporated with the linearized vector and G418 resistant clones were screened by PCR (**supplemental Fig.1**). Two clones (10 and 13) were reimplanted in C57BL/6 blastocysts. For each clone, chimeric founders gave rise to a IgJ^{GFP} lineage respectively named IgJ^{GFP}10 and IgJ^{GFP}13.

The Jchain$^{tm1(CreERT2_EGFP)Wtsi}$ mice, hereafter called IgJ^{CreERT2}, were generated by the EUCOMMTOOLS consortium at the Welcome Trust Sanger Institute of London (MGI:5633773). They were obtained from the French National Infrastructure for Mouse Phenogenomics (Phenomin) at the Mouse clinical institute (Illkirch, France). Briefly, the expression cassette consisting in an eGFP-F2A-Cre^{ERT2} was inserted in the intron between exons 1 and 2 of the J-chain allele. This cassette was preceded by a splice acceptor sequence followed by a F2A sequence allowing the independent expression of *eGFP* and *Cre^{ERT2}* genes under the control of the J chain promoter/enhancers. A puromycin resistance cassette flanked by Rox was also inserted in 3' of the construct. The full construction is depicted in **supplemental Fig.1**.

Rosa26-LSL-Tomato mice were obtained from The Jackson Laboratory (JAX, Bar Harbor, ME, stock number 7914). In a few words, mice contain in the Gt(ROSA)26Sor locus a floxed STOP

cassette preventing transcription of a CAG promoter-driven red fluorescent protein variant (tdTomato).

Finally, Heavy Chain Depostion Disease (HCDD)-CH1^{+} mice were generated as previously described[29]. Briefly, the gene coding for a human monoclonal heavy chain obtained from a HCDD patient was introduced into the mouse joining segments in the kappa locus with a floxed CH1 domain.

All the animals were bred and maintained in pathogen-free condition in our animal facility. Unless stated otherwise, heterozygous animals for every transgenic genes were used. All experimental procedures have received the approval of our institutional review board for animal experimentation and of the French Ministry of Research (N° 7655-2016112211028184).

Immunization and Tamoxifen induction

When needed, mice were immunized with one intra-peritoneal injection of 200µl of sheep red blood cells (Sigma-Aldrich) and analyzed at the indicated times. *In vivo* tamoxifen induction protocol consisted in two intraperitoneal injections of 4mg of Tamoxifen (Sigma-Aldrich) in sunflower oil (Sigma-Aldrich) with a two-day rest. Mice were sacrificed the day after the last tamoxifen injection (**supplemental Fig.2**).

Flow cytometry and cell sorting.

Antibodies and reagents used for staining and cell sorting experiments are detailed in supplemental **Table I**. Flow cytometry analyses were done on a BD Pharmingen LSRFortessa® cytometer. Cell sorting experiments were done on a BD Pharmingen FACSVantage® cell analyzer. Data were then analyzed with BD FACSDiva software (BD Biosciences) and FlowLogic (Miltenyi Biotec).

Confocal microscopy.

For confocal microscopy, organs were incubated 1 h in PBS/PFA 4 % followed by 12h in PBS/sucrose 30 % before freezing. Frozen 8 µm sections were prepared and incubated with PBS/BSA 3 %/Tween 0.05 % before staining. Images were acquired with a Zeiss LSM 510 Meta

confocal immunofluorescent microscope (Zeiss) and then analyzed with LSM Image Browser software (Zeiss).

Spleen cell culture.

Total spleen cells were cultured at a density of 1×10^6 cells/mL in RPMI 1640 supplemented with 10% fetal calf serum (FCS) with 5 ng/mL LPS (Invivogen). For 4-hydroxytamoxifen (OHTAM) (Sigma-Aldrich) induction, 1uM were dissolved in methanol were added in the culture media on the third day of culture.

Screening of CH1 deletion in HCDD-CH1+ mice

Screening of CH1 deletion was carried out using the following primers: pVHForEagI ACGGCCGAAGCTTAAAAACCTCAGAGGATTTGTCATCTCTA and GammaCH3HumRev GTGGTCTTGTAGTTGTTCTC.

ELISPOT assays.

For evaluation of Igκ or IgM secretion, sorted populations were seeded in duplicate at a density starting at 2 × 104 cells per well, followed by five-fold serial dilutions in culture medium on a 96-well plate MultiSreen HTS (Millipore) previously coated over-night at 4 °C with 1.5 µg per well of anti-Igκ or anti-IgM (Beckman Coulter) in PBS and saturated with culture medium. Cells were incubated 6 h at 37 °C and then removed by washing with PBS/Tween 0.01 %. Plate was then incubated 1 h à 37 °C with 1 µg per well of alkaline phosphatase-coupled anti-Igκ or anti-IgM (Beckman Coulter) in PBS. After washing PBS/Tween 0.01 %, plates were incubated 10 min with 100 µL of BCIP/NBT alkalin phosphatase substrate (Millipore). After washing and drying, pictures of wells were taken and images were analyzed for spots numbers and areas with ImageJ software.

Statistical analysis.

The statistical tests used to evaluate differences between variables were indicated in legends and were done using Prism GraphPad software (San Diego, CA). All P values < 0.05 were considered significant using Student's t-test.

RESULTS

Generation and characterization of the IgJ^{GFP} reporter model.

To follow *IgJ* expression and create a new reporter model for PC lineage, we generated a transgenic mouse strain that express the eGFP cDNA under the control of regulatory sequences from the IgJ locus (**supplemental Fig.1**). The transgene comprise the 1.4 kb promoter sequence of the *IgJ* gene including the Pax5 repression site [31] and a 1.5 kb genomic fragment from a region located between 6 and 7.5 kb upstream of the transcriptional start site, containing the main enhancer element controlling *IgJ* gene expression [27]. To limit the position effects, the transgene was flanked with two insulators sequences from the chicken β-globin. We obtained two different strains (clone 10 and 13) that were first analyzed by flow cytometry on 8 days SRBC immunized mice. In spleen, we detected two distinct cell populations expressing GFP: a bright population (GFP^{high}) characterized by a low expression of the pan-B cell marker B220 and a population expressing intermediate level of GFP (GFP^{low}) together with the B220 marker (**Fig.1A**). As expected, in both strains, CD138^{+} B220^{low} PCs were highly GFP positive with a slight difference in intensity between clones 10 and 13 (**Fig.1B**). As clone 13 presented the strongest level of GFP, further results presented in this study will focused on this strain. But, except when indicated, the pattern of expression of the GFP is similar in both strains. We also detected a GFP^{high} population in bone marrow (BM) corresponding to the CD138^{+}/B220^{low} PCs and no other GFP^{+} population showing the restriction of *IgJ* expression to the PC compartment. Interestingly, by contrast to previous assumptions [32], almost all CD138^{+} cells in spleen or BM were GFP^{high} and thus, express the *IgJ* gene (**Fig.1B**).

We also observed a B220^{+}/GFP^{low} population that expresses the germinal centers markers GL7 and Fas (Fig. 1C, top panel). About 75% of the GL7^{+} B cells in spleen are GFP positive. Similar

results were obtained with PNA/Fas staining in Peyers' patches (PP) (**supplemental Fig.3**). GFP^{low} GC B cells displayed both centroblast and centrocyte phenotypes as seen with CXCR4 staining (**Fig. 1B, middle panel**). Some of the GFP^{low} B cells are IgH-switched expressing IgG1 together with GL7 (**Fig.1C, lower panel**). Interestingly, IgH-switched cells that do not express GFP are also $GL7^{neg}$ showing that post-GC memory B cells do not express IgJ (**Fig. 1C, lower panel**).

Immunofluorescence on spleen sections confirmed that PCs are almost all GFP^{high} cells, localized mainly in the extrafollicular and peri-arteriolar areas (**Fig.1D**). GFP^{high} cells are readily observed in various organs including BM and lamina propria but also lung or kidney (**Fig.1E**), validating IgJ^{GFP} model as a valuable tool to study PC localization and migration. Consistent with flow cytometry results, GFP^{low} cells colocalized with GC area (IgD^{-}) in lymph nodes (**Fig.1F**), spleen and PP and are all $GL7^{+}$ cells (*not shown*). Strikingly, we also observed a significant number of GFP^{high} plasma cells in GCs of spleen and mesenteric lymph nodes of immunized mice (**Fig.1F**). As previously described, some PCs were localized at the periphery of the GCs but we also detected in significant number of GFP^{high} cells within the GC structure. Most of this intra-GC PCs were fully differentiated as seen by their CD138 staining and were mainly located in the light zone (Fig. 1F, right image). To further characterize these IgJ-expressing cells, we performed transcriptional analyses on sorted $B220^{+}/GFP^{low}$ and $CD138^{+}/GFP^{high}$ cells from spleen relative to $B220^{+}/GFP^{-}$ cells. Consistent with their GC phenotype, GFP^{low} B cells expressed high amount of *Aicda* gene together with a significant decrease of the anti-apoptotic transcription factor *Bcl2* compared with GFP^{neg} B cells. As expected, GFP^{low} B cells also expressed increased amount of IgJ transcripts but, interestingly, did not express increased amount of PC transcription factors like *Prdm1* or *Xbp1*. However, they displayed a significant reduction of about 4 fold of *Pax5* (Fig. 1G). Consistent with their PC phenotype, GFP^{high} cells presented with high expression of *IgJ*, *Prdm1*, *Xbp1* together with a strong decrease of *Pax5* (**Fig.1G**).

IgJ is an early marker of B cell terminal differentiation.

To verify if the *IgJ* gene is expressed during all stages of PC differentiation, we further performed *in vitro* LPS stimulations of spleen B cells from IgJ^{GFP} mice. As seen in **Fig.2A**, GFP was strongly detected from the first 48h in a significant proportion of cells, most of these cells remaining $CD138^{neg}$. At 72h, all the $CD138^{+}$ cells were also GFP^{+}, but a population of $GFP^{+}/CD138^{neg}$ cells was still present. Interestingly, κ light chain specific ELISPOT revealed that those $GFP^{+}/CD138^{neg}$ cells are secreting cells even if spots area were slightly smaller than $GFP^{+}/CD138^{+}$ plasmablasts cells (**Fig.2B**). By contrast, $GFP^{neg}/CD138^{neg}$ B cells secreted no or very low amount of Ig light chain. Real-time PCR analyses confirmed these results showing that $GFP^{+}/CD138^{neg}$ cells already express the master regulator of plasma cell *Prdm1* and the secreted form of Igμ heavy chain, together with a slight downregulation of *Pax5* (**Fig.2C**). These results seem to demonstrate that *IgJ* expression appears very early during the process of terminal differentiation of the B cell lineage, before the expression of CD138 and should therefore be an efficient marker of the previously described pre-plasmablast population [28,33].

Recombinase activity in $IgJ^{CreERT2}$ model only targets $CD138^{+}$ cells

Having shown that IgJ promoter/enhancers could be advantageously used to target PC lineage, we characterized the $IgJ^{CreERT2}$ mice line, created by the EUCOMMTOOLS consortium, which carries an eGFP and Cre^{ERT2} recombinase expression cassette under the control of regulatory sequences of the IgJ locus (**supplemental Fig.1**). In contrast with our IgJ^{GFP} model, spleen and BM analysis of these mice revealed a very weak fluorescence of the eGFP making it disadvantageous to follow up PCs and the expression of the Cre^{ERT2} recombinase by flow cytometry (**Fig.3A**). This was confirmed in LPS-stimulated cells that did not show detectable GFP in $CD138^{+}$ plasmablasts (**Fig.3B**).

To further characterize the $IgJ^{CreERT2}$ recombinase activity, mice were crossed with the Rosa26-LSL-Tomato mouse line (tdTomato) in which a loxP-flanked STOP cassette prevents transcription of the downstream red fluorescent protein tdTomato. Total spleen cells from $IgJ^{CreERT2}$ x tdTomato mice, were put in culture under LPS stimulation and treated with OHTAM after 3 days of culture.

On the following day (96h of culture), we achieved 77.13% ± 8.23 (mean ± SEM n=3) of CD138^{high}/tdTomato^{+} cells while the B220^{high}/CD138^{neg} remained low (8.51% ± 2.95 (mean ± SEM n=3)). However, about 25% of B220^{low}/CD138^{neg} cells acquired the tdTomato fluorescence. These cells likely correspond to the pre-plasmablasts described in our IgJ^{GFP} model, that expressed *IgJ* gene before the expression of CD138. There is no leaky Cre activity in the stimulated cells not treated with OHTAM (**Fig3.C**).

In vivo, the IgJ^{CreERT2} x tdTomato offspring was immunized with SRBC and treated with tamoxifen (**supplemental Fig.2**). At day 11 post-immunization, following 2 injections of tamoxifen, we detected the presence of tdTomato in 91.04% ± 1.14 (mean ± SEM n=3) of B220^{low}/CD138^{high} cells in spleen (**Fig.3D**) and 86.19% ± 6.49 (mean ± SEM) in BM. Less than 1% of B220^{high}/CD138^{neg} B-cells in the spleen were tdTomato^{+} likely accounting for few B cells already committed to the PC fate. No other cells were tdTomato^{+} demonstrating a high specificity of the IgJ activity as seen in IgJ^{GFP} mice (**Fig.3E**). In contrast with the IgJ^{GFP} model, we did not detected Cre^{ERT2} activity in GC B cells (**Fig.3F**). This discrepancy is likely due to the weak expression of Cre^{ERT2} in these cells as shown by the absence of the coexpressed GFP. In control mice injected with oil alone, we detected a leaky activity of the Cre^{ERT2} recombinase in PCs (10.25% ± 5.51 mean ± SEM; n=3 in the spleen and 22.56% ± 12.30 mean ± SEM; n=3 in BM), that was gender independent. Such leaky activity of the Cre^{ERT2} recombinase has already been described in other models[34,35] and will need to be taken in account for genetic manipulations of PCs in this model. Altogether, our data show that genetic manipulations of PCs can be efficiently and specifically obtained in IgJ^{CreERT2} mice.

Modifications affecting immunoglobulin structure affect PC survival

To further validate the IgJ^{CreERT2} model as an efficient tool to study PCs biology, we took advantage of our previously published mouse model for Heavy Chain Deposition Disease (HCDD)[29] in which the gene coding for a pathogenic human Igγ heavy chain was inserted in the Igκ locus of the mice. The CH1 domain of this HC was flanked by two loxP sites to allow its deletion upon Cre

recombinase activity since the disease is characterized by deposition of a truncated CH1-deleted HC. CH1 domain deletion was not supposed to affect PCs since CH1-deleted HCs do not interact with the binding immunoglobulin protein (BiP) chaperone and were then supposed to be freely secreted [36,37]. In our previous study, the deletion of the CH1 was done in the germline lineage so that all newly formed B cells expressed the truncated HC. While we did not detected any effect on the PC differentiation, we showed that the truncated HC was poorly secreted compared to the full-length and that PCs bearing this truncated Ig were more sensitive to proteasome inhibitors and displayed increased ER stress markers[29]. Therefore, to assess the real effect of deleting the CH1 only in PCs, we crossed the $IgJ^{CreERT2}$ mouse line with the HCDD-$CH1^{+}$ mouse, carrying a floxed CH1 domain. In a first validating experiment, we sorted spleen cells to obtain the following populations: plasma cells ($B220^{low}$/$CD138^{+}$ cells), germinal center B cells ($B220^{+}$/$GL7^{+}$), other B cells ($B220^{+}$) and the rest of cells. Cells were cultured without stimulation for 24h with OHTAM before gDNA from each population was extracted to carry out a PCR allowing the detection of the deleted CH1 allele. As seen in **Fig.4A**, the CH1-deleted band appeared only in the PC population. In contrast with the tdTomato *in vivo* experiment, we did not observe any leaky activity *in vitro* for this model as the non-treated PCs only displayed the band corresponding to the full-length HC. Then, total spleen cells from $IgJ^{CreERT2}$ x HCDD-$CH1^{+}$ mouse were stimulated with LPS for 4 days and treated with OHTAM or vehicle from day 3. We first confirmed that OHTAM treatment induced the deletion of the CH1 exon with no leaky activity in the non-treated cells (**Fig.4B**). As seen in **Fig.4C**, we observed a decreased of $CD138^{+}$/$B220^{low}$ cells treated with OHTAM compared to non-treated ones (32.91% ± 2.91 vs. 23.82% ± 4.54 mean ± SEM, $*P < 0.05$; n=3) showing that truncation of the CH1 domain could be toxic when occurring in PCs.

DISCUSSION

This study sheds light on a yet unknown pattern of expression of the IgJ chain in mouse. The lack of reliable antibodies has long precluded the efficient characterization of the IgJ-expressing cells in mouse. Here, using a transgenic reporter system in which the GFP gene was placed under the control of the IgJ promoter/enhancer, we show that IgJ chain is expressed in almost all PCs in

mouse, independently of their localization in spleen, BM, lamina propria or PP. Our transgenic model allowed us to precisely determine the stages of induction of the IgJ chain *in vitro*, following LPS stimulation of primary B cells, with IgJ/GFP expressed earlier than CD138. This result could be consistent with preplasmablasts (PPBs), an early subset of ASCs described by Kallies et al. [28]. Using mice rendered prdm1-deficient by the targeted insertion of a GFP gene, they characterized a population of low secreting cells that express IgJ together with markers of PC differentiation like XBP1 and IRF4. However, the $GFP^{+}/CD138^{neg}$ cells in our study secrete high amounts of Ig, comparable to $CD138^{+}$ cells. This difference could account for the absence of BLIMP1 in their model, limiting the secretion rate of Ig chains [22]. Whether PPBs in their study and our $GFP^{+}/CD138^{neg}$ cells represent different stages of PC differentiation or an equivalent population, remains to be addressed. In any case, IgJ expression appears as a reliable marker of ASCs *in vitro* as already shown in human B cells [23,38,39] and the IgJ^{GFP} model will be useful to accurately study the early steps of the PC differentiation. *In vivo*, we confirmed than no other hematologic cell lineage than the B lineage expressed the *IgJ* gene, making it a better reporter than other PC-related genes like Blimp-1[19,18], which are expressed in other cell lineages. Interestingly, we did not detected any IgJ activity in the pre-B and immature B cell stages as previously claimed [24]. However, we did detect IgJ activity in GC B cells. This activity could mirror cells that are already engaged in the PC differentiation. However, our observations showed that most GC B cells were GFP^{+} and all of them cannot be committed to PC differentiation. In fact, GFP expression in these cells could reflect a transient activity of the *IgJ* gene in GCs that, together with the long half-life of the GFP protein[40], could be misleading on the real activity of the IgJ promoters. More experiments are needed to conclude on this expression of the *IgJ* gene in GC and could elucidate new early steps of PC differentiation.

Since the IgJ^{GFP} model put light in the use of IgJ promoter as a good one to target PCs, the creation of a mouse model having an inducible recombinase under its control seemed like the path to take to improve, not only the study of the effects of modifying PC but the creation of mouse models for several PC-related malignancies. Here we presented the *in vitro/in vivo* characterization of the

inducible IgJ^{CreERT2} inducible model established by the EUCOMM consortium. As discussed above, this model also expressed an *eGFP* gene together with the tamoxifen-inducible Cre^{ERT2} recombinase. Contrastingly to IgJ^{GFP}, eGFP levels were very weak. We attributed this discrepancy to the complex architecture of the IgJ^{CreERT2} locus (artificial splice donor site, two consecutive T2A cleavage) that likely affects the global expression of the transgenes. However, we cannot exclude that the transgenic construct of the IgJ^{GFP} mice, which is not a knock-in and does not contain the full DNA region surrounding *IgJ* gene, could also be a bit further from the physiologic regulation of the locus. The low level of fluorescence of the eGFP in the IgJ^{CreERT2} model could be improved by the use of anti-GFP antibodies in flow cytrometry to correlate the expression of Cre^{ERT2} recombinase in future models if other reporter genes are not available. Nonetheless, with the reporter tdTomato model, we showed that the recombinase activity only targets CD138^{+} cells while B cells remain almost untouched. However, the leakiness of Cre recombinase in PCs (non subjected to tamoxifen) could be more worrying for temporal induction of oncogenes for example. This leaky affect has been well described in the literature [34] [35]. Reaching no-leak seems almost impossible, but it could likely be improved by separating the treated mice from those that are not to avoid the cross-contamination by coprophagia[34]. In any case, if temporal activity of the Cre recombinase is not fully ensured in this model, its spatial one seems to be high specific with a strict restriction of activity to antibody secreting cells and for the first time, no other hematopoietic cell lineage.

Our preliminary results with the HCDD-CH1^{+} model showed that PC survival is linked to the maintenance of its Ig integrity. This result demonstrated that even if CH1 domain is not strictly required for HC to be secreted[36], its deletion seems to affect PC survival. The absence of truncated band in untreated cells that would appear due to the leaky activity of the recombinase could be explained by this deleterious effect: those plasmablasts that spontaneously delete their CH1 domain are automatically eliminated during differentiation into ASCs and therefore cannot be retrieved by PCR. These results could account for the rare occurrence of heavy chain diseases (HCD) or heavy chain deposition diseases (HCDD) characterized by the production of CH1-

truncated HCs[41,37]. Moreover, the rare HCDD patients are mostly characterized by small, low-proliferative PC clones and low levels of circulating monoclonal HC. We have also shown in our mouse model of HCDD that the isolated truncated HC is far less secreted than the full-length HC associated with LC, highlighting that the CH1 domain, if not mandatory, at least greatly improved Ig trafficking into PCs[29]. This low secretion was also associated with increased ER stress and higher sensitivity to proteasome inhibitors[29]. Altogether, these previous findings and observations represented a body of evidence that CH1 deletion was somehow embarrassing for secreting cells. However, since CH1 deletion in these cases appears early in B cell development (mouse model) or is associated with oncogenic events (HCDD patients), it remained difficult to evaluate the real toxicity of a truncated HC for PCs. We now showed that CH1 deletion directly occurring in PCs is highly toxic, as previously shown in our laboratory for truncated LCs[30], paving the way for new therapeutics targeting monoclonal Ig. Currently, studies using of Antisense Oligo Nucleotides (ASOs) to induce exon skipping of Ig genes are being developed and could be adapted to be used in PC malignancies to generate toxic truncated Igs [42].

Altogether, we herein described two new models to study PCs using the restricted expression of *IgJ* gene to antibody secreting cells. IgJ^{GFP} mice will reinforce the pool of reporter models for PCs with a more specific pattern of expression. The use of IgJ^{CreERT2} model will be a huge step in the understanding of PC physiology and the modelling of PC neoplasm. The breeding of this novel inducible model with others carrying Cre-inducible genes or oncogenes opens new avenues to study this crucial but yet unexplored lineage.

REFERENCES

1. Delogu, A. *et al.* Gene repression by Pax5 in B cells is essential for blood cell homeostasis and is reversed in plasma cells. *Immunity* **24**, 269–281 (2006).
2. Nera, K.-P. *et al.* Loss of Pax5 promotes plasma cell differentiation. *Immunity* **24**, 283–293 (2006).
3. Tunyaplin, C. *et al.* Direct repression of prdm1 by Bcl-6 inhibits plasmacytic differentiation. *J. Immunol. Baltim. Md 1950* **173**, 1158–1165 (2004).
4. Muto, A. *et al.* Bach2 represses plasma cell gene regulatory network in B cells to promote antibody class switch. *EMBO J.* **29**, 4048–4061 (2010).
5. Sciammas, R. *et al.* Graded expression of interferon regulatory factor-4 coordinates isotype switching with plasma cell differentiation. *Immunity* **25**, 225–236 (2006).
6. Klein, U. *et al.* Transcription factor IRF4 controls plasma cell differentiation and class-switch recombination. *Nat. Immunol.* **7**, 773–782 (2006).
7. Shaffer, A. L. *et al.* Blimp-1 orchestrates plasma cell differentiation by extinguishing the mature B cell gene expression program. *Immunity* **17**, 51–62 (2002).
8. Lin, K.-I., Angelin-Duclos, C., Kuo, T. C. & Calame, K. Blimp-1-dependent repression of Pax-5 is required for differentiation of B cells to immunoglobulin M-secreting plasma cells. *Mol. Cell. Biol.* **22**, 4771–4780 (2002).
9. Reimold, A. M. *et al.* Plasma cell differentiation requires the transcription factor XBP-1. *Nature* **412**, 300–307 (2001).
10. Fiancette, R. *et al.* A myeloma translocation-like model associating CCND1 with the immunoglobulin heavy-chain locus 3' enhancers does not promote by itself B-cell malignancies. *Leuk. Res.* **34**, 1043–1051 (2010).
11. Katz, S. G. *et al.* Mantle cell lymphoma in cyclin D1 transgenic mice with Bim-deficient B cells. *Blood* **123**, 884–893 (2014).
12. Knittel, G. *et al.* B-cell-specific conditional expression of Myd88p.L252P leads to the development of diffuse large B-cell lymphoma in mice. *Blood* **127**, 2732–2741 (2016).
13. Dogan, I. *et al.* Multiple layers of B cell memory with different effector functions. *Nat. Immunol.* **10**, 1292–1299 (2009).

14. Wen, Z. *et al.* Expression of NrasQ61R and MYC transgene in germinal center B cells induces a highly malignant multiple myeloma in mice. *Blood* (2020) doi:10.1182/blood.2020007156.
15. Shaffer, A. L., Emre, N. C. T., Romesser, P. B. & Staudt, L. M. IRF4: Immunity. Malignancy! Therapy? *Clin. Cancer Res. Off. J. Am. Assoc. Cancer Res.* **15**, 2954–2961 (2009).
16. Linterman, M. A. & Vinuesa, C. G. Signals that influence T follicular helper cell differentiation and function. *Semin. Immunopathol.* **32**, 183–196 (2010).
17. Fairfax, K. A. *et al.* Different kinetics of blimp-1 induction in B cell subsets revealed by reporter gene. *J. Immunol. Baltim. Md 1950* **178**, 4104–4111 (2007).
18. Fooksman, D. R. *et al.* Development and migration of plasma cells in the mouse lymph node. *Immunity* **33**, 118–127 (2010).
19. Kallies, A. *et al.* Plasma cell ontogeny defined by quantitative changes in blimp-1 expression. *J. Exp. Med.* **200**, 967–977 (2004).
20. Linterman, M. A. *et al.* Foxp3+ follicular regulatory T cells control the germinal center response. *Nat. Med.* **17**, 975–982 (2011).
21. Xin, A. *et al.* A molecular threshold for effector CD8 + T cell differentiation controlled by transcription factors Blimp-1 and T-bet. *Nat. Immunol.* **17**, 422–432 (2016).
22. Tellier, J. *et al.* Blimp-1 controls plasma cell function through the regulation of immunoglobulin secretion and the unfolded protein response. *Nat. Immunol.* **17**, 323–330 (2016).
23. Koshland, M. E. The coming of age of the immunoglobulin J chain. *Annu. Rev. Immunol.* **3**, 425–453 (1985).
24. Max, E. E. & Korsmeyer, S. J. Human J chain gene. Structure and expression in B lymphoid cells. *J. Exp. Med.* **161**, 832–849 (1985).
25. Bjerke, K. & Brandtzaeg, P. Terminally differentiated human intestinal B cells. J chain expression of IgA and IgG subclass-producing immunocytes in the distal ileum compared with mesenteric and peripheral lymph nodes. *Clin. Exp. Immunol.* **82**, 411–415 (1990).
26. Brandtzaeg, P. & Johansen, F.-E. Mucosal B cells: phenotypic characteristics, transcriptional regulation, and homing properties. *Immunol. Rev.* **206**, 32–63 (2005).

27. Kang, C. J., Sheridan, C. & Koshland, M. E. A stage-specific enhancer of immunoglobulin J chain gene is induced by interleukin-2 in a presecretor B cell stage. *Immunity* **8**, 285–295 (1998).
28. Kallies, A. *et al.* Initiation of plasma-cell differentiation is independent of the transcription factor Blimp-1. *Immunity* **26**, 555–566 (2007).
29. Bonaud, A. *et al.* A mouse model recapitulating human monoclonal heavy chain deposition disease evidences the relevance of proteasome inhibitor therapy. *Blood* **126**, 757–765 (2015).
30. Srour, N. *et al.* A plasma cell differentiation quality control ablates B cell clones with biallelic Ig rearrangements and truncated Ig production. *J. Exp. Med.* **213**, 109–122 (2016).
31. Wallin, J. J. *et al.* B cell-specific activator protein prevents two activator factors from binding to the immunoglobulin J chain promoter until the antigen-driven stages of B cell development. *J. Biol. Chem.* **274**, 15959–15965 (1999).
32. Erlandsson, L. *et al.* Joining chain-expressing and -nonexpressing B cell populations in the mouse. *J. Exp. Med.* **194**, 557–570 (2001).
33. Jourdan, M. *et al.* Characterization of a transitional preplasmablast population in the process of human B cell to plasma cell differentiation. *J. Immunol. Baltim. Md 1950* **187**, 3931–3941 (2011).
34. Kristianto, J., Johnson, M. G., Zastrow, R. K., Radcliff, A. B. & Blank, R. D. Spontaneous recombinase activity of Cre–ERT2 in vivo. *Transgenic Res.* **26**, 411–417 (2017).
35. Álvarez-Aznar, A. *et al.* Tamoxifen-independent recombination of reporter genes limits lineage tracing and mosaic analysis using CreERT2 lines. *Transgenic Res.* **29**, 53–68 (2020).
36. Feige, M. J., Hendershot, L. M. & Buchner, J. How antibodies fold. *Trends Biochem. Sci.* **35**, 189–198 (2010).
37. Bridoux, F. *et al.* Unravelling the immunopathological mechanisms of heavy chain deposition disease with implications for clinical management. *Kidney Int.* **91**, 423–434 (2017).
38. Brandtzaeg, P. Immunohistochemical characterization of intracellular J-chain and binding site for secretory component (SC) in human immunoglobulin (Ig)-producing cells. *Mol. Immunol.* **20**, 941–966 (1983).

39. Hajdu, I., Moldoveanu, Z., Cooper, M. D. & Mestecky, J. Ultrastructural studies of human lymphoid cells. mu and J chain expression as a function of B cell differentiation. *J. Exp. Med.* **158**, 1993–2006 (1983).
40. Corish, P. & Tyler-Smith, C. Attenuation of green fluorescent protein half-life in mammalian cells. *Protein Eng.* **12**, 1035–1040 (1999).
41. Cogné, M., Preud'homme, J. L. & Guglielmi, P. Immunoglobulin gene alterations in human heavy chain diseases. *Res. Immunol.* **140**, 487–502 (1989).
42. Ashi, M. O. *et al.* Physiological and druggable skipping of immunoglobulin variable exons in plasma cells. *Cell. Mol. Immunol.* **16**, 810–819 (2019).

Figure Lengends:

Figure 1: **The vast majority of PCs expresses IgJ chain.** (A) Flow cytometry analysis of GFP expression in spleen and bone marrow B cells (left) and PCs (right) of IgJ^{GFP} mice. Two distinct populations of GFP expressing cells are observed (B) Flow cytometry analysis of GFP expression among PCs IgJ^{GFP} mice. PCs are gated based on the $CD138^{+}/B220^{low}$ staining (left) and analyzed for GFP expression (right). Percentages indicate the proportion of GFP-expressing PCs. Data shown in (A) and (B) are representative of 10 independent experiments with at least 2 mice of each strain. (C) Flow cytometry characterization of the GFP^{int} population in spleen cells of 8 days immunized $IgJ^{GFP}13$ mice. $GFP^{int}/B220^{+}$ (upper left panel) cells are framed in the left graph appears in black in the subsequent analysis of GL7 and Fas expression (upper right panel). Analysis of GFP expression among $B220^{+}/GL7^{+}$ GC B cells (middle left panel). $B220^{+}/GFP^{int}$ cells are framed and appear in black in the subsequent analysis for CXCR4 expression (middle right panel). GL7 and GFP expression in $IgG1^{+}$ B cells is also shown (bottom panels). Percentages of each population are indicated. Data shown are representative of 4 independent experiments with at least 2 mice. (D) Confocal microscopy analysis of spleen section. PC foci in extrafollicular zone from 8 days immunized IgJ^{GFP} mice stained with anti-CD138. Note that almost all PCs coexpress GFP (green) and CD138 (red). (E) GFP^{high} PC are observed in various organs. BM, Bone Marrow; LP, Lamina Propria. (F) GC in a mesenteric lymph node from a SRBC immunized mouse. GFP^{low} cells are in the IgD^{neg} GC area. Note the presence of a significant number of $GFP^{high}/CD138^{+}$ cells located within the GC area (arrows). (G) Transcription analysis of sorted $B220^{+}/GFP^{neg}$, $B220^{+}/GFP^{int}$ and $CD138^{+}/GFP^{high}$ cells from spleens of IgJ^{GFP} 13 mice. Fold change expression was established compared to $B220^{+}/GFP^{neg}$ B cells with Gapdh as housekeeping gene. Data are pooled from 7 experiments in which spleens from 2 mice were pooled and sorted, except for $CD138^{+}/GFP^{high}$ cells that were sorted in 5 experiments. Results are expressed in log scale as mean + SEM.

Figure 2: IgJ expression is an early marker of PC differentiation. (A) Flow cytometry analysis LPS-stimulated splenocytes from IgJ^{GFP} 13 mice at 48h and 72h. $B220^{+}/GFP^{int}$ cells are framed and percentages are indicated. GFP^{+} population framed in the left panel appears in black in the subsequent graphs. Percentages of $CD138^{+}$ plasmablasts are indicated (middle) and the expression of CD138 among GFP^{+} cells is shown in the right panel. Data shown are representative of 10 independent experiments with at least 2 mice. (B) Representative ELISPOT results from LPS-stimulated cells sorted at 72h according to the GFP and CD138 expression as indicated in images. Data shown are representative of 3 independent sorting experiments. (C) Gene expression relative to *Gapdh* of sorted $CD138^{neg}/GFP^{neg}$, $CD138^{neg}/GFP^{+}$ and $CD138^{+}/GFP^{+}$ cells. Results are shown as fold-change expression compared to the $CD138^{neg}/GFP^{+}$ cells. Results are from 3 independent sorting experiments. Data are shown as mean ± SD.

Figure 3: Recombinase activity in $IgJ^{CreERT2}$ targets $CD138^{+}$ cells. (A) Flow cytometry analysis of eGFP expression in spleen and bone marrow PCs of $IgJ^{CreERT2}$ mice denoting the low fluorescence (B) Flow cytometry analysis LPS-stimulated splenocytes at 72h for eGFP and $B220^{+}$ or $CD138^{+}$ (C) Flow cytometry analysis LPS-stimulated splenocytes from $IgJ^{CreERT2}$ x tdTomato mice at 96h. tdTomato expression in B cells (right) and PCs (left) for the control (CTL) vs 4-hydroxytamoxifen (OHTAM) treated cells. Cells expressing tdTomato are mostly found in the OHTAM group. As previously shown in IgJ^{GFP} mice, some $CD138^{-}$ cells already expressed tdTomato (right). (D) Representative flow cytometry analysis for tdTomato expression in spleen and bone marrow of $IgJ^{CreERT2}$ x tdTomato mice after *in vivo* treatment. (E) Representative flow cytrometry analysis of spleen cells for tdTomato expression. PCs are gated based on the $CD138^{+}/B220^{neg/low}$ staining (middle) and analyzed for tdTomato expression (left). B cells are gated based on $B220^{high}/CD138^{neg/low}$ (middle) and analysed for tdTomato expression (right). Percentages indicate the proportion of tdTomato-expressing cells. (F) Flow cytometry analysis of $B220^{+}/GL7^{+}$ GC B cells showing almost no expression of tdTomato.

Figure 4: PC survival correlates with Immunoglobulin modification. (A) genomicDNA analysis by PCR of sorted spleen cells of $IgJ^{CreERT2}$ x HCDD-$CH1^{+}$ mouse (Plasma cells : PC ; Germinal Center cells: GC, B cells and rest of cells) after being cultured for 24h with OHTAM. CTL non-TAM treated PCs do not exhibit the truncated band (right). (B) genomicDNA analysis by PCR of 4 days LPS-stimulated splenocytes from $IgJ^{CreERT2}$ x HCDD-$CH1^{+}$ mice to show the CH1 deletion only in OHTAM cells cultured with it for 24h. (C) Representaive flow cytometry analysis of 4 days LPS-stimulated splenocytes from $IgJ^{CreERT2}$ x HCDD-$CH1^{+}$ after 24h of treatment with gates showing the percentage of $CD138^{+}$ cells and $B220^{+}$ cells. (D) Histograms showing the significant decrease of plasmablasts ($B220^{low}$/$CD138^{+}$ population) following the deletion of CH1 in $IgJ^{CreERT2}$ x HCDD-$CH1^{+}$ mice splenocytes. $IgJ^{CreERT2}$ x tdTomato mice were used as control, showing that this decrease is not due to OHTAM treatement. ns, non significant; *$P < 0.05$.

Figure 1

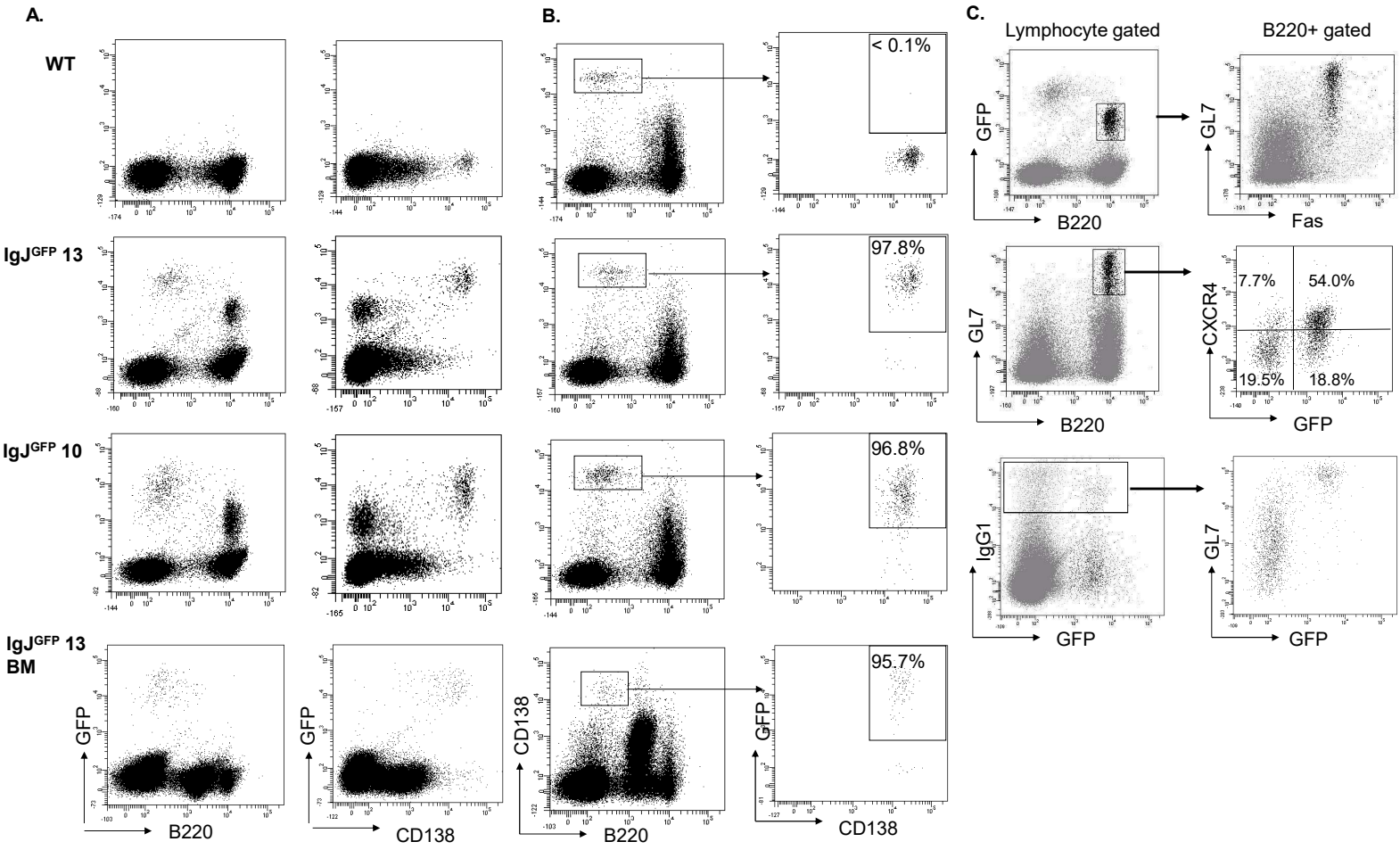
A.
B.
C.
WT
IgJGFP 13
IgJGFP 10
IgJGFP 13 BM
< 0.1%
97.8%
96.8%
95.7%
Lymphocyte gated
B220+ gated
GFP
B220
GL7
Fas
CXCR4
7.7%
54.0%
19.5%
18.8%
IgG1
CD138

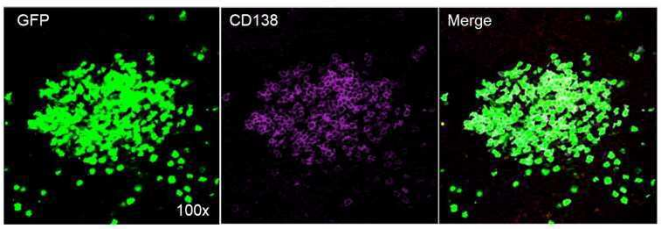
D.
GFP
CD138
Merge
100x

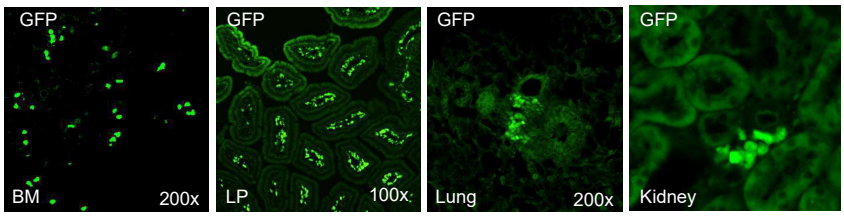
E.
GFP
BM
200x
LP
100x
Lung
200x
Kidney

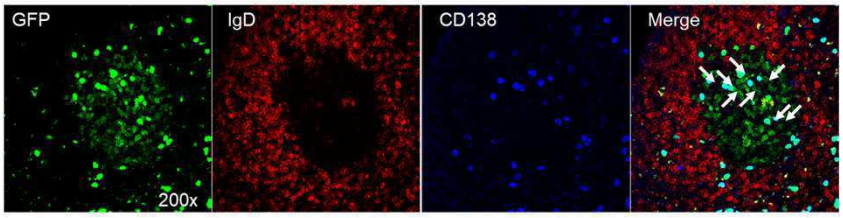
F.
GFP
IgD
CD138
Merge
200x

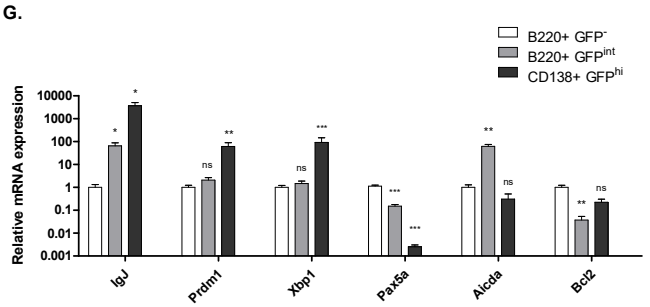
G.
B220+ GFP-
B220+ GFPint
CD138+ GFPhi
Relative mRNA expression
10000
1000
100
10
1
0.1
0.01
0.001
Igj
Prdm1
Xbp1
Pax5a
Aicda
Bcl2

Figure 2

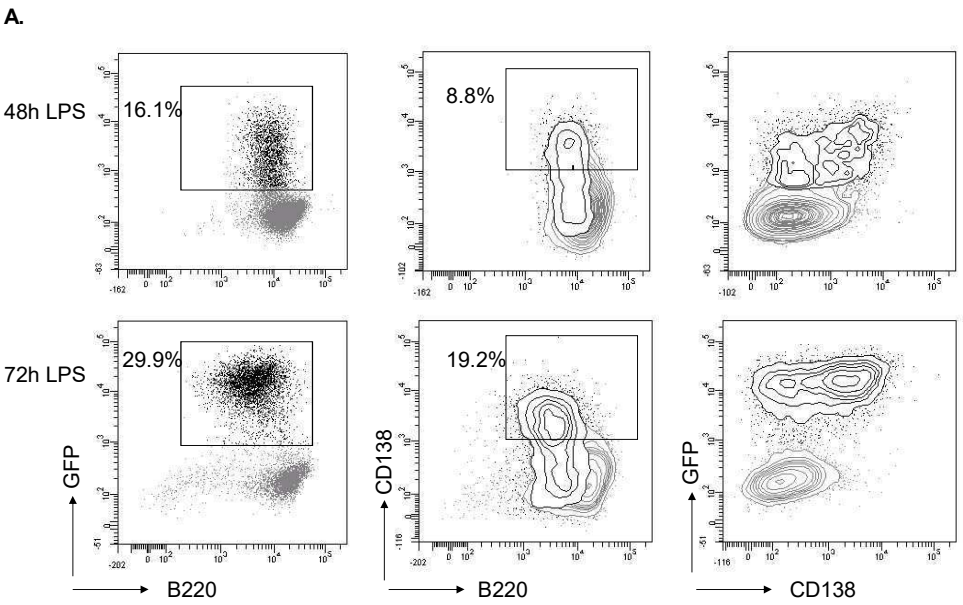
A.
48h LPS
16.1%
8.8%
72h LPS
29.9%
19.2%
GFP
B220
CD138
B220
GFP
CD138

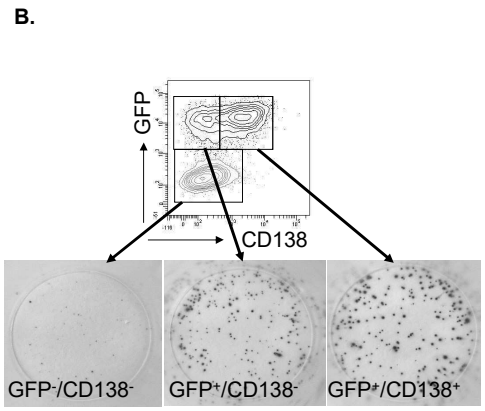
B.
GFP
CD138
GFP-/CD138-
GFP+/CD138-
GFP+/CD138+

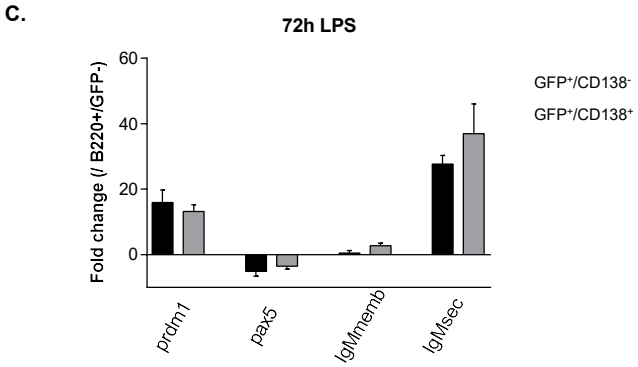
C.
72h LPS
Fold change (/ B220+/GFP-)
60
40
20
0
prdm1
pax5
IgMmemb
IgMsec
GFP+/CD138-
GFP+/CD138+

Figure 3

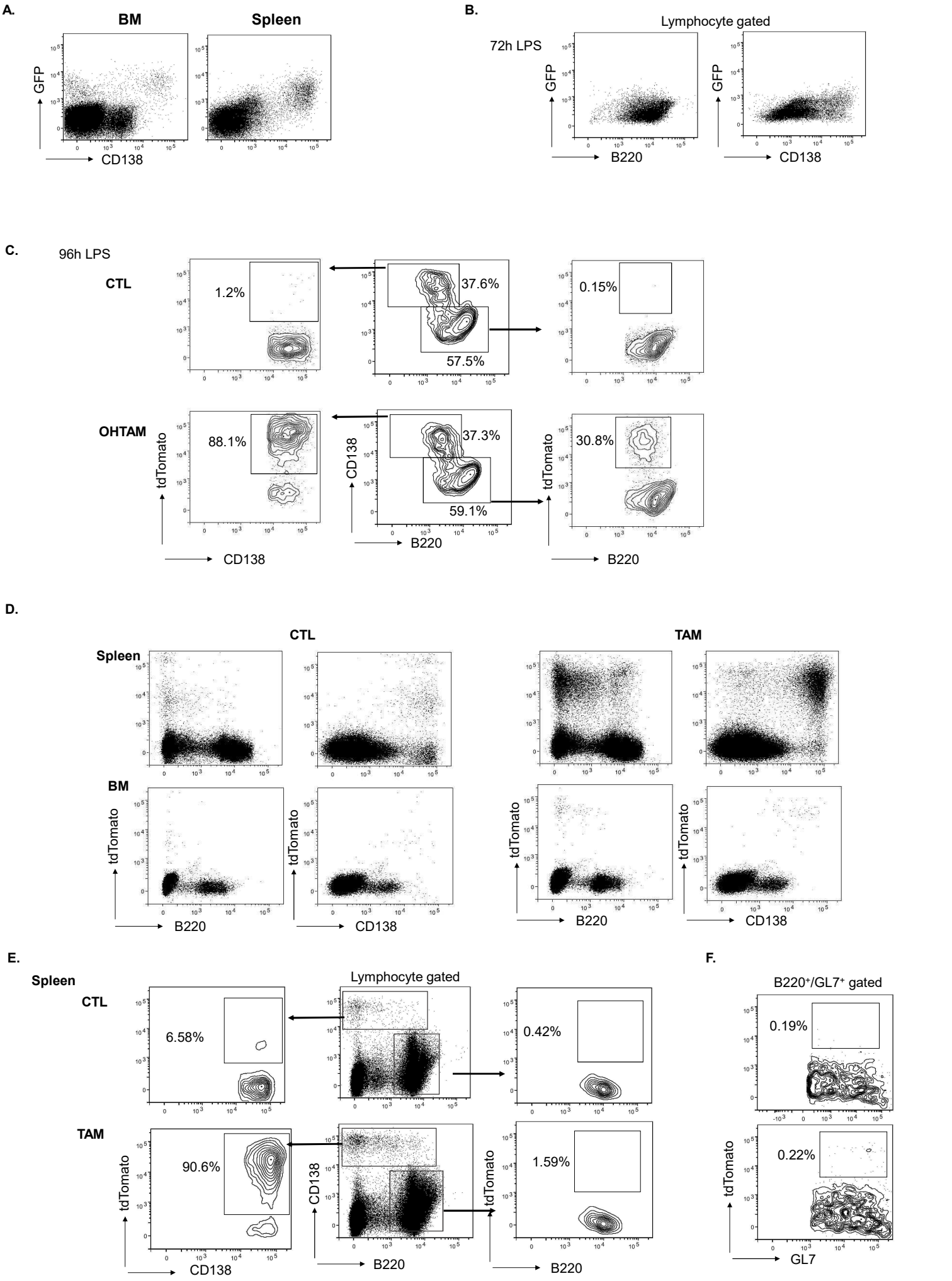
A.
BM
Spleen
GFP
CD138
B.
Lymphocyte gated
72h LPS
GFP
B220
GFP
CD138
C.
96h LPS
CTL
1.2%
37.6%
57.5%
0.15%
OHTAM
88.1%
tdTomato
CD138
37.3%
59.1%
B220
30.8%
tdTomato
CD138
B220
D.
CTL
TAM
Spleen
BM
tdTomato
B220
tdTomato
CD138
tdTomato
B220
tdTomato
CD138
E.
Spleen
Lymphocyte gated
CTL
6.58%
0.42%
TAM
90.6%
tdTomato
CD138
B220
CD138
1.59%
tdTomato
B220
F.
B220+/GL7+ gated
0.19%
0.22%
tdTomato
GL7

Figure 4

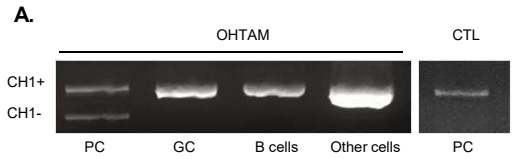
A.
OHTAM
CTL
CH1+
CH1-
PC
GC
B cells
Other cells
PC

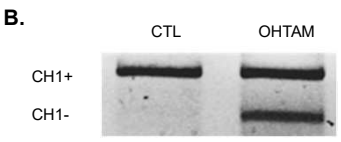
B.
CTL
OHTAM
CH1+
CH1-

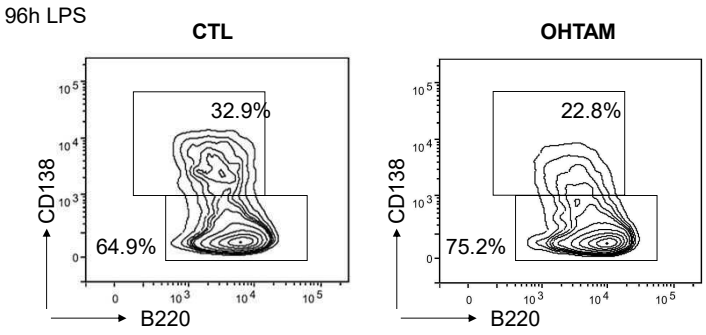
C.
96h LPS
CTL
OHTAM
32.9%
64.9%
22.8%
75.2%
CD138
B220

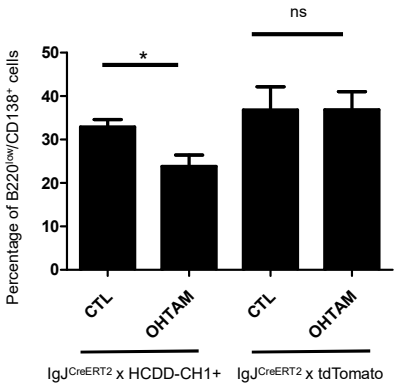
D.
ns
*
Percentage of B220low/CD138+ cells
CTL
OHTAM
CTL
OHTAM
IgJCreERT2 x HCDD-CH1+
IgJCreERT2 x tdTomato

Supp. Figure 1: (A) Representation of the IgJ^{GFP} mouse transgene for the expression eGFP (not in scale). (B) Representation of the IgJ^{CreERT} mouse insert for eGFP and Cre^{ERT2} recombinase expression in the mouse IgJ locus (not in scale). I, intron; PA, polyadenylation site; En2SA, En2 splice acceptor; F2A, foot-and-mouth disease virus 18 self-cleaving peptide

Supp. Figure 2: Protocol applied for tdTomato expression induction in vivo in IgJ^{CreERT} x tdTomato mice.

Supp. Figure 3: PNA^+/Fas^+ GC B cells in Peyers' patches express the IgJ chain. Flow cytometry analysis of PNA^+/Fas^+ B cells according to their expression of GFP in IgJ^{GFP} mice. Percentages indicate the proportion of GFP-expressing B cells among the population of GC B cells in Peyers' patches. Data shown are representative of 5 independent experiments.

Supp. Figure 1

A.

B.

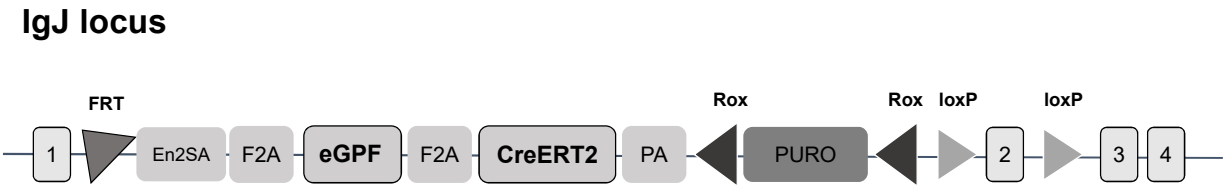

Supp. Figure 2

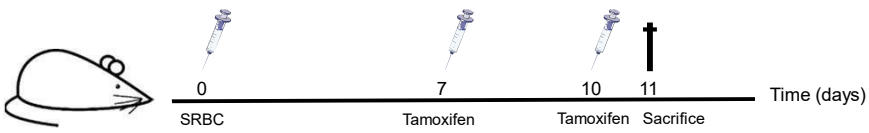

Supp. Figure 3

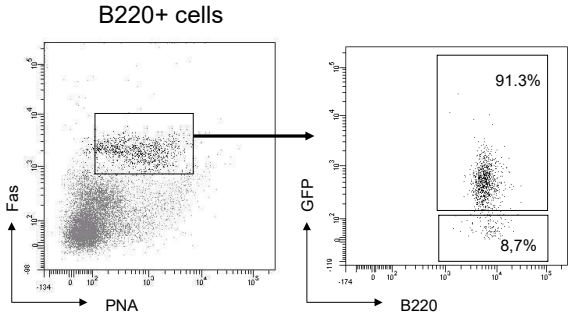

Supplemental Table. Antibodies used in flow cytometry and cell-sorting experiments

Antibody	Clone	Source
Anti-B220- BD Horizon™ V450	RA3-6B2	BD Biosciences
Anti-B220-APC	RA3-6B2	BioLegend
Anti-CD138-PE	281-1	BD Biosciences
Anti-CD138-APC	281-2	BD Biosciences
Anti-IgD-APC	11-26C.2a	BD
Anti-IgJ-PEa	NA	Santa Cruz Biotechnology
GL7-Alexa Fluor®647	GL7	BD Pharmingen
GL7-PEa	GL7	BD Pharmingen
Anti-CXCR4-PE	2B11	BD Pharmingen
Anti-IgG1-PE	A85-1	BD Pharmingen
Anti-Fas	JO2	BD Pharmingen
Anti-CD138-BV421	281-2	BD Biosciences
Anti-B220-BV786	RA3-6B2	BD Biosciences

The study of Ig-induced deposition diseases has greatly progressed in the last years thanks to the availability of novel or improved tools, such as the Cryo-EM, high-throughput sequencing, or mass spectrometry. However, to study the pathophysiology of these diseases and to evaluate new therapies, animal models are the main source of information and our research group focus on developing new murine models for the different MGCS. The creation of such models needs, not only the accrued knowledge from previous experiences but also the capacity of adapting our strategy accordingly. For example, in models that need the secretion of a LC in its free form, the crossing with the DH-LPM2A mice revealed to be crucial.

In any case, mouse models need to reproduce faithfully human diseases to be used in therapeutic investigations. Such mimicry was achieved with the LCDD model and we also showed that standard therapy for MIDD, *i.e.* cyclophosphamide and bortezomib, led to a similar hematological response as humans, with recovery of renal function and improved lifespan. Consequently, the model appears as highly relevant for further mechanistic and therapeutic investigations. Our transcriptomic results on sorted glomeruli will be further extended to younger and older mice to try to follow the evolution of the disease, from weak deposits to full-blown glomerulosclerosis. Besides a better understanding of renal function degradation in LCDD, our data could be extended to other diseases presenting with similar evolution, like diabetic nephropathy, that also suffers from the lack of reliable model (Betz and Conway, 2016). The quick decrease in LC deposits upon treatment will also be highly informative since such explorations cannot be conducted in humans. They could reveal the speed and mechanism of Ig-removal from the extracellular matrix (ECM) and if the abnormal ECM is replaced. Additionally, transcriptome modifications upon treatments could tell more about the recovery of kidney function. Finally, this model will be also useful to analyze the process of Ig deposition into ECM. We and others have shown that MIDD Igs are characterized by a striking high pI that could account for their deposition in negatively charged ECM (Bridoux et al., 2017; Joly et al., 2019; Kaplan et al., 2007). Treatments with heparanases or crossing with a transgenic model overexpressing heparanase could confirm the role of ECM charges in Ig deposition (van den Hoven et al., 2008). In an inverse study, we planned to create cell lines producing LCDD-LC with specific mutations that change their global charge. Such cells could then be used in tumor graft models as previously done in our laboratory (Khamlichi et al., 1995).

As described in the introduction, the genetic alterations are remarkably similar in MM or MGCS (Kuehl and Bergsagel, 2012; Paiva et al., 2016). Therefore, in addition to secondary events, PC fate may be conditioned also to the direct effect in proliferation exert by the different

Ig expressed. We had shown in our HCDD mouse model (Bonaud et al., 2015) and others in PCs from AL amyloidosis patients (Oliva et al., 2017), that PCs producing pathogenic Igs present abnormal cellular stress. This was confirmed by RNAseq analysis in the LCDD model, where PCs present with an exacerbated ER stress and are more sensitive to PI treatment. Our other models of MGCS (Fanconi Syndrome and AL Amyloidosis) will be also evaluated soon. With them, we could show if the different Igs provoke distinct sensitivity to PI in correlation to the ER stress they induce.

Despite the information on the influence of Igs on PCs provided by these different models, up to date there was no mouse model for its study in already differentiated PCs. To begin, we had to find a unique marker for ASCs and therefore the IgJ^{GFP} model was designed. By characterizing the poorly known J chain, thanks to the eGFP, we were able to show that its expression starts before the appearance of CD138 and it increases along PC development.

While further studies of GCs and the path taken by PCs or how other molecules can affect it, can be carried out with this novel animal model, it does not answer the question of how an Ig influences them. In contrast, this could be revealed using the $IgJ^{CreERT2}$ model. We first showed that inducing the expression of new protein, such as tdTomato, by itself does not affect PCs development. Contrastingly, the preliminary results obtained with $IgJ^{CreERT2}$ x HCDD-$CH1^{+}$ *in vitro* seem to indicate that altering protein homeostasis, by inducing the production of a different Ig in already differentiated cells, leads to PC death. The new ER stress balance encountered by the cell, which is now found producing a pathogenic $CH1^{-}$ HC, could shift the UPR into the PERK pathway inducing apoptosis. Additional *in vitro* studies with apoptosis markers will be carried out as well as *in vivo* inductions. Nonetheless, the current protocol used in tdTomato mice, in which we immunized them before the tamoxifen injections, may need to be adapted without such previous boost of PC proliferation. Furthermore, long-term periods of tamoxifen induction will be tried, with the goal of observing the appearance of PC that are resistant to the stress/death. Later on, a detailed analysis of the molecular mechanisms involved by RNA sequencing (RNAseq) as well as PI sensitivity could be carried out and compared to the results obtained with HCDD mice.

Additionally, other crossings with $IgJ^{CreERT2}$ are ongoing. The first one consists of our mouse model of FS, in which the pathogenic kappa LC is flanked by two LoxP sites. We would like to see the effect that eliminating a LC has, not only in PCs but on HCs too. As mentioned before, HCDD is a rare disease where PC freely secrete HC since it is devoid of the CH1 domain. We hypothesize that this deletion may arise when the PC finds itself without a LC, and consequently, the full HC would accumulate retained by Bip while a $CH1^{-}$ one could be secreted relieving ER stress, as previously shown in cell lines (see Appendix 2) (Bender et al., 2018).

In vivo assays on these mice could help induce the appearance of such rare PCs unraveling the pathological mechanism of HCDD.

Other crossings with mouse lines carrying floxed oncogenes would be of great interest, not only to model PC neoplasms but also to increase Ig secretion as needed in other Ig-deposition diseases, such as MM Cast Nephropathy. For example, we have crossed $IgJ^{CreERT2}$ with a model carrying $Myd88^{L265P}$, a mutated form of Myd88 commonly found in WM as indicated above, whose expression is blocked by a floxed STOP cassette.

While some diseases are amenable to model in mice, obtaining one for AL amyloidosis has been a challenge for several laboratories around the world. Despite haven achieved high FLC circulating levels thanks to our transgenic strategy, our AL-LC expressing mice remained resistant to forming LC fibrils. This pushed us to generate a rat model, that could be more susceptible to AL Amyloidosis, expressing an amyloidogenic LC obtained from a patient but unfortunately, here again, the results were disappointing. The creation of a rat model similar to DH-LPM2A mouse is likely needed to increase the FLC production. In the meantime, it will be interesting to carefully monitor intrinsic LC toxicity in this model. Failure to detect organ dysfunctions does not mean that more subtle molecular changes could not be observed in specific experiments, such as cardiac or renal transcriptomic, detection of stress markers, etc.

However, as expected, our main future projects will be focused on the mouse model of AL amyloidosis that we finally obtained. Thanks to this long story, we learned that serum levels of amyloid LCs are not the sole factor needed for fibril formation in mice and that many approaches successful in other amyloidosis to trigger fibril formation were not applicable to AL amyloidosis.

Finally, our attempts to get *in vitro* fibrils unblocked this long-standing issue and shed new light on the amyloid fibril formation in mice. We showed the VL domain from our amyloid LC alone is able to form fibrils *in vitro* and that full-length LC or serum from mouse and human were highly inhibitory in this process. Nevertheless, since we got short but readily detectable fibrils when we seeded full-length LC with VL-formed seeds, we decided to inject the transgenic mice line with VL seeds and VL pre-formed fibrils. This proved to be a valuable initiative since we finally observed CR-positive deposits in spleen and heart of the injected mice. Additionally, we confirmed by IF that the deposits are composed of the transgenic LC. The same protocol did not yield deposits in another transgenic mouse model expressing a non-amyloidogenic LC from a MM patient validating that only the amyloidogenic LC can elongate the injected seeds/fibrils. We are currently confirming the nature and composition of the deposits by immune-EM and mass spectrometry and other mice are being injected with seeds for a full characterization of the model, with life-long follow-up. We have also started new collaborations

to finely analyzed cardiac function such as NT-proBNP dosage, *in vivo* imaging or histological study of stress markers previously described in the literature. Of course, kidneys will be observed in older mice since the absence of amyloid deposits in this organ was surprising taking into account the origin and the VL subgroup of the LC. However, this discrepancy between mouse and human could help decipher the process of amyloid formation.

This long-awaited successful outcome to obtain a mouse AL amyloidosis model undoubtedly raises many questions that we will endeavor to answer for untangling the pathophysiology of this disease. First, the soluble VL domain, shown to be highly amyloidogenic *in vitro*, will be injected in the λS-DH mice to see if they can spontaneously seed amyloid fibril formation. This will offer new insights into the mechanistic of fibrilization: a positive result would argue in favor of the requirement for a partial degradation of the LC to become amyloidogenic *in vivo*, opening new avenues in search of the culprit proteases, their location and activity in AL amyloidosis patients. Comparison of human and mouse degradomes, made available by recent databases (Pérez-Silva et al., 2016), will be likely informative as will be the comparative transcriptomic analyses of these proteases in human and mouse. On the contrary, if VL alone is unable to induce amyloidosis in λS-DH mice, it will mean that other factors, absent in the mouse, are implicated in the initiation of amyloid fibrils.

Our model already faithfully reproduce amyloid deposits in heart, which is the most severe form in human. Consequently, it stands as an exquisite model to test new therapeutics aiming at removing amyloid fibrils. As soon as possible, AL amyloid positive λS-DH mice will be used to evaluate our SAP-Fc molecule that proved efficiency in AA mouse models but not in other amyloidosis *in vivo*. Then, we plan to make this model available for the amyloid community since many other therapeutic approaches still suffer from the lack of reliable in vivo experimental models for amyloidosis in general and cardiac amyloidosis in particular (Buxbaum, 2009; Wall et al., 2018; Morgan et al., 2019).

In the longer term, and depending on our results with VL injections, we have planned to create a new transgenic model able to produce an amyloidogenic VL upon tamoxifen induction. For this, we have rederived ES cells from double homozygous λS-DH mice and one kappa allele will be targeted using Crispr-Cas9 technology to introduce the inducible (floxed STOP cassette) λS-VL. Then, the mice will continuously produce the full-length amyloid LC and upon tamoxifen induction, they will start to produce a burst of VL, with the hope it will trigger amyloidosis. For this, our PC-specific Cre model, $IgJ^{CreERT2}$, will be an invaluable tool.

To conclude, all the work carried out along my thesis, as well as the legacy from previous laboratory fellows, has allowed me to better understand the pathologies associated with the deregulation of PC development. With success models as LCDD that work on a first try and those that required more effort and dedication to achieve the desired results, as AL Amyloidosis that took us more than 20 years, our collaborative group work has put light in this group of rare diseases. As the first phrase in the present manuscript says “You will succeed if you persevere, and you will find joy in overcoming obstacles” and we will, therefore, continue to innovate and seek answers for the passion of science, but also in the hope of improving the outcome of patients touched by these diseases.

APPENDICES

Appendix 1. Animal models of monoclonal immunoglobulin-related renal diseases

Sirac C, Herrera GA, Sanders PW, Batuman V, Bender S, **Ayala MV**, Javaugue V, Teng J, Turbat-Herrera EA, Cogné M, Touchard G, Leung N, Bridoux F.

Nat Rev Nephrol. 2018 Apr;14(4):246-264. DOI: 10.1038/nrneph.2018.8

PMID: 29456245

ONCONEPHROLOGY

Animal models of monoclonal immunoglobulin-related renal diseases

*Christophe Sirac[1] *, Guillermo A. Herrera[2], Paul W. Sanders[3], Vecihi Batuman[4], Sebastien Bender[1], Maria V. Ayala[1], Vincent Javaugue[1,5], Jiamin Teng[2], Elba A. Turbat-Herrera[2], Michel Cogné[1], Guy Touchard[5], Nelson Leung[6] and Frank Bridoux[1,5]*

Abstract | The renal deposition of monoclonal immunoglobulins can cause severe renal complications in patients with B cell and plasma cell lymphoproliferative disorders. The overproduction of a structurally unique immunoglobulin can contribute to the abnormal propensity of monoclonal immunoglobulins to aggregate and deposit in specific organs. A wide range of renal diseases can occur in multiple myeloma or monoclonal gammopathy of renal significance, including tubular and glomerular disorders with organized or unorganized immunoglobulin deposits. The development of reliable experimental models is challenging owing to the inherent variability of immunoglobulins and the heterogeneity of the pathologies they produce. However, although imperfect, animal models are invaluable tools to understand the molecular pathogenesis of these diseases, and advances in creating genetically modified animals might provide novel approaches to evaluate innovative therapeutic interventions. We discuss the strategies employed to reproduce human monoclonal immunoglobulin-induced kidney lesions in animal models, and we highlight their advantages and shortcomings. We also discuss how these models have affected the management of these deposition diseases and might do so in the future. Finally, we discuss hypotheses that explain some limitations of the various models, and how these models might improve our understanding of other nephropathies without immunoglobulin involvement that have similar pathogenic mechanisms.

Plasma cell dyscrasias are characterized by the secretion of either a complete monoclonal immunoglobulin or immunoglobulin fragments — either free light chains or truncated free heavy chains. These fragments are often unstable owing to their abnormal physicochemical properties and may cause various pathological conditions as a consequence of their precipitation, aggregation or crystallization within cells or tissues[1,2] (BOX 1). Current treatment options for plasma cell dyscrasias mostly target the underlying haematological disorder to decrease the production of the toxic protein[3], whereas only a few treatments directly target the aggregated proteins. Thistreatment focus reflects, in part, a lack of knowledge of how and why the proteins precipitate, aggregate and deposit in specific organs and of how these aggregates modify the functions of the affected cells and organs. This shortcoming has been partially addressed by the establishment and study of *in vitro* experimental models. However, the multifactorial causes of these diseases, including the nature of the producing clone, the structural features of pathogenic immunoglobulins and their organ tropism for deposition, have complicated the establishment of animal models that faithfully reproduce human disorders. In this Review, we summarize the different strategies used to create animal models of monoclonal immunoglobulin deposition diseases, with a specific focus on transgenic approaches. In addition, we evaluate the limitations of each animal model and their contribution to the understanding and treatment of these pathological conditions. We also discuss how dissecting the pathogenic mechanisms in these experimental models of immunoglobulin deposition diseases could benefit research into other non-immunoglobulin-related nephropathies that produce similar alterations in the structure and function of the kidneys and have similar pathogenic mechanisms, such as diabetic nephropathy and inherited forms of Fanconi syndrome.

Immunoglobulin deposition diseases

Although monoclonal immunoglobulin deposition may affect a number of organs and tissues, the kidneys are the most common target. Renal disorders associated

*e-mail: christophe.sirac@unilim.fr

doi:10.1038/nrneph.2018.8
Published online 19 Feb 2018

Key points

- Numerous renal diseases occur owing to the deposition of a monoclonal immunoglobulin, including multiple myeloma and monoclonal gammopathy of renal significance
- Understanding the molecular pathogenesis of human immunoglobulin deposition diseases and testing new therapeutic strategies requires relevant animal models, which is a challenge owing to the heterogeneity of these diseases
- Models based on the injection of purified human immunoglobulins and on tumour grafts that produce the monoclonal immunoglobulin have revealed several early pathogenic events in immunoglobulin deposition and demonstrated the efficacy of innovative therapeutic agents
- Advances in transgenic techniques have allowed the creation of mouse models that faithfully reproduce the human diseases and have aided in unravelling the pathogenic mechanisms of monoclonal immunoglobulin deposition
- Animal models are invaluable tools to study the process of deposition and to explore the direct toxicity of monoclonal immunoglobulins in tissues and immunoglobulin-producing plasma cells

with the deposition of monoclonal immunoglobulins are classified according to the immunochemical nature of the deposited immunoglobulins and the pattern of renal lesions that are observed by light microscopy, immunofluorescence analysis and electron microscopy[1,4] (FIG. 1). Various conditions are thus defined, including immunoglobulin-related amyloidosis (most often involving the immunoglobulin light chain (AL)), 'non-amyloid' Randall-type monoclonal immunoglobulin deposition disease (MIDD), monoclonal light chain-induced proximal tubulopathy with or without Fanconi syndrome and myeloma cast nephropathy (MCN). Other disorders involving deposition of complete monoclonal immunoglobulins (comprising two heavy chains and two light chains), such as type 1 and type 2 cryoglobulinaemia, immunotactoid glomerulopathy and proliferative glomerulonephritis with monoclonal immunoglobulin deposits, are not discussed in this Review.

The kidneys are frequently affected by the toxicity of monoclonal immunoglobulin fragments during symptomatic multiple myeloma, in which large amounts of free monoclonal antibody light chains are filtered by the glomerulus, overwhelming the reabsorption capacity of the endocytic receptors megalin and cubilin in the proximal tubule[5,6]. Specific light chains may induce the production of inflammatory cytokines in the proximal tubule cells, and some light chains precipitate with uromodulin in the distal tubules, which results in tubular obstruction, interstitial inflammation and renal failure, a condition that is termed MCN[7]. However, most other types of renal injury occur in patients with small B cell or plasma cell clones, a condition that is termed monoclonal gammopathy of undetermined significance (MGUS)[8,9]. In these cases, even low amounts of free light chains can aggregate and deposit in organs, which can lead to organ damage and/or dysfunction[2]. Consequently, the International Kidney and Monoclonal Gammopathy (IKMG) Research Group introduced the term 'monoclonal gammopathy of renal significance' (MGRS) to define kidney diseases that are induced by a nephrotoxic immunoglobulin that is produced by a small, otherwise indolent B cell clone[10]. This disease definition is similar to that for diseases caused by pathogenic monoclonal immunoglobulin fragments in other organs, including, among others, the heart, the skin and the peripheral nervous system[2].

Proximal tubulopathy is induced by monoclonal immunoglobulin light chains, and although it is a common pathology, its clinical significance varies[7,11], including an association with renal light chain-induced Fanconi syndrome, which is a rare complication of plasma cell dyscrasias in which tumour mass is usually low. Renal Fanconi syndrome is characterized by generalized proximal tubular dysfunction leading to the urinary leakage of low-molecular-mass proteins, phosphate, uric acid, glucose and amino acids, which is often associated with osteomalacia and slowly progressive renal failure[12,13]. Fanconi syndrome is typically associated with the accumulation of light chain crystals within the endolysosomal compartment of proximal tubule cells[12,13]. The other non-crystalline proximal tubulopathies are characterized by tubular damage that may or may not be associated with interstitial inflammation, but they are not routinely associated with Fanconi syndrome. These disorders exemplify how interactions of the tubulopathic light chains with the endolysosomal system might result in different pathological and functional alterations in the proximal tubule[14]. To date, little is known about the mechanisms that underlie the distinct pathologies in these tubulopathies.

By contrast, immunoglobulin-related amyloidosis is a systemic disease that affects various organs, predominantly the kidneys and the heart, although the liver, soft tissue and nervous system are also frequently affected. This amyloidosis features extracellular deposits that are organized into fibrils comprising monoclonal immunoglobulin fragments, most commonly light chains (AL amyloidosis), although the deposits may rarely comprise truncated heavy chains only (AH amyloidosis) or both heavy chains and light chains (AHL amyloidosis). Immunoglobulin-related amyloidosis is the most frequent form of systemic amyloidosis[15,16] and in many cases is particularly aggressive. Amyloidogenic protein precursors share a number of properties, including reduced stability and solubility and a propensity to aggregate into β-pleated sheets[17]. Fibrils are enwrapped by additional molecules, including serum amyloid P component (SAP), apolipoprotein E and proteoglycans[15]. Amyloid fibrils

Immunoglobulin-related amyloidosis
Accumulation of abnormal immunoglobulin fragments that form fibrils and deposit in organs and tissues, causing their dysfunction.

Monoclonal immunoglobulin deposition disease
(MIDD). Accumulation of abnormal immunoglobulin fragments that form granular deposits in organs and tissues, mainly the kidneys, causing their dysfunction.

Myeloma cast nephropathy
(MCN). Acute kidney disease that occurs in multiple myeloma and is characterized by the obstruction of distal tubules by casts composed of a monoclonal immunoglobulin light chain.

Author addresses

[1]CNRS UMR 7276-CRIBL, University of Limoges, Limoges, France, and French National Reference Centre for "AL Amyloidosis and Other Monoclonal Immunoglobulin Deposition Diseases", University Hospital Dupuytren, Limoges, France.
[2]Department of Pathology and Translational Pathobiology, Louisiana State University Health Sciences Center, Shreveport, LA, USA.
[3]Division of Nephrology, Department of Medicine, University of Alabama at Birmingham and Birmingham Veterans Affairs Medical Center, Birmingham, AL, USA.
[4]Department of Medicine, Southeast Louisiana Veterans Health Care System, New Orleans, LA, USA, and Department of Medicine, Nephrology Section-SL45, Tulane University Medical School, New Orleans, LA, USA.
[5]Department of Nephrology and Transplantation, University Hospital of Poitiers, Poitiers, France.
[6]Division of Nephrology and Hypertension and Division of Hematology, Mayo Clinic, Rochester, MN, USA.

Box 1 | **Immunoglobulin rearrangements, synthesis and deposition**

Imperfect joining of variable (V), diversity (D) and joining (J) gene segments during V(D)J recombination, followed by activation-induced cytidine-deaminase-induced somatic hypermutations during the immune response (in germinal centres), leads to the large diversity (repertoire) of antibodies that are required for protection against pathogens (see the figure). However, some amino acid changes may also decrease the stability and folding of immunoglobulins, especially in monoclonal gammopathies, resulting in the excess production of unstable immunoglobulins or immunoglobulin fragments (light chains or heavy chains). Imbalanced production of immunoglobulin subunits is common in monoclonal gammopathies and usually results in the secretion of free light chains. Free heavy chains are normally retained in the cell by endoplasmic reticulum chaperones (immunoglobulin heavy chain-binding protein (BiP; also known as GRP78)) unless a genetic deletion of the heavy chain constant domain 1 (CH1) occurs, which is rare. The abnormal physicochemical properties of these monoclonal immunoglobulin fragments may result in various pathological conditions as a consequence of fragment precipitation, aggregation or crystallization in cells or tissues. AH amyloidosis; immunoglobulin heavy chain amyloidosis; AL amyloidosis, immunoglobulin light chain amyloidosis; $A_{(n)}$, polyadenylation; C, constant region; FS, Fanconi syndrome; GOMMID, glomerulonephritis with organized microtubular monoclonal immunoglobulin deposits; HCDD, heavy chain deposition disease; LC, light chain; LCDD, light chain deposition disease; MIDD, monoclonal immunoglobulin deposition disease; PGNMID, proliferative glomerulonephritis with monoclonal immunoglobulin deposits.

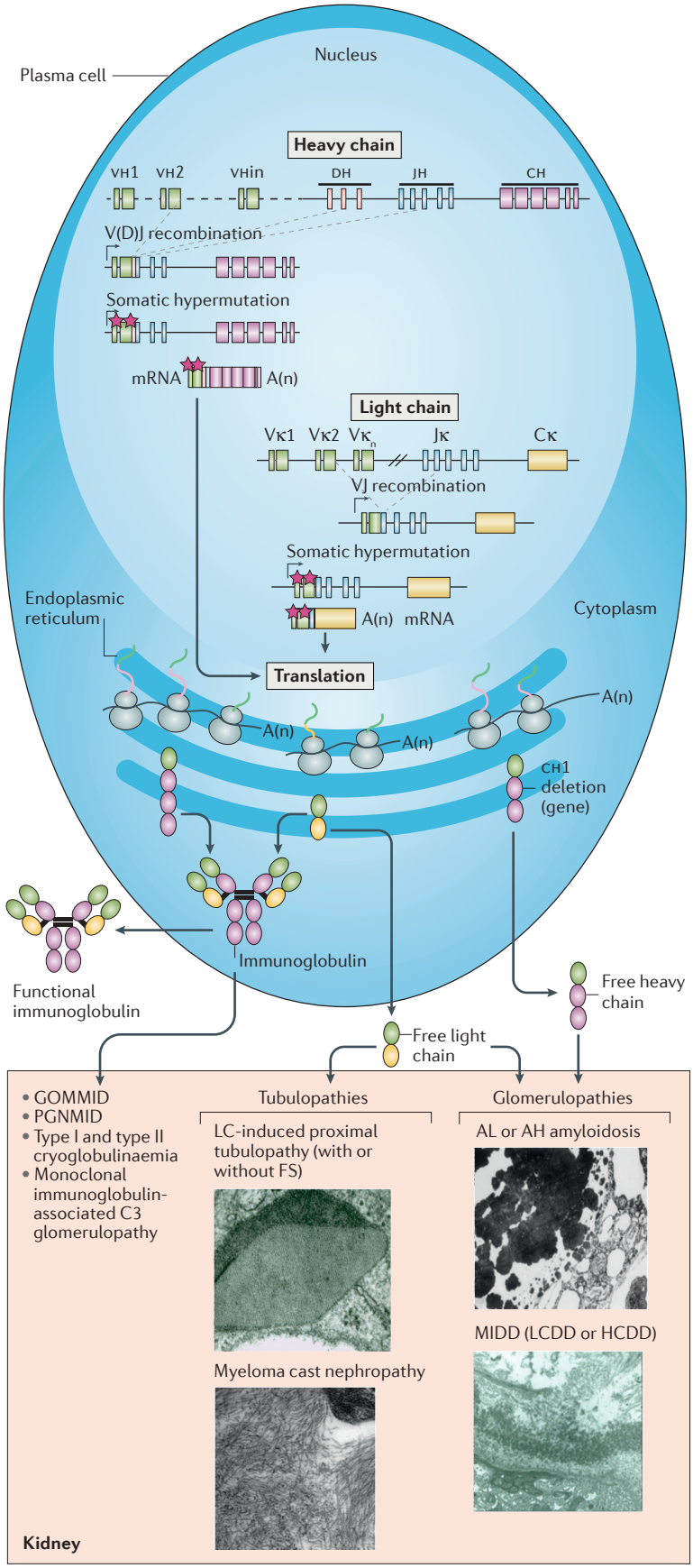

Light chain-induced Fanconi syndrome
Generalized dysfunction of reabsorption in proximal tubules due to the intracellular accumulation of a monoclonal immunoglobulin light chain.

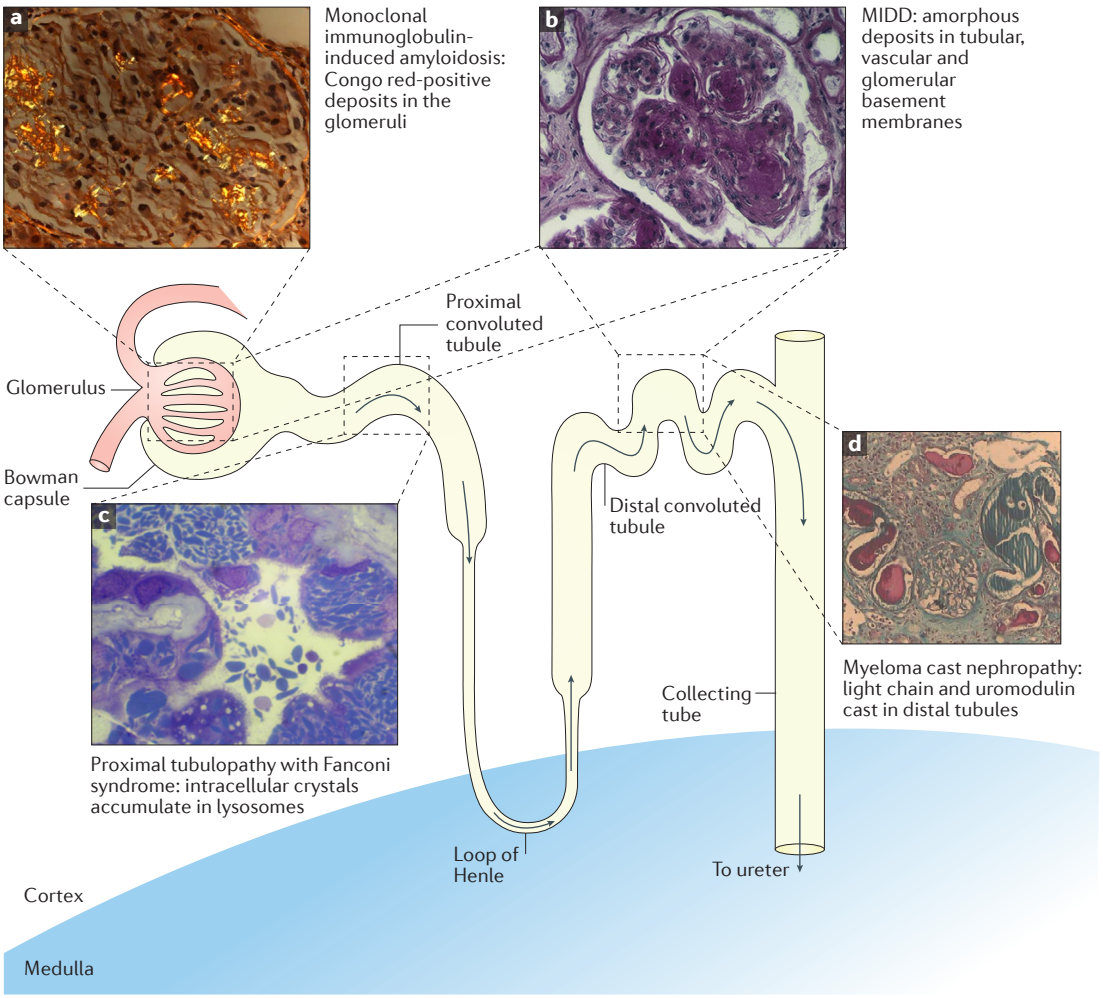

Figure 1 | **The localization of monoclonal immunoglobulin-induced lesions in the kidneys. a** | Monoclonal immunoglobulin-induced amyloidoses, which include immunoglobulin light chain amyloidosis (AL amyloidosis), immunoglobulin heavy chain amyloidosis (AH amyloidosis) and immunoglobulin heavy chain and light chain amyloidosis (AHL amyloidosis). Congo red-positive glomerular deposits in the mesangium, capillary walls and Bowman capsule with typical green birefringence under polarized light. **b** | Monoclonal immunoglobulin deposition diseases (MIDDs), which include light chain deposition disease, heavy chain deposition disease and light chain and heavy chain deposition disease. Light microscopy (periodic acid–Schiff staining) on a section of the renal cortex showing nodular glomerulosclerosis and diffuse tubular basement membrane thickening. **c** | Monoclonal immunoglobulin-induced proximal tubulopathy (with Fanconi syndrome). Light microscopy (toluidine blue staining) showing multiple crystalline inclusions in proximal tubule cells. **d** | Myeloma cast nephropathy. Light microscopy (Masson's trichrome staining) showing numerous casts in a tubular lumen together with inflammatory cell infiltrate and interstitial fibrosis.

progressively invade the extracellular spaces in various organs, inducing physical disruption of organ structure and, most likely, alteration of organ function due to the toxicity of persistent deposits and of unstable protein oligomers that initiate the formation of fibrils[18–20].

Randall-type MIDD features non-amyloid extracellular deposits that comprise monoclonal immunoglobulin fragments and are shown to have an amorphous structure by electron microscopy. The deposits are usually systemic, but have a prominent renal association and, to a lesser extent, liver and heart manifestations[21–23]. Renal lesions typically consist of linear immunoglobulin deposits along tubular and glomerular basement membranes, which are often associated with nodular glomerulosclerosis, leading to progressive kidney failure. Light chain deposition disease (LCDD) is the most common subtype of MIDD, but heavy chain deposition disease (HCDD) and light chain and heavy chain deposition disease (LHCDD) have also been described[24–27].

Pathogenic monoclonal immunoglobulins

Pathogenic light chains. Only a minority of light chains that are produced in clonal B cell disorders are pathogenic, and those that are toxic cause heterogeneous organ injury. It is now widely acknowledged that sequence peculiarities in the variable (V) domain cause the abnormal physicochemical characteristics of light chains that govern their toxicity and their propensity to aggregate and deposit in specific organs. Tremendous efforts have been made to obtain informative sequence data to help in predicting

the pathogenic properties of specific monoclonal light chains, but with limited success. In MCN, no bias in the use of any light chain isotype or V domain subgroup has been observed. However, the secondary structure and a few amino acids in complementarity-determining region 3 (CDR3) of free light chains greatly influence their binding affinity for uromodulin[28]. Amyloidogenic light chains have been extensively studied by several groups[29–31], and although a common structural motif that confers amyloidogenicity has not been identified, specific amino-acid changes due to somatic mutations seem to be involved in the reduced folding stability of the native light chain structure[32–36]. However, the most relevant feature of amyloidogenic light chains is the strong bias in germline immunoglobulin V gene usage. Of note, there is a high prevalence of the λ-light chain isotype in AL amyloidosis, and two germline Vλ genes, immunoglobulin lambda variable 6–57 (*IGLV6-57*) and *IGLV3-1*, are implicated in almost half of the λ-light chain-associated AL amyloidoses[37–39]. The use of *IGLV6-57* is predominantly associated with kidney lesions, whereas *IGLV1-44* use is frequently associated with cardiac lesions[40]. More importantly, the bias in the use of these germline genes is almost exclusively associated with AL amyloidosis and is not observed for other types of diseases that are related to monoclonal immunoglobulin deposition. Consequently, germline immunoglobulin V gene usage may be an even more reliable predictor of the amyloidogenic potential of a monoclonal light chain than somatic mutations in light chains. Structural peculiarities of light chains have also been reported in LCDD, including more frequent glycosylation of the V region, the exposure of large hydrophobic patches at the surface of the light chain and overrepresentation of the IGKV4-1 germline V domain[25,41,42,43]. The κ-light chain isotypes are most commonly involved but, again, there is no common peptide or primary sequence feature that might help in predicting the pathogenicity of a light chain. Finally, the predominant characteristic of the light chains that are involved in LCDD is their high isoelectric point, which could account for their propensity to deposit along the anionic proteoglycans of the basement membranes[44]. In contrast to other monoclonal immunoglobulin-related deposition disorders, molecular studies have revealed a striking homogeneity in the genetic and biochemical attributes of monoclonal immunoglobulin light chains that are associated with Fanconi syndrome. With few exceptions[13,45,46], the light chains belong mostly to the Vκ1 subgroup of variability genes and derive from only two germline genes, *IGKV1-33* and *IGKV1-39*[13]. The crystallization propensity of the light chains in Fanconi syndrome is associated with the resistance of a 12-kDa portion of the Vκ domain to proteolysis, and the light chains contain unusual hydrophobic residues in the CDRs[47,48]. Substitution of a polar residue with a hydrophobic residue at position 30 in the CDR1 loop of the IGKV1–39 domain has been detected in all Fanconi syndrome-associated light chains studied to date. The involvement of this residue change in light chain aggregation propensity has been demonstrated by site-directed mutagenesis experiments[49,50] (discussed below).

Pathogenic heavy chains. The deposition of free monoclonal heavy chains in organs is a rare event that is characteristic of AH amyloidosis and Randall-type HCDD[51,23]. The circulating monoclonal heavy chain is often undetectable by electrophoresis and immunofixation, reflecting the extreme toxicity of even small amounts of free truncated heavy chains[27]. The most striking feature of heavy chains that are deposited is the deletion of the first constant (CH1) domain in the heavy chain gene[24,52], a mutation that is required for the free heavy chain to be secreted[53]. No structural peculiarities in the heavy chain that could account for their propensity to form fibrils or granular deposits have been reported to date, but the remarkably high isoelectric point of almost all the heavy chain variable (VH) domains that are involved in HCDD has been highlighted[27]. The presence of a complete VH domain seems to be strictly required for deposition of a free heavy chain, as the absence or partial deletion of the VH domain precludes tissue deposition, which is exemplified by heavy chain disease (HCD), in which circulating free truncated heavy chains are present but no organ deposits are detectable[54]. Perhaps even more striking, no reports exist of free truncated heavy chains with a complete VH domain that are not deposited in organs. Whether all truncated heavy chains with a complete VH domain are pathogenic remains to be experimentally determined.

Overview of animal models

The first attempts to reproduce MGRS in animals relied on massive and/or repeated injections of human pathogenic monoclonal immunoglobulin light chains (FIG. 2a), which was possible owing to the availability of large quantities of light chains (Bence Jones proteins) in the urine from patients with multiple myeloma or MGUS[55–59]. Protein in the urine samples was precipitated and dialysed, and the light chains were purified using size-exclusion and/or affinity chromatography. Checking the purity of purified light chains is essential to avoid the presence of preformed aggregates that could skew results, especially when the direct toxicity of the light chain or the aggregation process is evaluated *in vivo*. Several groups have used recombinant human immunoglobulins to overcome the restricted availability of a specific light chain[49,60,61], whereby a monoclonal immunoglobulin gene is cloned from the bone marrow of patients with a defined MGRS and is expressed in *Escherichia coli* or mammalian cell lines. Recombinant protein production also offers the possibility of introducing desired mutations in the original gene, thereby modifying potentially important amino acid residues or domains in the light chain[49]. Intravenous (via the tail vein) or intraperitoneal injections are the most frequent methods of delivery, but injection in the penile vein revealed an unsuspected advantage in its efficiency in delivering large amounts of light chains to the kidneys[62]. The first animal model using light chain injection was established in 1976 (REF. 63) and was later improved owing to a better understanding of the underlying human pathologies associated with injected Bence Jones proteins[55–58]. The main drawback of the injection

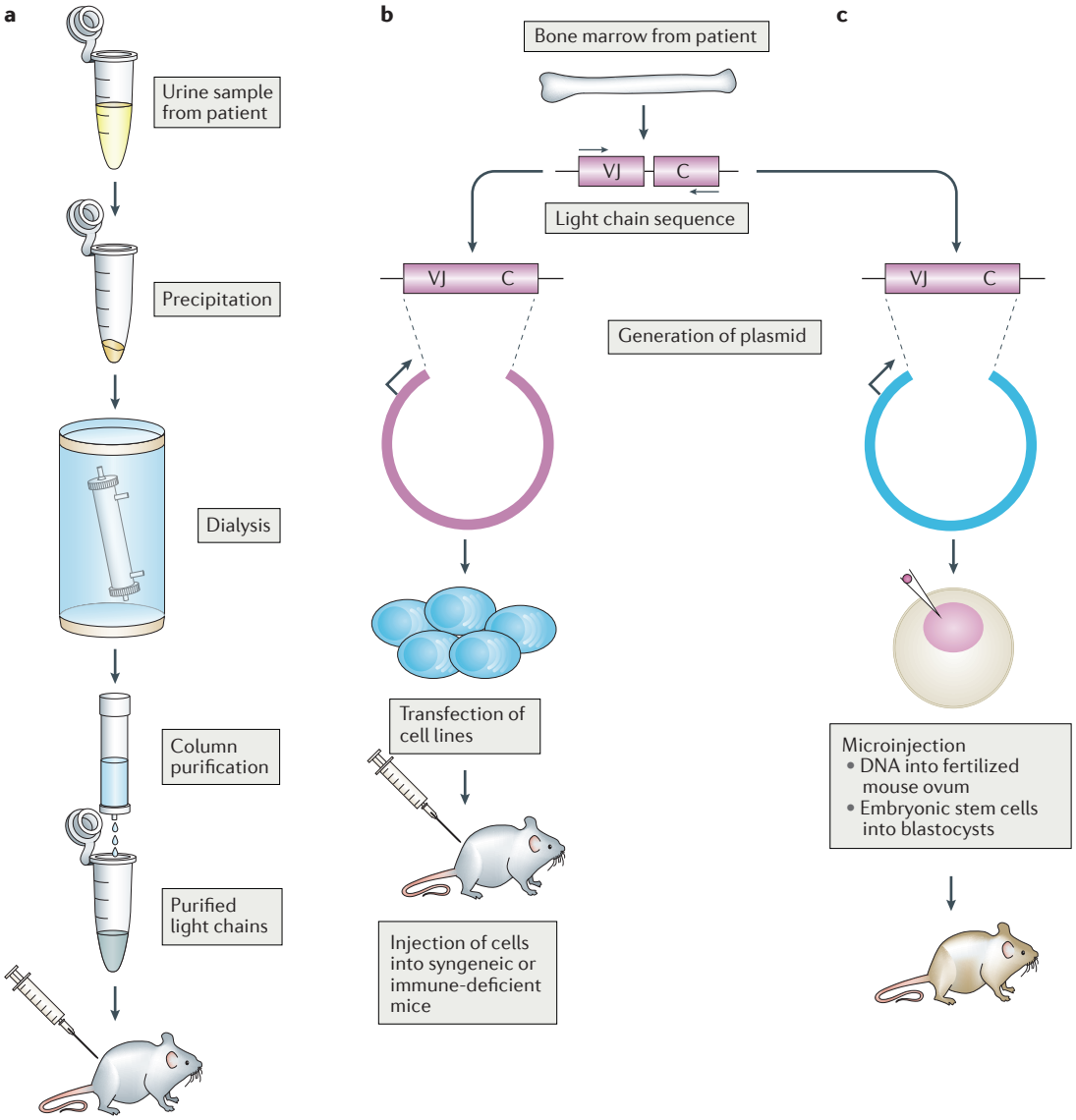

Figure 2 | **Strategies to model immunoglobulin-induced kidney diseases in rodents. a** | Injection of purified human immunoglobulin light chains. Light chains are purified from a patient's urine by salt precipitation, dialysis and column purification. The light chains are then injected into a mouse via intraperitoneal injection or intravenously into the lateral tail vein or the penile vein. The doses, concentrations and number of injections can easily be adapted depending on experimental requirements. **b** | Tumour grafts. After isolation of the pathogenic immunoglobulin from a patient's bone marrow aspirate and sequencing, an expression vector containing the immunoglobulin sequence and adapted regulatory elements (promoters and enhancers) is constructed and transfected into tumour cell lines (typically, plasma cell lines or hybridomas). The best-producing clones are injected into mice to allow a tumour to develop, which continuously secretes large amounts of the light chain of interest. Alternatively, human plasma cell lines can be directly derived from primary cells isolated from patients with the disease of interest. **c** | Transgenic approaches. Expression vectors containing the human pathogenic immunoglobulin sequence and adapted regulatory elements are used to generate transgenic mice in which the human gene is randomly integrated into the genome. Alternatively, the transgene can be targeted to specific loci using embryonic stem cell transfection, selection and injection into blastocysts to generate knock-in mice. C, constant domain; J, joining domain; V, variable domain.

method is that the acute delivery of large quantities of light chains poorly reflects the pathologies in patients with MGRS, who usually have a low tumour burden and low serum levels of free light chains. In addition, the skill required to repeatedly inject proteins into the tail or penile veins of mice or rats and the short half-life of light chains in serum also complicate this method. However, although most of these experiments were performed in rodents (mice or rats), studies have highlighted the benefit and relevance of utilizing phylogenetically remote species[64,65].

Tumour graft models of MGRS represent an interesting alternative to injection models (FIG. 2b). To establish this model, SP2/0 cells, a non-producing hybridoma

from BALB/c mice, were stably transfected with the gene encoding a human monoclonal immunoglobulin fragment. The best-producing clones were then grafted into BALB/c mice, allowing tumour growth over a period of weeks with proportionally increasing production of the human pathogenic immunoglobulin[49,60]. Using immunodeficient mice, this strategy was extended to other mouse or human cell lines[66,67]. In addition to the advantage of continuous secretion of immunoglobulins over the course of the experiment, which closely mimics the human disease, mutational analysis could be used in this strategy to dissect the role of individual residues of the V domain in the propensity of light chains to aggregate and deposit[49]. However, the short-term survival of animals due to rapid tumour growth prevents full characterization of disease phenotypes and limits investigation of potential therapies.

Transgenic models are used to reproduce monoclonal immunoglobulin-induced organ lesions in mice (FIG. 2c). The first transgenic mouse model was developed in the late 1990s using a monoclonal light chain that was obtained from a patient with AL amyloidosis (C.S. and M.C., unpublished observations). At the time, an additive transgenic approach was used to introduce the light chain gene flanked by the main regulatory elements of the immunoglobulin H (IgH) locus[68] to induce 'physiological' production of the pathogenic immunoglobulin by the plasma cells. Transgenic mice were obtained with a B lineage-restricted expression of the human light chain and abundant light chain production in serum (>1 g/l). However, human light chains associated with murine heavy chains to form hybrid immunoglobulins, resulting in a very low level of free light chains, which poorly reproduces the conditions leading to monoclonal light chain deposition. Accordingly, neither tissue deposits nor physiological abnormalities were seen in these mice. Many other models were subsequently developed using a similar strategy. Ubiquitous or liver-specific expression of light chains was also tested, with disappointing results, as light chain production was low[69]; however, one of these models had sufficient localized production of light chains to induce amyloid deposits in the stomach[70]. To further increase the production of human immunoglobulins in the serum, transgene expression was induced by replacing random integration into the mouse genome by homologous recombination within the highly expressed endogenous κ-light chain locus, a strategy that was successful in establishing a model of renal Fanconi syndrome and of Randall-type HCDD[71–73]. Replacement of the Jκ segments of the κ-light chain locus by the transgene allowed the exclusive expression of the human immunoglobulin by all B cells and plasma cells. Only traces of mouse λ-light chains were detected in these mice, but again, most human light chains were associated with mouse heavy chains owing to the absence of the imbalanced light chain:heavy chain stoichiometry observed in humans. An improvement to this transgenic approach was achieved by the creation of a mouse line in which the JH segments in the IgH locus were replaced by the gene encoding latent membrane protein 2A (LMP2A) from the Epstein–Barr virus, termed the LMP2A mouse[74]. In these mice, LMP2A efficiently replaces B cell receptor signalling, allowing complete B cell development in the absence of immunoglobulin heavy chains. LMP2A mice also have an increased number of plasma cells, making them the ideal model for the production of large amounts of free light chains without the complication of an underlying haematological disorder[75]. Accordingly, following crossing of LMP2A mice with human κ-light chain knock-in mice, the levels of circulating human light chains exceeded those observed in the patients from whom the light chains were isolated (BOX 2).

Immunoglobulin light chain amyloidosis. Attempts to create a reliable animal model of AL amyloidosis have had limited success, despite considerable effort from numerous groups. Initially, it was thought that AL amyloid formation could be achieved if the level of circulating light chains equalled or exceeded that observed in patients. The challenge was to create conditions that mimic the excess of monoclonal free light chains. The first *in vivo* model of AL amyloidosis was created in the early 1990s[57,58] by repeated injection of large amounts of human Bence Jones proteins into mice (up to 5.3 g per mouse or 2 g after the mice had undergone a period of dehydration), which resulted in the formation of Congo red-positive deposits in organs and vessel walls. Although artificial, this model provided proof of concept that human light chains could form amyloid deposits in rodents. Strikingly, the use of injections of free light chains to recreate gammopathies was abandoned during the following decades. For subsequent studies, researchers validated the efficacy of monoclonal antibodies against amyloid-related epitopes by subcutaneous injection of water-soluble amyloid extracts ('amyloidomas'), which are being tested in clinical trials[76–79]. The use of the light chain injection method resumed after utilization of an alternative injection route in the penile vein[62] (FIG. 3Aa,b). Compared with intraperitoneal injections used in earlier studies, injections in the dorsal penile vein deliver light chains directly to the systemic circulation, the light chains do not enter the portal circulation where dilution takes place and a first-pass effect on light chain metabolism in the liver is not expected[80]. The resultant burst of light chains delivered to the kidneys might explain the efficacy of this route in inducing amyloid formation in glomeruli. Although this repeated, acute delivery of light chains differs from the pathology of the human disease, this study provided new insights into the molecular mechanisms of amyloid fibril formation in the kidneys. As previously observed *in vitro*[81], light chains from patients with AL amyloidosis are internalized by mesangial cells via clathrin-mediated endocytosis and are delivered to mature lysosomes, in which the acidic pH probably participates in the formation of fibrils. This process is possible because the mesangial cells acquire a macrophage-like phenotype on exposure to AL amyloidosis light chains (FIG. 3Ac). Newly formed amyloid fibrils are released from mesangial cells to invade the

extracellular space[82] (FIG. 3Ad–f). This process closely resembles amyloid formation in an *in vitro* model of amyloid A amyloidosis (AA amyloidosis)[83], which occurs following internalization of serum amyloid A (SAA) protein by macrophages. Accordingly, *in vivo* depletion of macrophages delays the development of AA amyloidosis[84,85]. These observations suggest that the lysosome is an 'amyloid factory' in a number of gammopathies and potentially represents a novel target for therapy.

Other strategies to induce AL amyloidosis in mice have been unsuccessful. Amyloid deposits were not detected in grafts of SP2/0 cells expressing AL amyloidosis light chains in BALB/c mice (C.S, M.C., S.B. and M.V.A., unpublished observations) or grafts of human AL amyloidosis plasma cell lines in immunodeficient mice (REFS 86,87; D. Jelinek, personal communication), probably owing to the extremely rapid growth of tumour cells[86,87]. However, this result is difficult to explain, as the other immunoglobulin-related deposition diseases have all been reproduced using tumour graft models[49,60]. As injection of light chains leads to the formation of amyloid deposits in 24–48 hours[58,62], it is surprising that cells producing large amounts of light chains over several weeks do not produce amyloid deposits. Whether this reflects the absence of a 'burst' of free light chains induced by injections of large quantities of light chains or the absence of unfolded amyloid-prone light chains produced by cell lines remains to be established.

The discouraging results obtained with transgenic models are even more striking. To date, only one model of ubiquitous expression of a human λ6 light chain (CMV-λ6) has successfully induced a few immunoglobulin-containing amyloid deposits in the

Box 2 | **Transgenic strategy to generate mouse models of monoclonal immunoglobulin deposition diseases**

Transgenic strategies have been used to generate mice that produce free human monoclonal immunoglobulin. A two-step strategy to obtain high, continuous production of free light chain involves crossing two mouse lines: a line that has the mouse κ-light chain locus replaced with the human pathogenic immunoglobulin gene cloned from a number of affected patients (see the figure, part **a**) and a second line that has the mouse immunoglobulin H locus replaced with the latent membrane protein 2A (*lmp2a*) gene from the Epstein–Barr virus (EBV), which can functionally replace B cell receptor (BCR) signalling and is used to increase the number of spleen plasma cells (PCs) that exclusively express a human immunoglobulin light chain (see the figure, part **b**; a model of a light chain deposition disease (LCDD) is shown as an example). The serum levels of the pathogenic human immunoglobulin in transgenic mice might even exceed those in patients with the corresponding disease (see the figure, part **c**; values are means ± SEM; for patients, $n \geq 2$ samples from each patient; for mice, $n \geq 10$ mice). AL amyloidosis, immunoglobulin light chain amyloidosis; CH, heavy chain constant domain; D, diversity domain; J, joining domain; DH, immunoglobulin H diversity gene; Eiκ, intronic enhancer of the κ-light chain locus; Eμ, intronic enhancer of the heavy chain locus; HCDD, heavy chain deposition disease; κ-LC, κ-light chain; λ-LC, λ-light chain; L, leader sequence; MCN, myeloma cast nephropathy; MGRS, monoclonal gammopathy of renal significance; ND, not determined; pDH, DH promoter; V, variable domain.

a Mouse with a targeted insertion of the human pathogenic immunoglobulin genes into the mouse κ-light chain locus

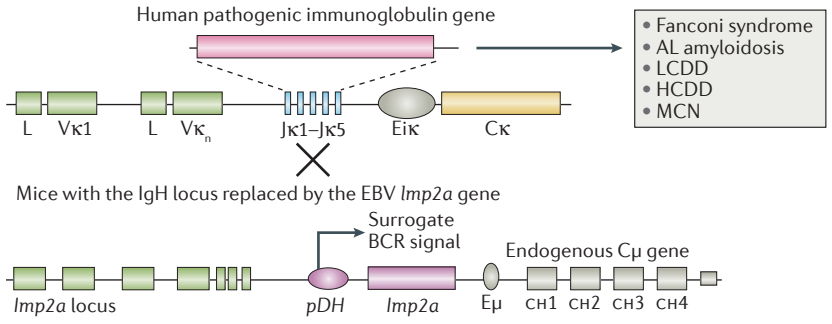

b

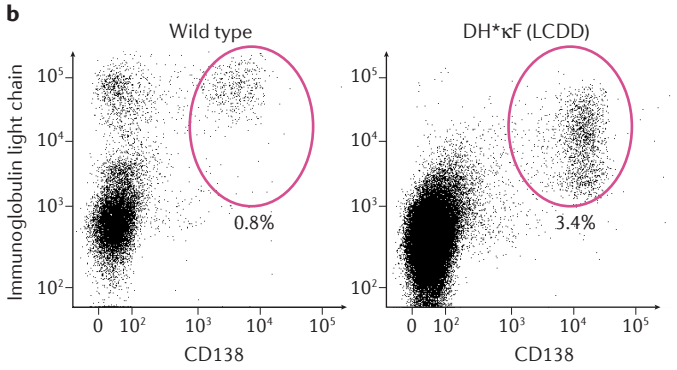

Advantages of the two-step knock-in strategy to mimic MGRS
- High number of PCs
- Only free light chain
- Quasi-monoclonal

c

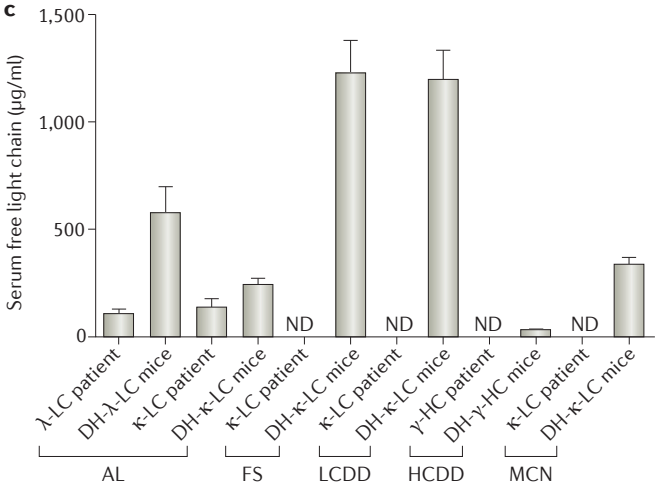

lumen of the gastric glands of the stomach[70]. However, in this model, the light chains are produced locally, and the acidic environment of the stomach probably participates in the unfolding of the light chains and in fibril formation, which does not reflect the pathophysiology of the human disease, in which fibrils are formed at a distance from the light chain-producing cells. Accordingly, the levels of circulating human light chains in the transgenic mice were below the limit of detection, and no deposit was detected in other tissues. Nevertheless, this model provided insights about the ability of doxycycline to directly interfere with amyloid fibril formation[70] — a result that was later confirmed in clinical studies[88]. Other efforts to establish a transgenic mouse model that produces high levels of human immunoglobulins achieved success by combining the κ-light chain knock-in strategy with the LMP2A genetic background (BOX 2). Two mouse knock-in lines were established (expressing IGLV6-57 or IGLK1-33 from patients with renal or cardiac amyloidosis, respectively), in which circulating free immunoglobulin light chain levels exceed those in patients by up to fivefold. Unfortunately, features of the human disease, such as amyloid deposits, organ dysfunction and reduced lifespan, were not observed in these mice. This result was surprising, as the serum levels of the amyloidogenic proteins SAA, transthyretin (TTR) or apolipoprotein A-II in some similar mouse models of amyloidosis are lower than those of the free light chains in the knock-in model[89–92]. However, an inducible transgenic model of systemic AA amyloidosis elegantly demonstrated that a threshold level of SAA exists below which amyloidosis is not, or is minimally, triggered[93]. One hypothesis to explain this discrepancy is that this threshold is reached by the burst of light chain delivery that occurs in the injection model but that the threshold is not reached in transgenic or tumour graft models of AL amyloidosis. This hypothesis could be tested by crossing AL amyloidosis transgenic mice with mouse models of plasma cell proliferation and/or multiple myeloma, which might further increase light chain production, and by using inducible transgenes that create the initial burst of light chain production[94–96].

Other non-mutually exclusive hypotheses might explain the absence of amyloid deposits in transgenic mice — in particular, the association of proteins that are invariably found in amyloid fibrils, such as SAP, apolipoprotein E or heparan sulfate, with the amyloid precursor may differ between species. For example, the lower affinity of mouse SAP for amyloid is well documented[15]. The identification of such factors would be invaluable for deciphering the mechanisms of amyloid formation and to develop new therapeutic approaches.

We believe that without fibrils, animal models cannot accurately recapitulate amyloidosis; however, some features of the disease (especially the toxicity of soluble oligomers) can be studied in the absence of fibrils. For example, although cardiac dysfunction during AL amyloidosis is usually associated with extensive myocardial infiltration by fibrils, soluble amyloidogenic light chains might initiate direct toxicity to cardiomyocytes, even in the absence of Congo red-positive amyloid deposits. The direct toxicity of cardiac amyloid light chains was first observed *in vitro* in cardiomyocytes and *ex vivo* in perfused isolated mouse hearts exposed to purified light chains[18,19,97,98], as well as in *in vivo* models, including in zebrafish embryos[64,99] and in the nematode *Caenorhabditis elegans*[65]. Direct and specific cellular toxicity of amyloid light chains (through oxidative stress that is associated with lysosomal and mitochondrial dysfunction) was observed in both zebrafish and nematodes. These results accord with clinical observations that improved survival of patients with cardiac AL amyloidosis is directly associated with a decrease in the levels of free light chain, even when the amount of amyloid deposits remains unchanged[20]. These *in vivo* models allowed the evaluation of new therapeutics, including p38 mitogen-activated protein kinase (MAPK) inhibitors[97] (to block oxidative stress), inhibitors of mechanistic target of rapamycin (mTOR)[98] (to activate autophagy) and metal chelators or metal-binding molecules[100] (to block toxic effects mediated by reactive oxygen species (ROS)). These studies demonstrate that non-mammalian models of AL amyloidosis can be used to develop and validate novel therapeutic approaches, even in the absence of amyloid deposits. However, these studies were focused on cardiac amyloidosis — a similar direct toxicity and its consequences have not been confirmed *in vivo* in the kidneys. In addition, the normal lifespan of transgenic animals that continuously produce large amounts of cardiac or renal amyloid light chains suggests that the effects of the direct toxicity of the light chain in the pathophysiology of the disease are not as great as previously thought. However, the absence of an effect of light chains on lifespan might also reveal interesting differences in the factors that are involved in light chain toxicity (such as receptors, signalling pathways, circulating chaperones and so on) between mice and humans.

Randall-type monoclonal immunoglobulin deposition disease. Modelling Randall-type MIDD in mice was successfully carried out using several strategies. The first well-characterized mouse model of MIDD was created by establishing grafts of SP2/0 cells expressing a κ-light chain from a patient with biopsy-confirmed LCDD[60]. Mice injected with SP2/0 cells expressing LCDD light chains, but not control light chains, showed faint but detectable tubular and glomerular basement membrane immunoglobulin deposits by immunofluorescence. However, light and electron microscopy studies did not reveal the basement membrane thickening or glomerulosclerosis that is typically seen in LCDD, probably because the animals were sacrificed early owing to rapid tumour growth. Penile injection of biopsy-confirmed human LCDD light chains into mice reproduced the typical mesangial pathology of LCDD, including the increased extracellular matrix that is associated with the deposition of light chains. Interestingly, caveolin 1 (*Cav1*)-knockout mice do not develop the mesangial pathology, highlighting the importance of CAV1 in the signalling mechanisms that are integral to the development and/or progression of mesangial alterations in LCDD[101].

In contrast to AL amyloidosis, the development of reliable, reproducible mouse models of MIDD was possible using transgenic strategies[73]. A reconstituted complete human γ1 heavy chain gene from a patient with an established diagnosis of HCDD was inserted in the mouse κ-light chain locus. Removal of the CH1 domain to produce the truncated pathogenic heavy chain was possible using Cre-mediated conditional deletion. This model replicated several cardinal features of HCDD, including the high pathogenicity specific to the truncated form of the heavy chain and the full histological characteristics of MIDD lesions in the kidneys, including linear heavy chain deposits in tubular basement membranes and the mesangium and thickening of basement membranes (FIG. 3Ba,b). Serum concentrations of truncated monoclonal heavy chain as low as 25 μg/ml were sufficient to induce the disease, which highlights the strong propensity of heavy chains to aggregate. Of note, a similarly high pathogenicity probably accounts for the high percentage (40%) of patients without detectable M-spikes by standard electrophoresis[27]. Finally, the only shortcoming of this model is the absence of nodular glomerulosclerosis, despite early signs of extracellular matrix remodelling by mesangial cells. This shortcoming is frequently

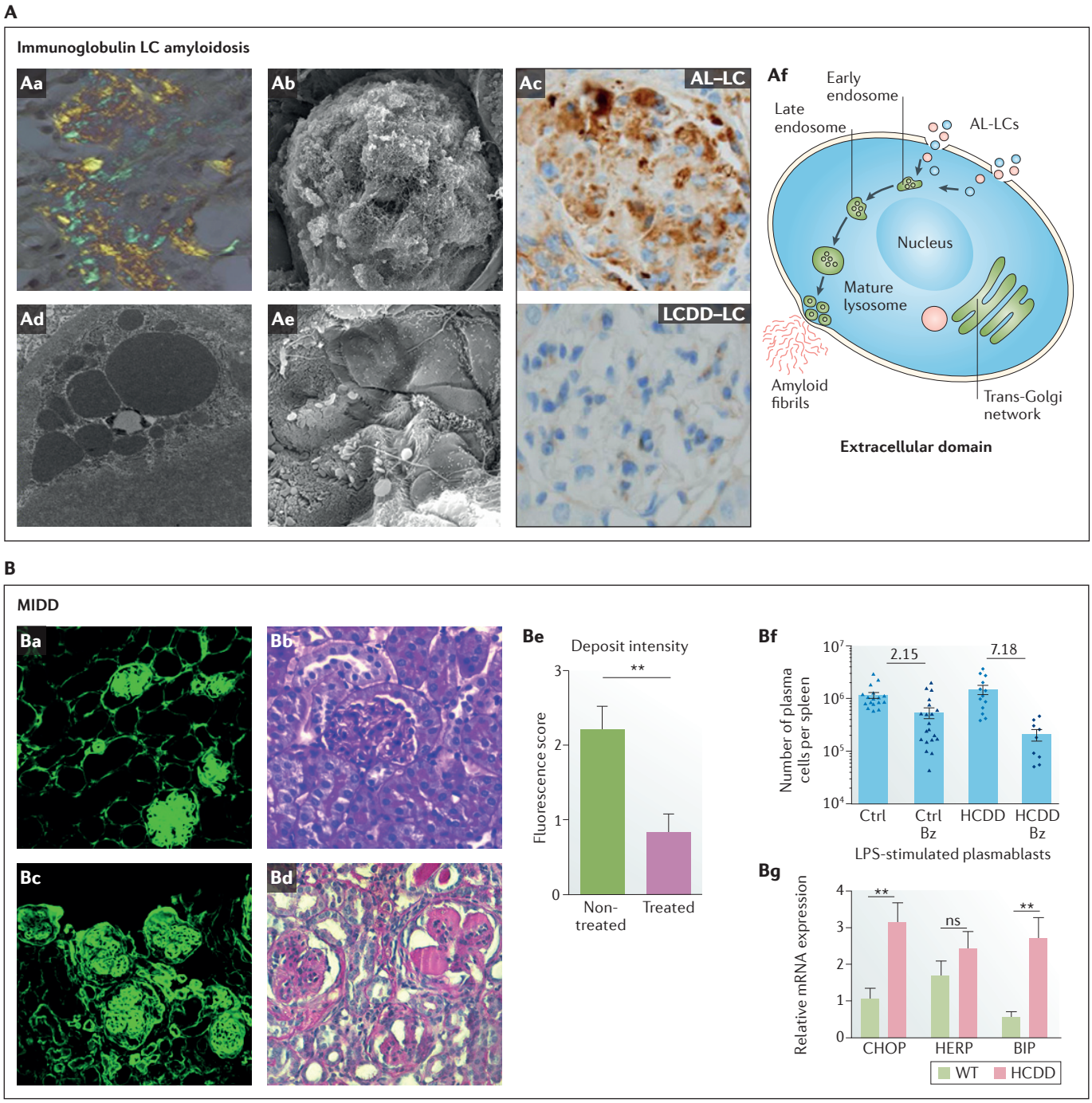

encountered in mouse models of other renal diseases — in particular, diabetic nephropathy[102] — and is thought to be related to the genetic background of the mouse strain that is used to generate transgenic animals, which is resistant to renal fibrosis and glomerulosclerosis[103,104]. However, a transgenic model of Randall-type LCDD developed all the features of the human disease, including nodular glomerulosclerosis, nephrotic-range proteinuria and kidney failure that results in death (median survival of 8.5 months) (S.B., M.V.A., V.J., M.C., G.T., F.B. and C.S., unpublished observations) (FIG. 3Bc,d). In addition to providing a better understanding of the renal toxicity that is induced by LCDD light chains, this model could help elucidate more general pathogenic mechanisms, especially those shared with diabetic nephropathy, which causes similar alterations in kidney structure and function.

Similar to humans, removal of the heavy chain-producing or the light chain-producing cells in mouse models leads to a significant improvement in kidney lesions (FIG. 3Be), and this finding will probably improve our understanding of the mechanisms of kidney recovery in these pathologies. The HCDD mouse model also sheds light on key haematological features of MIDD. Isolated truncated heavy chains induce endoplasmic reticulum stress that sensitizes plasma cells to proteasome inhibitor-based therapy (FIG. 3Bf,g), a feature that is also observed in plasma cells producing AL amyloidosis light chains[105], which might reflect a general intracellular toxicity of aggregation-prone immunoglobulin[106]. Accordingly, several clinical investigations have demonstrated the striking efficacy of proteasome inhibitor-based regimens in the treatment of AL amyloidosis and Randall-type MIDD, including HCDD[107–112].

Proximal tubulopathies. In view of the rarity of proximal tubulopathies with Fanconi syndrome in humans[13], it is striking that pioneering experimental approaches involving *ex vivo* or *in vivo* exposure of renal tubules to human monoclonal light chains frequently detected a tubular toxicity that closely resembles renal light chain-induced Fanconi syndrome. Following the first *in vitro* demonstration that Bence Jones proteins inhibit the uptake of amino acids and glucose by proximal tubular cells[113], an *ex vivo* system of perfused rat nephrons was used to evaluate the differential and specific toxicity of monoclonal light chains in relation to their distinct physicochemical characteristics[56]. In this study, one of the perfused Bence Jones proteins induced morphological and functional changes in the tubular epithelium, including abnormal lysosomes filled with crystals, and reduced reabsorption of water, chloride and glucose, which are all features of light chain-induced Fanconi syndrome[13]. In a later study, the accumulation of crystals was observed in proximal tubules after injection of three Bence Jones proteins into mice (of the 40 proteins tested)[57], but the effect on reabsorption function was not evaluated. These studies were carried out with light chains purified from patients with myeloma who did not have a diagnosis of overt Fanconi syndrome. Furthermore, the acute infusion of proximal tubules with massive quantities of light chains poorly reflects the pathology in light chain-associated Fanconi syndrome, which almost always occurs in the setting of smouldering myeloma or MGRS. Consequently, these studies, together with *in vitro* experiments[114–119], mostly describe the formation of proximal tubule lesions induced by massive reabsorption of light chains with specific physicochemical characteristics, a phenomenon that seems to occur in acute kidney injury and in the rapid development of tubulointerstitial fibrosis observed in cast nephropathy[7,11]. The next step was to generate mouse models using human light chains from patients with well-characterized Fanconi syndrome. Using the SP2/0 tumour graft system, the first mouse model of human monoclonal light chain-associated Fanconi syndrome was developed[49], which displayed proximal tubular lesions highly similar to those observed in the patient from whom the light chain sequence was cloned[47] (FIG. 4Aa). For the first time, site-directed mutagenesis was carried out to substitute residues at

Figure 3 | **Models of monoclonal immunoglobulin-induced glomerulopathies.** **A** | Mouse model of immunoglobulin light chain amyloidosis (AL amyloidosis). **Aa** | Penile vein injections of purified light chains from a patient with AL amyloidosis leads to Congo red-positive light chain deposits in the kidneys after 2 weeks of repeated injections. **Ab** | Scanning electron micrograph of a glomerulus showing tangled, non-branching fibrils that are typical of amyloidosis. **Ac** | Mesangial cells undergo a phenotypic change from a smooth muscle-like to a macrophage-like phenotype, as shown by intracytoplasmic staining for CD68, after injection of AL amyloidosis light chains (top) but not of light chain deposition disease (LCDD)-associated light chains (bottom). **Ad** | Transmission electron microscopy showing abundant, heterogeneous lysosomes that are closely associated with the plasma membrane in mesangial cells. **Ae** | Scanning electron microscopy of mesangial cells 1 week after initial injection of AL amyloidosis light chains, showing extrusion of single amyloid fibrils from a cell. **Af** | Schematic representation of the amyloidogenesis process in mesangial cells. AL amyloidosis-associated light chains are endocytosed and trafficked to the endolysosomal compartment, where they are processed and fibrils are formed. Amyloid fibrils are then extruded to the exterior of the cell. **B** | Transgenic mouse models of monoclonal immunoglobulin deposition disease (MIDD) using the κ-light chain knock-in strategy. **Ba**,**Bb** | Transgenic model of heavy chain deposition disease (HCDD). **Bc**,**Bd** | Transgenic model of light chain deposition disease (LCDD). These transgenic models faithfully reproduce human renal lesions, with typical glomerular and tubular deposits (parts **Ba** and **Bc**; immunofluorescence with anti-human immunoglobulin antibodies). A slight expansion of mesangial matrix is observed in the kidneys of the HCDD model but no glomerulosclerosis (part **Bb**), probably owing to the very low level of free heavy chains in the serum. By contrast, LCDD mice develop a typical nodular glomerulosclerosis (part **Bd**). Parts **Bb** and **Bd** show periodic acid–Schiff staining. **Be** | On bortezomib (Bz)-based treatment, a rapid reduction in immunoglobulin deposits (5 weeks) was observed in the kidneys in the HCDD model. Means ± SEM are shown; $n = 6–7$ mice in two independent experiments. **Bf** | Mouse plasma cells producing the HCDD heavy chain are highly sensitive to proteasome inhibitors, as seen by the substantial decrease in plasma cell number following two daily injections of low-dose Bz. Each symbol represents a mouse, and numbers indicate the overall means of the fold-decrease in each strain. **Bg** | Proteasome inhibitor sensitivity seems to be due to the intrinsic toxicity of the truncated heavy chain, causing a terminal endoplasmic reticulum (ER) stress response, as shown by the markedly elevated expression of the ER stress markers C/EBP-homologous protein (CHOP; also known as DDIT3), hairy/enhancer-of-split related with YRPW motif protein 2 (HEY2; also known as HERP) and immunoglobulin heavy chain-binding protein (BiP)) in the plasma cells producing the HCDD heavy chain. The data are means ± SEM of three independent experiments with two mice of each strain. All statistical tests are unpaired Student's *t* tests (*$P < 0.05$ and **$P < 0.01$). Ctrl, control; LC, light chain; LPS, lipopolysaccharide; ns, not significant; WT, wild type. Parts **Aa–e** reproduced with permission from REF. 62, International Society of Nephrology. Part **Ba** is reproduced and parts **Be–g** are adapted with permission from REF. 73, American Society of Hematology. Parts **Bc** and **Bd**: C.S., S.B., M.V.A., V.J., M.C., G.T. and F.B., unpublished observations.

position 30 or position 94 of the light chain with their germline counterpart, which prevented the appearance of crystalline inclusions in proximal tubule cells in mice (FIG. 4Ab–d). This result was the first demonstration that the propensity of the light chain to crystallize is dependent on individual unusual hydrophobic residues. Unfortunately, the rapid tumour growth in these mice precluded complete *in vivo* metabolic analysis and testing of therapeutic approaches. To overcome this issue, a κ-light chain knock-in mouse, which overexpresses a chimeric κ-light chain comprising the human Vκ1–39 domain from a patient with Fanconi

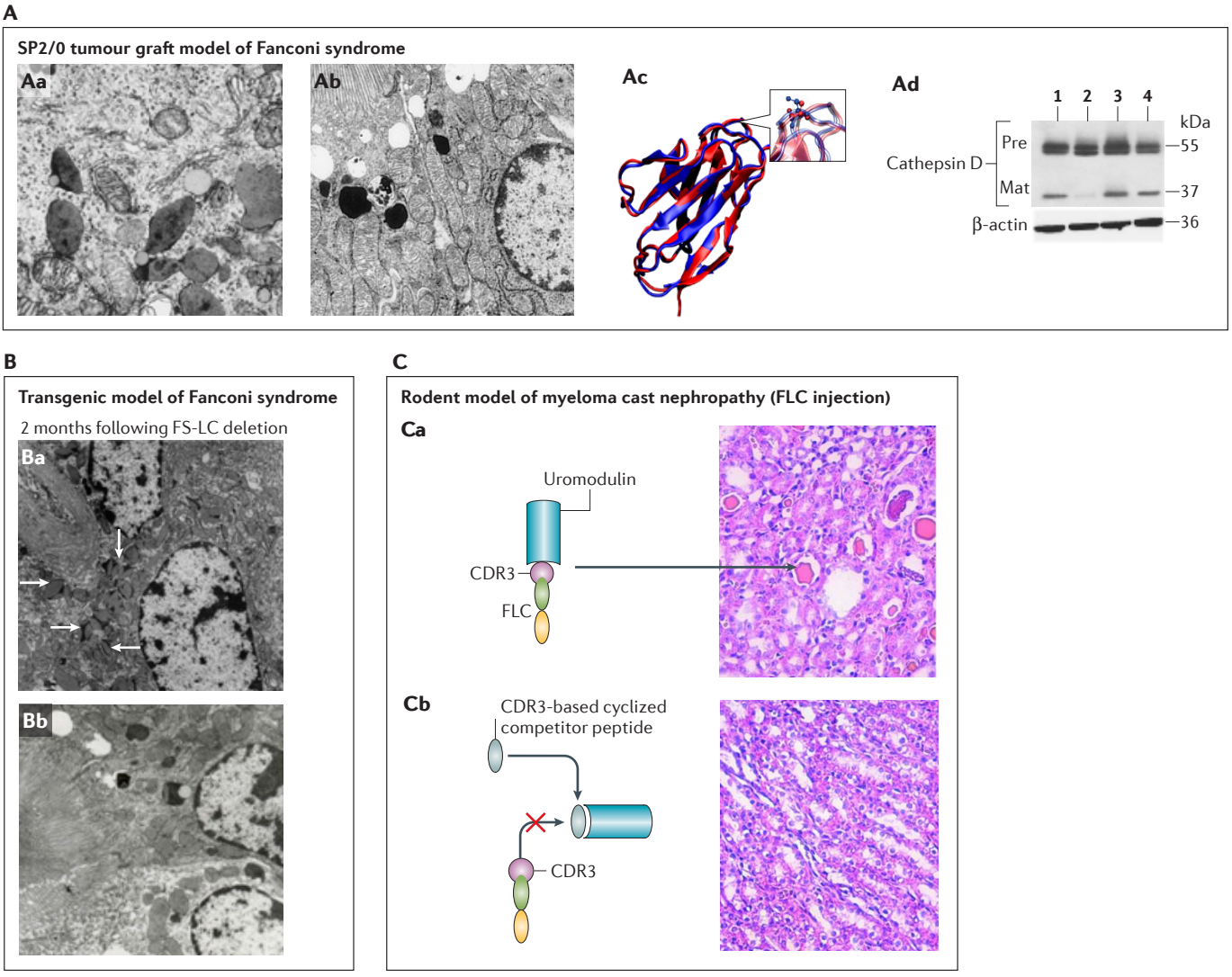

Figure 4 | **Models of monoclonal immunoglobulin-induced tubulopathies.** **A** | The SP2/O tumour graft model in mice of light chain-related Fanconi syndrome. **Aa** | Transmission electron microscopy (TEM) showing tubular lesions induced by crystals of Fanconi syndrome light chains (FS-LCs) in the lysosomes of proximal tubular cells. **Ab** | Substitution of a single amino acid (Ala30Ser) in the FS-LC completely abrogates the appearance of crystals in tubule cells of grafted mice as shown by TEM. **Ac** | The Ala30Ser substitution does not drastically alter the 3D structure of the variable (V) domain (the inset shows a superimposition of the V domains of the pathogenic light chain and the pathogenic light chain containing the Ala30Ser substitution). **Ad** | FS-LCs (lane 2) inhibit lysosomal function by inhibiting cathepsin D maturation (immunoblot of mouse tissue using an anti-cathepsin D antibody). Inhibition of cathepsin D maturation is not observed in mice expressing an empty vector (lane 1), a control light chain (lane 3) or the FS-LCs containing the Ala30Ser substitution (lane 4). **B** | Transgenic mouse model of light chain-related Fanconi syndrome. **Ba** | The transgenic model reproduces the human pathogenic lesions, with massive intracellular accumulation of crystals in proximal tubule cells (white arrows). **Bb** | Cre-recombinase-mediated deletion of the human light chain gene leads to an almost complete absence of tubular lesions after 2 months, arguing for the use of myeloma-based chemotherapy in this usually low-grade neoplastic disorder. **C** | Rat model of myeloma cast nephropathy using injections of immunoglobulin light chains. **Ca** | The light chain interacts with uromodulin through complementarity-determining region 3 (CDR3) to form casts (microscopic cylindrical structures; arrow) that obstruct the lumen of the distal tubules (shown by haematoxylin and eosin staining). **Cb** | Injection of cyclized competitor peptides that mimick CDR3 of the light chain inhibits the interaction between the light chain and uromodulin and, consequently, the formation of casts in the rodent model of myeloma cast nephropathy (haematoxylin and eosin staining). FLC, free light chain; Mat, mature; Pre, pre-pro-enzyme. Parts **Ac** and **Ad** are reproduced with permission from REF. 50, American Society of Nephrology. Parts **Ba** and **Bb** are reproduced with permission from REF. 71, American Society of Hematology. Part **C** is reproduced with permission from REF. 28, The American Society for Clinical Investigation.

syndrome and the mouse Cκ region, was created[71]. Pathological studies detected characteristic proximal tubular lesions in these mice, including intracellular light chain crystals, enlargement of mitochondria and alterations of the apical brush border (FIG. 4Ba). Studies of this light chain architecture definitively established that nephrotoxicity is a consequence of alterations to the V domain structure. Proximal tubular lesions in this mouse model rapidly disappear following Cre-mediated deletion of the pathogenic light chain from the mouse genome (FIG. 4Bb), arguing for the use of chemotherapy to eliminate the underlying light chain-producing plasma cell clone. In the absence of an underlying haematological disorder, the transgenic mice showed no obvious alteration in their general condition and were easily amenable to physiological analysis, which revealed a phenotype that was almost identical to Fanconi syndrome, including polyuria, phosphaturia, glucosuria and low-molecular-mass proteinuria. All these features are absent in mice expressing another chimeric κ-light chain from a patient with AL amyloidosis, highlighting the specific nephrotoxicity of the light chains associated with renal Fanconi syndrome[50]. Exposure of both proximal tubules in transgenic mice and proximal tubular cells *in vitro* to light chains from patients with Fanconi syndrome strongly inhibits receptor-mediated endocytosis and impairs lysosomal function (that is, it results in defective proteolysis and acidification), which are associated with dedifferentiation and proliferation of proximal tubular cells[50]. Taken together, these changes highlight the defective reabsorption that is observed in patients with Fanconi syndrome. Interestingly, all of these cellular alterations are observed in the absence of detectable crystals *in vitro*, which indicates that there is direct toxicity of the light chain. Studies are ongoing to further dissect these pathogenic mechanisms, which resemble those observed in congenital lysosomal disorders causing renal Fanconi syndrome, including nephropathic cystinosis[120,121], opening new avenues to establish common treatments for Fanconi syndrome resulting from distinct aetiologies. Lysosomes in proximal tubule cells are also crucial in the pathogenesis of proximal tubulopathies with features of acute tubular necrosis or those associated with interstitial inflammation[14,122]. As such, lysosomes could be a therapeutic target to ameliorate tubular injury. The generation of animal models to better understand these proximal tubulopathies is in progress.

Myeloma cast nephropathy. Cast nephropathy is the first monoclonal light chain-induced renal disorder for which murine models were created[63,123]. In contrast to MGRS, the injection of large quantities of purified Bence Jones proteins into mice efficiently reproduces the human disease, in which light chains precipitate with uromodulin when they exceed a threshold concentration (aided by triggering factors, such as low pH, high salt concentration, contrast agents or furosemide treatment)[7]. The sequences involved in the interaction between the immunoglobulin light chain and uromodulin have been mapped[56,124–128]. Key amino acids in CDR3 of the light chain account for its binding affinity for uromodulin, which facilitates the development of cyclized competitor peptides that inhibit cast formation in rats[28] (FIG. 4Ca,b).

Casts have been induced in tumour-grafted mice using SP2/0 cells that express a control human light chain[49], mirroring the frequent occurrence of this renal lesion during myeloma progression[129,130]. However, the inconsistent formation and rarity of myeloma casts in this model precluded any further investigation. A κ-light chain knock-in transgenic model of cast nephropathy is under investigation and involves the inducible production of the human light chain and the use of plasma cell-specific oncogenes, such as *CCND1* or *MYC*, to further increase plasma cell number and light chain production. This model might represent a valuable tool to better understand the disease and evaluate new therapeutic strategies[28].

Lessons and future challenges

AL amyloidosis is the most frequent cause of systemic amyloidosis and remains a devastating disease despite the advent of effective therapeutic agents and treatments[3,79,131]. Whereas zebrafish[64] and *C. elegans*[65] models have helped researchers to elucidate the biological effects of specific mutant light chains, the absence of a reliable experimental model hinders research into the mechanisms of light chain deposition and removal in AL amyloidosis (TABLE 1). Consequently, the light chain penile-vein injection model is a major step forward in the field. This model laid the foundations of our understanding of the pathophysiological mechanisms leading to light chain amyloid formation in the kidneys[62], but its drawbacks include the requirement for specialized technical skills and that it poorly recapitulates the human disease. The transgenic approach now allows free amyloid light chains to be produced in amounts equivalent to or greater than those in patients, but these high concentrations do not induce disease. In fact, creating an animal model of AL amyloidosis is far more complicated than for the other monoclonal immunoglobulin-related diseases, as even high concentrations of the mutant protein are not necessarily sufficient to induce the formation of amyloid fibrils. Of note, the only models that reproduce amyloid deposits in mice were obtained by injection of massive amounts of purified human light chains, with the exception of the random transgenic model that develops nonphysiological amyloid owing to the specific acidic conditions in the stomach. To date, no model in which there is constant production of a recombinant light chain has shown evidence of amyloid deposits. Consequently, the results from AL amyloidosis models pose a number of questions. First, is a burst of light chains required to initiate the nucleation and polymerization of light chains and, if so, how does this burst occur in patients? Of note, an *in vitro* study demonstrated that nucleation and polymerization are not concentration-dependent processes[132]. Second, do human light chains that are produced by neoplastic plasma cells differ from the recombinant light chains that are produced by normal mouse plasma cells? Furthermore, do light chains remain the

Table 1 | **Animal models of monoclonal immunoglobulin-related deposition diseases**

Model	Kidney deposits*	Effect on kidney function	Effect on other organs	Advantages	Disadvantages	Comparison with human disease	Refs
AL amyloidosis							
LC injection (i.v.)	+/–	ND	The liver, heart, lungs and spleen	Rapid, cost-effective and technically simple; mammalian model	LC availability; short-term analysis; kidney function analysis is not possible	CR^+ deposits; injection of a nonphysiological quantity of immunoglobulins; acute instead of chronic disease	57,58
LC injection (PV)	++ (glomeruli)	ND	ND	Rapid; analysis of early amyloidogenic processes possible; mammalian model	LC availability; requires specific technical skills; kidney function analysis is not possible	CR^+ deposits; injection of a nonphysiological quantity of immunoglobulins; acute instead of chronic disease	62
Amyloidomas	No	NA	NA	Rapid, cost-effective and technically simple; testing of therapies possible (amyloid removal)	Nonphysiological	No similarities to human disease	76–78
Transgenic (random)	No	NA	CR^+ deposits in the stomach; neurological dysfunction	Long-term delivery of AL amyloidosis LCs; testing of some therapies possible (doxycycline)	Lengthy protocol; expensive; no kidney or other typical organ lesions	CR^+ deposits in tissue; chronic delivery of monoclonal immunoglobulin but very low level of free LCs and unusual location of deposits; no organ dysfunction except nervous system, without deposits	70
Transgenic (random)	No	NA	No	Doxycycline-inducible expression of the LCs	Lengthy protocol; expensive; no kidney or other typical organ lesions	Chronic delivery of monoclonal immunoglobulins, but very low levels of free LCs; no organ dysfunction	69
Transgenic (immunoglobulin κ-LC KI)	No	None	No	Long-term delivery of AL amyloidosis LCs at physiological levels; might allow study of direct immunoglobulin toxicity in tissues and plasma cells	Lengthy protocol; expensive; no kidney or other typical organ lesions	Monoclonal gammopathy; production by plasma cells but no CR^+ deposits despite a high level of free LCs; no organ dysfunction	72
Zebrafish	No	NA	Cardiac dysfunction; cell death	Rapid, cost-effective test to check *in vivo* amyloidogenicity of immunoglobulin; study of direct immunoglobulin toxicity possible	Phylogenetically remote species; effect on mammalian physiology cannot be studied; no CR^+ deposits	NA	64, 99
Caenorhabditis elegans	NA	NA	Decreased pharyngeal pumping	Rapid, cost-effective test to check *in vivo* amyloidogenicity of immunoglobulin; study of direct immunoglobulin toxicity possible	Phylogenetically remote species; effect on mammalian physiology cannot be studied; no CR^+ deposits	NA	65

Table 1 (cont.) | **Animal models of monoclonal immunoglobulin-related deposition diseases**

Model	Kidney deposits*	Effect on kidney function	Effect on other organs	Advantages	Disadvantages	Comparison with human disease	Refs
MIDD							
LC injection (PV)	+ (glomeruli)	ND	ND	Rapid; analysis of early glomerular lesions is possible; mammalian model; demonstrated the role of caveolin 1 in the mesangial alteration	LC availability; requires specific technical skills; kidney function analysis is not possible	Early lesions are similar to those in humans; easy follow-up; nonphysiological burst; no CKD or glomerular proteinuria	101
Tumour grafts (SP2/O)	+ (glomeruli and tubules)	ND	Few deposits in the lungs, liver and heart	Rapid and technically simple mammalian model; recombinant immunoglobulin so unlimited material available; mutagenesis studies are possible	Rapid tumour growth; general condition of the animals due to tumour growth limits study of kidney function	Continuous delivery of large amounts of free LCs associated with plasma cell proliferation but highly proliferating cells; localization of tumour	60
Transgenic (KI) HCDD	++ (glomeruli and tubules)	Mild albuminuria	Few deposits in the lungs and liver (similar to patients)	Long-term delivery of pathogenic HCs at physiological levels; allows study of effects on kidney function; suitable for testing therapies; allows study of direct immunoglobulin toxicity	Lengthy protocol; expensive; complex follow-up (no external sign of the disease)	Monoclonal gammopathy; production by plasma cells; faithfully reproduces early lesions of the disease but no late lesions (glomerulosclerosis) or end-stage renal disease	73
Transgenic (KI) LCDD	+++ (glomeruli, tubules; glomerulosclerosis)	Albuminuria and terminal kidney failure	Few deposits in the lungs, liver and heart	Long-term delivery of pathogenic LCs at physiological levels; long-term studies possible; suitable for testing therapies; allows study of direct immunoglobulin toxicity	Lengthy protocol; expensive; complex follow-up (no external sign of the disease)	Monoclonal gammopathy; production by plasma cells; faithfully reproduces early and late kidney lesions (glomerulosclerosis) and end-stage renal disease	NP
Proximal tubulopathy (with or without Fanconi syndrome)							
LC injection (i.v. or i.p.)	++ (crystals in tubular cells; casts)	ND	ND	Rapid, cost-effective and technically simple mammalian model; study of early events in LC-induced inflammation possible	LC availability; only short-term analysis possible; kidney function analysis is not possible	Lesions similar to those in patients with high-mass myeloma and with proximal tubulopathy and MCN; does not mimic renal Fanconi syndrome, which is mostly associated with low-mass myeloma	55–57
Tumour grafts (SP2/O)	++ (some crystals in proximal tubules)	Phosphaturia	Crystals in plasma cells	Rapid, technically simple mammalian model; recombinant immunoglobulin so unlimited material available; mutagenesis studies are possible	Rapid tumour growth; poor general condition of the animals due to tumour growth limits study of kidney function	Continuous delivery of large amounts of free LC associated with plasma cell proliferation but highly proliferative cells; localization of tumour	49
Transgenic (KI)	+++ (many crystals in proximal tubules)	Fanconi syndrome	Crystals in plasma cells and spleen macrophages	Long-term delivery of pathogenic LCs at physiological levels; allows study of effects on kidney function; suitable for testing therapies; allows study of direct immunoglobulin toxicity	Lengthy protocol; expensive; complex follow-up (no external sign of the disease)	Monoclonal gammopathy; production by plasma cells; faithfully reproduces early kidney lesions (crystals in tubular cells) and Fanconi syndrome, but no evolution to end-stage renal disease	50,71

Table 1 (cont.) | **Animal models of monoclonal immunoglobulin-related deposition diseases**

Model	Kidney deposits*	Effect on kidney function	Effect on other organs	Advantages	Disadvantages	Comparison with human disease	Refs
Myeloma cast nephropathy							
Injection of LCs into rat or mouse (i.v. or i.p.)	• ++ (casts in distal tubules) • +/– (proximal tubulopathy)	Mild AKI	NA	Rapid, cost-effective and simple mammalian model; rapid induction of casts; suitable for testing therapies (inhibition of cast formation)	LC availability; only short-term analysis possible	Injection of LCs mimics the AKI observed in patients; lesions are similar to those in patients with MCN but requires production of nonphysiological quantities of immunoglobulins	28,63, 123, 124
Transgenic (KI)	Under investigation	Under investigation	NA	NA	NA	NA	NP

*The intensity (+/–, low; +, moderate; ++, high; +++, very high) and location of immunoglobulin deposits are indicated. AKI, acute kidney injury; AL amyloidosis, immunoglobulin light chain amyloidosis; CKD, chronic kidney disease; CR, Congo red; HC, heavy chain; HCDD, heavy chain deposition disease; i.p., intraperitoneal; i.v., intravenous; KI, knock-in; LC, light chain; LCDD, light chain deposition disease; MCN, myeloma cast nephropathy; MIDD, monoclonal immunoglobulin deposition disease; NA, not applicable; ND, not determined; NP, not published; PV, penile vein.

same in the serum in humans and mice (that is, are they as stable, are they similarly modified and so on)? Even if the primary sequences of the light chains are identical in human neoplastic plasma cells and mouse normal plasma cells, it is difficult to monitor the 3D structure of the light chains in circulation. Unfolded or misfolded proteins, which might be more prone to initiate the nucleation or polymerization process, might be produced by the neoplastic plasma cells but not by the normal plasma cells. These misfolded light chains that are present in human urine could be injected in mice to test this idea and might eventually create the conditions for amyloid fibril formation. This hypothesis could explain why transgenic mouse models of AL amyloidosis do not develop the disease. Third, are specific circulating factors or receptors required for amyloid formation and are they absent or less efficient in mice? A comparison of the light chain 'interactome' from the serum of human patients and of transgenic mice might be useful to answer these questions. Fourth, can higher production of light chains overcome the lack of amyloid formation in mice and can this be tested using plasma cell proliferation models[94,95]?

In contrast to AL amyloidosis, creating animal models of the other monoclonal immunoglobulin-related deposition diseases requires only a sufficient level of the light chain in serum, which is either produced by plasma cells or injected into mice. The first lesson learned from these models is that the pathogenicity of a specific light chain is similar in humans and rodents, which means that the structural peculiarities of a light chain that results in nephrotoxicity are independent of the species. Consequently, the pathophysiological mechanisms of MIDD are, at least in part, similar in humans and mice, validating the use of these animal models. The available models of MIDDs efficiently reproduce the typical pathological features of the diseases in humans, including immunoglobulin deposits in basement membranes and the mesangium. Light chain injection or tumour graft models can be used to quickly monitor and study early lesions in the kidneys (and therapeutics aiming at inhibiting their formation), but only transgenic models recapitulate the complete features of the diseases and their progressive evolution[73]. The HCDD model demonstrated that, similar to findings in humans, a very low amount of pathogenic truncated heavy chains induces kidney lesions and that the truncated heavy chains are toxic to the producing plasma cells, which should facilitate investigation of the toxicity of pathogenic monoclonal immunoglobulins for plasma cells. Similarly, only the transgenic mouse model of light chain-induced Fanconi syndrome recapitulates both the lesions and the tubular dysfunctions of the human disease, and this model has been useful in understanding the direct toxicity of Fanconi syndrome light chains in proximal tubular cells[50,71]. However, models based on light chain injections or tumour grafts can be used to quickly test the pathogenicity of a mutant light chain and to validate therapeutic interventions aimed at limiting the aggregation of light chains and their trafficking to lysosomes. Models of light chain-induced proximal tubulopathies without Fanconi syndrome are being created and will probably clarify the differences between crystalline and non-crystalline tubulopathies. At present, although the creation of transgenic models of MCN is ongoing, the injection of light chains accurately recapitulates MCN — in particular, the acute phase of the human disease — and this method was used to design a new therapy that inhibits the interaction between the light chain and uromodulin[28]. However, transgenic models could provide insights into the early events that trigger the precipitation of light chains in distal tubules.

Despite the tremendous advances that have been made using these models, areas to investigate still exist — in particular, the pathophysiological consequences of immunoglobulin deposits. As discussed here (TABLE 1), glomerulosclerosis, tubulointerstitial fibrosis and progressive renal failure are only rarely recapitulated in animal models of monoclonal immunoglobulin deposition. The standard use of inbred mouse strains that

are known to be resistant to the development of these phenotypes to generate transgenic mice may account for this phenomenon and could be addressed by backcrossing with more permissive strains[104,133]. High-throughput technologies, especially transcriptomic studies carried out on damaged tissues or cells, should also aid in evaluating the relevance of animal models in modelling the human diseases, by allowing comparisons of the available data from patients with data from mouse models. These studies could also highlight new pathological pathways and produce innovative therapeutic strategies. Finally, aside from the organ injuries induced by immunoglobulins, little is known about the specific attributes of the underlying haematological disorders. As discussed earlier, accumulating experimental evidence suggests that misfolded immunoglobulin fragments are intrinsically toxic to plasma cells[66,73,105,134], which should be explored further. A new animal model allowing the inducible production of pathogenic immunoglobulins specifically in plasma cells is under investigation and might be useful to dissect the mechanisms of immunoglobulin toxicity to the immunoglobulin-producing plasma cells and to explore novel treatment strategies.

Conclusions

Since the creation of the first models of immunoglobulin deposition diseases using injections of Bence Jones protein, considerable progress has been made to better reproduce human monoclonal immunoglobulin-related diseases in animals. The advent of recombinant protein production and transgenic approaches has provided new tools to study the complex pathophysiology of these diseases, and several therapeutic advances have already been made using these disease models. However, the unresolved issue of the failure to create a model of AL amyloidosis is still present, and scope exists to more faithfully reproduce all aspects of human monoclonal immunoglobulin deposition disorders.

1. Bridoux, F. et al. Diagnosis of monoclonal gammopathy of renal significance. *Kidney Int.* **87**, 698–711 (2015).
2. Merlini, G. & Stone, M. J. Dangerous small B-cell clones. *Blood* **108**, 2520–2530 (2006).
3. Fermand, J.-P. et al. How I treat monoclonal gammopathy of renal significance (MGRS). *Blood* **122**, 3583–3590 (2013).
4. Preud'homme, J. L. et al. Monoclonal immunoglobulin deposition disease: a review of immunoglobulin chain alterations. *Int. J. Immunopharmacol.* **16**, 425–431 (1994).
5. Batuman, V. et al. Myeloma light chains are ligands for cubilin (gp280). *Am. J. Physiol.* **275**, F246–254 (1998).
6. Christensen, E. I., Birn, H., Storm, T., Weyer, K. & Nielsen, R. Endocytic receptors in the renal proximal tubule. *Physiology* **27**, 223–236 (2012).
7. Hutchison, C. A. et al. The pathogenesis and diagnosis of acute kidney injury in multiple myeloma. *Nat. Rev. Nephrol.* **8**, 43–51 (2012).
8. Kyle, R. A. et al. Prevalence of monoclonal gammopathy of undetermined significance. *N. Engl. J. Med.* **354**, 1362–1369 (2006).
9. Dispenzieri, A. et al. Prevalence and risk of progression of light-chain monoclonal gammopathy of undetermined significance: a retrospective population-based cohort study. *Lancet* **375**, 1721–1728 (2010).
10. Leung, N. et al. Monoclonal gammopathy of renal significance: when MGUS is no longer undetermined or insignificant. *Blood* **120**, 4292–4295 (2012).
11. Sanders, P. W. Mechanisms of light chain injury along the tubular nephron. *J. Am. Soc. Nephrol.* **23**, 1777–1781 (2012).
12. Maldonado, J. E. et al. Fanconi syndrome in adults. A manifestation of a latent form of myeloma. *Am. J. Med.* **58**, 354–364 (1975).
13. Messiaen, T. et al. Adult Fanconi syndrome secondary to light chain gammopathy. Clinicopathologic heterogeneity and unusual features in 11 patients. *Medicine* **79**, 135–154 (2000).
14. Herrera, G. A. Proximal tubulopathies associated with monoclonal light chains: the spectrum of clinicopathologic manifestations and molecular pathogenesis. *Arch. Pathol. Lab. Med.* **138**, 1365–1380 (2014).
15. Pepys, M. B. Amyloidosis. *Annu. Rev. Med.* **57**, 223–241 (2006).
16. Desport, E. et al. AL Amyloidosis. *Orphanet J. Rare Dis.* **7**, 54 (2012).
17. Chiti, F. & Dobson, C. M. Protein misfolding, functional amyloid, and human disease. *Annu. Rev. Biochem.* **75**, 333–366 (2006).
18. Liao, R. et al. Infusion of light chains from patients with cardiac amyloidosis causes diastolic dysfunction in isolated mouse hearts. *Circulation* **104**, 1594–1597 (2001).
19. Brenner, D. A. et al. Human amyloidogenic light chains directly impair cardiomyocyte function through an increase in cellular oxidant stress. *Circ. Res.* **94**, 1008–1010 (2004).
20. Palladini, G. et al. Circulating amyloidogenic free light chains and serum N-terminal natriuretic peptide type B decrease simultaneously in association with improvement of survival in AL. *Blood* **107**, 3854–3858 (2006).
21. Buxbaum, J. & Gallo, G. Nonamyloidotic monoclonal immunoglobulin deposition disease. Light-chain, heavy-chain, and light- and heavy-chain deposition diseases. *Hematol. Oncol. Clin. North Am.* **13**, 1235–1248 (1999).
22. Lin, J. et al. Renal monoclonal immunoglobulin deposition disease: the disease spectrum. *J. Am. Soc. Nephrol.* **12**, 1482–1492 (2001).
23. Cohen, C. et al. Randall-type monoclonal immunoglobulin deposition disease: from diagnosis to treatment [French]. *Nephrol. Ther.* **12**, 131–139 (2016).
24. Aucouturier, P. et al. Brief report: heavy-chain deposition disease. *N. Engl. J. Med.* **329**, 1389–1393 (1993).
25. Preud'homme, J. L. et al. Monoclonal immunoglobulin deposition disease (Randall type). Relationship with structural abnormalities of immunoglobulin chains. *Kidney Int.* **46**, 965–972 (1994).
26. Kambham, N. et al. Heavy chain deposition disease: the disease spectrum. *Am. J. Kidney Dis. Off. J. Natl Kidney Found.* **33**, 954–962 (1999).
27. Bridoux, F. et al. Unravelling the immunopathological mechanisms of heavy chain deposition disease with implications for clinical management. *Kidney Int.* **91**, 423–434 (2017).
28. Ying, W.-Z., Allen, C. E., Curtis, L. M., Aaron, K. J. & Sanders, P. W. Mechanism and prevention of acute kidney injury from cast nephropathy in a rodent model. *J. Clin. Invest.* **122**, 1777–1785 (2012).
29. Stevens, F. J. & Argon, Y. Pathogenic light chains and the B-cell repertoire. *Immunol. Today* **20**, 451–457 (1999).
30. Bellotti, V., Mangione, P. & Merlini, G. Review: immunoglobulin light chain amyloidosis — the archetype of structural and pathogenic variability. *J. Struct. Biol.* **130**, 280–289 (2000).
31. Blancas-Mejía, L. M. & Ramirez-Alvarado, M. Systemic amyloidoses. *Annu. Rev. Biochem.* **82**, 745–774 (2013).
32. Davis, D. P. et al. Both the environment and somatic mutations govern the aggregation pathway of pathogenic immunoglobulin light chain. *J. Mol. Biol.* **313**, 1021–1034 (2001).
33. Wall, J. S. et al. Structural basis of light chain amyloidogenicity: comparison of the thermodynamic properties, fibrillogenic potential and tertiary structural features of four Vlambda6 proteins. *J. Mol. Recognit.* **17**, 323–331 (2004).
34. Poshusta, T. L. et al. Mutations in specific structural regions of immunoglobulin light chains are associated with free light chain levels in patients with AL amyloidosis. *PLoS ONE* **4**, e5169 (2009).
35. Hernández-Santoyo, A. et al. A single mutation at the sheet switch region results in conformational changes favoring lambda6 light-chain fibrillogenesis. *J. Mol. Biol.* **396**, 280–292 (2010).
36. Kobayashi, Y. et al. Decreased amyloidogenicity caused by mutational modulation of surface properties of the immunoglobulin light chain BRE variable domain. *Biochemistry* **53**, 5162–5173 (2014).
37. Comenzo, R. L., Zhang, Y., Martinez, C., Osman, K. & Herrera, G. A. The tropism of organ involvement in primary systemic amyloidosis: contributions of Ig V(L) germ line gene use and clonal plasma cell burden. *Blood* **98**, 714–720 (2001).
38. Perfetti, V. et al. Analysis of V(lambda)-J(lambda) expression in plasma cells from primary (AL) amyloidosis and normal bone marrow identifies 3r (lambdaIII) as a new amyloid-associated germline gene segment. *Blood* **100**, 948–953 (2002).
39. Abraham, R. S. et al. Immunoglobulin light chain variable (V) region genes influence clinical presentation and outcome in light chain-associated amyloidosis (AL). *Blood* **101**, 3801–3808 (2003).
40. Perfetti, V. et al. The repertoire of λ light chains causing predominant amyloid heart involvement and identification of a preferentially involved germline gene, IGLV1-44. *Blood* **119**, 144–150 (2012).
41. Rocca, A. et al. Primary structure of a variable region of the V kappa I subgroup (ISE) in light chain deposition disease. *Clin. Exp. Immunol.* **91**, 506–509 (1993).
42. Denoroy, L., Déret, S. & Aucouturier, P. Overrepresentation of the V kappa IV subgroup in light chain deposition disease. *Immunol. Lett.* **42**, 63–66 (1994).
43. Decourt, C., Cogné, M. & Rocca, A. Structural peculiarities of a truncated V kappa III immunoglobulin light chain in myeloma with light chain deposition disease. *Clin. Exp. Immunol.* **106**, 357–361 (1996).
44. Kaplan, B., Livneh, A. & Gallo, G. Charge differences between in vivo deposits in immunoglobulin light chain amyloidosis and non-amyloid light chain deposition disease. *Br. J. Haematol.* **136**, 723–728 (2007).
45. Isobe, T., Kametani, F. & Shinoda, T. V-Domain deposition of lambda Bence Jones protein in the renal tubular epithelial cells in a patient with the adult Fanconi syndrome with myeloma. *Amyloid* **5**, 117–120 (1998).
46. Bridoux, F. et al. Fanconi's syndrome induced by a monoclonal Vkappa3 light chain in Waldenstrom's macroglobulinemia. *Am. J. Kidney Dis.* **45**, 749–757 (2005).
47. Aucouturier, P. et al. Monoclonal Ig L chain and L chain V domain fragment crystallization in myeloma-associated Fanconi's syndrome. *J. Immunol.* **150**, 3561–3568 (1993).
48. Leboulleux, M. et al. Protease resistance and binding of Ig light chains in myeloma-associated tubulopathies. *Kidney Int.* **48**, 72–79 (1995).

49. Decourt, C. et al. Mutational analysis in murine models for myeloma-associated Fanconi's syndrome or cast myeloma nephropathy. *Blood* **94**, 3559–3566 (1999).
50. Luciani, A. et al. Impaired lysosomal function underlies monoclonal light chain-associated renal Fanconi syndrome. *J. Am. Soc. Nephrol.* **27**, 2049–2061 (2016).
51. Nasr, S. H. et al. The diagnosis and characteristics of renal heavy-chain and heavy/light-chain amyloidosis and their comparison with renal light-chain amyloidosis. *Kidney Int.* **83**, 463–470 (2013).
52. Khamlichi, A. A., Aucouturier, P., Preud'homme, J. L. & Cogné, M. Structure of abnormal heavy chains in human heavy-chain-deposition disease. *Eur. J. Biochem.* **229**, 54–60 (1995).
53. Hendershot, L., Bole, D., Köhler, G. & Kearney, J. F. Assembly and secretion of heavy chains that do not associate posttranslationally with immunoglobulin heavy chain-binding protein. *J. Cell Biol.* **104**, 761–767 (1987).
54. Cogné, M., Silvain, C., Khamlichi, A. A. & Preud'homme, J. L. Structurally abnormal immunoglobulins in human immunoproliferative disorders. *Blood* **79**, 2181–2195 (1992).
55. Sanders, P. W., Herrera, G. A. & Galla, J. H. Human Bence Jones protein toxicity in rat proximal tubule epithelium in vivo. *Kidney Int.* **32**, 851–861 (1987).
56. Sanders, P. W., Herrera, G. A., Chen, A., Booker, B. B. & Galla, J. H. Differential nephrotoxicity of low molecular weight proteins including Bence Jones proteins in the perfused rat nephron in vivo. *J. Clin. Invest.* **82**, 2086–2096 (1988).
57. Solomon, A., Weiss, D. T. & Kattine, A. A. Nephrotoxic potential of Bence Jones proteins. *N. Engl. J. Med.* **324**, 1845–1851 (1991).
58. Solomon, A., Weiss, D. T. & Pepys, M. B. Induction in mice of human light-chain-associated amyloidosis. *Am. J. Pathol.* **140**, 629–637 (1992).
59. Khan, A.-M. et al. Myeloma light chain-induced renal injury in mice. *Nephron Exp. Nephrol.* **116**, e32–e41 (2010).
60. Khamlichi, A. A. et al. Role of light chain variable region in myeloma with light chain deposition disease: evidence from an experimental model. *Blood* **86**, 3655–3659 (1995).
61. Rognoni, P. et al. A strategy for synthesis of pathogenic human immunoglobulin free light chains in *E. coli*. *PLoS ONE* **8**, e76022 (2013).
62. Teng, J., Turbat-Herrera, E. A. & Herrera, G. A. An animal model of glomerular light-chain-associated amyloidogenesis depicts the crucial role of lysosomes. *Kidney Int.* **86**, 738–746 (2014).
63. Koss, M. N., Pirani, C. L. & Osserman, E. F. Experimental Bence Jones cast nephropathy. *Lab. Invest.* **34**, 579–591 (1976).
64. Mishra, S. et al. Human amyloidogenic light chain proteins result in cardiac dysfunction, cell death, and early mortality in zebrafish. *Am. J. Physiol. Heart Circ. Physiol.* **305**, H95–H103 (2013).
65. Diomede, L. et al. A *Caenorhabditis elegans*-based assay recognizes immunoglobulin light chains causing heart amyloidosis. *Blood* **123**, 3543–3552 (2014).
66. Zhou, P., Ma, X., Iyer, L., Chaulagain, C. & Comenzo, R. L. One siRNA pool targeting the λ constant region stops λ light-chain production and causes terminal endoplasmic reticulum stress. *Blood* **123**, 3440–3451 (2014).
67. Hovey, B. M. et al. Preclinical development of siRNA therapeutics for AL amyloidosis. *Gene Ther.* **18**, 1150–1156 (2011).
68. Chauveau, C., Decourt, C. & Cogné, M. Insertion of the IgH locus 3' regulatory palindrome in expression vectors warrants sure and efficient expression in stable B cell transfectants. *Gene* **222**, 279–285 (1998).
69. Nuvolone, M. et al. Regulated expression of amyloidogenic immunoglobulin light chains in mice. *Amyloid* **24**, 52–53 (2017).
70. Ward, J. E. et al. Doxycycline reduces fibril formation in a transgenic mouse model of AL amyloidosis. *Blood* **118**, 6610–6617 (2011).
71. Sirac, C. et al. Role of the monoclonal kappa chain V domain and reversibility of renal damage in a transgenic model of acquired Fanconi syndrome. *Blood* **108**, 536–543 (2006).
72. Sirac, C. et al. Strategies to model AL amyloidosis in mice. *Amyloid* **18** (Suppl. 1), 40–42 (2011).
73. Bonaud, A. et al. A mouse model recapitulating human monoclonal heavy chain deposition disease evidences the relevance of proteasome inhibitor therapy. *Blood* **126**, 757–765 (2015).
74. Casola, S. et al. B cell receptor signal strength determines B cell fate. *Nat. Immunol.* **5**, 317–327 (2004).
75. Lechouane, F. et al. B-Cell receptor signal strength influences terminal differentiation. *Eur. J. Immunol.* **43**, 619–628 (2013).
76. Hrncic, R. et al. Antibody-mediated resolution of light chain-associated amyloid deposits. *Am. J. Pathol.* **157**, 1239–1246 (2000).
77. Solomon, A., Weiss, D. T. & Wall, J. S. Therapeutic potential of chimeric amyloid-reactive monoclonal antibody 11-1F4. *Clin. Cancer Res.* **9**, 3831S–3838S (2003).
78. Wall, J. S. et al. AL amyloid imaging and therapy with a monoclonal antibody to a cryptic epitope on amyloid fibrils. *PLoS ONE* **7**, e52686 (2012).
79. Gertz, M. A. et al. First-in-Human Phase I/II Study of NEOD001 in Patients With Light Chain Amyloidosis and Persistent Organ Dysfunction. *J. Clin. Oncol.* **34**, 1097–1103 (2016).
80. Nightingale, C. H. & Mouravieff, M. Reliable and simple method of intravenous injection into the laboratory rat. *J. Pharm. Sci.* **62**, 860–861 (1973).
81. Teng, J. et al. Different types of glomerulopathic light chains interact with mesangial cells using a common receptor but exhibit different intracellular trafficking patterns. *Lab. Invest.* **84**, 440–451 (2004).
82. Teng, J., Turbat-Herrera, E. A. & Herrera, G. A. Extrusion of amyloid fibrils to the extracellular space in experimental mesangial AL-amyloidosis: transmission and scanning electron microscopy studies and correlation with renal biopsy observations. *Ultrastruct. Pathol.* **38**, 104–115 (2014).
83. Kluve-Beckerman, B., Manaloor, J. J. & Liepnieks, J. J. A pulse-chase study tracking the conversion of macrophage-endocytosed serum amyloid A into extracellular amyloid. *Arthritis Rheum.* **46**, 1905–1913 (2002).
84. Lundmark, K., Vahdat Shariatpanahi, A. & Westermark, G. T. Depletion of spleen macrophages delays AA amyloid development: a study performed in the rapid mouse model of AA amyloidosis. *PLoS ONE* **8**, e79104 (2013).
85. Kennel, S. J. et al. Phagocyte depletion inhibits AA amyloid accumulation in AEF-induced huIL-6 transgenic mice. *Amyloid* **21**, 45–53 (2014).
86. Arendt, B. K. et al. Biologic and genetic characterization of the novel amyloidogenic lambda light chain-secreting human cell lines, ALMC-1 and ALMC-2. *Blood* **112**, 1931–1941 (2008).
87. Buxbaum, J. N. Animal models of human amyloidoses: are transgenic mice worth the time and trouble? *FEBS Lett.* **583**, 2663–2673 (2009).
88. Wechalekar, A. D. & Whelan, C. Encouraging impact of doxycycline on early mortality in cardiac light chain (AL) amyloidosis. *Blood Cancer J.* **7**, e546 (2017).
89. Rokita, H., Shirahama, T., Cohen, A. S. & Sipe, J. D. Serum amyloid A gene expression and AA amyloid formation in A/J and SJL/J mice. *Br. J. Exp. Pathol.* **70**, 327–335 (1989).
90. Takeda, T. et al. A novel murine model of aging, Senescence-Accelerated Mouse (SAM). *Arch. Gerontol. Geriatr.* **19**, 185–192 (1994).
91. Ge, F. et al. Amyloidosis in transgenic mice expressing murine amyloidogenic apolipoprotein A-II (Apoa2c). *Lab. Invest.* **87**, 633–643 (2007).
92. Kohno, K. et al. Analysis of amyloid deposition in a transgenic mouse model of homozygous familial amyloidotic polyneuropathy. *Am. J. Pathol.* **150**, 1497–1508 (1997).
93. Simons, J. P. et al. Pathogenetic mechanisms of amyloid A amyloidosis. *Proc. Natl Acad. Sci. USA* **110**, 16115–16120 (2013).
94. Chesi, M. et al. AID-dependent activation of a MYC transgene induces multiple myeloma in a conditional mouse model of post-germinal center malignancies. *Cancer Cell* **13**, 167–180 (2008).
95. Carrasco, D. R. et al. The differentiation and stress response factor XBP-1 drives multiple myeloma pathogenesis. *Cancer Cell* **11**, 349–360 (2007).
96. Hamouda, M.-A. et al. BCL-B (BCL2L10) is overexpressed in patients suffering from multiple myeloma (MM) and drives an MM-like disease in transgenic mice. *J. Exp. Med.* **213**, 1705–1722 (2016).
97. Shi, J. et al. Amyloidogenic light chains induce cardiomyocyte contractile dysfunction and apoptosis via a non-canonical p38alpha MAPK pathway. *Proc. Natl Acad. Sci. USA* **107**, 4188–4193 (2010).
98. Guan, J. et al. Lysosomal dysfunction and impaired autophagy underlie the pathogenesis of amyloidogenic light chain-mediated cardiotoxicity. *EMBO Mol. Med.* **6**, 1493–1507 (2014).
99. Shin, J. T. et al. Overexpression of human amyloidogenic light chains causes heart failure in embryonic zebrafish: a preliminary report. *Amyloid* **19**, 191–196 (2012).
100. Diomede, L. et al. Cardiac light chain amyloidosis: the role of metal ions in oxidative stress and mitochondrial damage. *Antioxid. Redox Signal.* **27**, 567–582 (2017).
101. Herrera, G. A., Turbat-Herrera, E. A. & Teng, J. Animal models of light chain deposition disease provide a better understanding of nodular glomerulosclerosis. *Nephron* **132**, 119–136 (2016).
102. Ronco, P., Plaisier, E. & Aucouturier, P. Monoclonal immunoglobulin light and heavy chain deposition diseases: molecular models of common renal diseases. *Contrib. Nephrol.* **169**, 221–231 (2011).
103. Zheng, F., Striker, G. E., Esposito, C., Lupia, E. & Striker, L. J. Strain differences rather than hyperglycemia determine the severity of glomerulosclerosis in mice. *Kidney Int.* **54**, 1999–2007 (1998).
104. Ma, L.-J. & Fogo, A. B. Model of robust induction of glomerulosclerosis in mice: importance of genetic background. *Kidney Int.* **64**, 350–355 (2003).
105. Oliva, L. et al. The amyloidogenic light chain is a stressor that sensitizes plasma cells to proteasome inhibitor toxicity. *Blood* **129**, 2132–2142 (2017).
106. Meister, S. et al. Extensive immunoglobulin production sensitizes myeloma cells for proteasome inhibition. *Cancer Res.* **67**, 1783–1792 (2007).
107. Nasr, S. H. et al. Renal monoclonal immunoglobulin deposition disease: a report of 64 patients from a single institution. *Clin. J. Am. Soc. Nephrol.* **7**, 231–239 (2012).
108. Cohen, C. et al. Bortezomib produces high hematological response rates with prolonged renal survival in monoclonal immunoglobulin deposition disease. *Kidney Int.* **88**, 1135–1143 (2015).
109. Venner, C. P. et al. A matched comparison of cyclophosphamide, bortezomib and dexamethasone (CVD) versus risk-adapted cyclophosphamide, thalidomide and dexamethasone (CTD) in AL amyloidosis. *Leukemia* **28**, 2304–2310 (2014).
110. Palladini, G. et al. Melphalan and dexamethasone with or without bortezomib in newly diagnosed AL amyloidosis: a matched case-control study on 174 patients. *Leukemia* **28**, 2311–2316 (2014).
111. Jaccard, A. et al. Efficacy of bortezomib, cyclophosphamide and dexamethasone in treatment-naïve patients with high-risk cardiac AL amyloidosis (Mayo Clinic stage III). *Haematologica* **99**, 1479–1485 (2014).
112. Kastritis, E. et al. Bortezomib with or without dexamethasone in primary systemic (light chain) amyloidosis. *J. Clin. Oncol.* **28**, 1031–1037 (2010).
113. Batuman, V., Sastrasinh, M. & Sastrasinh, S. Light chain effects on alanine and glucose uptake by renal brush border membranes. *Kidney Int.* **30**, 662–665 (1986).
114. Batuman, V., Guan, S., O'Donovan, R. & Puschett, J. B. Effect of myeloma light chains on phosphate and glucose transport in renal proximal tubule cells. *Ren. Physiol. Biochem.* **17**, 294–300 (1994).
115. Pote, A., Zwizinski, C., Simon, E. E., Meleg-Smith, S. & Batuman, V. Cytotoxicity of myeloma light chains in cultured human kidney proximal tubule cells. *Am. J. Kidney Dis.* **36**, 735–744 (2000).
116. Sengul, S., Zwizinski, C. & Batuman, V. Role of MAPK pathways in light chain-induced cytokine production in human proximal tubule cells. *Am. J. Physiol. Renal Physiol.* **284**, F1245–F1254 (2003).
117. Wang, P.-X. & Sanders, P. W. Immunoglobulin light chains generate hydrogen peroxide. *J. Am. Soc. Nephrol.* **18**, 1239–1245 (2007).
118. Li, M., Balamuthusamy, S., Simon, E. E. & Batuman, V. Silencing megalin and cubilin genes inhibits myeloma light chain endocytosis and ameliorates toxicity in human renal proximal tubule epithelial cells. *Am. J. Physiol. Renal Physiol.* **295**, F82–F90 (2008).
119. Ying, W.-Z., Wang, P.-X., Aaron, K. J., Basnayake, K. & Sanders, P. W. Immunoglobulin light chains activate nuclear factor-κB in renal epithelial cells through a Src-dependent mechanism. *Blood* **117**, 1301–1307 (2011).
120. Sirac, C. et al. Toward understanding renal Fanconi syndrome: step by step advances through experimental models. *Contrib. Nephrol.* **169**, 247–261 (2011).

121. Raggi, C. et al. Dedifferentiation and aberrations of the endolysosomal compartment characterize the early stage of nephropathic cystinosis. *Hum. Mol. Genet.* **23**, 2266–2278 (2014).
122. Aufman, J. & Herrera, G. A. Circulating monoclonal light chains and acute kidney injury: the role of the renal biopsy with emphasis on ultrastructural evaluation in assessing and understanding renal injury. *Ultrastruct. Pathol.* **39**, 159–168 (2015).
123. Weiss, J. H. et al. Pathophysiology of acute Bence-Jones protein nephrotoxicity in the rat. *Kidney Int.* **20**, 198–210 (1981).
124. Sanders, P. W. & Booker, B. B. Pathobiology of cast nephropathy from human Bence Jones proteins. *J. Clin. Invest.* **89**, 630–639 (1992).
125. Huang, Z. Q., Kirk, K. A., Connelly, K. G. & Sanders, P. W. Bence Jones proteins bind to a common peptide segment of Tamm-Horsfall glycoprotein to promote heterotypic aggregation. *J. Clin. Invest.* **92**, 2975–2983 (1993).
126. Huang, Z. Q. & Sanders, P. W. Biochemical interaction between Tamm-Horsfall glycoprotein and Ig light chains in the pathogenesis of cast nephropathy. *Lab. Invest.* **73**, 810–817 (1995).
127. Huang, Z. Q. & Sanders, P. W. Localization of a single binding site for immunoglobulin light chains on human Tamm-Horsfall glycoprotein. *J. Clin. Invest.* **99**, 732–736 (1997).
128. Ying, W. Z. & Sanders, P. W. Mapping the binding domain of immunoglobulin light chains for Tamm-Horsfall protein. *Am. J. Pathol.* **158**, 1859–1866 (2001).
129. Korbet, S. M. & Schwartz, M. M. Multiple myeloma. *J. Am. Soc. Nephrol.* **17**, 2533–2545 (2006).
130. Drayson, M. et al. Effects of paraprotein heavy and light chain types and free light chain load on survival in myeloma: an analysis of patients receiving conventional-dose chemotherapy in Medical Research Council UK multiple myeloma trials. *Blood* **108**, 2013–2019 (2006).
131. Richards, D. B. et al. Therapeutic clearance of amyloid by antibodies to serum amyloid P component. *N. Engl. J. Med.* **373**, 1106–1114 (2015).
132. Blancas-Mejía, L. M., Misra, P. & Ramirez-Alvarado, M. Differences in protein concentration dependence for nucleation and elongation in light chain amyloid formation. *Biochemistry* **56**, 757–766 (2017).
133. Becker, G. J. & Hewitson, T. D. Animal models of chronic kidney disease: useful but not perfect. *Nephrol. Dial. Transplant.* **28**, 2432–2438 (2013).
134. Srour, N. et al. A plasma cell differentiation quality control ablates B cell clones with biallelic Ig rearrangements and truncated Ig production. *J. Exp. Med.* **213**, 109–122 (2016).

Acknowledgements
The authors thank the members of the International Kidney and Monoclonal Gammopathy Research Group for their intellectual support in this project. C.S. thanks C. Carrion, A. Rinsant, S. Kaaki, N. Quellard, J.M. Goujon, A. Jaccard and D. Lavergne for their technical and intellectual support. C.S. is supported by a grant from Fondation Française pour le Recheche contre le Myelome et les Gammapathies Monoclonales. G.A.H. is supported by a grant from the Amyloidosis Foundation. P.W.S. is supported by grants from the Office of Research and Development, Medical Research Service, US Department of Veterans Affairs (I01 CX001326) and the US National Institutes of Health George M. O'Brien Kidney and Urological Research Centers Program (P30 DK079337). M.V.A. is funded by a fellowship from region Nouvelle Aquitaine. S.B. is supported by the French Ministry of Research 'Plan maladies rares'.

Author contributions
All authors contributed to researching data for the article and writing, reviewing and editing the article before submission.

Competing interests
The authors declare no competing interests.

Publisher's note
Springer Nature remains neutral with regard to jurisdictional claims in published maps and institutional affiliations.

Appendix 2. Comprehensive molecular characterization of a heavy chain deposition disease case

Bender S, **Ayala MV**, Javaugue V, Bonaud A, Cogné M, Touchard G, Jaccard A, Bridoux F, Sirac C.

Haematologica. 2018 Nov;103(11):e557-e560. DOI: 10.3324/haematol.2018.196113

PMID: 30026336 PMCID: PMC6278990

Comprehensive molecular characterization of a heavy chain deposition disease case

We herein report the complete characterization of the monoclonal Ig fragments produced by the plasma cell clone in a 65-year-old patient with a typical heavy chain deposition disease (HCDD).[1–3] The patient was referred for nephrotic syndrome and the main biological parameters are summarized in *Online Supplementary Table S1*. Kidney biopsy at diagnosis revealed a typical HCDD with nodular glomerulosclerosis and thickening of tubular and vascular basement membranes by a refractile ribbon-like material. HCDD was confirmed by immunofluorescence studies, showing linear γ1 heavy chain (HC) deposits along basement membranes and the absence of κ and λ light chain (LC) stainings, and later by electron microscopy with ultrastructural feature of monoclonal immunoglobulin deposition disease (MIDD) (*Online Supplementary Figure S1*). The patient was treated with vincristine, doxorubicin and oral dexamethasone. Overall, the treatment was well tolerated and laboratory tests conducted three months after chemotherapy showed a complete hematological and renal response (*Online Supplementary Table S1*). Ten years later, the patient relapsed with stage 3 multiple myeloma and died due to pulmonary infection.

We have recently published the most important series of HCDD cases,[3] unraveling some pathophysiological mechanisms of the disease. However, the molecular events leading to HC deposits are still incompletely understood. Deletion of the CH1 domain is supposed to be a prerequisite for the secretion of HC in the absence of a LC since unassembled HC is normally trapped in the endoplasmic reticulum (ER) by a non-covalent association with BiP/GRP78 until its association with a LC.[4] However, whether HC truncation in HCDD results from similar defect in LC production or other independent abnormalities remains to be determined. Our present study highlights the molecular events leading to the production of a monoclonal pathogenic HC in this HCDD patient.

Western blot analysis carried out on serum collected at diagnosis confirmed the presence of a truncated γ1 HC corresponding to the deposited HC (Figure 1A). Despite not being detected by immunofixation in serum, a λ-type Bence-Jones protein was observed in urine. Therefore, we sought for a λ LC in bone marrow protein extracts and serum by western blot. Interestingly, it revealed the presence of both a full-length λ LC and a shortened λ LC of approximatively 17 kDa (Figure 1B). Immunofluorescence studies carried out on medullary bone biopsy showed that both γHC and λLC are produced by the same plasma cell clone (Figure 1C).

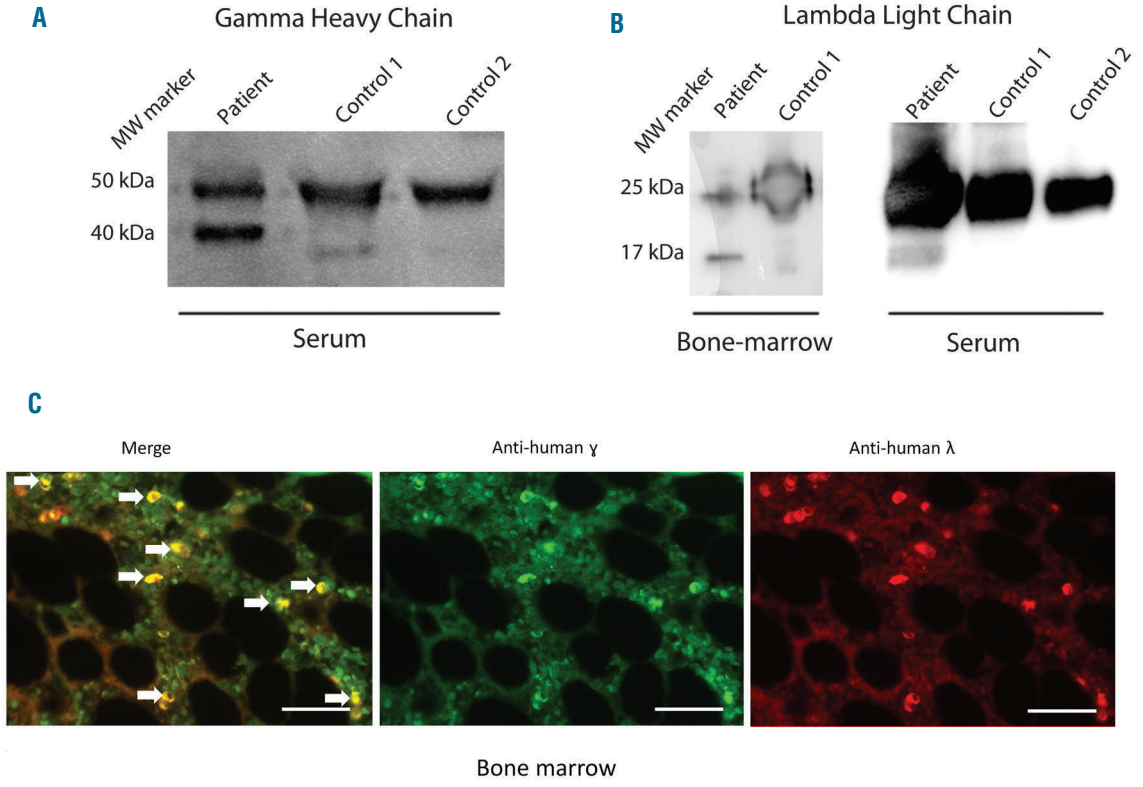

Figure 1. Detection of truncated γ HC and λ LC in bone marrow and serum. Western blot analysis of γ HC (A) and λ LC (B) in the serum and/or bone marrow (protein extracts) from the patient and controls. (A) The upper band (50 kDa) corresponds to the full-length γ HC, the lower band (40 kDa) corresponds to the truncated γ HC. (B) The upper band (25 kDa) corresponds to the full-length λ LC and the lower band (around 17 kDa) corresponds to the truncated LC. The truncated LC chain is detectable in both bone marrow and serum. (C) Immunofluorescence studies of a dewaxed paraffin embedded sample of medullary bone biopsy co-stained with anti-γ HC (middle) and anti-λ LC (right), the merge (left) indicating that PCs are double positive for γ and λ (white arrows). Original magnification x200, Bar = 100μM).

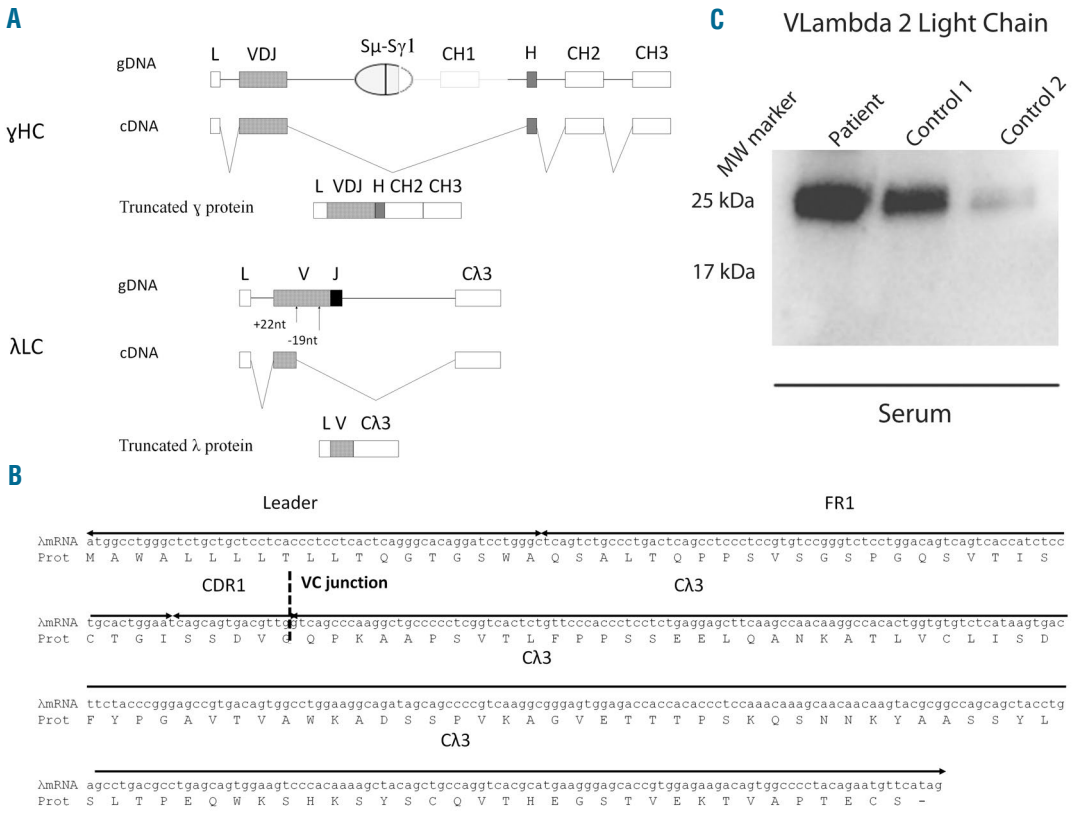

Figure 2. Determination of LC and HC mutations. (A) Schematic representation of the transcripts and proteins alterations observed on the γ HC and λ LC. (B) λ mRNA sequence and the deduced amino-acid sequence. (C) Western blot analysis of the circulating λ LC with an anti-Vλ2 antibody compared to the western blot carried out with an anti-λ antibody. Note the absence of the 17 kDa band, corresponding to the truncated λ LC detected with the anti-λ LC.

We determined the corresponding sequences from cDNAs derived from bone marrow extracts. We confirmed the presence of a monoclonal CH1-truncated HC sequence, composed of the rearranged VH3-30/DH2-15/JH4-derived germline genes (identity = 93.06 % for VH gene and 83.3 % for JH gene) directly spliced to the hinge/CH2/CH3 exons (*Online Supplementary Figure 2*). Further analysis of the monoclonal γ1 HC primary transcripts showed a large genomic deletion from the end of switch γ1 region to the middle of the CH1/hinge intron (Figure 2A). The PCR amplifications of λ LC cDNA confirmed the presence of a monoclonal truncated LC with a large deletion of the 3' part of the variable (V) domain, from the end of the CDR1 to the junction (J) region (Figure 2A). The remaining 5' part of the V domain, derived from the germline Vλ2-18 gene, was directly spliced onto the Cλ3 exon to form an in-frame truncated λ LC (Figure 2B and *Online Supplementary Figure S2*). We next analyzed the λ LC primary transcripts and found two abnormalities in the V domain: a 22 pb addition in FR2 and a 19 pb deletion in FR3. The 22 pb addition corresponded to a duplication of the CDR1/FR2 upstream region leading to a frameshift with the appearance of a stop codon at the beginning of the FR2 (*Online Supplementary Figure 2*). Frameshift in the Vλ exon may result from somatic hypermutations as it was previously shown for HC V domains.[5] When occurring in such HC V regions, a frameshift may lead to a complete decay of the transcript,[6] consequently resulting in free LC secretion (as seen in ~10% of plasma cell dyscrasias) since LCs are not retained in the ER in the absence of HC pairing. Alternatively, a frameshift may result in an alternative splicing leading to the production of a HC with a truncated V domain as observed in heavy chain diseases (HCD).[5] In the present case, an alternative splicing in the Vλ exon using the cryptic site TG/GTAGT in CDR1 led to the skipping of the premature stop codon and the production of truncated in-frame mRNA λ LC (*Online Supplementary Figure S2*). Since most of the Vλ domain is missing in the truncated LC, we performed a western blot using an anti-Vλ2 domain antibody[7] which proved positive for the full length polyclonal λ LC containing Vλ2 domains but failed to detect the shortened monoclonal V domain (Figure 2C).

Given our findings, we decided to study the capacity of this truncated LC to associate with a HC in an *in vitro* model. For this purpose, we stably transfected the murine hybridoma/myeloma cell line SP2/0 with the truncated λ LC and the patient's truncated HC or full-length HC obtained by the addition of the CH1 domain. A control full-length λ LC was also transfected with the full-length or the truncated HC. We confirmed that despite its abnormalities, the truncated λ LC can be secreted, as observed in the patient (Figure 3A). Then, to detect HC/LC association, we performed a hybrid ELISA using anti-γ HC antibodies for coating and anti-λ LC for revealing. Our results showed that the truncated LC do not associate with the full-length HC (Figure 3A). Finally, the intracellular/secreted ratio for the full-length HC in cell culture was nearly ten times higher compared to the

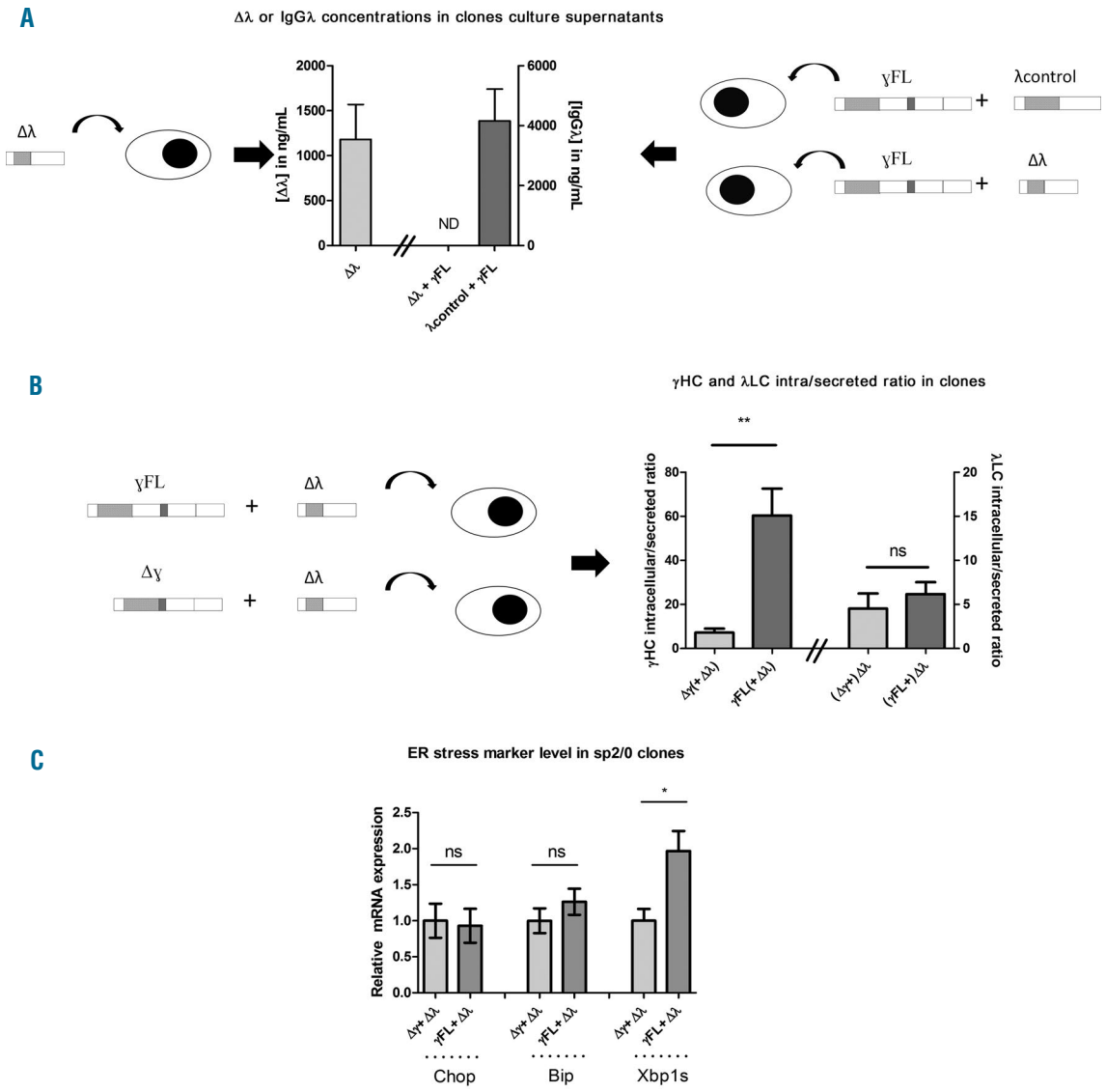

Figure 3. *In vitro* study of the truncated LC/HC mispairing and resulting higher ER stress in cells expressing a solitary complete γ HC in a SP2/0 cell line. model. (A, left) ELISA analysis of supernatants from SP2/0 cells transfected with the truncated λ LC (Δλ) or (right) transfected with the full-length HC (γFL) and the truncated λ LC (Δλ) or a control λ LC (λ control). Note the absence of association between the truncated λ LC and the normal reconstituted HC (ND=non detectable). (B) Determination of the intracellular/secreted ratio of SP2/0 clones expressing the full-length (γFL) or truncated HC (Δγ) co-transfected with the truncated λ LC. The high ratio indicates that products were retained intracellularly. Note that the intracellular/secreted ratio of the truncated λ LC was similar in both cases, demonstrating that the full-length HC retention is not due to a general secretory defect of the cells. (C) Quantitative expression of ER stress marker *Chop*, *Bip* and *Xbp1s* in a SP2/0 cell model containing a full-length HC (γFL) or a truncated HC (Δγ) associated with the truncated λ LC. Note the two-fold increased rate of *Xbp1s* in cells expressing the γ FL HC. Data are shown as mean ± SEM from 6 clones obtained per condition which express the highest levels of HC and/or LC. ** =*P*<0.01; *=*P*<0.05; ns: non-significant.

truncated HC (Figure 3B). These results confirmed that in absence of a pairing LC, a complete HC is retained intracellulary and that CH1 domain deletion facilitates HC secretion. This result prompted us to determine if the deletion of the HC CH1 domain could benefit plasma cell fitness. We analyzed the transcriptional expression of endoplasmic reticulum stress markers *Chop, Bip* and *Xbp1s* on SP2/0 clones expressing complete or truncated HC. We found that clones expressing a solitary full-length HC present a two-fold increased rate of *Xbp1s* (*P*=0.01) compared to clones expressing the truncated one (Figure 3C). We also observed a slight but non-significant increase of *Bip* (*P*=0.3) while *Chop* was unchanged. As previously mentioned, in the absence of LC, the HC is retained in the ER by BiP binding to CH1 domain,[4] a situation which was shown to lead to few CH1-truncated HC in a LC-deficient mouse model.[8] Consequently, we suggest that in the present case, the defect of the LC could have been the first event promoting the deletion of the CH1 domain of the HC in order to avoid HC intracellular retention and alleviate reticulum stress. Recently, several studies have shown that excessive ER stress induced apoptosis of PCs,[9] that inhibition of LC production by siRNA triggered apoptosis due to unpaired HC accumulation in ER and unfolded protein response[10] and that truncated LC selectively inhibited plasma cell differentiation and survival.[11] Consequently, we hypothesize that the CH1 deletion could act as a prosurvival event

since the intracellular retention of the full-length HC would likely have caused the loss of the PC clone due to ER stress. Accordingly, the very rare occurrence of true nonsecretory plasma cell disorders likely accounts for the toxicity of solitary HCs, the loss of LC or H/L pairing being lethal for the plasma cell except in case of HC truncation.

Truncated LC were not observed in other HCDD cases with LC characterization[3] but shortened LC transcripts resulting from internal deletions of the VJ exon and/or of splicing aberrations were also found in cases of Burkitt's lymphoma[12] or in non-secreting myeloma[13] and it cannot be excluded that point mutations without effects on the LC length could also impede H/L association. Our study gives an example of the relevance to monitor free LC in HCDD or other HC-related diseases since the same clone is producing both HC and LC. The intrinsic toxicity of isolated full-length HC in plasma cells also underpins the relevance of therapeutics aimed at inhibiting or altering LCs, for instance by siRNA[10] or antisense oligonucleotide (AON)-induced exon skipping.[11]

To conclude, we hypothesize that in this patient the onset of HCDD started with the alteration of the LC, followed by the deletion of the CH1 domain of the HC. This eventually relieved ER stress and thus improved the fitness and survival of the abnormal plasma cells. Further investigations must be conducted on other cases, in order to appreciate on a larger series how often H/L mispairing occurs in HCDD and can thus be considered as the initial alterations affecting these malignant B-cell clones.

Sébastien Bender,[1,2] Maria Victoria Ayala,[1] Vincent Javaugue,[1,2,3] Amélie Bonaud,[4] Michel Cogné,[1,2] Guy Touchard,[3] Arnaud Jaccard,[1,2,5] Frank Bridoux[1,2,3] and Christophe Sirac[1,2]

[1]Centre National de la recherche Scientifique UMR CNRS 7276/INSERM U1262, Université de Limoges; [2]Centre National de l'Amylose AL et Autres Maladies par Dépôt d'Immunoglobulines Monoclonales, Centre Hospitalier Universitaire de Limoges; [3]Service de Néphrologie et Transplantation, Centre Hospitalier Universitaire de Poitiers; [4]Institut national de la santé et de la recherche médicale INSERM UMR996 - Cytokines, Chimiokines, Immunopathologie, Université Paris-Sud et Université Paris-Saclay and [5]Service d'Hématologie Clinique, Centre Hospitalier Universitaire de Limoges, France

MVA, VJ and AB contributed equally to this work.

Correspondence: christophe.sirac@unilim.fr
doi:10.3324/haematol.2018.196113

Information on authorship, contributions, and financial & other disclosures was provided by the authors and is available with the online version of this article at www.haematologica.org.

References

1. Aucouturier P, Khamlichi AA, Touchard G, et al. Heavy-chain deposition disease. N Engl J Med. 1993;329(19):1389-1393.
2. Bridoux F, Leung N, Hutchison CA, et al. Diagnosis of monoclonal gammopathy of renal significance. Kidney Int. 2015;87(4):698-711.
3. Bridoux F, Javaugue V, Bender S, et al. Unravelling the immunopathological mechanisms of heavy chain deposition disease with implications for clinical management. Kidney Int. 2017;91(2):423-434.
4. Feige MJ, Hendershot LM, Buchner J. How antibodies fold. Trends Biochem Sci. 2010;35(4):189-198.
5. Goossens T, Klein U, Küppers R. Frequent occurrence of deletions and duplications during somatic hypermutation: implications for oncogene translocations and heavy chain disease. Proc Natl Acad Sci USA. 1998;95(5):2463-2468.
6. Tinguely A, Chemin G, Péron S, et al. Cross talk between immunoglobulin heavy-chain transcription and RNA surveillance during B cell development. Mol Cell Biol. 2012;32(1):107-117.
7. Davern S, Tang LX, Williams TK, et al. Immunodiagnostic capabilities of anti-free immunoglobulin light chain monoclonal antibodies. Am J Clin Pathol. 2008;130(5):702-711.
8. Zou X, Osborn MJ, Bolland DJ, et al. Heavy chain-only antibodies are spontaneously produced in light chain-deficient mice. J Exp Med. 2007;204(13):3271-3283.
9. Bianchi G, Oliva L, Cascio P, et al. The proteasome load versus capacity balance determines apoptotic sensitivity of multiple myeloma cells to proteasome inhibition. Blood. 2009;113(13):3040-3049.
10. Zhou P, Ma X, Iyer L, Chaulagain C, Comenzo RL. One siRNA pool targeting the λ constant region stops λ light-chain production and causes terminal endoplasmic reticulum stress. Blood. 2014; 123(22):3440-3451.
11. Srour N, Chemin G, Tinguely A, et al. A plasma cell differentiation quality control ablates B cell clones with biallelic Ig rearrangements and truncated Ig production. J Exp Med. 2016;213(1):109-122.
12. Cogné M, Mounir S, Aucouturier P, Preud'homme JL, Nau F, Guglielmi P. Immunoglobulin light chain transcripts with altered V regions in Burkitt's lymphoma cell lines producing short mu chains. Eur J Immunol. 1990;20(9):1905-1910.
13. Cogné M, Guglielmi P. Exon skipping without splice site mutation accounting for abnormal immunoglobulin chains in nonsecretory human myeloma. Eur J Immunol. 1993;23(6):1289-1293.

Appendix 3. Other papers

- Physiological and druggable skipping of immunoglobulin variable exons in plasma cells. Ashi MO, Srour N, Lambert JM, Marchalot A, Martin O, Le Noir S, Pinaud E, **Ayala MV**, Sirac C, Saulière J, Moreaux J, Cogné M, Delpy L. *Cell Mol Immunol*. 2019 Oct;16(10):810-819.

Abstract

The error-prone V(D)J recombination process generates considerable amounts of nonproductive immunoglobulin (Ig) pre-mRNAs. We recently demonstrated that aberrant Ig chains lacking variable (V) domains can be produced after nonsense-associated altered splicing (NAS) events. Remarkably, the expression of these truncated Ig polypeptides heightens endoplasmic reticulum stress and shortens plasma cell (PC) lifespan. Many questions remain regarding the molecular mechanisms underlying this new truncated Ig exclusion (TIE-) checkpoint and its restriction to the ultimate stage of B-cell differentiation. To address these issues, we evaluated the extent of NAS of Ig pre-mRNAs using an Ig heavy chain (IgH) knock-in model that allows for uncoupling of V exon skipping from TIE-induced apoptosis. We found high levels of V exon skipping in PCs compared with B cells, and this skipping was correlated with a biallelic boost in IgH transcription during PC differentiation. Chromatin analysis further revealed that the skipped V exon turned into a pseudo-intron. Finally, we showed that hypertranscription of Ig genes facilitated V exon skipping upon passive administration of splice-switching antisense oligonucleotides (ASOs). Thus, V exon skipping is coupled to transcription and increases as PC differentiation proceeds, likely explaining the late occurrence of the TIE-checkpoint and opening new avenues for ASO-mediated strategies in PC disorders.

- Immunoglobulin variable domain high-throughput sequencing reveals specific novel mutational patterns in POEMS syndrome. Bender S, Javaugue V, Saintamand A, **Ayala MV**, Alizadeh M, Filloux M, Pascal V, Gachard NN, Lavergne D, Auroy F, Cogné M, Bridoux F, Sirac C, Jaccard A. *Blood.*2020 May 14;135(20):1750-1758.

Abstract

Polyneuropathy, organomegaly, endocrinopathy, monoclonal gammopathy, and skin changes (POEMS) syndrome is a rare multisystem disease resulting from an underlying plasma cell (PC) dyscrasia. The pathophysiology of the disease remains unclear, but the role of the monoclonal immunoglobulin (Ig) light chain (LC) is strongly suspected because of the highly restrictive usage of 2 λ variable (V) domains (IGLV1-40 and IGLV1-44) and the general improvement of clinical manifestations after PC clone-targeted treatment. However, the diagnostic value of Ig LC sequencing, especially in the case of incomplete forms of the disease, remains to be determined. Using a sensitive high-throughput Ig repertoire sequencing on RNA (rapid amplification of cDNA ends-based repertoire sequencing [RACE-RepSeq]), we detected a λ LC monoclonal expansion in the bone marrow (BM) of 83% of patients with POEMS syndrome, including some in whom BM tests routinely performed to diagnose plasma cell dyscrasia failed to detect λ+ monoclonal PCs. Twenty-four (83%) of the 29 LC clonal sequences found were derived from the *IGLV1-40* and *IGLV1-44* germline genes, as well as 2 from the closely related *IGLV1-36* gene, and all were associated with an *IGLJ3*02* junction (J) gene, confirming the high restriction of VJ region usage in POEMS syndrome. RACE-RepSeq VJ full-length sequencing additionally revealed original mutational patterns, the strong specificity of which might crucially help establish or eliminate the diagnosis of POEMS syndrome in uncertain cases. Thus, RACE-RepSeq appears as a sensitive, rapid, and specific tool to detect low-abundance PC clones in BM and assign them to POEMS syndrome, with all the consequences for therapeutic options.

BIBLIOGRAPHY

Aguirre, M.A., Boietti, B.R., Nucifora, E., Sorroche, P.B., González Bernaldo de Quirós, F., Giunta, D.H., Posadas-Martínez, M.L., 2016. Incidence rate of amyloidosis in patients from a medical care program in Buenos Aires, Argentina: a prospective cohort. Amyloid 23, 184–187. https://doi.org/10.1080/13506129.2016.1207626

Amin, R., Mourcin, F., Uhel, F., Pangault, C., Ruminy, P., Dupré, L., Guirriec, M., Marchand, T., Fest, T., Lamy, T., Tarte, K., 2015. DC-SIGN-expressing macrophages trigger activation of mannosylated IgM B-cell receptor in follicular lymphoma. Blood 126, 1911–1920. https://doi.org/10.1182/blood-2015-04-640912

Arnaout, R., Lee, W., Cahill, P., Honan, T., Sparrow, T., Weiand, M., Nusbaum, C., Rajewsky, K., Koralov, S.B., 2011. High-Resolution Description of Antibody Heavy-Chain Repertoires in Humans. PLoS ONE 6, e22365. https://doi.org/10.1371/journal.pone.0022365

Bak, S.T., Sakellariou, D., Pena-Diaz, J., 2014. The dual nature of mismatch repair as antimutator and mutator: for better or for worse. Front. Genet. 5. https://doi.org/10.3389/fgene.2014.00287

Basso, K., Dalla-Favera, R., 2015. Germinal centres and B cell lymphomagenesis. Nat. Rev. Immunol. 15, 172–184. https://doi.org/10.1038/nri3814

Becker, G.J., Hewitson, T.D., 2013. Animal models of chronic kidney disease: useful but not perfect. Nephrol. Dial. Transplant. 28, 2432–2438. https://doi.org/10.1093/ndt/gft071

Belnoue, E., Pihlgren, M., McGaha, T.L., Tougne, C., Rochat, A.-F., Bossen, C., Schneider, P., Huard, B., Lambert, P.-H., Siegrist, C.-A., 2008. APRIL is critical for plasmablast survival in the bone marrow and poorly expressed by early-life bone marrow stromal cells. Blood 111, 2755–2764. https://doi.org/10.1182/blood-2007-09-110858

Bender, S., Ayala, M.V., Javaugue, V., Bonaud, A., Cogné, M., Touchard, G., Jaccard, A., Bridoux, F., Sirac, C., 2018. Comprehensive molecular characterization of a heavy chain deposition disease case. Haematologica 103, e557–e560. https://doi.org/10.3324/haematol.2018.196113

Bergman, L.W., Kuehl, W.M., 1979. Formation of intermolecular disulfide bonds on nascent immunoglobulin polypeptides. J. Biol. Chem. 254, 5690–5694.

Betz, B., Conway, B.R., 2016. An Update on the Use of Animal Models in Diabetic Nephropathy Research. Curr. Diab. Rep. 16, 18. https://doi.org/10.1007/s11892-015-0706-2

Bianchi, G., Munshi, N.C., 2015. Pathogenesis beyond the cancer clone(s) in multiple myeloma. Blood 125, 3049–3058. https://doi.org/10.1182/blood-2014-11-568881

Bird, S.A., Boyd, K., 2019. Multiple myeloma: an overview of management. Palliat. Care Soc. Pract. 13, 117822421986823. https://doi.org/10.1177/1178224219868235

Bjerke, K., Brandtzaeg, P., 1990. Terminally differentiated human intestinal B cells. J chain expression of IgA and IgG subclass-producing immunocytes in the distal ileum compared with mesenteric and peripheral lymph nodes. Clin. Exp. Immunol. 82, 411–415.

Blancas-Mejía, L.M., Ramirez-Alvarado, M., 2013. Systemic Amyloidoses. Annu. Rev. Biochem. 82, 745–774. https://doi.org/10.1146/annurev-biochem-072611-130030

Blancas-Mejía, Luis.M., Tischer, A., Thompson, J.R., Tai, J., Wang, L., Auton, M., Ramirez-Alvarado, M., 2014. Kinetic Control in Protein Folding for Light Chain Amyloidosis and the Differential Effects of Somatic Mutations. J. Mol. Biol. 426, 347–361. https://doi.org/10.1016/j.jmb.2013.10.016

Bodin, K., Ellmerich, S., Kahan, M.C., Tennent, G.A., Loesch, A., Gilbertson, J.A., Hutchinson, W.L., Mangione, P.P., Gallimore, J.R., Millar, D.J., Minogue, S., Dhillon, A.P., Taylor, G.W., Bradwell, A.R., Petrie, A., Gillmore, J.D., Bellotti, V., Botto, M., Hawkins, P.N., Pepys, M.B., 2010. Antibodies to human serum amyloid P component eliminate visceral amyloid deposits. Nature 468, 93–97. https://doi.org/10.1038/nature09494

Bonaud, A., Bender, S., Touchard, G., Lacombe, C., Srour, N., Delpy, L., Oblet, C., Druilhe, A., Quellard, N., Javaugue, V., Cogne, M., Bridoux, F., Sirac, C., 2015. A mouse model recapitulating human monoclonal heavy chain deposition disease evidences the relevance of proteasome inhibitor therapy. Blood 126, 757–765. https://doi.org/10.1182/blood-2015-03-630277

Bordon, Y., 2016. The many sides of Paul Ehrlich. Nat. Immunol. 17, S6–S6. https://doi.org/10.1038/ni.3601

Brekke, O.H., Sandlie, I., 2003. Therapeutic antibodies for human diseases at the dawn of the twenty-first century. Nat. Rev. Drug Discov. 2, 52–62. https://doi.org/10.1038/nrd984

Bridoux, F., Javaugue, V., Bender, S., Leroy, F., Aucouturier, P., Debiais-Delpech, C., Goujon, J.-M., Quellard, N., Bonaud, A., Clavel, M., Trouillas, P., Di Meo, F., Gombert, J.-M., Fermand, J.-P., Jaccard, A., Cogné, M., Touchard, G., Sirac, C., 2017. Unravelling the immunopathological mechanisms of heavy chain deposition disease with implications for clinical management. Kidney Int. 91, 423–434. https://doi.org/10.1016/j.kint.2016.09.004

Bridoux, F., Leung, N., Hutchison, C.A., Touchard, G., Sethi, S., Fermand, J.-P., Picken, M.M., Herrera, G.A., Kastritis, E., Merlini, G., Roussel, M., Fervenza, F.C., Dispenzieri, A., Kyle, R.A., Nasr, S.H., on behalf of the International Kidney and Monoclonal Gammopathy Research Group, 2015. Diagnosis of monoclonal gammopathy of renal significance. Kidney Int. 87, 698–711. https://doi.org/10.1038/ki.2014.408

Bruhns, P., Jönsson, F., 2015. Mouse and human FcR effector functions. Immunol. Rev. 268, 25–51. https://doi.org/10.1111/imr.12350

Bryce, A.H., Ketterling, R.P., Gertz, M.A., Lacy, M., Knudson, R.A., Zeldenrust, S., Kumar, S., Hayman, S., Buadi, F., Kyle, R.A., Greipp, P.R., Lust, J.A., Russell, S., Rajkumar, S.V., Fonseca, R., Dispenzieri, A., 2009. Translocation t(11;14) and survival of patients with light chain (AL) amyloidosis. Haematologica 94, 380–386. https://doi.org/10.3324/haematol.13369

Burnet, F.M., 1957. A Modification of Jerne's Theory of Antibody Production using the Concept of Clonal Selection. Aust. J. Sci. 20, 67–9.

Burrows, P.D., Stephan, R.P., Wang, Y.-H., Lassoued, K., Zhang, Z., Cooper, M.D., 2002. The transient expression of pre-B cell receptors governs B cell development. Semin. Immunol. 14, 343–349. https://doi.org/10.1016/S1044-5323(02)00067-2

Buxbaum, J.N., 2009. Animal models of human amyloidoses: are transgenic mice worth the time and trouble? FEBS Lett. 583, 2663–2673. https://doi.org/10.1016/j.febslet.2009.07.031

Cambier, J.C., Gauld, S.B., Merrell, K.T., Vilen, B.J., 2007. B-cell anergy: from transgenic models to naturally occurring anergic B cells? Nat. Rev. Immunol. 7, 633–643. https://doi.org/10.1038/nri2133

Casola, S., Otipoby, K.L., Alimzhanov, M., Humme, S., Uyttersprot, N., Kutok, J.L., Carroll, M.C., Rajewsky, K., 2004. B cell receptor signal strength determines B cell fate. Nat. Immunol. 5, 317–327. https://doi.org/10.1038/ni1036

Castillo, J.J., 2016. Plasma Cell Disorders. Prim. Care Clin. Off. Pract. 43, 677–691. https://doi.org/10.1016/j.pop.2016.07.002

Castro, C.D., Flajnik, M.F., 2014. Putting J Chain Back on the Map: How Might Its Expression Define Plasma Cell Development? J. Immunol. 193, 3248–3255. https://doi.org/10.4049/jimmunol.1400531

Cerutti, A., Cols, M., Puga, I., 2013. Marginal zone B cells: virtues of innate-like antibody-producing lymphocytes. Nat. Rev. Immunol. 13, 118–132. https://doi.org/10.1038/nri3383

Chemin, G., Tinguely, A., Sirac, C., Lechouane, F., Duchez, S., Cogné, M., Delpy, L., 2010. Multiple RNA surveillance mechanisms cooperate to reduce the amount of nonfunctional Ig kappa transcripts. J. Immunol. Baltim. Md 1950 184, 5009–5017. https://doi.org/10.4049/jimmunol.0902949

Chi, X., Li, Y., Qiu, X., 2020. V(D)J Recombination, Somatic Hypermutation and Class Switch Recombination of Immunoglobulins: Mechanism and Regulation. Immunology imm.13176. https://doi.org/10.1111/imm.13176

Cobaleda, C., Schebesta, A., Delogu, A., Busslinger, M., 2007a. Pax5: the guardian of B cell identity and function. Nat. Immunol. 8, 463–470. https://doi.org/10.1038/ni1454

Cobaleda, C., Schebesta, A., Delogu, A., Busslinger, M., 2007b. Pax5: the guardian of B cell identity and function. Nat. Immunol. 8, 463–470. https://doi.org/10.1038/ni1454

Cogné, M., Preud'homme, J.L., Bauwens, M., Touchard, G., Aucouturier, P., 1991. Structure of a monoclonal kappa chain of the V kappa IV subgroup in the kidney and plasma cells in light chain deposition disease. J. Clin. Invest. 87, 2186–2190. https://doi.org/10.1172/JCI115252

Collins, A.M., Watson, C.T., 2018. Immunoglobulin Light Chain Gene Rearrangements, Receptor Editing and the Development of a Self-Tolerant Antibody Repertoire. Front. Immunol. 9, 2249. https://doi.org/10.3389/fimmu.2018.02249

Comenzo, R.L., Zhang, Y., Martinez, C., Osman, K., Herrera, G.A., 2001. The tropism of organ involvement in primary systemic amyloidosis: contributions of Ig V(L) germ line gene use and clonal plasma cell burden. Blood 98, 714–720.

Corti, D., Lanzavecchia, A., 2014. Efficient Methods To Isolate Human Monoclonal Antibodies from Memory B Cells and Plasma Cells. Microbiol. Spectr. 2. https://doi.org/10.1128/microbiolspec.AID-0018-2014

Crotty, S., Johnston, R.J., Schoenberger, S.P., 2010. Effectors and memories: Bcl-6 and Blimp-1 in T and B lymphocyte differentiation. Nat. Immunol. 11, 114–120. https://doi.org/10.1038/ni.1837

Davies, F.E., Raje, N., Hideshima, T., Lentzsch, S., Young, G., Tai, Y.-T., Lin, B., Podar, K., Gupta, D., Chauhan, D., Treon, S.P., Richardson, P.G., Schlossman, R.L., Morgan, G.J., Muller, G.W., Stirling, D.I., Anderson, K.C., 2001. Thalidomide and immunomodulatory derivatives augment natural killer cell cytotoxicity in multiple myeloma. Blood 98, 210–216. https://doi.org/10.1182/blood.V98.1.210

De Silva, N.S., Klein, U., 2015. Dynamics of B cells in germinal centres. Nat. Rev. Immunol. 15, 137–148. https://doi.org/10.1038/nri3804

Decourt, C., Cogne, M., Rocca, A., 1996. Structural peculiarities of a truncated VkappaIII immunoglobulin light chain in myeloma with light chain deposition disease. Clin. Exp. Immunol. 106, 351–356. https://doi.org/10.1046/j.1365-2249.1996.d01-841.x

Decourt, C., Rocca, A., Bridoux, F., Vrtovsnik, F., Preud'homme, J.L., Cogné, M., Touchard, G., 1999. Mutational analysis in murine models for myeloma-associated Fanconi's syndrome or cast myeloma nephropathy. Blood 94, 3559–3566.

Denoroy, L., Déret, S., Aucouturier, P., 1994. Overrepresentation of the VκIV subgroup in light chain deposition disease. Immunol. Lett. 42, 63–66. https://doi.org/10.1016/0165-2478(94)90036-1

Desport, E., Bridoux, F., Sirac, C., Delbes, S., Bender, S., Fernandez, B., Quellard, N., Lacombe, C., Goujon, J.-M., Lavergne, D., Abraham, J., Touchard, G., Fermand, J.-P., Jaccard, A., Centre national de référence pour l'amylose AL et les autres maladies par dépôts d'immunoglobulines monoclonales, 2012. AL Amyloidosis. Orphanet J. Rare Dis. 7, 54. https://doi.org/10.1186/1750-1172-7-54

Diomede, L., Rognoni, P., Lavatelli, F., Romeo, M., del Favero, E., Cantù, L., Ghibaudi, E., di Fonzo, A., Corbelli, A., Fiordaliso, F., Palladini, G., Valentini, V., Perfetti, V., Salmona, M., Merlini, G., 2014. A Caenorhabditis elegans-based assay recognizes immunoglobulin light chains causing heart amyloidosis. Blood 123, 3543–3552. https://doi.org/10.1182/blood-2013-10-525634

Dispenzieri, A., Katzmann, J.A., Kyle, R.A., Larson, D.R., Melton, L.J., Colby, C.L., Therneau, T.M., Clark, R., Kumar, S.K., Bradwell, A., Fonseca, R., Jelinek, D., Rajkumar, S.V., 2010. Prevalence and risk of progression of light-chain monoclonal gammopathy of undetermined significance: a retrospective population-based cohort study. The Lancet 375, 1721–1728. https://doi.org/10.1016/S0140-6736(10)60482-5

Dispenzieri, A., Stewart, A.K., Chanan-Khan, A., Rajkumar, S.V., Kyle, R.A., Fonseca, R., Kapoor, P., Bergsagel, P.L., McCurdy, A., Gertz, M.A., Lacy, M.Q., Lust, J.A., Russell, S.J., Zeldenrust, S.R., Reeder, C., Roy, V., Buadi, F., Dingli, D., Hayman, S.R., Leung, N., Lin, Y., Mikhael, J., Kumar, S.K., 2013. Smoldering multiple myeloma requiring treatment: time for a new definition? Blood 122, 4172–4181. https://doi.org/10.1182/blood-2013-08-520890

Dranoff, G., 2004. Cytokines in cancer pathogenesis and cancer therapy. Nat. Rev. Cancer 4, 11–22. https://doi.org/10.1038/nrc1252

Duhamel, S., Mohty, D., Magne, J., Lavergne, D., Bordessoule, D., Aboyans, V., Jaccard, A., 2017. Incidence and Prevalence of Light Chain Amyloidosis: A Population-Based Study. Blood 130, 5577–5577. https://doi.org/10.1182/blood.V130.Suppl_1.5577.5577

Edwards, C.V., Gould, J., Langer, A.L., Mapara, M., Radhakrishnan, J., Maurer, M.S., Raza, S., Mears, J.G., Wall, J., Solomon, A., Lentzsch, S., 2017. Interim analysis of the phase 1a/b study of chimeric fibril-reactive monoclonal antibody 11-1F4 in patients with AL amyloidosis. Amyloid 24, 58–59. https://doi.org/10.1080/13506129.2017.1292900

Eisenberg, D., Jucker, M., 2012. The Amyloid State of Proteins in Human Diseases. Cell 148, 1188–1203. https://doi.org/10.1016/j.cell.2012.02.022

Eyer, K., Doineau, R.C.L., Castrillon, C.E., Briseño-Roa, L., Menrath, V., Mottet, G., England, P., Godina, A., Brient-Litzler, E., Nizak, C., Jensen, A., Griffiths, A.D., Bibette, J., Bruhns, P., Baudry, J., 2017a. Single-cell deep phenotyping of IgG-secreting cells for high-resolution immune monitoring. Nat. Biotechnol. 35, 977–982. https://doi.org/10.1038/nbt.3964

Eyer, K., Doineau, R.C.L., Castrillon, C.E., Briseño-Roa, L., Menrath, V., Mottet, G., England, P., Godina, A., Brient-Litzler, E., Nizak, C., Jensen, A., Griffiths, A.D., Bibette, J., Bruhns, P., Baudry, J., 2017b. Single-cell deep phenotyping of IgG-secreting cells for high-resolution immune monitoring. Nat. Biotechnol. 35, 977–982. https://doi.org/10.1038/nbt.3964

Fazilleau, N., Mark, L., McHeyzer-Williams, L.J., McHeyzer-Williams, M.G., 2009a. Follicular Helper T Cells: Lineage and Location. Immunity 30, 324–335. https://doi.org/10.1016/j.immuni.2009.03.003

Fazilleau, N., McHeyzer-Williams, L.J., Rosen, H., McHeyzer-Williams, M.G., 2009b. The function of follicular helper T cells is regulated by the strength of T cell antigen receptor binding. Nat. Immunol. 10, 375–384. https://doi.org/10.1038/ni.1704

Feige, M.J., Hendershot, L.M., Buchner, J., 2010. How antibodies fold. Trends Biochem. Sci. 35, 189–198. https://doi.org/10.1016/j.tibs.2009.11.005

Fermand, J.-P., Bridoux, F., Dispenzieri, A., Jaccard, A., Kyle, R.A., Leung, N., Merlini, G., 2018. Monoclonal gammopathy of clinical significance: a novel concept with therapeutic implications. Blood 132, 1478–1485. https://doi.org/10.1182/blood-2018-04-839480

Fermand, J.-P., Bridoux, F., Kyle, R.A., Kastritis, E., Weiss, B.M., Cook, M.A., Drayson, M.T., Dispenzieri, A., Leung, N., 2013. How I treat monoclonal gammopathy of renal significance (MGRS). Blood 122, 3583–3590. https://doi.org/10.1182/blood-2013-05-495929

Ferreira, N., Cardoso, I., Domingues, M.R., Vitorino, R., Bastos, M., Bai, G., Saraiva, M.J., Almeida, M.R., 2009. Binding of epigallocatechin-3-gallate to transthyretin modulates its amyloidogenicity. FEBS Lett. 583, 3569–3576. https://doi.org/10.1016/j.febslet.2009.10.062

Fiancette, R., Amin, R., Truffinet, V., Vincent-Fabert, C., Cogné, N., Cogné, M., Denizot, Y., 2010. A myeloma translocation-like model associating CCND1 with the immunoglobulin heavy-chain locus 3' enhancers does not promote by itself B-cell malignancies. Leuk. Res. 34, 1043–1051. https://doi.org/10.1016/j.leukres.2009.11.017

Fonseca, R., Debes-Marun, C.S., Picken, E.B., Dewald, G.W., Bryant, S.C., Winkler, J.M., Blood, E., Oken, M.M., Santana-Dávila, R., González-Paz, N., Kyle, R.A., Gertz, M.A., Dispenzieri, A., Lacy, M.Q., Greipp, P.R., 2003. The recurrent IgH translocations are highly associated with nonhyperdiploid variant multiple myeloma. Blood 102, 2562–2567. https://doi.org/10.1182/blood-2003-02-0493

Foster, J.S., Williams, A.D., Macy, S., Richey, T., Stuckey, A., Wooliver, D.C., Koul-Tiwari, R., Martin, E.B., Kennel, S.J., Wall, J.S., 2017. A Peptide-Fc Opsonin with Pan-Amyloid Reactivity. Front. Immunol. 8, 1082. https://doi.org/10.3389/fimmu.2017.01082

Gass, J.N., Gunn, K.E., Sriburi, R., Brewer, J.W., 2004. Stressed-out B cells? Plasma-cell differentiation and the unfolded protein response. Trends Immunol. 25, 17–24. https://doi.org/10.1016/j.it.2003.11.004

Gokden, N., Barlogie, B., Liapis, H., 2008. Morphologic Heterogeneity of Renal Light-Chain Deposition Disease. Ultrastruct. Pathol. 32, 17–24. https://doi.org/10.1080/01913120701854002

Hayes, J.M., Cosgrave, E.F.J., Struwe, W.B., Wormald, M., Davey, G.P., Jefferis, R., Rudd, P.M., 2014. Glycosylation and Fc Receptors, in: Daeron, M., Nimmerjahn, F. (Eds.), Fc Receptors. Springer International Publishing, Cham, pp. 165–199. https://doi.org/10.1007/978-3-319-07911-0_8

Helmreich, E., Kern, M., Eisen, H.N., 1961. The secretion of antibody by isolated lymph node cells. J. Biol. Chem. 236, 464–473.

Hora, M., Carballo-Pacheco, M., Weber, B., Morris, V.K., Wittkopf, A., Buchner, J., Strodel, B., Reif, B., 2017. Epigallocatechin-3-gallate preferentially induces aggregation of amyloidogenic immunoglobulin light chains. Sci. Rep. 7, 41515. https://doi.org/10.1038/srep41515

Hwang*, J.K., Alt*, F.W., Yeap, L.-S., 2015. Related Mechanisms of Antibody Somatic Hypermutation and Class Switch Recombination. Microbiol. Spectr. 3. https://doi.org/10.1128/microbiolspec.MDNA3-0037-2014

Iannaccone, P.M., Jacob, H.J., 2009. Rats! Dis. Model. Mech. 2, 206–210. https://doi.org/10.1242/dmm.002733

Ise, W., Kurosaki, T., 2019. Plasma cell differentiation during the germinal center reaction. Immunol. Rev. 288, 64–74. https://doi.org/10.1111/imr.12751

Jaccard, A., Desport, E., Mohty, D., Bridoux, F., 2015. Amylose AL. Rev. Médecine Interne 36, 89–97. https://doi.org/10.1016/j.revmed.2014.08.003

Jaccard, A., Moreau, P., Leblond, V., Leleu, X., Benboubker, L., Hermine, O., Recher, C., Asli, B., Lioure, B., Royer, B., Jardin, F., Bridoux, F., Grosbois, B., Jaubert, J., Piette, J.-C., Ronco, P., Quet, F., Cogne, M., Fermand, J.-P., 2007. High-dose melphalan versus melphalan plus dexamethasone for AL amyloidosis. N. Engl. J. Med. 357, 1083–1093. https://doi.org/10.1056/NEJMoa070484

Janssens, S., Pulendran, B., Lambrecht, B.N., 2014. Emerging functions of the unfolded protein response in immunity. Nat. Immunol. 15, 910–919. https://doi.org/10.1038/ni.2991

Jelinek, T., Kufova, Z., Hajek, R., 2016. Immunomodulatory drugs in AL amyloidosis. Crit. Rev. Oncol. Hematol. 99, 249–260. https://doi.org/10.1016/j.critrevonc.2016.01.004

Joly, F., Cohen, C., Javaugue, V., Bender, S., Belmouaz, M., Arnulf, B., Knebelmann, B., Nouvier, M., Audard, V., Provot, F., Gnemmi, V., Nochy, D., Goujon, J.M., Jaccard, A., Touchard, G., Fermand, J.P., Sirac, C., Bridoux, F., 2019. Randall-type monoclonal immunoglobulin deposition disease: novel insights from a nationwide cohort study. Blood 133, 576–587. https://doi.org/10.1182/blood-2018-09-872028

Jordan, T.L., Maar, K., Redhage, K.R., Misra, P., Blancas-Mejia, L.M., Dick, C.J., Wall, J.S., Williams, A., Dietz, A.B., van Wijnen, A.J., Lin, Y., Ramirez-Alvarado, M., 2020. Light chain amyloidosis induced inflammatory changes in cardiomyocytes and adipose-derived mesenchymal stromal cells. Leukemia 34, 1383–1393. https://doi.org/10.1038/s41375-019-0640-4

Jung, D., Giallourakis, C., Mostoslavsky, R., Alt, F.W., 2006. MECHANISM AND CONTROL OF V(D)J RECOMBINATION AT THE IMMUNOGLOBULIN HEAVY CHAIN LOCUS. Annu. Rev. Immunol. 24, 541–570. https://doi.org/10.1146/annurev.immunol.23.021704.115830

Kang, C.-J., Sheridan, C., Koshland, M.E., 1998. A Stage-Specific Enhancer of Immunoglobulin J Chain Gene Is Induced by Interleukin-2 in a Presecretor B Cell Stage. Immunity 8, 285–295. https://doi.org/10.1016/S1074-7613(00)80534-8

Kaplan, B., Livneh, A., Gallo, G., 2007. Charge differences between in vivo deposits in immunoglobulin light chain amyloidosis and non-amyloid light chain deposition disease. Br. J. Haematol. 136, 723–728. https://doi.org/10.1111/j.1365-2141.2006.06488.x

Kapoor, P., Ansell, S.M., Braggio, E., 2016. Waldenstrom Macroglobulinemia: Genomic Aberrations and Treatment, in: Roccaro, A.M., Ghobrial, I.M. (Eds.), Plasma Cell Dyscrasias, Cancer Treatment and Research. Springer International Publishing, Cham, pp. 321–361. https://doi.org/10.1007/978-3-319-40320-5_16

Kaufman, G.P., Schrier, S.L., Lafayette, R.A., Arai, S., Witteles, R.M., Liedtke, M., 2017. Daratumumab yields rapid and deep hematologic responses in patients with heavily pretreated AL amyloidosis. Blood 130, 900–902. https://doi.org/10.1182/blood-2017-01-763599

Kaufmann, S.H.E., 2017. Remembering Emil von Behring: from Tetanus Treatment to Antibody Cooperation with Phagocytes. mBio 8, e00117-17, /mbio/8/1/e00117-17.atom. https://doi.org/10.1128/mBio.00117-17

Keeling, J., Herrera, G.A., 2005. Matrix metalloproteinases and mesangial remodeling in light chain-related glomerular damage. Kidney Int. 68, 1590–1603. https://doi.org/10.1111/j.1523-1755.2005.00571.x

Khamlichi, A.A., Rocca, A., Touchard, G., Aucouturier, P., Preud'homme, J.L., Cogné, M., 1995. Role of light chain variable region in myeloma with light chain deposition disease: evidence from an experimental model. Blood 86, 3655–3659.

Kim, M.-S., Lapkouski, M., Yang, W., Gellert, M., 2015. Crystal structure of the V(D)J recombinase RAG1–RAG2. Nature 518, 507–511. https://doi.org/10.1038/nature14174

Kinoshita, K., Honjo, T., 2001. Linking class-switch recombination with somatic hypermutation. Nat. Rev. Mol. Cell Biol. 2, 493–503. https://doi.org/10.1038/35080033

Kiyoshi, M., Tsumoto, K., Ishii-Watabe, A., Caaveiro, J.M.M., 2017. Glycosylation of IgG-Fc: a molecular perspective. Int. Immunol. 29, 311–317. https://doi.org/10.1093/intimm/dxx038

Klein, U., Casola, S., Cattoretti, G., Shen, Q., Lia, M., Mo, T., Ludwig, T., Rajewsky, K., Dalla-Favera, R., 2006. Transcription factor IRF4 controls plasma cell differentiation and class-switch recombination. Nat. Immunol. 7, 773–782. https://doi.org/10.1038/ni1357

Klein, U., Dalla-Favera, R., 2008. Germinal centres: role in B-cell physiology and malignancy. Nat. Rev. Immunol. 8, 22–33. https://doi.org/10.1038/nri2217

Knight, K.L., Rhee, K.-J., 2005. Organization and Expression of Genes Encoding IgA Heavy Chain, Polymeric Ig Receptor, and J Chain, in: Mucosal Immunology. Elsevier, pp. 183–194. https://doi.org/10.1016/B978-012491543-5/50014-0

Kourelis, T.V., Dasari, S., Theis, J.D., Ramirez-Alvarado, M., Kurtin, P.J., Gertz, M.A., Zeldenrust, S.R., Zenka, R.M., Dogan, A., Dispenzieri, A., 2017. Clarifying immunoglobulin gene usage in systemic and localized immunoglobulin light-chain amyloidosis by mass spectrometry. Blood 129, 299–306. https://doi.org/10.1182/blood-2016-10-743997

Krammer, P.H., 2000. CD95's deadly mission in the immune system. Nature 407, 789–795. https://doi.org/10.1038/35037728

Kuehl, W.M., Bergsagel, P.L., 2012. Molecular pathogenesis of multiple myeloma and its premalignant precursor. J. Clin. Invest. 122, 3456–3463. https://doi.org/10.1172/JCI61188

Kumar, S., Murray, D., Dasari, S., Milani, P., Barnidge, D., Madden, B., Kourelis, T., Arendt, B., Merlini, G., Ramirez-Alvarado, M., Dispenzieri, A., 2019. Assay to rapidly screen for immunoglobulin light chain glycosylation: a potential path to earlier AL diagnosis for a subset of patients. Leukemia 33, 254–257. https://doi.org/10.1038/s41375-018-0194-x

Kumar, S.K., Rajkumar, V., Kyle, R.A., van Duin, M., Sonneveld, P., Mateos, M.-V., Gay, F., Anderson, K.C., 2017. Multiple myeloma. Nat. Rev. Dis. Primer 3, 17046. https://doi.org/10.1038/nrdp.2017.46

Kyle, R.A., Larson, D.R., Kurtin, P.J., Kumar, S., Cerhan, J.R., Therneau, T.M., Rajkumar, S.V., Vachon, C.M., Dispenzieri, A., 2019. Incidence of AL Amyloidosis in Olmsted County, Minnesota, 1990 through 2015. Mayo Clin. Proc. 94, 465–471. https://doi.org/10.1016/j.mayocp.2018.08.041

Kyle, R.A., Larson, D.R., Therneau, T.M., Dispenzieri, A., Kumar, S., Cerhan, J.R., Rajkumar, S.V., 2018. Long-Term Follow-up of Monoclonal Gammopathy of Undetermined Significance. N. Engl. J. Med. 378, 241–249. https://doi.org/10.1056/NEJMoa1709974

Kyle, R.A., Therneau, T.M., Rajkumar, S.V., Larson, D.R., Plevak, M.F., Offord, J.R., Dispenzieri, A., Katzmann, J.A., Melton, L.J., 2006. Prevalence of monoclonal

gammopathy of undetermined significance. N. Engl. J. Med. 354, 1362–1369. https://doi.org/10.1056/NEJMoa054494

Laidlaw, B.J., Duan, L., Xu, Y., Vazquez, S.E., Cyster, J.G., 2020. The transcription factor Hhex cooperates with the corepressor Tle3 to promote memory B cell development. Nat. Immunol. https://doi.org/10.1038/s41590-020-0713-6

Lambert, J.-M., Srour, N., Delpy, L., 2019. The Yin and Yang of RNA surveillance in B lymphocytes and antibody-secreting plasma cells. BMB Rep. 52, 671–678. https://doi.org/10.5483/BMBRep.2019.52.12.232

Landgren, O., Kyle, R.A., Pfeiffer, R.M., Katzmann, J.A., Caporaso, N.E., Hayes, R.B., Dispenzieri, A., Kumar, S., Clark, R.J., Baris, D., Hoover, R., Rajkumar, S.V., 2009. Monoclonal gammopathy of undetermined significance (MGUS) consistently precedes multiple myeloma: a prospective study. Blood 113, 5412–5417. https://doi.org/10.1182/blood-2008-12-194241

Lanzavecchia, A., 2018. Dissecting human antibody responses: useful, basic and surprising findings. EMBO Mol. Med. 10. https://doi.org/10.15252/emmm.201808879

LeBien, T.W., Tedder, T.F., 2008. B lymphocytes: how they develop and function. Blood 112, 1570–1580. https://doi.org/10.1182/blood-2008-02-078071

Lechouane, F., Bonaud, A., Delpy, L., Casola, S., Oruc, Z., Chemin, G., Cogné, M., Sirac, C., 2013. B-cell receptor signal strength influences terminal differentiation. Eur. J. Immunol. 43, 619–628. https://doi.org/10.1002/eji.201242912

Lefranc, M.-P., Giudicelli, V., Ginestoux, C., Jabado-Michaloud, J., Folch, G., Bellahcene, F., Wu, Y., Gemrot, E., Brochet, X., Lane, J., Regnier, L., Ehrenmann, F., Lefranc, G., Duroux, P., 2009. IMGT(R), the international ImMunoGeneTics information system(R). Nucleic Acids Res. 37, D1006–D1012. https://doi.org/10.1093/nar/gkn838

Leung, N., Bridoux, F., Hutchison, C.A., Nasr, S.H., Cockwell, P., Fermand, J.-P., Dispenzieri, A., Song, K.W., Kyle, R.A., 2012. Monoclonal gammopathy of renal significance: when MGUS is no longer undetermined or insignificant. Blood 120, 4292–4295. https://doi.org/10.1182/blood-2012-07-445304

Leung, N., Thomé, S.D., Dispenzieri, A., 2018. Venetoclax induced a complete response in a patient with immunoglobulin light chain amyloidosis plateaued on cyclophosphamide, bortezomib and dexamethasone. Haematologica 103, e135–e137. https://doi.org/10.3324/haematol.2017.183749

Lightman, S.M., Utley, A., Lee, K.P., 2019. Survival of Long-Lived Plasma Cells (LLPC): Piecing Together the Puzzle. Front. Immunol. 10, 965. https://doi.org/10.3389/fimmu.2019.00965

Liu, H., May, K., 2012. Disulfide bond structures of IgG molecules: structural variations, chemical modifications and possible impacts to stability and biological function. mAbs 4, 17–23. https://doi.org/10.4161/mabs.4.1.18347

Ma, C.S., Deenick, E.K., Batten, M., Tangye, S.G., 2012. The origins, function, and regulation of T follicular helper cells. J. Exp. Med. 209, 1241–1253. https://doi.org/10.1084/jem.20120994

Ma, Y., Shimizu, Y., Mann, M.J., Jin, Y., Hendershot, L.M., 2010. Plasma cell differentiation initiates a limited ER stress response by specifically suppressing the PERK-dependent branch of the unfolded protein response. Cell Stress Chaperones 15, 281–293. https://doi.org/10.1007/s12192-009-0142-9

Martin, F., Kearney, J.F., 2002. Marginal-zone B cells. Nat. Rev. Immunol. 2, 323–335. https://doi.org/10.1038/nri799

Martínez, A., Marín, V.G., Junquera, S.R. y C., Martínez-Murillo, R., Freire, M., 2005. The contributions of Santiago Ramón y Cajal to cancer research — 100 years on. Nat. Rev. Cancer 5, 904–909. https://doi.org/10.1038/nrc1741

Meffre, E., Casellas, R., Nussenzweig, M.C., 2000. Antibody regulation of B cell development. Nat. Immunol. 1, 379–385. https://doi.org/10.1038/80816

Meister, S., Schubert, U., Neubert, K., Herrmann, K., Burger, R., Gramatzki, M., Hahn, S., Schreiber, S., Wilhelm, S., Herrmann, M., Jäck, H.-M., Voll, R.E., 2007. Extensive immunoglobulin production sensitizes myeloma cells for proteasome inhibition. Cancer Res. 67, 1783–1792. https://doi.org/10.1158/0008-5472.CAN-06-2258

Merlini, G., Bellotti, V., 2003. Molecular Mechanisms of Amyloidosis. N. Engl. J. Med. 349, 583–596. https://doi.org/10.1056/NEJMra023144

Merlini, G., Dispenzieri, A., Sanchorawala, V., Schönland, S.O., Palladini, G., Hawkins, P.N., Gertz, M.A., 2018. Systemic immunoglobulin light chain amyloidosis. Nat. Rev. Dis. Primer 4, 38. https://doi.org/10.1038/s41572-018-0034-3

Merlini, G., Seldin, D.C., Gertz, M.A., 2011. Amyloidosis: pathogenesis and new therapeutic options. J. Clin. Oncol. Off. J. Am. Soc. Clin. Oncol. 29, 1924–1933. https://doi.org/10.1200/JCO.2010.32.2271

Milde, R., Ritter, J., Tennent, G.A., Loesch, A., Martinez, F.O., Gordon, S., Pepys, M.B., Verschoor, A., Helming, L., 2015. Multinucleated Giant Cells Are Specialized for Complement-Mediated Phagocytosis and Large Target Destruction. Cell Rep. 13, 1937–1948. https://doi.org/10.1016/j.celrep.2015.10.065

Mishra, S., Guan, J., Plovie, E., Seldin, D.C., Connors, L.H., Merlini, G., Falk, R.H., MacRae, C.A., Liao, R., 2013. Human amyloidogenic light chain proteins result in cardiac dysfunction, cell death, and early mortality in zebrafish. Am. J. Physiol. Heart Circ. Physiol. 305, H95-103. https://doi.org/10.1152/ajpheart.00186.2013

Mishra, S., Joshi, S., Ward, J.E., Buys, E.P., Mishra, Deepak, Mishra, Deepa, Morgado, I., Fisch, S., Lavatelli, F., Merlini, G., Dorbala, S., MacRae, C.A., Liao, R., 2019. Zebrafish model of amyloid light chain cardiotoxicity: regeneration versus degeneration. Am. J. Physiol.-Heart Circ. Physiol. 316, H1158–H1166. https://doi.org/10.1152/ajpheart.00788.2018

Monroe, J.G., 2006. ITAM-mediated tonic signalling through pre-BCR and BCR complexes. Nat. Rev. Immunol. 6, 283–294. https://doi.org/10.1038/nri1808

Morgan, G.J., Yan, N.L., Mortenson, D.E., Rennella, E., Blundon, J.M., Gwin, R.M., Lin, C.-Y., Stanfield, R.L., Brown, S.J., Rosen, H., Spicer, T.P., Fernandez-Vega, V., Merlini, G., Kay, L.E., Wilson, I.A., Kelly, J.W., 2019. Stabilization of amyloidogenic immunoglobulin light chains by small molecules. Proc. Natl. Acad. Sci. U. S. A. 116, 8360–8369. https://doi.org/10.1073/pnas.1817567116

Mosmann, T.R., Gravel, Y., Williamson, A.R., Baumal, R., 1978. Modification and fate of J chain in myeloma cells in the presence and absence of polymeric immunoglobulin secretion. Eur. J. Immunol. 8, 94–101. https://doi.org/10.1002/eji.1830080205

Mostoslavsky, R., Alt, F.W., Rajewsky, K., 2004. The Lingering Enigma of the Allelic Exclusion Mechanism. Cell 118, 539–544. https://doi.org/10.1016/j.cell.2004.08.023

Naito, Y., Takematsu, H., Koyama, S., Miyake, S., Yamamoto, H., Fujinawa, R., Sugai, M., Okuno, Y., Tsujimoto, G., Yamaji, T., Hashimoto, Y., Itohara, S., Kawasaki, T., Suzuki, A., Kozutsumi, Y., 2007. Germinal center marker GL7 probes activation-dependent repression of N-glycolylneuraminic acid, a sialic acid species involved in the negative modulation of B-cell activation. Mol. Cell. Biol. 27, 3008–3022. https://doi.org/10.1128/MCB.02047-06

Nasr, S.H., Galgano, S.J., Markowitz, G.S., Stokes, M.B., D'Agati, V.D., 2006. Immunofluorescence on pronase-digested paraffin sections: a valuable salvage technique for renal biopsies. Kidney Int. 70, 2148–2151. https://doi.org/10.1038/sj.ki.5001990

Nasr, S.H., Valeri, A.M., Cornell, L.D., Fidler, M.E., Sethi, S., D'Agati, V.D., Leung, N., 2012. Renal monoclonal immunoglobulin deposition disease: a report of 64 patients from a single institution. Clin. J. Am. Soc. Nephrol. CJASN 7, 231–239. https://doi.org/10.2215/CJN.08640811

Nauta, J., Goedbloed, M.A., Herck, H.V., Hesselink, D.A., Visser, P., Willemsen, R., Dokkum, R.P., Wright, C.J., Guay-Woodford, L.M., 2000. New rat model that phenotypically resembles autosomal recessive polycystic kidney disease. J. Am. Soc. Nephrol. JASN 11, 2272–2284.

Nutt, S.L., Hodgkin, P.D., Tarlinton, D.M., Corcoran, L.M., 2015. The generation of antibody-secreting plasma cells. Nat. Rev. Immunol. 15, 160–171. https://doi.org/10.1038/nri3795

Nuvolone, M., Sorce, S., Pelczar, P., Rushing, E., Lavatelli, F., Rognoni, P., Valentini, V., Palladini, G., Merlini, G., Aguzzi, A., 2017. Regulated expression of amyloidogenic immunoglobulin light chains in mice. Amyloid Int. J. Exp. Clin. Investig. Off. J. Int. Soc. Amyloidosis 24, 52–53. https://doi.org/10.1080/13506129.2017.1289914

Oliva, L., Orfanelli, U., Resnati, M., Raimondi, A., Orsi, A., Milan, E., Palladini, G., Milani, P., Cerruti, F., Cascio, P., Casarini, S., Rognoni, P., Touvier, T., Marcatti, M., Ciceri, F., Mangiacavalli, S., Corso, A., Merlini, G., Cenci, S., 2017. The amyloidogenic light chain is a stressor that sensitizes plasma cells to proteasome inhibitor toxicity. Blood 129, 2132–2142. https://doi.org/10.1182/blood-2016-08-730978

on behalf of the International Myeloma Working Group, Kyle, R.A., Durie, B.G.M., Rajkumar, S.V., Landgren, O., Blade, J., Merlini, G., Kröger, N., Einsele, H., Vesole, D.H., Dimopoulos, M., San Miguel, J., Avet-Loiseau, H., Hajek, R., Chen, W.M., Anderson, K.C., Ludwig, H., Sonneveld, P., Pavlovsky, S., Palumbo, A., Richardson, P.G., Barlogie, B., Greipp, P., Vescio, R., Turesson, I., Westin, J., Boccadoro, M., 2010. Monoclonal gammopathy of undetermined significance (MGUS) and smoldering (asymptomatic) multiple myeloma: IMWG consensus perspectives risk factors for progression and guidelines for monitoring and management. Leukemia 24, 1121–1127. https://doi.org/10.1038/leu.2010.60

Paiva, B., Martinez-Lopez, J., Corchete, L.A., Sanchez-Vega, B., Rapado, I., Puig, N., Barrio, S., Sanchez, M.-L., Alignani, D., Lasa, M., García de Coca, A., Pardal, E., Oriol, A., Garcia, M.-E.G., Escalante, F., González-López, T.J., Palomera, L., Alonso, J., Prosper, F., Orfao, A., Vidriales, M.-B., Mateos, M.-V., Lahuerta, J.-J., Gutierrez, N.C., San Miguel, J.F., 2016. Phenotypic, transcriptomic, and genomic features of clonal plasma cells in light-chain amyloidosis. Blood 127, 3035–3039. https://doi.org/10.1182/blood-2015-10-673095

Parrondo, R.D., Majeed, U., Sher, T., 2020. Antibody-based immunotherapy for treatment of immunoglobulin light-chain amyloidosis. Br. J. Haematol. https://doi.org/10.1111/bjh.16697

Pepys, M.B., 2006. Amyloidosis. Annu. Rev. Med. 57, 223–241. https://doi.org/10.1146/annurev.med.57.121304.131243

Pepys, M.B., Herbert, J., Hutchinson, W.L., Tennent, G.A., Lachmann, H.J., Gallimore, J.R., Lovat, L.B., Bartfai, T., Alanine, A., Hertel, C., Hoffmann, T., Jakob-Roetne, R., Norcross, R.D., Kemp, J.A., Yamamura, K., Suzuki, M., Taylor, G.W., Murray, S., Thompson, D., Purvis, A., Kolstoe, S., Wood, S.P., Hawkins, P.N., 2002. Targeted

pharmacological depletion of serum amyloid P component for treatment of human amyloidosis. Nature 417, 254–259. https://doi.org/10.1038/417254a

Pérez-Silva, J.G., Español, Y., Velasco, G., Quesada, V., 2016. The Degradome database: expanding roles of mammalian proteases in life and disease. Nucleic Acids Res. 44, D351-355. https://doi.org/10.1093/nar/gkv1201

Perfetti, V., Palladini, G., Casarini, S., Navazza, V., Rognoni, P., Obici, L., Invernizzi, R., Perlini, S., Klersy, C., Merlini, G., 2012. The repertoire of λ light chains causing predominant amyloid heart involvement and identification of a preferentially involved germline gene, IGLV1-44. Blood 119, 144–150. https://doi.org/10.1182/blood-2011-05-355784

Petro, J.B., Gerstein, R.M., Lowe, J., Carter, R.S., Shinners, N., Khan, W.N., 2002. Transitional Type 1 and 2 B Lymphocyte Subsets Are Differentially Responsive to Antigen Receptor Signaling. J. Biol. Chem. 277, 48009–48019. https://doi.org/10.1074/jbc.M200305200

Pillai, S., Cariappa, A., 2009. The follicular versus marginal zone B lymphocyte cell fate decision. Nat. Rev. Immunol. 9, 767–777. https://doi.org/10.1038/nri2656

Pinaud, E., Marquet, M., Fiancette, R., Péron, S., Vincent-Fabert, C., Denizot, Y., Cogné, M., 2011. The IgH locus 3' regulatory region: pulling the strings from behind. Adv. Immunol. 110, 27–70. https://doi.org/10.1016/B978-0-12-387663-8.00002-8

Preud'homme, J.-L., Aucouturier, P., Touchard, G., Striker, L., Khamlichi, A.A., Rocca, A., Denoroy, L., Cogné, M., 1994. Monoclonal immunoglobulin deposition disease (Randall type). Relationship with structural abnormalities of immunoglobulin chains. Kidney Int. 46, 965–972. https://doi.org/10.1038/ki.1994.355

Radamaker, L., Lin, Y.-H., Annamalai, K., Huhn, S., Hegenbart, U., Schönland, S.O., Fritz, G., Schmidt, M., Fändrich, M., 2019. Cryo-EM structure of a light chain-derived amyloid fibril from a patient with systemic AL amyloidosis. Nat. Commun. 10, 1103. https://doi.org/10.1038/s41467-019-09032-0

Rajkumar, S.V., Dimopoulos, M.A., Palumbo, A., Blade, J., Merlini, G., Mateos, M.-V., Kumar, S., Hillengass, J., Kastritis, E., Richardson, P., Landgren, O., Paiva, B., Dispenzieri, A., Weiss, B., LeLeu, X., Zweegman, S., Lonial, S., Rosinol, L., Zamagni, E., Jagannath, S., Sezer, O., Kristinsson, S.Y., Caers, J., Usmani, S.Z., Lahuerta, J.J., Johnsen, H.E., Beksac, M., Cavo, M., Goldschmidt, H., Terpos, E., Kyle, R.A., Anderson, K.C., Durie, B.G.M., Miguel, J.F.S., 2014. International Myeloma Working Group updated criteria for the diagnosis of multiple myeloma. Lancet Oncol. 15, e538–e548. https://doi.org/10.1016/S1470-2045(14)70442-5

Ramirez-Alvarado, M., 2012. Amyloid formation in light chain amyloidosis. Curr. Top. Med. Chem. 12, 2523–2533.

Randall, R.E., Williamson, W.C., Mullinax, F., Tung, M.Y., Still, W.J.S., 1976. Manifestations of systemic light chain deposition. Am. J. Med. 60, 293–299. https://doi.org/10.1016/0002-9343(76)90440-X

Reimold, A.M., Iwakoshi, N.N., Manis, J., Vallabhajosyula, P., Szomolanyi-Tsuda, E., Gravallese, E.M., Friend, D., Grusby, M.J., Alt, F., Glimcher, L.H., 2001. Plasma cell differentiation requires the transcription factor XBP-1. Nature 412, 300–307. https://doi.org/10.1038/35085509

Richards, D.B., Cookson, L.M., Berges, A.C., Barton, S.V., Lane, T., Ritter, J.M., Fontana, M., Moon, J.C., Pinzani, M., Gillmore, J.D., Hawkins, P.N., Pepys, M.B., 2015. Therapeutic Clearance of Amyloid by Antibodies to Serum Amyloid P Component. N. Engl. J. Med. 373, 1106–1114. https://doi.org/10.1056/NEJMoa1504942

Romeuf, C.D., Sirac, C., 2015. Chimeric protein in the treatment of amyloidosis. WO2015063728A1.

Ronco, P., Plaisier, E., Mougenot, B., Aucouturier, P., 2006. Immunoglobulin Light (Heavy)-Chain Deposition Disease: From Molecular Medicine to Pathophysiology-Driven Therapy. Clin. J. Am. Soc. Nephrol. 1, 1342–1350. https://doi.org/10.2215/CJN.01730506

Ronco, P.M., Alyanakian, M.A., Mougenot, B., Aucouturier, P., 2001. Light chain deposition disease: a model of glomerulosclerosis defined at the molecular level. J. Am. Soc. Nephrol. JASN 12, 1558–1565.

Roth, K., Oehme, L., Zehentmeier, S., Zhang, Y., Niesner, R., Hauser, A.E., 2014. Tracking plasma cell differentiation and survival: Molecular Events of Plasma Cell Differentiation and Survival. Cytometry A 85, 15–24. https://doi.org/10.1002/cyto.a.22355

Roussel, M., Merlini, G., Chevret, S., Arnulf, B., Stoppa, A.M., Perrot, A., Palladini, G., Karlin, L., Royer, B., Huart, A., Macro, M., Morel, P., Frenzel, L., Touzeau, C., Boyle, E., Dorvaux, V., Le Bras, F., Lavergne, D., Bridoux, F., Jaccard, A., 2020. A prospective phase 2 trial of daratumumab in patients with previously treated systemic light-chain amyloidosis. Blood 135, 1531–1540. https://doi.org/10.1182/blood.2019004369

Sanders, P.W., Herrera, G.A., Galla, J.H., with the technical assistance of James R. Hancock, Lott, R.L., 1987. Human Bence Jones protein toxicity in rat proximal tubule epithelium in vivo. Kidney Int. 32, 851–861. https://doi.org/10.1038/ki.1987.286

Sayed, R.H., Wechalekar, A.D., Gilbertson, J.A., Bass, P., Mahmood, S., Sachchithanantham, S., Fontana, M., Patel, K., Whelan, C.J., Lachmann, H.J., Hawkins, P.N., Gillmore, J.D., 2015. Natural history and outcome of light chain deposition disease. Blood 126, 2805–2810. https://doi.org/10.1182/blood-2015-07-658872

Schatz, D.G., Swanson, P.C., 2011. V(D)J Recombination: Mechanisms of Initiation. Annu. Rev. Genet. 45, 167–202. https://doi.org/10.1146/annurev-genet-110410-132552

Schrezenmeier, E., Jayne, D., Dörner, T., 2018. Targeting B Cells and Plasma Cells in Glomerular Diseases: Translational Perspectives. J. Am. Soc. Nephrol. ASN.2017040367. https://doi.org/10.1681/ASN.2017040367

Schroeder, H.W., Cavacini, L., 2010. Structure and function of immunoglobulins. J. Allergy Clin. Immunol. 125, S41–S52. https://doi.org/10.1016/j.jaci.2009.09.046

Sciammas, R., Shaffer, A.L., Schatz, J.H., Zhao, H., Staudt, L.M., Singh, H., 2006. Graded Expression of Interferon Regulatory Factor-4 Coordinates Isotype Switching with Plasma Cell Differentiation. Immunity 25, 225–236. https://doi.org/10.1016/j.immuni.2006.07.009

Shaffer, A.L., Lin, K.I., Kuo, T.C., Yu, X., Hurt, E.M., Rosenwald, A., Giltnane, J.M., Yang, L., Zhao, H., Calame, K., Staudt, L.M., 2002. Blimp-1 orchestrates plasma cell differentiation by extinguishing the mature B cell gene expression program. Immunity 17, 51–62. https://doi.org/10.1016/s1074-7613(02)00335-7

Shapiro-Shelef, M., Calame, K., 2005. Regulation of plasma-cell development. Nat. Rev. Immunol. 5, 230–242. https://doi.org/10.1038/nri1572

Shinnakasu, R., Inoue, T., Kometani, K., Moriyama, S., Adachi, Y., Nakayama, M., Takahashi, Y., Fukuyama, H., Okada, T., Kurosaki, T., 2016. Regulated selection of germinal-center cells into the memory B cell compartment. Nat. Immunol. 17, 861–869. https://doi.org/10.1038/ni.3460

Sidiqi, M.H., Al Saleh, A.S., Leung, N., Jevremovic, D., Aljama, M.A., Gonsalves, W.I., Buadi, F.K., Kourelis, T.V., Warsame, R., Muchtar, E., Hobbs, M.A., Lacy, M.Q., Dingli, D., Go, R.S., Hayman, S.R., Rajkumar, S.V., Dispenzieri, A., Gertz, M.A., Kumar, S.K., Fonseca, R., Kapoor, P., 2020. Venetoclax for the treatment of translocation (11;14) AL amyloidosis. Blood Cancer J. 10, 1–4. https://doi.org/10.1038/s41408-020-0321-6

Sipe, J.D., Benson, M.D., Buxbaum, J.N., Ikeda, S., Merlini, G., Saraiva, M.J.M., Westermark, P., 2016. Amyloid fibril proteins and amyloidosis: chemical identification and clinical classification International Society of Amyloidosis 2016 Nomenclature Guidelines. Amyloid 23, 209–213. https://doi.org/10.1080/13506129.2016.1257986

Sirac, C., 2006. Role of the monoclonal chain V domain and reversibility of renal damage in a transgenic model of acquired Fanconi syndrome. Blood 108, 536–543. https://doi.org/10.1182/blood-2005-11-4419

Sirac, C., Herrera, G.A., Sanders, P.W., Batuman, V., Bender, S., Ayala, M.V., Javaugue, V., Teng, J., Turbat-Herrera, E.A., Cogné, M., Touchard, G., Leung, N., Bridoux, F., 2018. Animal models of monoclonal immunoglobulin-related renal diseases. Nat. Rev. Nephrol. 14, 246–264. https://doi.org/10.1038/nrneph.2018.8

Sitia, R., Palladini, G., Merlini, G., 2007. Bortezomib in the treatment of AL amyloidosis: targeted therapy? Haematologica 92, 1302–1307. https://doi.org/10.3324/haematol.12136

Smadja, N.V., Fruchart, C., Isnard, F., Louvet, C., Dutel, J.L., Cheron, N., Grange, M.J., Monconduit, M., Bastard, C., 1998. Chromosomal analysis in multiple myeloma: cytogenetic evidence of two different diseases. Leukemia 12, 960–969. https://doi.org/10.1038/sj.leu.2401041

Solomon, A., Weiss, D.T., Kattine, A.A., 1991. Nephrotoxic Potential of Bence Jones Proteins. N. Engl. J. Med. 324, 1845–1851. https://doi.org/10.1056/NEJM199106273242603

Solomon, A., Weiss, D.T., Wall, J.S., 2003a. Immunotherapy in Systemic Primary (AL) Amyloidosis Using Amyloid-Reactive Monoclonal Antibodies. Cancer Biother. Radiopharm. 18, 853–860. https://doi.org/10.1089/108497803322702824

Solomon, A., Weiss, D.T., Wall, J.S., 2003b. Therapeutic potential of chimeric amyloid-reactive monoclonal antibody 11-1F4. Clin. Cancer Res. Off. J. Am. Assoc. Cancer Res. 9, 3831S–8S.

Steward, A., Adhya, S., Clarke, J., 2002. Sequence Conservation in Ig-like Domains: The Role of Highly Conserved Proline Residues in the Fibronectin Type III Superfamily. J. Mol. Biol. 318, 935–940. https://doi.org/10.1016/S0022-2836(02)00184-5

Stewart, I., Radtke, D., Phillips, B., McGowan, S.J., Bannard, O., 2018. Germinal Center B Cells Replace Their Antigen Receptors in Dark Zones and Fail Light Zone Entry when Immunoglobulin Gene Mutations are Damaging. Immunity 49, 477-489.e7. https://doi.org/10.1016/j.immuni.2018.08.025

Suresh, R., Mosser, D.M., 2013. Pattern recognition receptors in innate immunity, host defense, and immunopathology. Adv. Physiol. Educ. 37, 284–291. https://doi.org/10.1152/advan.00058.2013

Swuec, P., Lavatelli, F., Tasaki, M., Paissoni, C., Rognoni, P., Maritan, M., Brambilla, F., Milani, P., Mauri, P., Camilloni, C., Palladini, G., Merlini, G., Ricagno, S., Bolognesi, M., 2019. Cryo-EM structure of cardiac amyloid fibrils from an immunoglobulin light chain AL amyloidosis patient. Nat. Commun. 10, 1269. https://doi.org/10.1038/s41467-019-09133-w

Teng, J., Turbat-Herrera, E.A., Herrera, G.A., 2014. An animal model of glomerular light-chain-associated amyloidogenesis depicts the crucial role of lysosomes. Kidney Int. 86, 738–746. https://doi.org/10.1038/ki.2014.122

Tiselius, A., Kabat, E.A., 1939. AN ELECTROPHORETIC STUDY OF IMMUNE SERA AND PURIFIED ANTIBODY PREPARATIONS. J. Exp. Med. 69, 119–131. https://doi.org/10.1084/jem.69.1.119

van den Hoven, M.J., Wijnhoven, T.J., Li, J.-P., Zcharia, E., Dijkman, H.B., Wismans, R.G., Rops, A.L., Lensen, J.F., van den Heuvel, L.P., van Kuppevelt, T.H., Vlodavsky, I., Berden, J.H.M., van der Vlag, J., 2008. Reduction of anionic sites in the glomerular basement membrane by heparanase does not lead to proteinuria. Kidney Int. 73, 278–287. https://doi.org/10.1038/sj.ki.5002706

van Erp, E.A., Luytjes, W., Ferwerda, G., van Kasteren, P.B., 2019. Fc-Mediated Antibody Effector Functions During Respiratory Syncytial Virus Infection and Disease. Front. Immunol. 10. https://doi.org/10.3389/fimmu.2019.00548

van Nieuwenhuijzen, N., Spaan, I., Raymakers, R., Peperzak, V., 2018. From MGUS to Multiple Myeloma, a Paradigm for Clonal Evolution of Premalignant Cells. Cancer Res. 78, 2449–2456. https://doi.org/10.1158/0008-5472.CAN-17-3115

Varettoni, M., Zibellini, S., Defrancesco, I., Ferretti, V.V., Rizzo, E., Malcovati, L., Gallì, A., Porta, M.G.D., Boveri, E., Arcaini, L., Candido, C., Paulli, M., Cazzola, M., 2017. Pattern of somatic mutations in patients with Waldenström macroglobulinemia or IgM monoclonal gammopathy of undetermined significance. Haematologica 102, 2077–2085. https://doi.org/10.3324/haematol.2017.172718

Varga, C., Titus, S.E., Toskic, D., Comenzo, R.L., 2019. Use of novel therapies in the treatment of light chain amyloidosis. Blood Rev. 37, 100581. https://doi.org/10.1016/j.blre.2019.05.005

Vembar, S.S., Brodsky, J.L., 2008. One step at a time: endoplasmic reticulum-associated degradation. Nat. Rev. Mol. Cell Biol. 9, 944–957. https://doi.org/10.1038/nrm2546

Vettermann, C., Schlissel, M.S., 2010. Allelic exclusion of immunoglobulin genes: models and mechanisms: Allelic exclusion of immunoglobulin genes. Immunol. Rev. 237, 22–42. https://doi.org/10.1111/j.1600-065X.2010.00935.x

Victora, G.D., Nussenzweig, M.C., 2012. Germinal centers. Annu. Rev. Immunol. 30, 429–457. https://doi.org/10.1146/annurev-immunol-020711-075032

Wajant, H., 2002. The Fas Signaling Pathway: More Than a Paradigm. Science 296, 1635–1636. https://doi.org/10.1126/science.1071553

Wall, J., Schell, M., Murphy, C., Hrncic, R., Stevens, F.J., Solomon, A., 1999. Thermodynamic instability of human lambda 6 light chains: correlation with fibrillogenicity. Biochemistry 38, 14101–14108.

Wall, J.S., Gupta, V., Wilkerson, M., Schell, M., Loris, R., Adams, P., Solomon, A., Stevens, F., Dealwis, C., 2004. Structural basis of light chain amyloidogenicity: comparison of the thermodynamic properties, fibrillogenic potential and tertiary structural features of four Vlambda6 proteins. J. Mol. Recognit. JMR 17, 323–331. https://doi.org/10.1002/jmr.681

Wall, J.S., Kennel, S.J., Stuckey, A.C., Long, M.J., Townsend, D.W., Smith, G.T., Wells, K.J., Fu, Y., Stabin, M.G., Weiss, D.T., Solomon, A., 2010. Radioimmunodetection of amyloid deposits in patients with AL amyloidosis. Blood 116, 2241–2244. https://doi.org/10.1182/blood-2010-03-273797

Wall, J.S., Kennel, S.J., Williams, A., Richey, T., Stuckey, A., Huang, Y., Macy, S., Donnell, R., Barbour, R., Seubert, P., Schenk, D., 2012. AL Amyloid Imaging and Therapy with a Monoclonal Antibody to a Cryptic Epitope on Amyloid Fibrils. PLoS ONE 7, e52686. https://doi.org/10.1371/journal.pone.0052686

Wall, J.S., Williams, A.D., Foster, J.S., Richey, T., Stuckey, A., Macy, S., Wooliver, C., Campagna, S.R., Tague, E.D., Farmer, A.T., Lands, R.H., Martin, E.B., Heidel, R.E., Kennel, S.J., 2018. Bifunctional amyloid-reactive peptide promotes binding of antibody 11-1F4 to diverse amyloid types and enhances therapeutic efficacy. Proc. Natl. Acad. Sci. U. S. A. 115, E10839–E10848. https://doi.org/10.1073/pnas.1805515115

Ward, J.E., Ren, R., Toraldo, G., SooHoo, P., Guan, J., O'Hara, C., Jasuja, R., Trinkaus-Randall, V., Liao, R., Connors, L.H., Seldin, D.C., 2011. Doxycycline reduces fibril formation in a transgenic mouse model of AL amyloidosis. Blood 118, 6610–6617. https://doi.org/10.1182/blood-2011-04-351643

Westermark, G.T., Fändrich, M., Lundmark, K., Westermark, P., 2018. Noncerebral Amyloidoses: Aspects on Seeding, Cross-Seeding, and Transmission. Cold Spring Harb. Perspect. Med. 8, a024323. https://doi.org/10.1101/cshperspect.a024323

Xu, Z., Zan, H., Pone, E.J., Mai, T., Casali, P., 2012. Immunoglobulin class-switch DNA recombination: induction, targeting and beyond. Nat. Rev. Immunol. 12, 517–531. https://doi.org/10.1038/nri3216

Yancopoulos, G.D., Alt, F.W., 1986. Regulation of the Assembly and Expression of Variable-Region Genes. Annu. Rev. Immunol. 4, 339–368. https://doi.org/10.1146/annurev.iy.04.040186.002011

Zhang, K., Kaufman, R.J., 2008. From endoplasmic-reticulum stress to the inflammatory response. Nature 454, 455–462. https://doi.org/10.1038/nature07203

Zhou, P., Ma, X., Iyer, L., Chaulagain, C., Comenzo, R.L., 2014. One siRNA pool targeting the λ constant region stops λ light-chain production and causes terminal endoplasmic reticulum stress. Blood 123, 3440–3451. https://doi.org/10.1182/blood-2013-10-535187

Mouse models to study plasma cells and monoclonal immunoglobulin-related diseases

Abnormal plasma cells (PC) proliferation is frequent (approximately 5% of people over 50) but in most cases remains asymptomatic, detected by the presence of a monoclonal Immunoglobulin (Ig) in excess. These Ig can be unstable and cause complications related to their precipitation, aggregation or crystallization in different organs. Due to the inherent variability of Igs, with different sequences from one patient to the other, and the wide spectrum of the different pathologies, reliable experimental models for Ig-induced deposition diseases are challenging to obtain. In our laboratory, we were able to develop a Light Chain Deposition Disease (LCDD) mouse model that reproduces the renal lesions found in patients and that allowed us to show that pathogenic Light Chain (LC) expressed sensitizes the PC to proteasome inhibitors by the activation of the endoplasmic reticulum stress response pathway. Additionally, we proved that eliminating the pathogenic LC mice recovered their renal function. Over the years, different strategies have been carried out to obtain a model for AL Amyloidosis , the most frequent and severe form of Ig-related deposition disease. We have created a rat and a mouse transgenic model expressing an amyloidogenic LC that did not spontaneously develop amyloidosis. Thanks to *in vitro* studies, we have showed that the Variable LC domain (VL) is the key for fibril formation and mice injected with them generate amyloid deposits in heart and spleen. We have also focused in the targeting and modification of PCs. For this, we searched for a gene only expressed in this cell lineage, the J Chain. Using a conditional deletion mouse model expressing a tamoxifen-dependent Cre recombinase under the regulatory elements of the J Chain, we were able to modify gene expression specifically in PCs. Thanks to this model and others already available in the laboratory, we started the exploration of the therapeutic potential of targeting the Ig.

Mots-clés : Plasma Cell, Ig-related deposition disease, AL Amyloidosis, Light Chain Deposition Disease (LCDD), J Chain

Modèles des souris pour étudier les plasmocytes et les maladies liées aux immunoglobulines monoclonales.

La prolifération anormale des plasmocytes (PC) est fréquente (environ 5% des personnes de plus de 50 ans) mais reste dans la plupart des cas asymptomatique, détectée par la présence d'une Immunoglobuline (Ig) monoclonale en excès. Ces Ig peuvent être instables et entraîner des complications liées à leur précipitation, agrégation ou cristallisation dans différents organes. En raison de la variabilité inhérente des Ig, avec des séquences différentes d'un patient à l'autre, et du large spectre des différentes pathologies, des modèles expérimentaux fiables pour les maladies à dépôt induit par des Ig sont difficiles à obtenir. Dans notre laboratoire, nous avons pu développer un modèle de souris pour la Light Chain Deposition Disease (LCDD) qui reproduit les lésions rénales retrouvées chez les patients et qui nous a permis de montrer que la chaîne légère (LC) pathogène exprimée sensibilise le PC aux inhibiteurs du protéasome par l'activation de la voie de réponse au stress du réticulum endoplasmique. De plus, nous avons prouvé que l'élimination des LC pathogènes conduis à la récupération de la fonction rénale des souris. Au fil des ans, différentes stratégies ont été mises en œuvre pour obtenir un modèle de l'amylose AL, la forme la plus fréquente et sévère des maladies liées aux dépôts d'Ig monoclonales. Nous avons développé une lignée transgénique de rat et une de souris exprimant une LC amyloïdogène. Grâce à des études *in vitro*, nous avons montré que le domaine LC variable (VL) est essentiel pour la formation de fibrilles et que les souris injectées avec génèrent des dépôts amyloïdes dans le cœur et la rate. Nous nous sommes également intéressés au ciblage et à la modification des PC. Pour cela, nous avons recherché un gène exprimé uniquement dans ce groupe de cellules, la chaîne J. En utilisant un modèle de souris à délétion conditionnelle exprimant une recombinase Cre dépendante du tamoxifène sous les éléments régulateurs de la chaîne J, nous avons pu modifier l'expression de gènes spécifiquement dans les PC. Grâce à ce modèle et à d'autres déjà disponibles au laboratoire, nous avons commencé l'exploration du potentiel thérapeutique du ciblage des Ig.

Keywords: Plasmocyte, maladie des dépôts liés aux Ig, Amylose AL, Light Chain Deposition Disease (LCDD), Chaîne J